Crystallisation behaviour of commercial polyethylenes: a fundamental study

by

Megan Matthews

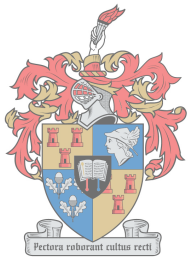

UNIVERSITEIT
iYUNIVESITHI
STELLENBOSCH
UNIVERSITY

Supervisor: Prof A.J. van Reenen

University of Stellenbosch
Department of Chemistry and Polymer Science

December 2018

Declaration

I declare that the entirety of the work contained herein is my own, original work, that I am the sole author thereof (save to the extent explicitly otherwise stated), that reproduction and publication thereof by Stellenbosch University will not infringe any third party rights and that I have not previously in its entirety or in part submitted it for obtaining any qualification.

December 2018

Abstract

Commercial films are generally made of polyolefins, often using a blend of two different polyolefins. Specifically, low density polyethylene (LDPE) and linear low density polyethylene (LLDPE) are blended due to the mechanical strength of LLDPE and the processability of LDPE. However the behaviour of these blends is unpredictable due to the lack of understanding of the underlying processes which determine the final properties.

This study focused on developing an understanding of the interactions between LDPE and LLDPE in the blended form through the crystallisation behaviour of the blends. The criteria for co-crystallisation are presented and systematically investigated in order to determine whether the blends meet the criteria. By analysing the blend miscibility in the melt, the crystal structure of the individual blend components as well as the crystallisation kinetics, conclusions can be made about the co-crystallisation potential of LDPE/LLDPE blends.

Melt miscibility was investigated by using fluorescent labelling of both polymer components and tracking their movements after the blending process. No isolated domains could be detected with fluorescence microscopy indicating that phase separation did not occur during the melt blending process. However, differential scanning calorimetry (DSC) displayed a number of different crystalline environments which implied that phase separation occurred during the crystallisation process. DSC was also used to verify this through kinetics and showed that the LLDPE crystallised at a faster rate than the LDPE, making co-crystallisation unlikely. Solid state nuclear magnetic resonance (SS NMR) was used to probe the phase separation within the blends and was used to identify a number of different regions which had formed within the amorphous and interfacial areas which seemed to be the cause of the interactions. This disproved the hypothesis that the difference in rate and extent of crystallisation directly affected the ultimate blend properties but rather showed that the amorphous and interfacial regions determine blend behaviour.

Opsomming

Kommersiële films bestaan hoofsaaklik uit poliolefiene en meestal uit ‘n samestelling van twee verskillende poliolefiene. Spesifieke verwysing word gemaak na die samestelling van lae digtheid poliëtileen (LDPE) en liniêre lae digtheid poliëtileen (LLDPE) as gevolg van die meganiese sterkte van LLDPE en die verwerkbaarheid van LDPE. Die werkverrigtinge van hierdie samestellings is onvoorspelbaar as gevolg van ‘n gebrek aan begrip oor die onderliggende prosesse wat die finale eienskappe daarvan bepaal.

Die fokus van hierdie studie is om begrip te ontwikkel van die interaksie tussen LDPE en LLDPE in ‘n samestellende vorm, deur die kristallisasie van die samestellings. Die kriteria vir ko-kristallisasie word voorgelê en sistematies ondersoek om te bepaal of die samestellings aan die vereistes voldoen.

‘n Ontleding van die mengbaarheid van die samestelling in die smeltsel, die kristalstruktuur van die individuele komponente van die samestelling asook die kristallisasie kinetika kan lei tot bevindings oor die ko-kristallisasie potensiaal van die LDPE/LLDPE samestellings.

Fluorosserende merkers van beide polimeer komponente word gebruik om die mengbaarheid van die smeltsel te ondersoek asook om die bewegings na die smeltingsproses te volg. Resultate toon dat fase skeiding nie gedurende die smeltingsproses voorgekom het nie. ‘n Bewys hiervan is die gebrek aan geÏsoleerde domeine wat waargeneem is deur die toepassing van fluoressensie mikroskopie. Differensieel skandering kalorimetrie (DSC) het wel bewys gelewer van ‘n aantal verskillende kristallyne areas wat impliseer dat fase skeiding plaasgevind het gedurende die kristallisasie proses. DSC was ook gebruik om fase skeiding deur kinetika te bewys. Dit het ook aangedui dat kristallisasie van LLDPE teen ‘n vinniger tempo as LDPE plaasvind, wat ko-kristallisasie onwaarskynlik maak. Soliede fase kern magnetiese resonansie (KMR) was gebruik om die fase skeiding binne die amorfe en skeidingsvlak areas te ondersoek wat die oorsaak van die interaksies blyk te wees. Die hipotese dat die verskille in die tempo en omvang van kristallisasie die mengsel eienskappe direk affekteer, is verkeerd bewys. Die resultate toon wel dat mengbaarheid bepaal word deur die amorfe en skeidingsvlak areas.

This thesis is dedicated to my mother, Denyse, for all the small things.

Acknowledgements

I would like to thank the following people for their support throughout the year:

Prof A.J. van Reenen for his guidance during this project and for believing in me even when I didn't.

The **Olefins group** for their problem solving expertise and for creating a fun working environment, **Ben van der Westhuizen** for image processing, **Marehette le Grange** for assistance in the field of cellulose nanowhiskers and my friend **Chandré Smit** for her input and advice on this project and everything else.

My family and the **Bowes family** for unwavering support and understanding and many years of continuous prayer.

Finally, I would like to thank the following for their contributions to this project:

Sasol polymers for providing the materials which were studied in this work

Central Analytical Facility (CAF) specifically, **Dumisile Lumkwana** and **Rozanne Adams** for assistance with confocal fluorescence microscopy and **Dr Elrika Harmzen-Pretorius** and **Nelisa Dyayiya** for assistance with electron microscopy. Also **Dr Jaco Brand**, **Elsa Malherbe** and **Heidi Duveskog** for assistance with solid state NMR.

Prof Alejandro J. Müller and **Ricardo Pérez** for providing me with the CrystFit software for processing kinetics by DSC

The **National Research Foundation** (NRF) for funding

Table of Contents

Chapter 5

Chapter 6

Appendices

List of Figures

Chapter 2

Chapter 3

Chapter 4

Chapter 5

Appendices

List of Tables

Chapter 2

Chapter 3

Chapter 4

Chapter 5

List of Equations

List of Abbreviations

CP	Cross-polarisation
Crystaf	Crystallisation analysis fractionation
DD	Dipolar decoupled
DP	Degree of polymerisation
DSC	Differential scanning calorimetry
Exo	Exothermic
FITC	Fluoroscein-5'-isothiocyanate
FTIR	Fourier transform infrared
HDPE	High density polyethylene
HT-SEC	High temperature size exclusion chromatography
LCST	Lower critical solution temperature
LDPE	Low density polyethylene
LLDPE	Linear low density polyethylene
MAO	Methylaluminoxane
MAS	Magic angle spinning
MDPE	Medium density polyethylene
m-LLDPE	Metallocene-linear low density polyethylene
M_n	Number average molar mass
MSL	Methylene sequence length
M_w	Weight average molar mass
NMR	Nuclear magnetic resonance
o-DCB	*ortho*-dichlorobenzene
PET	Poly(ethylene terephthalate)
PLA	Poly(lactic acid)
PMMA	Poly(methyl methacrylate)
POM	Polarised optical microscopy
PS	Polystyrene
RhB	Rhodamine B
SAN	Poly(styrene-co-acrylonitrile)
SAXS	Small angle x-ray scattering
Scalls	Solution crystallisation analysis by laser light scattering
SE	Solvent extracted
SEM	Scanning electron microscopy
SPE	Single pulse excitation
SSA	Successive self-nucleation and annealing
T_c	Crystallisation temperature
TEM	Transmission electron microscopy
T_g	Glass transition temperature
T_m	Melting temperature
TREF	Temperature rising elution fractionation
UCST	Upper critical solution temperature
UHMWPE	Ultra-high molecular weight polyethylene
VT	Variable temperature

VYHH	Poly(vinyl chloride-co-vinyl acetate)
WAXD	Wide angle x-ray diffraction
wt%	Weight percentage
XRD	X-ray diffraction

List of Symbols

Å	Angstrom
A	Area
β	X-ray half-width at maximum intensity
°C	Celsius
cm^{-1}	Reciprocal centimetres
δ	Keith-Padden length term
Đ	Dispersity index
d	Interplanar distance
D	Diffusion coefficient
ε	Strain
E	Young's modulus
ϕ	Blend volume fraction
F	Force
g	Growth rate
G	Radial growth rate
g/mol	Gram per mole
J/g	Joules per gram
χ	Cooling rate
h	Thickness
H	Crystallisation peak half-width
ΔH_m	Change in enthalpy of mixing
I_a	X-ray scattering intensity (semi-crystalline)
I_a^0	X-ray scattering intensity (fully amorphous)
Hz	Hertz
j	Number of blend components
κ	Strain-optic coefficient
K	Crystallisation rate constant
K*	Cooling crystallisation function
kN	kilo Newton
kPa	kilo Pascal
kV	kilo Volt
λ	Wavelength
ℓ	Number of nuclei formed sporadically
L	Number of nuclei formed instantaneously
L_g	Gauge length
MPa	Mega pascal
mV	milli Volt
n	Avrami index
N	Fringe order
n_d	Dimensional dependent nucleation
N_i	Number of interfaces
nm	Nanometer
n_n	Time dependent nucleation
N_n	Nucleation sites per centimetre
Ψ	Flory-Huggins interaction parameter
P	Cooling function
ppm	Parts per million
ρ_a	Fully amorphous density
ρ_c	Fully crystalline density
R	Universal gas constant

σ	Stress
ΔS_m	Change in entropy of mixing
S_n	Niche separation distance
t	Time
T	Temperature
$t_{0.5}$	Crystallisation half-time
$T_{1\rho}$	Spin-lattice relaxation time in the rotating frame
T_2	Spin-spin relaxation time
ΔT_c	Degree of undercooling
ΔT_c^0	Theoretical undercooling at zero cooling rate
ν	Poisson's ratio
W_c	Weight fraction of crystalline material
W/g	Watt per gram
X	Volume fraction of crystalline material
Y	Mole fraction of methylene carbons
Z	Kinetic crystallinity

Chapter 1: General introduction and aims

1.1 Introduction

Modern commercial films consist mainly of a blend of linear low density polyethylene (LLDPE) and low density polyethylene (LDPE).[1] The blending of these two polymers allows for the properties of the final material to be expanded to cover a broader range. Blending, in general, allows specific properties to be targeted such as enhanced impact resistance or decreased flammability. Blending also has economic advantages in that particular polymer properties can be obtained without the extensive amount of time and cost associated with the development of a new polymer system with the desired properties. Through blending it is possible to increase the ease of processing of polymers with high viscosities or processing temperatures.[2] High performance polymers can also exhibit an enhanced lifetime and be made more affordable by blending with other inexpensive polymers. These desirable properties are highly dependent on the blend morphology. The phase behaviour associated with the blend morphology can either result in compatibility or phase separation and, in special cases, co-crystallisation.

As of 2015 the consumption of LDPE and LLDPE reached 300 000 tons in South Africa.[3] Despite these polymers having the highest consumption among polymeric materials in South Africa, the blending process through which these products are produced is not sufficiently understood. Films blown from the blends of LDPE with LLDPE can display both phase separation and co-crystallisation, depending on the blending conditions and the type of blending process. Although phase separation is quite common since many polymers are insoluble in each other due to their long chain nature[4], co-crystallisation is very rare due to the highly specific conditions required for it to occur.[5] The circumstances which lead to both of these states is currently not understood for the LDPE/LLDPE system and thus is the main purpose of this research.

1.2 Aims

This study aims to develop an understanding of the crystallisation behaviour of blends of LDPE with LLDPE. This overarching theme can be separated into the following components:

- Understanding the crystallisation of LDPE/LLDPE blends in terms of kinetics
- To clarify why co-crystallisation occurs in these blends
- Discover the effect which co-crystallisation has on the manner in which stored elastic energy is dissipated within these blends, leading to an understanding of the mechanical properties of the final material

1.3 Objectives

The proposed aims can be achieved through the following objectives:

- Modelling the kinetic parameters under isothermal and non-isothermal conditions
- Identification of the key component which acts as the compatibilising phase between the two homopolymers leading to the fulfilment of the criteria for co-crystallisation
- Comparison of stress-strain behaviour to established models for failure of polymers

1.4 Outline

1.4.1 Chapter 2

Chapter two provides a theoretical background for the concepts upon which this research is based. It offers a brief introduction to the polymers used as well as the techniques employed in this study.

1.4.2 Chapter 3

Chapter three introduces the specifications of the materials used in this work. It also details the experimental procedures followed in order to obtain the results.

1.4.3 Chapter 4

Chapter four provides a detailed description of the neat polymers used for blending. A full characterisation of the materials in bulk as well as fractionated is discussed.

1.4.4 Chapter 5

Chapter five lists the results obtained for solution blended samples as well as analysis of these results.

1.4.5 Chapter 6

Chapter six summarises the conclusions of the previous chapters, combining them for a detailed view of the LDPE/LLDPE blend system.

References

1. Ajji, A., Sammut, P. & Huneault, M. A. Elongational rheology of LLDPE / LDPE blends. *J. Appl. Polym. Sci.* **88,** 3070–3077 (2003).

2. Utracki, L. A. Introduction to polymer blends. *Polym. blends Handb.* **1,** 1–122 (2003).

3. Plastic industry facts. *Plastics South Africa* Available at: http://www.plasticsinfo.co.za/industry-news/. (Accessed: 21st September 2017)

4. Huggins, M. L. Some properties of solutions of long-chain compounds. *J. Phys. Chem.* **46,** 151–158 (1942).

5. Paul, D. R. & Bucknall, C. B. *Polymer blends: formulation and performance*. (Wiley, 2000).

Chapter 2: Theoretical background

2.1 Polyethylene

2.1.1 Structure and Crystallography

Polyethylenes are some of the most extensively used polymers globally due to its light weight nature, low production costs and insulating properties.[1] Its chain structure, the most basic of which contains no pendant groups as shown in Figure 2.1, leads to a highly flexible polymer with a high rate of crystallisation.[1]

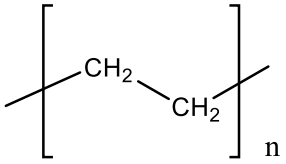

Figure 2. 1: Repeat unit structure of polyethylene

Polymerisation of ethylene monomer via a repeated insertion reaction yields the polyethylene polymer. Depending on the polymerisation conditions and catalyst or initiator used the amount and distribution of chain branching varies leading to the specific properties of the different forms of polyethylene. The degree of polymerisation varies greatly, from 100 to 250 000 or more units.[2]

The small size of the repeat units as well as the regularity of the chain structure allows for the formation of crystalline structures. The greater the degree of crystallinity the greater the density of the polyethylene. Due to the long chain nature of polymers and the folding mechanism which facilitates crystallisation, polymers never obtain full crystallinity.[3] The driving force for this crystallisation is the relaxation of the polymer melt[4], which is not thermodynamically stable at a temperature below the equilibrium melting temperature, which is referred to as the undercooling.

The most stable polyethylene unit cell can be classified as orthorhombic. These unit cells pack into a lamellar structure[5,6], which is the structure most commonly observed for polyethylene bulk crystals. Figure 2 shows a representation of the orthorhombic unit cell which incorporates two ethylene monomers per unit cell, one unit from a single chain and segments of ethylene units from adjacent chains.[2,3] The variation in branching content, which results in the different varieties of polyethylene, will result in differing unit cell dimensions. A hexagonal crystal structure has been observed at high temperatures and pressures, however, these conditions are not common to industrial processes.[7] At pressures near or above 5 000 bar the crystal structure which is thermodynamically stable is the extended chain crystal which is a rod-like structure.[3]

In order to form these unit cell structures polymer chains fold back on themselves along the (110) plane.[3] Crystallisation from the melt, or at high concentrations, yields many-layered, sphere-shaped dendritic structures known as spherulites which have a specific pattern resembling a Maltese cross.[3] The initial structure formed upon cooling from the melt is the single crystal, described above, which then grow into two dimensional clusters called axialites.[3] Axialites progressively fan outwards forming spherulites. The spherical morphology is maintained until the end of primary crystallisation, where after the spherulites extend into neighbouring spherulites, forming either straight or hyperbolic boundaries depending on whether nucleation was simultaneous or sporadic.[3] It is thus clear that the conditions have an effect on the crystal structure and morphology of polyethylene.

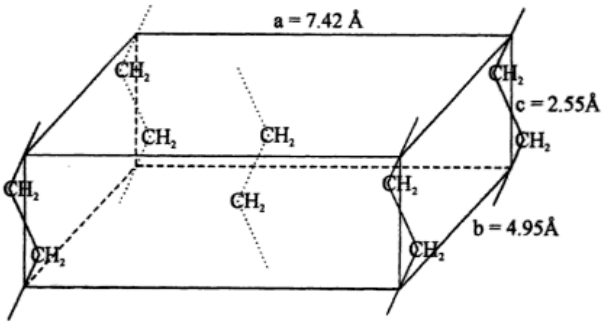

Figure 2. 2: Orthorhombic unit cell of polyethylene [2]

2.1.2 Crystallisation Kinetics

2.1.2.1 Isothermal kinetics

Under isothermal conditions the kinetics of polyethylene crystallisation can be described by the Avrami equation given by Equation 2.1, where *X (t,T)* represents the volume fraction of the crystalline polymer at a time *t* and a temperature *T* which is constant. K is a temperature dependent rate constant providing a sense of the rate of crystal nucleation while *n* is known as the Avrami exponent which qualitatively describes nucleation and crystal growth processes.[8]

$$X(t,T) = 1 - e^{-K(T)t^{n(T)}} \qquad (2.1)$$

The Avrami equation is usually effective during the initial crystallisation stages, or until the end of primary crystallisation, before spherulites begin to impinge upon each other's boundaries.[3,9] The values of K and *n* are indicative of the crystallisation mechanism. The Avrami index has been described as the sum of two terms n_d and n_n.[9] The n_d relates to the dimensional growth of the crystal, where values of 1, 2 and 3 describe one dimensional, two dimensional and three dimensional growth respectively. The n_n term describes the time dependence of crystal growth. Theoretically n_n is limited to values of either 0, indicating instantaneous nucleation, or 1, indicating periodic nucleation.[9] Values of 0.5 have been reported and explained as the result of a diffusion controlled nucleation process.[9,10,11] The Avrami index for the case of polyethylenes ranges from 2.6 – 4.0.[12] Sperling has tabulated the constants representing the Avrami parameters for various crystallisation mechanisms.[3] The most relevant of these are summarised in Table 2.1 where g indicates a constant growth rate and the term L represents the number of nuclei formed under instantaneous crystallisation conditions while l denotes the number of nuclei under sporadic crystallisation conditions.[3] The value of K was derived using a constant disc thickness *h* for the disc structure and a constant radius *d* for the rod structure.[3]

Values for K and *n* are conventionally determined through taking the double logarithm of Equation 2.1 to yield a linear plot according to Equation 2.2.[8] K and *n* can thus be determined from the intercept and slope of the line respectively.

$$\ln[-\ln(1 - X(t))] = \ln K + n \ln t \qquad (2.2)$$

Although useful, this method has been criticised due to the inherent low accuracy of a double logarithm plot. López and Wilkes addressed this issue in 1988 by proposing the use of a crystallisation half time, $t_{0.5}$, which is defined as the time taken to reach 50 %

of the maximum obtainable crystallinity.[8] The logarithm of Equation 2.1 at $t_{0.5}$ then gives the value of K, shown in Equation 2.3.

$$K = \frac{\ln 2}{{t_{0.5}}^n} \tag{2.3}$$

Table 2. 1: Selected Avrami parameters for crystallisation of polymers

Structure	Mechanism	Avrami constants		Dimensions
		K	*n*	
Spheres	Sporadic	$\frac{2}{3}\pi g^3 l$	4.0	3
	Simultaneous	$\frac{4}{3}\pi g^3 L$	3.0	3
Discs	Sporadic	$\frac{\pi}{3}\pi g^2 ld$	3.0	2
	Simultaneous	$\pi g^3 Ld$	2.0	2
Rods	Sporadic	$\frac{1}{2}\pi gld^2$	2.0	1
	Simultaneous	$\frac{1}{2}\pi gLd^2$	1.0	1

After integration and a series of substitutions, the Avrami exponent is then given by Equation 2.4.

$$-t_{0.5} K n t_{0.5}^{n-1} e^{-K t_{0.5}^n} = \frac{n \ln 2}{2} \tag{2.4}$$

López and Wilkes, however, observed an excellent agreement between the results obtained using crystallisation half time and the original Avrami double logarithm, implying that the double logarithm method is not inaccurate or, at least, that both methods are equally inaccurate.[8]

The model proposed by Keith and Padden provides insight into the crystal structure during crystallisation. They introduced a length term, δ, which is defined in Equation 2.5 as the ratio between the diffusion coefficient for melt impurities and the radial growth rate of a crystal spherulite.[3,13]

$$\delta = \frac{D}{G} \tag{2.5}$$

Through logarithmic differentiation of Equation 2.5, Equation 2.6 can be obtained where a positive value for the sum $\frac{1}{D}\left(\frac{dD}{dT}\right) - \frac{1}{G}\left(\frac{dG}{dT}\right)$ indicates that an increase in spherulites roughness with temperature can be expected.[3,14]

$$\frac{1}{\delta}\left(\frac{d\delta}{dT}\right) = \frac{1}{D}\left(\frac{dD}{dT}\right) - \frac{1}{G}\left(\frac{dG}{dT}\right) \tag{2.6}$$

The Keith-Padden theory implies that low temperature crystallisation is dominated by diffusion while at high temperatures the nucleation rate is the more important factor.[3]

The nucleation kinetics theory proposed by Hoffman defines three crystallisation regimes. In each regime the kinetics vary according to the rate at which polymer chains are placed on the crystallisation front. A surface nucleus is defined as a polymer chain fragment positioned on an already existing lamellar surface.[3] In Regime I the chains crystallise individually, or the entire layer crystallises onto a single surface nucleus.[3] The rate at which the surface nuclei sporadically crystallise onto the layer

below is dependent on the temperature.[15] The length of the chain which exists between folds is defined as a stem.

Regime II is characterised by the presence of multiple surface nuclei on the crystallisation subtstrate.[3] The transition to Regime II usually requires a greater undercooling than for Regime I, which for polyethylene has been reported as approximately 16 °C difference in temperature.[15] Crystal growth rates in Regime II have a quadratic dependence on the rate of surface nucleus deposition.[15] The assumption for both Regime I and Regime II is that chains fold in order to facilitate re-entry into the crystal structure adjacent to the exit point. An important parameter is the niche separation distance, S_n, defined in Equation 2.7 where N_n represent the amount of nucleation sites per centimetre.[3]

$$S_n = {}^{1}/_{N_n} \tag{2.7}$$

Regime III is achieved when the niche separation distance approaches the length of a stem.[15] Crystallisation in Regime III occurs very rapidly and chains do not often undergo adjacent re-entry.[3] Transitions from Regimes I – III occur with decreasing temperature and are accompanied by a decrease in the rate of successful completion of a crystal surface.[3] Increases in growth rate at the Regime II – III transition have been observed by some researchers.[15] The growth rate in Regime III is determined by the rate at which nuclei are deposited onto the crystallisation substrate in a linear fashion.[15] Due to the close proximity of niches in Regime III chains are most likely to re-enter the crystal lamella in a switchboard manner and not according to adjacent re-entry.[15] For branched polyethylenes the chain motion occurs sufficiently rapidly so that portions of branches may be accommodated into the chain structure, however this applies only to Regimes I and II.[15] During the initial stages of Regime III this may still occur until the temperature becomes too low for the incorporation of branch segments to occur.

2.1.2.2 Non-isothermal kinetics

Although the isothermal kinetic studies have provided better understanding of crystallisation kinetics, industrial processes are rarely conducted under isothermal conditions. The kinetics of polymer crystallisation under non-isothermal conditions are substantially more complex as the kinetics include the addition of the time-dependent temperature as another variable. In addition, instrumental temperature delays between the instrument and the sample as well as temperature gradients within the samples cannot be ignored as with isothermal crystallisation.[16]

Methods for the treatment of non-isothermal crystallisation kinetics are mostly derived from the Avrami theory. The first theory, put forward by Ziabicki, suggested that non-isothermal kinetics can be treated as a series of isothermal stages.[16] The theory expresses the crystalline volume at a specific time as an expansion series of the Avrami equation using the crystallisation half time.[16] The Ziabicki theory, however, is only valid for a limited temperature range; the range for which isothermal crystallisation values can be obtained.[16] A different method was suggested by the group of Nakamura which derived a variation of the Avrami equation, shown in Equation 2.8, where *n* is the Avrami index and *K'* is associated with the Avrami rate constant K through Equation 2.9.[16] This method was found to be in good agreement with experimental changes in crystallinity in HDPE samples as detected by X-ray scattering measurements.

$$X(t) = 1 - e^{-\left(\int_0^t K'(T)dt\right)^n} \quad (2.8)$$

$$K' = K^{1/n} \quad (2.9)$$

The Nakamura model does not account for the influence of the induction time on the crystallisation kinetics. Jeziorny attempted to describe the kinetic crystallinity, Z, through Equation 2.10, a modification of the Avrami theory, where K_{max} is the value of the rate constant for the highest rate of crystallisation and *H* is the half-width of the crystallisation peak.[16]

$$Z = \left(\frac{\pi}{\ln 2}\right) K_{max} \frac{H}{2} \quad (2.10)$$

One of the simpler methods is that proposed by Nadkarni *et al*. which relates empirical values to a linear kinetic plot of the form shown in Equation 2.11 where ΔT_c is the degree of undercooling, χ is the cooling rate, ΔT_c^0 is the theoretical undercooling at a cooling rate of zero and P is a kinetic factor which is dependent on the crystallisation process.[17]

$$\Delta T_c = P\chi + \Delta T_c^0 \quad (2.11)$$

The Ozawa equation, shown in Equation 2.12,[18,19] is perhaps the most well-known method for the analysis of non-isothermal crystallisation.

$$\ln\left(1 - \frac{x_T}{x_\infty}\right) = \frac{K^*(T)}{\chi^n} \quad (2.12)$$

The ratio $\frac{x_T}{x_\infty}$ represents the fraction of crystalline material at a specific temperature *T* relative to the fraction of crystalline material upon completion of crystallisation, while χ^n is the cooling rate with *n* describing the nucleation process as the *n* in the Avrami equation in Equation 2.1.[20] The Ozawa approach was demonstrated to be ineffective in describing the crystallisation of high density polyethylene (HDPE) under non-isothermal conditions due to factors which the equation does not account for. First, the Ozawa theory does not consider secondary crystallisation which results in a continual improvement of crystal order which occurs at a lesser rate compared to the initial crystal formation.[19] Second, the thickness of the crystal lamellae has some dependence on the crystallisation temperature as does the Avrami exponent, *n*.[19] The Ozawa model has not yet been applied to the crystallisation of branched polyethylenes but has been demonstrated to be effective in describing the crystallisation of polypropylene.[19]

Supaphol et al. investigated the effect of molar mass on non-isothermal kinetics of HDPE of molar mass 77 000 and 101 000 g/mol.[21] They found an increase in crystallisation rate for the lower molar mass polymer due to its higher mobility in solution. They theorised that low molar mass chains experienced less difficulty disentangling from the melt, resulting in faster crystallisation. This theory was corroborated by the work of Minkova et al. who analysed HDPE and UHMWPE and found a similar trend.[22] When these polymers were blended the parent polymers crystallised independently the rates of crystallisation were greater than the crystallisation rates of the homopolymers as well as the additive rate between the two polymers.[22] Minkova et al. proposed that the built in stress in the UHMWPE and the entanglements between the chains of both components resulted in an increase in the

crystallisation rate of HDPE, while possible co-crystallisation events in the blend caused an increase in the rate of UHMWPE crystallisation.

The study conducted by Gupta et al. on the non-isothermal kinetics of blends of HDPE with LLDPE revealed co-crystallisation of these components.[23] The Avrami indices were determined as 2.9 and 1.7 for HDPE and LLDPE respectively, while the Avrami indices for the blends varied with blend composition as a result of the variation in nucleation due to co-crystallisation.[23] The method of Jeziorny (Equation 2.10) has been applied to blends of LDPE with bimodal MDPE with good agreement. The same system was tested using the Ozawa theory however the Ozawa equation could only describe discrete aspects of the crystallisation and not the total process.[24] Xu et al. conducted non-isothermal crystallisation experiments on blends of LDPE with copolymers of ethylene and 1-butene and found that the crystallisation rate showed a dependence on the distribution of short chain branching in the copolymers.[25] The kinetic crystallisation rate, Z, was found to decrease as the short chain branching distribution broadened while the overall crystallisation rate increased upon blending with LDPE as result of the association of the highly branched fractions with the LDPE.[25]

2.2 Low density polyethylene

Low density polyethylenes (LDPEs) contain a large number of short and long chain branches, effectively hindering the crystallisation process and the formation of a closely packed or dense structure.[2] Short chain branches are formed through backbiting reactions where a chain radical abstracts a proton from the main polymer chain, typically through a six-membered transition state.[2] This leads to branches of four monomer units in length. Densities are typically restricted to the range 0.90 – 0.94 g/cm^3.[2] LDPEs are produced by free radical polymerisation. The polymerisation is conducted at high pressure in order to ensure that the reagents are homogeneously distributed.[26] The high pressures often result in a higher density of ethyl or butyl groups in one region between extended linear regions while the long chain branches are randomly distributed.[2] A peroxide initiator is commonly used, leading to a highly branched polymer structure. It is also likely that the branches are themselves branched. By controlling the temperature and pressure of the reaction mixture the molar mass of the resulting polymer as well as the density can be affected. The free radical process has little to no control over the position of the radical leading to a random branching distribution.

LDPEs find use where low cost, moisture resistance or flexibility at low temperatures are of importance. They are commonly used for film packaging due to their flexible nature. They also find use as insulators for electrical cables as well as in injection moulded objects.

2.3 Linear low density polyethylene

Linear low density polyethylene (LLDPE) consists of a linear polyethylene main chain with short chain branches distributed randomly throughout the chain. LLDPEs are produced by the copolymerisation of ethylene with other α-olefins by either gas phase or slurry polymerisation at low pressures. The LLDPE used in this study is produced commercially using a supported Ziegler-Natta catalyst system. LLDPEs can be produced by metallocene catalysts leading to more regular co-monomer distributions than that obtained with Ziegler-Natta catalysts. The tendency of Ziegler-Natta catalysts to produce polymer systems with broader molar mass distributions has advantages;

these polymers are more easily processed resulting in faster outputs.[1] LLDPEs are used in film applications where a higher tensile strength is required than that which LDPE can offer for a lower film thickness. LLDPE is common to the food packaging industry which requires films of lower permeability resulting in a longer shelf-life of the packaged product.

2.4 LDPE/LLDPE blends

2.4.1 Definitions

A polymer blend is described as a mixture of a minimum of 2 % by weight of two or more polymers or copolymers.[27] Miscible blends are defined by the size of their domains which should be of the same order of dimension as a statistical length segment.[27] Miscibility can also be assumed from a negative value for the free energy of mixing of the blend. Immiscible blends do not meet these criteria but can be compatibilised to form a polymer alloy.[27]

2.4.2 Thermodynamics of polymer blends

Thermodynamic theories of polymer blends developed from the theories of polymer solutions, assuming that a polymer blend can be treated as a solution of one polymer in another polymer. Early methods treat a polymer solution as a type of lattice structure. The most widely used approach is that of Flory and Huggins. The theory is based on Raoult's Law in which the entropy of mixing, ΔS_{m}, is described by Equation 2.13.[28] Polymers have shown to deviate significantly from Raoult's Law.[28]

$$\Delta S_{\mathrm{m}} = R \ln \frac{(N_A+N_B)!}{N_A!N_B!} \tag{2.13}$$

Polymer molecules were described as consisting of sub molecules which each occupy a lattice site and the number of ways of arranging the lattice can then be calculated. The lattice method quantitatively describes the activities of solution components which allows the derivation of Equation 2.14, as was done by Huggins.[28] In Equation 2.14 m is the chain length, N_A^* the volume fraction of solute in the solution and B is a correction factor.

$$Bm \approx -\ln N_A^* - (m-1)N_A^* + m - 1 \tag{2.14}$$

The relationship between N_A^*, which can be related to the solubility of A, and n indicates that the solubility tends towards 1 – *B* (for values of *B* less than one) or zero (for values of *B* greater than one).[28] This implies that long chain molecules are inherently poorly soluble.

The low solubility of polymers often leads to phase separation in blends. The formation of phases is controlled by the Gibbs free energy of mixing.[29] Dissolution of one polymer in another occurs when the free energy of mixing is less than zero. In terms of the Flory-Huggins lattice theory dissolution occurs first by the conversion of the solid lattice to a solution with an increased degree of disorder followed by the mixing of the chains with molecules of solvent.[30] Polymer molecules are much larger than solvent molecules and the number of configurations which the chain can assume is less than that of the solvent molecules due to the covalent bonds between repeat units. This leads to deviation from ideal solution behaviour for polymer blends. For small molecules the entropy of the solution increases upon dissolution, however, polymers have a negligible contribution of entropy to the mixing process.[31] Miscibility is thus dependent on the enthalpy of mixing, described by Equation 2.15, where ΔH_m is the molar enthalpy of mixing, R is the gas constant, T is the temperature, Ψ is the Flory-

Huggins interaction parameter and ϕ represents the volume fractions of the blend components.[31]

$$\Delta H_m = RT\Psi\phi_1\phi_2 \quad (2.15)$$

A negative value for the Flory-Huggins interaction parameter results in a negative value for the enthalpy of mixing, resulting in a negative free energy of mixing and implying miscibility. The Gibbs free energy of mixing can then be described by Equation 2.16 where *DP* denotes the degree of polymerisation of the blend components.[31] The free energy of mixing can therefore be affected by the molar mass, the volume fraction of each component as well as the temperature.

$$\Delta G_m = RT\left[\Psi\phi_1\phi_2 + \frac{\phi_1}{DP_1 \ln \phi_1} + \frac{\phi_2}{DP_2 \ln \phi_2}\right] \quad (2.16)$$

Phase separation can also be thermally induced, which was not explained by the Flory-Huggins theory.[31,32] Two temperature values are of importance. First, the lower critical solution temperature (LCST) where phase separation is driven by an unfavourable value for entropy of mixing.[32] Second, at the upper critical solution temperature (UCST) phase separation is induced by unfavourable values for the energy of mixing.[32] Phase diagrams of polymer blends can therefore be constructed with these temperatures being the limits of temperature dependent miscibility. Polyolefin blends often display UCST type phase diagrams with a few cases having LCST behaviour or a combination of both.[32]

The homogeneity of the blend also plays a role in the lifetime of the polymer product. This is most important for blends containing more than two components as the number of interfaces (which are possible causes of fractures) increases according to Equation 2.17, where *j* is the number of blend components.[27]

$$N_i = \frac{j(j-1)}{2} \quad (2.17)$$

2.4.3 Blending methods

Blending involves the mixing of two or more polymers after the polymerisation process. From the thermodynamics it can be concluded that most polymer blends are immiscible on the basis of the low entropy change upon mixing. The blending method employed may affect the compatibility of the blend components. Before determining the miscibility of the blend the blending process is key in ensuring that equilibrium conditions were reached.[33]

Solution blending requires the dissolution of the polymers in a solvent. Depending on the polymer this may be done at room temperature or at elevated temperatures for semi-crystalline polymers which require the melting of the crystalline regions before dissolution. In order to isolate the blended polymer, the solvent needs to be separated from the mixture. Solution methods have shown to either enhance or worsen miscibility depending on the affinity of the polymer system to the solvent used.[33]

Polyolefins can be blended in the melt phase upon completion of the polymerisation process, preventing the use of large amounts of solvent, as in the solution blending process.[32] Melt blending of polyolefins is often less costly.[34] Melt blending works particularly well for polyolefins due to the high elasticity in the melt as well as high

melt strength.[35] The disadvantage of melt blending is the difficulty in obtaining a blend where the components are homogeneously distributed as well as the longer blending times required.[34] Das et al. tested a number of blending methods and observed that poly(vinyl chloride-co-vinyl acetate) (VYHH) blends with polystyrene (PS), poly(methyl methacrylate) (PMMA) and poly(styrene-co-acrylonitrile) (SAN) were all immiscible when melt-mixed despite PMMA/VYHH and SAN/VYHH being miscible when blended in solution.[33]

In-reactor blending originated in 1979 with the blending of polyethylene, polypropylene and ethylene-propylene rubber for impact modification of polypropylene.[27] The method involves blending of materials during the polymerisation, allowing the use of the polymerisation catalyst to aid the blending. Reactor blending may make use of multiple reactors with differing reaction conditions in every reactor or a single reactor containing multiple catalysts.[36] LLDPE is often blended with other polyolefins by this method, incorporating species of varying ethylene contents into the blends.[32]

2.4.4 Blends of semi-crystalline polymers

Most commercial polymers are semi-crystalline and therefore it is not uncommon to find a blend of which at least one component is semi-crystalline. For miscible blends the temperature range over which crystallisation of one component can occur may be increased or decreased relative to the neat semi-crystalline polymer depending on the glass transition temperature (T_g) and concentration of the second polymer.[32] This implies that the melting temperature (T_m) is also dependent upon the concentration of each component within the blend and will tend to decrease as the concentration of the second component increases, where the second component is amorphous.

An interesting phenomenon which may occur in blends where two or more components are semi-crystalline is co-crystallisation. Co-crystallisation is defined as the crystallisation of two semi-crystalline polymers into the same crystal lamella.[32] The criteria for co-crystallisation to occur is miscibility or partial miscibility in the melt, similarity in chemical structure as well as similarity in crystal structure or unit cell parameters.[32] Due to these stringent criteria co-crystallisation is not often observed. The crystallisation kinetics also affect the possibility of co-crystallisation, with a high cooling rate promoting co-crystallisation in blends which meet the above criteria.[32,37,38] The similarity in crystallisation rate also appears to be an important factor in promoting co-crystallisation of blends.[38,25] Since the total rate of crystallisation depends on the growth rate of the crystal spherulites as well as the rate of primary crystal nucleation, immiscible blends can experience a decrease in the crystal growth rate, and thus the overall crystallisation rate, through the formation of growth barriers as a result of rejection or deformation of the second blend component.[32] The presence of homopolymer in blends containing copolymers tends to influence the crystallisation of the blend by nucleating the formation of crystal structures increasing the overall crystallisation rate.[32] It has also been observed that for the specific case of LDPE/butene-LLDPE blends the composition distribution of the LLDPE significantly affected the occurrence of co-crystallisation.[39] Ziegler-Natta LLDPE possesses a broader chemical composition distribution than metallocene-LLDPE, leading to the segregation of the co-crystals from the LDPE and LLDPE crystals and the formation of three separate crystalline environments.[39,40]

One may expect that due to the similarity in chemical structure of polyolefin blends, especially polyethylene blends, they would display miscibility. In reality, as

polyethylenes contain only saturated hydrocarbon moieties, the lack of functional groups leads to the absence of any strong intermolecular forces indicating low miscibility.[32]

2.4.5 Performance of LDPE/LLDPE blends

The basic strategy for obtaining a specific property through blending is to combine components which display the desired characteristics.[27] Blends of polyolefins display properties which are rarely intermediate to those of the parent polymers. For many polyolefin blends the properties vary with composition in a non-linear fashion.[35] The properties of the parent polymers are not the only determining factors for the blend properties as the morphology of the resultant blend also determines the final properties. For polyethylene blends the properties are a compromise between ease of processing and mechanical properties depending on the specific application.

The successful blending of polyolefins in the molten state is determined by the rheology of the polymers which have viscosity that is dependent on stress and shear rate.[35] LLDPE films provide a higher strength than that of LDPE films, however LLDPE is often difficult to process due to its high melt viscosity.[41] For this reason LLDPE is blended with small quantities of LDPE to improve its rheology. Due to the direct impact of rheology on processing behaviour this topic has been investigated extensively with regard to LDPE/LLDPE blends.[41,42,43,44,45] The rheological studies revealed that the molar mass of the LLDPE component affected the miscibility of the blend, with increasing molar mass decreasing the blend miscibility.[42] The catalyst used during the polymerisation of LLDPE was also significant as Ziegler-Natta LLDPE was found to be more miscible with LDPE when compared with metallocene-LLDPE.[46] As immiscibility may lead to an increase in viscosity[46] it is of industrial importance that the blend should be miscible in order to achieve the intended purpose of blending.

A concept that is also of importance in blending of materials is the strength of the interface that exists between the components. In most cases the strength of polymers arises from the entanglements between chains or chemical crosslinks leading to small scale, non-planar, interfaces.[32] Before the formation of a crack in a polymeric material the stored elastic energy is dissipated through distortion in the region of the crack which is induced by the stress concentrations on the polymer chains in the vicinity of the crack.[32] Where the blend components are immiscible the interfacial region has significantly smaller dimensions than the distance between chain entanglements meaning that entanglements spanning the interfacial region are few.[32] For this reason polymer interfaces have low toughness unless the miscibility of the polymers are high. The conventional method for strengthening polymer interfaces involves the formation of a copolymer which will associate with both blend components and create sufficient chain entanglements on both sides of the interface. Copolymers also aid in the homogeneous mixing of the two components by decreasing the surface tension at the interface and preventing the formation of polymer domains.[32] Reactor blending allows the *in situ* formation of copolymers by reacting with both blend components.[32] Although the kinetics of *in situ* copolymerisation for interfacial toughening is not well understood it is known that these kinetics as well as the topology of the copolymer chain affects the ability of the copolymer to strengthen the interface.[32] Copolymer chains of low molar mass which cannot form a strong polymer on their own may have difficulty forming sufficient chain entanglements with the original homopolymer, preventing strengthening by co-crystallisation.[32] Oyama investigated this effect on reactor blends of poly(lactic acid)

(PLA) with poly(ethylene – glycidyl methacrylate) with a di-block copolymer of both components, finding that above the entanglement molar mass of the PLA block (approximately 9 000 g/mol) the PLA fragment becomes included within the PLA homopolymer crystalline structure through co-crystallisation leading to enhanced adhesion at the interface.[47]

Mechanical properties of blends can be most easily understood by conducting tensile tests. The method involves the extension of the polymer sample of a cross-sectional area *A* at constant velocity while the distance L_g between the gauges is measured while the load cell applies a force *F.* The tensile properties can then be inferred from a plot of stress (Equation 2.18) as a function of strain (Equation 2.19).[32]

$$\sigma = F/A \tag{2.18}$$

$$\varepsilon = \Delta L_g / L_{g0} \tag{2.19}$$

The tensile strength is then defined as the maximum amount of stress the sample can sustain during the test while the tensile strength at break is the stress on the sample upon rupture.[48] At the yield point the strain increases without a corresponding increase in the stress upon the sample.[48] Semi-crystalline polymers often undergo a localised yielding referred to as necking as well as cold drawing. The neck frequently originates at both ends of the sample and extends towards the centre resulting in strain hardening of the material in the neck.[32]

The tensile properties of reactor blends of LDPE/octene-LLDPE displayed a decrease in tensile stress at yield and at break as determined by Li et al., however this behaviour changed when the molar mass of the LLDPE component was decreased.[49] Tensile tests conducted on LLDPE independently have shown a broad yield region which is sometimes referred to as a double yield point due to, first temporary deformation and partial recrystallisation followed by permanent deformation involving the tearing apart of the crystal structures.[50] Yamaguchi et al. determined that the hardness of the polymer blend depends on the relative percentage of the more crystalline component.[44] Tensile tests conducted by Yamaguchi showed an increase in yield stress with increasing percentages of the more crystalline component which, in their case, was LPDE.[44]

2.5 Fractionation of polyethylenes

2.5.1 Temperature Rising Elution Fractionation

TREF is a fractionation technique which allows separation by crystallisability or molecular structure, as this affects crystallinity. The degree of crystallisability yields information about the microstructure of a semi-crystalline polymer system. TREF is commonly used with polyolefins in order to determine the distribution of crystallisable segments.[51]

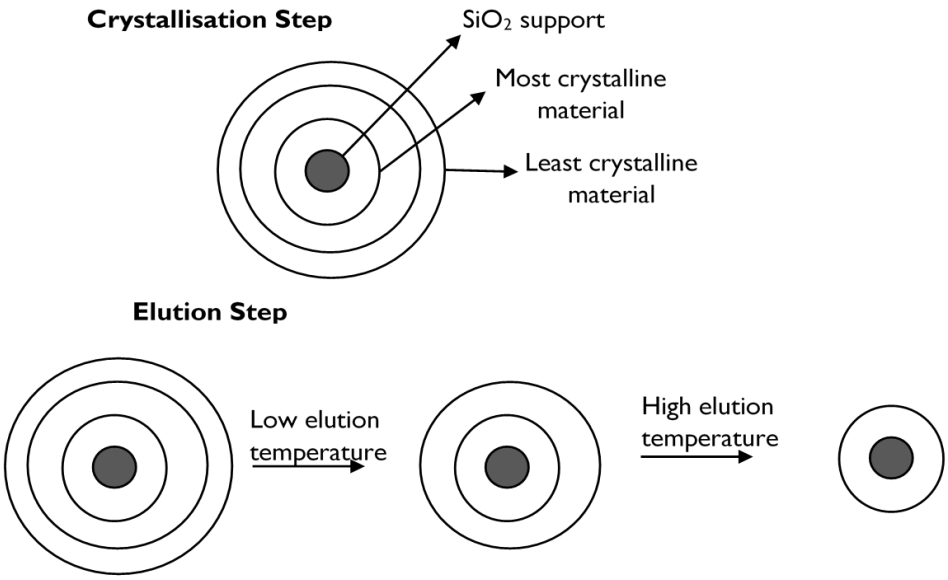

Figure 2. 3 Diagram illustrating TREF temperature cycles[52]

Two temperature cycles occur; during the first cycle fractionation occurs by crystallisation of the components from the most crystalline to the least crystalline onto the column stationary phase as the temperature is slowly decreased while during the second cycle the temperature is increased and melting occurs from the stationary phase particles in the reverse order in which crystallisation occurred. As the fractions melt they enter the mobile phase and are eluted from the column. The stationary phase needs to be an inert solid particle such as silica, with sea sand being the most commonly used support. This is demonstrated in Figure 2.3.Typically the polymer is dissolved in hot solvent before loading onto the column, therefore a high boiling solvent such as xylene is necessary. The slower the cooling rate the greater the resolution obtained.

TREF can be operated in the analytical mode or preparative mode. Analytical TREF involves a slow cooling process during which crystallisation occurs onto the support. After the heating process the polymer fractions are eluted and the solution concentrations are detected online by various detectors.[53] Preparative-TREF is used in this study in order to isolate the constituent fractions of the polyethylene for further offline analysis. Preparative TREF applies a stepwise heating profile and collection of the entire range of polymers eluting within that step interval takes place, with each fraction possessing a more limited compositional variation than the original polymer.[51]

2.6 Characterisation of polyethylenes

2.6.1 Differential Scanning Calorimetry

DSC measurements are representative of thermodynamic and kinetic events which take place in a sample upon heating. In a conventional heat flux DSC setup, the sample and a reference are placed in a furnace where the heating rate can be controlled. The difference in temperature of the sample relative to the reference is measured by thermocouples at the base of each container within the furnace.

Various events result in heat flow changes, these can be characterised as either first order or second order thermal transitions within the sample being analysed. First order thermal transitions are associated with a latent heat and result in peaks in the DSC curve. Second order thermal transitions have no latent heat associated with them and therefore only result in changes in the baseline of the DSC curve.

This study will focus on the melting and crystallisation events of each polyethylene, which can be seen using DSC. Isothermal and non-isothermal kinetics of polyethylene crystallisation will attempt to be determined using DSC. The volume of crystalline material present, which is a parameter in the Avrami equation, can be calculated from Equation 2.20.[9]

$$X = \frac{Wc}{Wc + \left(\rho_c / \rho_a\right)(1 - Wc)} \tag{2.20}$$

In Equation 2.20 ρ_c and $\rho_a$are the fully crystalline and amorphous densities respectively, *Wc* is the fraction of crystalline material by mass which can be determined with Equation 2.21. In Equation 2.21 ΔH_{total} is the total enthalpy attained for an isothermal experiment and $\Delta H(t)$ represents the change in enthalpy with the duration of time at s specified temperature.[9]

$$Wc = \frac{\Delta H(t)}{\Delta H_{\text{total}}} \tag{2.21}$$

Eder and Wlochowicz[19] analysed polyethylene and polypropylene under non-isothermal conditions using DSC. The degree of conversion from amorphous to crystalline material was obtained from the DSC thermograms and plotted as a function of the constant cooling rate according to Equation 2.12. As was mentioned in Section 2.1.2.2, the results for the polyethylene was found to not fit the Ozawa equation.[19] Jeziorny investigated the non-isothermal crystallisation of PET using DSC with the aim of calculating the crystallisation rate constant as well as the kinetic crystallisability.[54] The rate constant (K_c) was determined first through obtaining the isothermal rate constant (K) according to the conventional Avrami method, then second dividing the isothermal rate constant by the cooling rate (χ) as shown in Equation 2.22.[54]

$$\log K_c = \frac{\log K}{\chi} \tag{2.22}$$

The kinetic crystallisability (Z) was calculated according to Equation 2.10. The half-width (H) could be obtained directly from the DSC thermogram.

The number of melting endotherms observed with DSC should also indicate the number of crystalline environments within the blends. Should co-crystallisation occur this would immediately be observed by the presence of a single melting endotherm suggesting that both blend components form part of the same crystalline environment.[32]

Thermal fractionation of ethylene-α-olefin copolymers in the solid state was first reported by Müller et al[55] who then coined the term Successive Self-Nucleation and Annealing (SSA). SSA allows fractionation on a much shorter timescale than conventional solution fractionation techniques such as TREF. Xue et al. used SSA as a means of characterising short-chain branched polyethylenes by performing SSA on TREF fractions to determine the methylene sequence length.[56] As a peak obtained from an SSA experiment is indicative of methylene sequences of similar lengths, this

is a useful technique in characterising highly heterogeneous samples.[56] The method proposed by Zhang and Wanke[57] to calculate the methylene sequence length (MSL) using SSA fractionation can be applied to the polymers used in this work. By performing SSA on a series of linear hydrocarbons Zhang and Wanke established a calibration curve yielding Equation 2.23, where Y is the mole fraction of methylene carbons and *T* is the SSA peak temperature in Kelvin.[57]

$$\ln Y = 0.3451 - \frac{142.2}{T} \tag{2.23}$$

The value of X can then be inserted into Equation 2.24 to obtain the MSL.[57]

$$\mathrm{MSL} = \frac{2Y}{1-Y} \tag{2.24}$$

2.6.2 Nuclear Magnetic Resonance Spectroscopy

^{13}C nuclear magnetic resonance (NMR) signals have shown to be sensitive to microstructural changes. The variation in the chemical shifts occur due to changes in the average chain conformation in a specific area directly resulting from changes in the microstructure. In polyethylene this is predominantly due to the γ-gauche effect, depicted in Figure 2.4. The γ-gauche effect justifies the occurrence of the amorphous carbon signal in polyethylene approximately 2-3 ppm further upfield from the carbons in crystalline regions since the γ-gauche effect results in increased shielding in the amorphous regions.[58,59] No γ-gauche effect occurs in the crystalline regions as the chains assumes as all-trans zig-zag conformation.[58,59]

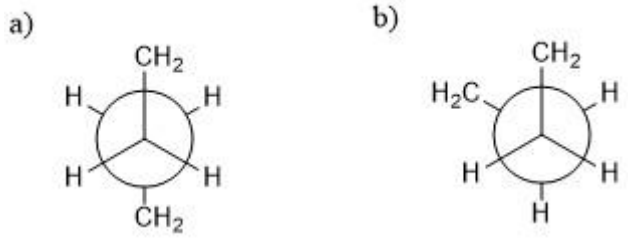

Figure 2. 4: Newman projections showing a) no γ-gauche effect and b) γ -gauche effect

In the solid state the properties pertinent to this state are commonly the polymer structure, morphology and chain mobility. In order to elucidate secondary structural characteristics solid state NMR can yield high resolution spectra using cross polarisation (CP) and rapid magic angle sample spinning (MAS) experiments. The purpose of CP is to enhance the sensitivity towards nuclei of low natural abundance while the MAS increases the resolution of the resonances produced from solid state experiments to similar resolution of solution experiments by removing the effects of chemical shift anisotropy and heteronuclear dipolar coupling.[60] MAS ^{13}C NMR spectroscopy therefore allows the study of molecular motion in the solid state at high resolution. ^{13}C CPMAS NMR spectra of large cycloalkanes indicates that slower reptation corresponds to chains in the crystalline regions while faster motion is associated with unbound chains in the amorphous areas.[61] The comparison between large cycloalkanes and polyethylene was drawn due to the tendency of large cycloalkanes to form lamellar crystals, similarly to polyethylenes.[61] During VT experiments it is also common for an increase in signal intensity to be observed as well as for line broadening to occur with increasing temperature, or as the temperature approaches that of a thermal transition until the resonances coalesce to a single signal.[59,61]

^{13}C CPMAS NMR spectra of polyethylene show a resonance at approximately 33.0 ppm due to the crystalline regions and another resonance at approximately 31.0 ppm due to the amorphous regions.[62,63,64] The resonance at 33.0 ppm due to the internal methylene units in the crystalline regions arises from the orthorhombic crystal structure, however the chemical shift remains largely constant for changes in crystal structure, excepting the triclinic structure which exhibits a resonance at approximately 34.9 ppm.[64] The chemical shift of the branching carbon occurs at approximately 38.2 ppm for branch lengths greater than three carbons.[65,66]

An interesting method of probing the mobility of polymers and their components in solid state NMR is the proton wideline experiment. The ^{1}H wideline experiment is a static solid state NMR experiment specifically performed for nuclei which result in broad signals due to dipolar interactions (such as protons) and can span hundreds of kHz.[67] The line width of the signal corresponds to the mobility of the molecules within the sample. Samples with high mobility display narrow line widths or conversely highly rigid samples display broader signals as a result of the strength of the dipolar interactions. Samples with greater mobility approach the random motion associated with the solvated state resulting in averaged dipolar interactions and narrow line widths.[68] It is also common, in the case of semi-crystalline polymers, for the wideline signal to be a combination of both the crystalline and amorphous domains, where the broad base would correspond to the rigid, crystalline domain and the more Lorentzian shaped signal emerging from the broad base represents the amorphous, mobile domains.

Relaxation times in solid state NMR can also provide an indication of sample mobility. Nuclear relaxation processes are due to fluctuations in nuclear spin interactions and these fluctuations can be attributed to molecular motions.[69] In this work the focus is mainly on relaxation on the nanoscale or lower meaning that spin-lattice in the rotating frame ($T_{1\rho}$) and spin-spin (T_2) relaxation times are more relevant as these parameters yield information on relaxation which occurs on the millisecond timescale or faster.[70] The determination of proton $T_{1\rho}$ is a CP MAS experiment with variable spin-lock times while the measurement of T_2 uses a spin echo experiment.

Solid state NMR spectroscopy is thus a useful tool in the characterisation of the chemical environment within the polyethylene blends. In addition, the changes which occur in the blend morphology will be detectable using this technique.

2.6.3 Visualisation of crystal structure and morphology

2.6.3.1 Scanning Electron Microscopy and Transmission Electron Microscopy

Scanning electron microscopy (SEM) provides a direct means to visualise three dimensional structures at high resolution. The image is obtained by scanning a sample with a beam of electrons. The electrons can interact with the polymer in various ways which produce characteristic signals containing information about the polymer structure and topology. The types of signals produced and their interaction volumes within the sample are shown in Figure 2.5.

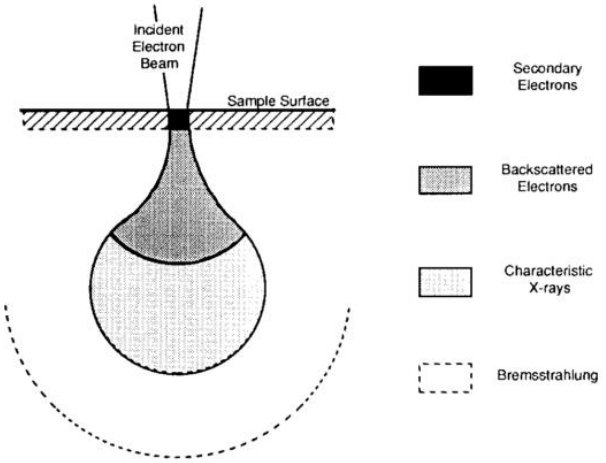

Figure 2. 5 Schematic indicating the interaction volumes of each type of signal produced upon interaction of the sample with the electron beam[71]

SEM of polymers has posed a number of difficulties due to the low degree of electron scattering, especially of polyolefins, which yields poor contrast.[72] In addition, polymers are known to be poor conductors resulting in an accumulation of charge and heat upon exposure to an electron beam.[71] For this reason SEM images of polymers are commonly obtained at low voltages (0.5 – 5.0 kV).[72]

The charging of polymer samples can be overcome and the image resolution enhanced by the use of transmission electron microscopy (TEM).[71] In a TEM experiment the sample is exposed to an electron beam with accelerating voltages of approximately 80 – 120 kV.[73] Polymers do not scatter electrons effectively and therefore produce insufficient contrast in TEM. Contrast in TEM is produced by electron scattering and can be enhanced by decreasing the accelerating voltage.[73] Imaging by transmission requires the use of thin samples in order for the electrons to enter the surface without losing significant energy and in order to achieve enhanced contrast even thinner samples are required.[73] For polyethylenes, which are rubbery polymers at room temperature, it is not simple to slice thin films and typically has to be done by cryo-ultramicrotomy. The sample preparation also adds difficulties with regards to repeatability as the films need to be cut to the same thickness. In the case of semi-crystalline polymers the intensity of the scattered electrons is highly dependent on the orientation of the crystals as well as the crystal thickness.[73]

In this study SEM and TEM images of crystal structures will provide a qualitative means for assessing differences in crystal structure between homopolymers and blends. Quantitatively, the crystal radius can be obtained from both TEM and SEM images at different stages of the isothermal and non-isothermal experiments in order to calculate crystallisation kinetics.

2.6.4 X-Ray Diffraction

X-Ray Diffraction (XRD) provides a means of directly measuring sample crystallinity instead of properties which depend on crystallinity, as in the case of many thermal analysis techniques such as DSC. An X-Ray diffraction pattern is a destructive interference pattern generated when incident X-rays are diffracted by the electrons surrounding the atoms comprising the crystal within polymer samples.[74] XRD experiments can be classified into either wide angle X-ray diffraction (WAXD) or small angle X-ray scattering (SAXS) depending on the angle of deviation from the

incident beam, referred to as 2θ.[75] WAXD will be used in this study as this method provides information on the polymer microstructure while SAXS yields information about polymer macrostructure. For atoms which have an ordered arrangement the scattering angle 2θ is related to the interplanar distance *d* by Bragg's Law, given in Equation 2.25, where *i* is an integer.[75]

$$i\lambda = 2dsin\theta \tag{2.25}$$

X-ray diffraction patterns of polymers can be quite complex due to the slight scattering of amorphous regions creating a characteristic "amorphous halo" in the diffraction pattern. In addition, polymer crystals are often buried within amorphous regions resulting in broadening of the scattering peaks of these crystals due to the necessity of the scattered beam to travel through the amorphous regions before being detected. Thus, for a polymer sample, the intensity of the scattering of a completely amorphous sample (I_a^0) is measured and compared to that of the semi-crystalline sample of the same thickness(I_a). The crystallinity can then be defined according to Equation 2.26.

$$1 - w_{c,x} = \frac{I_a}{I_a^0} \tag{2.26}$$

The Scherrer equation has been used to determine crystallite dimensions for perfectly crystalline solids (Equation 2.27), where $L_{hkl}$is the average size of the crystallites orthogonal to the *hkl* planes, β is the width at half-maximum intensity in radians and *Q* is normally a constant value of one.[75]

$$L_{hkl} = \frac{Q\lambda}{\beta \cos\theta} \tag{2.27}$$

XRD is thus a useful tool to monitor any changes in the polyethylene crystal structure under isothermal or non-isothermal conditions. In addition, the effect of the blending of LDPE with LLDPE on the crystal structures could be determined using XRD. Through XRD measurements of crystal lattice parameters it can be determined whether changes in blend composition affect these parameters.

2.6.5 Solution crystallisation by laser light scattering (Scalls)

The fractionation of semi-crystalline polymers by crystallisation is by now common practice and has been introduced in section 2.5.1 under the heading of TREF. A technique which is similar to TREF with the advantage of faster analysis times is Crystallisation analysis fractionation (Crystaf). The Crystaf technique monitors the decrease in the concentration of the polymer solution during the crystallisation process.[76] Although providing a wealth of information regarding polymer crystallisability, both of these techniques use complex equipment which can only be obtained at high cost. As an alternative to these techniques an instrument was developed at Stellenbosch University which measures the change in turbidity of a polymer solution with temperature. In semi-crystalline polymer solutions an increase in turbidity can be related to an increase density of the solution.[77] Since crystalline materials are denser than their amorphous counterparts, an increase in density can be interpreted as the increase in size or quantity of crystalline material in the solution. The turbidity analysis method presented advantages over both TREF and Crystaf as the analysis times are relatively fast and instrumentation is inexpensive. Additionally, it can provide a real-time analysis of the crystallisation and dissolution process in the same experiment.

This technique was termed Scalls and involves measurement of the intensities of three wavelengths of laser light with the idea being that an increase in the turbidity of the solution (or crystallinity of the sample) upon cooling would increase the amount of scattering of the laser light, leading to a corresponding decrease in the intensity of the beams transmitted through to an in-line detector.[78] Conversely, an increase in the intensity of the transmitted beam would be observed upon polymer dissolution. A schematic of the Scalls setup is shown in Figure 2.6. The developmental procedure has been explained elsewhere.[76,79]

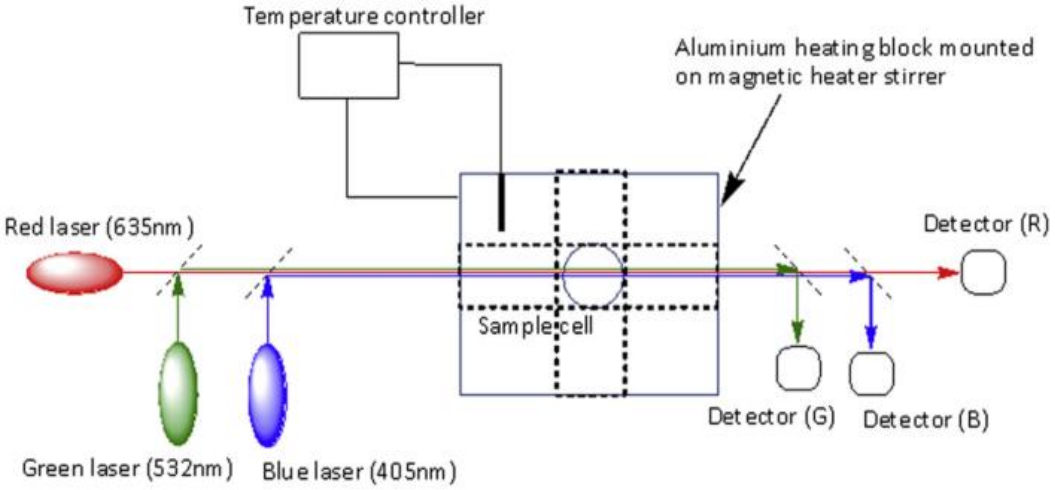

Figure 2. 6: General schematic of Scalls setup[78]

The polymer solution is added to a quartz vial which is then placed in an aluminium heating block, as shown in Figure 2.6. The wavelengths of laser light used were 405 nm, 532 nm and 635 nm denoted blue, green and red respectively. The raw data obtained is a voltage versus temperature plot, depicted in Figure 2.7a. In order to obtain the final crystallisation profile (Figure 2.7b) the first derivative of the raw data is used.

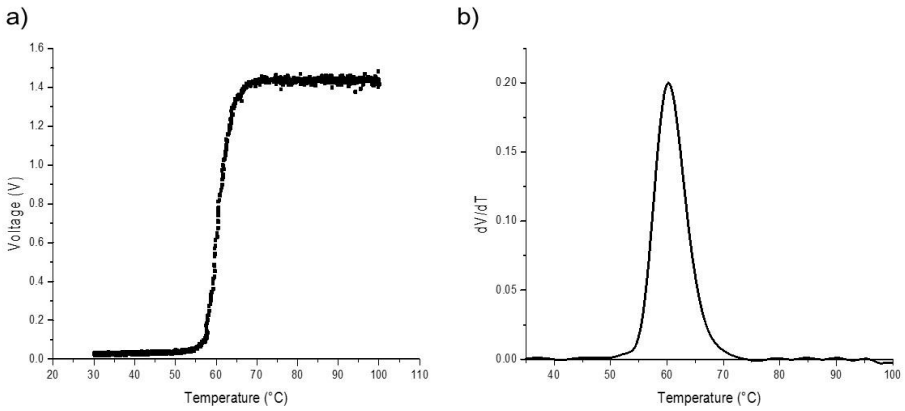

Figure 2. 7: Generalised Scalls plots showing a) raw voltage data as a function of temperature and b) final crystallisation profile

2.7 Summary

The purpose of this background was to clarify the aims and objectives listed in chapter one. A brief overview of current kinetic models was provided. These models will attempt to be fitted to the kinetic data obtained for the LDPE/LLDPE blends. The thermodynamics of blending has shown that in order to draw conclusions about miscibility the interaction parameter needs to be experimentally determined to yield the enthalpy of mixing, since the change in entropy does not contribute significantly to free energy of mixing. The criteria for co-crystallisation were listed. The combination of kinetic results and structural characterisation techniques detailed above will therefore aid in the identification of the compatibilising phase.

Literature on performance of polyethylene blends was presented, providing guidelines for the treatment and interpretation of stress-strain data. The results will be separated according to blending methods and many of the techniques described in this chapter will be used on the blends prepared by both solution and reactive methods.

2.8 References

1. Shamiri, A., Chakrabarti, M. H., Jahan, S., Hussain, M. A., Kaminsky, W., Aravind, P. V. & Yehye, W. A. The influence of Ziegler-Natta and metallocene catalysts on polyolefin structure, properties, and processing ability. *Materials (Basel).* **7,** 5069–5108 (2014).

2. Peacock, A. *Handbook of polyethylene: structures: properties, and applications*. (Marcel Dekker Inc., 2000).

3. Sperling, L. H. *Introduction to physical polymer science*. (John Wiley & Sons, 2006).

4. Cheng, S. Z. D. & Lotz, B. Enthalpic and entropic origins of nucleation barriers during polymer crystallization: The Hoffman-Lauritzen theory and beyond. *Polymer (Guildf).* **46,** 8662–8681 (2005).

5. Toda, A. Polyethylene crystallization from dilute solutions : adsorption isotherm on the growth face. *J. Chem. Soc. Faraday Trans.* **91,** 3581–2586 (1995).

6. Keller, A. A note on single crystals in polymers: evidence for a folded chain configuration. *Philos. Mag.* **2,** 1171–1175 (1957).

7. Tashiro, K., Sasaki, S. & Kobayashi, M. Structural investigation of orthorhombic-to-hexagonal phase transition in polyethylene crystal: the experimental confirmation of the conformationally disordered structure by x-ray diffraction and infrared / raman spectroscopic measurements. *Macromolecules* **26,** 7460–7469 (1996).

8. Lopez, L. C. & Wilkes, G. L. Crystallization kinetics of poly (p-phenylene sulphide): effect of molecular weight. *Polymer (Guildf).* **29,** 106–113 (1988).

9. Lorenzo, A. T., Arnal, M. L., Albuerne, J. & Müller, A. J. DSC isothermal polymer crystallization kinetics measurements and the use of the Avrami equation to fit the data: guidelines to avoid common problems. *Polym. Test.* **26,** 222–231 (2007).

10. Pradell, T., Crespo, D., Clavaguera, N. & Clavaguera-Mora, M. T. Diffusion controlled grain growth in primary crystallization: Avrami exponents revisited. *J. Phys. Condens. Matter* **10,** 3833–3844 (1999).

11. Brucato, V., Crippa, G., Piccarolo, S. & Titomanlio, G. Crystallization of polymer melts under fast cooling. I: Nucleated polyamide 6. *Polym. Eng. Sci.* **31,** 1411–1416 (1991).

12. Banks, W., Gordon, M. & Sharples, A. The crystallization of polyethylene after partial melting. *Polymer (Guildf).* **4,** 289–302 (1963).

13. Keith, H. D. & Padden, F. J. A phenomenological theory of spherulitic crystallization. *J. Appl. Phys.* **34,** 2409–2421 (1963).

14. Keith, H. D. & Padden, F. J. Spherulitic crystallization from the melt. I. Fractionation and impurity segregation and their influence on crystalline morphology. *J. Appl. Phys.* **35,** 1270–1285 (1964).

15. Hoffman, J. D. Regime III crystallization in melt-crystallized polymers: the variable cluster model of chain

folding. *Polymer (Guildf).* **24,** 3–26 (1983).

16. Di Lorenzo, M. L. & Silvestre, C. Non-isothermal crystallization of polymers. *Prog. Polym. Sci.* **24,** 917–950 (1999).

17. Krishnaswamy, R. K., Yang, Q., Fernandez-Ballester, L. & Kornfield, J. A. Effect of the distribution of short-chain branches on crystallization kinetics and mechanical properties of high-density polyethylene. *Macromolecules* **41,** 1693–1704 (2008).

18. Ozawa, T. Kinetics of non-isothermal crystallization. *Polymer (Guildf).* **12,** 150–158 (1971).

19. Eder, M. & Wlochowicz, A. Kinetics of non-isothermal crystallization of polyethylene and polypropylene. *Polymer (Guildf).* **24,** 1593–1595 (1983).

20. Ozawa, T. Kinetics of non-isothermal crystallization. *Polymer (Guildf).* **12,** 150–158 (1971).

21. Supaphol, P. & Spruiell, J. E. Nonisothermal bulk crystallization studies of high density polyethylene using light depolarizing microscopy. *J. Polym. Sci. Part B Polym. Phys.* **36,** 681–692 (1998).

22. Minkova, L. & Mihailov, M. Kinetics of nonisothermal crystallization and melting of normal high density and ultra-high molecular weight polyethylene blends. *Colloid Polym. Sci.* **267,** 577–582 (1989).

23. Gupta, A. K., Rana, S. K. & Deopura, B. L. Crystallization kinetics of high-density polyethylene/linear low-density polyethylene blend. *J. Appl. Polym. Sci.* **51,** 231–239 (1994).

24. Gao, J., Yu, M. & Li, Z.-T. Nonisothermal crystallization kinetics and melting behavior of bimodal medium density polyethylene/low density polyethylene blends. *Eur. Polym. J.* **40,** 1533–1539 (2004).

25. Xu, X., Xu, J., Chen, L., Liu, R. & Feng, L. Nonisothermal crystallization kinetics of ethylene-butene copolymer/low-density polyethylene blends. *J. Appl. Polym. Sci.* **80,** 123–129 (2001).

26. Davis, T. P. & Matyjaszewski, K. *Handbook of Radical Polymerization*. (John Wiley & Sons, 2002).

27. Utracki, L. A. Introduction to polymer blends. *Polym. blends Handb.* **1,** 1–122 (2003).

28. Huggins, M. L. Some properties of solutions of long-chain compounds. *J. Phys. Chem.* **46,** 151–158 (1942).

29. Koningsveld, R. & Staverman, A. J. Liquid–liquid phase separation in multicomponent polymer solutions. I. Statement of the problem and description of methods of calculation. *J. Polym. Sci. Part A-2 Polym. Phys.* **6,** 305–323 (1968).

30. Flory, P. J. Statistical thermodynamics of semi-flexible chain molecules. *Proc. R. Soc. London A Math. Phys. Eng. Sci.* **234,** (1956).

31. Robeson, L. M. Polymer blends. *Hanser, Munich* 24–149 (2007).

32. Paul, D. R. & Bucknall, C. B. *Polymer blends: formulation and performance*. (Wiley, 2000).

33. Das, G. & Banerjee, A. N. Role of methods of blending on polymer-polymer compatibility. *J. Appl. Polym. Sci.* **61,** 1473–1478 (1996).

34. Wallace, R. G. Melt blending of polyolefins. US3299186A. 1–3 (1967).

35. Paul, D. R. & Newman, S. *Polymer blends*. (Academic Press, 1978).

36. Mecking, S. Reactor blending with early / late transition metal catalyst combinations in ethylene polymerization. *Macromolecules* **143,** 139–143 (1999).

37. Puig, C. C. On the cocrystallization phenomenon in blends of high density polyethylene and low density polyethylene. *Polym. Bull.* **38,** 715–720 (1997).

38. Galante, M. J., Mandelkern, L. & Alamo, R. G. The crystallization of blends of different types of polyethylene: the role of crystallization conditions. *Polymer (Guildf).* **39,** 5105–5119 (1998).

39. Xu, J., Xu, X., Chen, L., Feng, L. & Chen, W. Effect of composition distribution on miscibility and co-crystallization phenomena in the blends of low density polyethylene with conventional and metallocene-based ethylene–butene copolymers. *Polymer (Guildf).* **42,** 3867–3874 (2001).

40. Fonseca, C. A. & Harrison, I. R. An investigation of co-crystallization in LDPE/HDPE blends using DSC and TREF. *Thermochim. Acta* **313,** 37–41 (1998).

41. Hussein, I. A., Hameed, T., Sharkh, B. F. A. & Mezghani, K. Miscibility of hexene-LLDPE and LDPE

blends: influence of branch content and composition distribution. *Polymer (Guildf).* **44,** 4665–4672 (2003).

42. Hameed, T. & Hussein, I. A. Rheological study of the influence of Mw and comonomer type on the miscibility of m-LLDPE and LDPE blends. *Polymer (Guildf).* **43,** 6911–6929 (2002).

43. Delgadillo-Velázquez, O., Hatzikiriakos, S. G. & Sentmanat, M. Thermorheological properties of LLDPE/LDPE blends. *Rheol. Acta* **47,** 19–31 (2007).

44. Yamaguchi, M. & Shigehiko, A. LLDPE/LDPE blends. I. Rheological, thermal, and mechanical properties. *J. Appl. Polym. Sci.* **74,** 3153–3159 (1999).

45. Abraham, D., George, K. E. & Francis, D. J. Rheological characterization of blends of low density with linear low density polyethylene using a torque rheometer. *Eur. Polym. J.* **26,** 197–200 (1990).

46. Hussein, I. A. Influence of composition distribution and branch content on the miscibility of m-LLDPE and HDPE blends: rheological investigation. *Macromolecules* **36,** 2024–2031 (2003).

47. Oyama, H. T. Super-tough poly (lactic acid) materials : reactive blending with ethylene copolymer. *Polymer (Guildf).* **50,** 747–751 (2009).

48. Brown, W. E. *Testing of polymers*. (Interscience Publishers, 1969).

49. Soares, B. P., Penlidis, A., Li, C. & Shan, P. HDPE / LLDPE reactor blends with bimodal microstructures — part I : mechanical properties. *Polymer (Guildf).* **43,** 7345–7365 (2002).

50. Li Pi Shan, C., Soares, J. B. P. & Penlidis, A. Mechanical properties of ethylene/1-hexene copolymers with tailored short chain branching distributions. *Polymer (Guildf).* **43,** 767–773 (2001).

51. Anantawaraskul, S., Soares, J. B. P. & Wood-Adams, P. M. Fractionation of semicrystalline polymers by crystallization analysis fractionation and temperature rising elution fractionation. *Adv. Polym. Sci.* **182,** 1–54 (2005).

52. Sweed, M. Co-crystallization in polyolefin blends studied by various crystallization analysis techniques (MSc). (Stellenbosch University, 2006).

53. Gabriel, C. & Lilge, D. Comparison of different methods for the investigation of the short-chain branching distribution of LLDPE. *Polymer (Guildf).* **42,** 297–303 (2001).

54. Jeziorny, A. Parameters characterizing the kinetics of the non-isothermal crystallization of poly(ethylene terephthalate) determined by d.s.c. *Polymer (Guildf).* **19,** 1142–1144 (1978).

55. Muller, a J., Hernandez, Z. H., Arnal, M. L. & Sanchez, J. J. A novel technique to study molecular segregation during crystallization. *Polym. Bull.* **472,** 465–472 (1997).

56. Xue, Y., Fan, Y., Bo, S. & Ji, X. Microstructure characterization of a complex branched low-density. *Chinese J. Polym. Sci.* **33,** 508–522 (2015).

57. Zhang, M. & Wanke, S. E. Branching content and distribution in commercial polyethylenes by thermally fractionated differential scanning calorimetry. *Polym. Eng. Sci.* **43,** 1878–1888 (2003).

58. Tonelli, A. E., Gomez, M. A., Tanaka, H. & Cozine, M. H. Solid state ^{13}C NMR studies of the structures, conformations, and dynamics of semi-crystalline polymers. in *Solid State NMR of Polymers* 81–105 (Springer US, 1991). doi:10.1007/978-1-4899-2474-2_4

59. Ando, I., Yamanobe, T., Akiyama, S., Komoto, T., Sato, H., Fujito, T., Deguchi, K. & Imanari, M. Polyethylene structure in the solid state as studied by variable-temperature ^{13}C CP/MAS n.m.r. spectroscopy. *Solid State Commun.* **62,** 785–788 (1987).

60. Colletti, R. F. & Mathias, L. J. Solid-state 2H NMR: overview with specific examples. in *Solid State NMR of Polymers* 23–60 (Springer US, 1991).

61. Moller, M., Kogler, G., Oelfin, D. & Drotloff, H. Molecular motion in crystalline and mesomorphous phases of large size cycloalkanes as a model for polyethylene. in *Solid State NMR of Polymers* 245–259 (Springer US, 1991).

62. Botha, L. & Van Reenen, A. J. The effect of in-process ethylene incorporation on the evolution of particle morphology and molecular characteristics of commercial heterophasic ethylene propylene copolymers (HEPCs). *Eur. Polym. J.* **49,** 2202–2213 (2013).

63. Ando, I., Yamanobe, T., Sorita, T., Komoto, T., Sato, H., Deguchi, K. & Imanari, M. Conformation of cyclic paraffins and polyethylene in the solid- state as studied by C-13 CP MAS NMR. *Macromolecules* **17,**

1955–1958 (1984).

64. Ando, I., Yamanobe, T. & Asakura, T. Primary and secondary structures of synthetic polymer systems as studied by 13C N M R spectroscopy. *Prog. Nucl. Magn. Reson. Spectrosc.* **22,** 349–400 (1990).

65. Galland, G. B., de Souza, R. F., Mauler, R. S. & Nunes, F. F. ^{13} C NMR determination of the composition of linear low-density polyethylene obtained with [η ^{3} -Methallyl-nickel-diimine]PF $_{6}$ complex. *Macromolecules* **32,** 1620–1625 (1999).

66. Assumption, H. J., Vermeulen, J. P., Jarrett, W. L., Mathias, L. J. & Van Reenen, A. J. High resolution solution and solid state NMR characterization of ethylene/1-butene and ethylene/1-hexene copolymers fractionated by preparative temperature rising elution fractionation. *Polymer (Guildf).* **47,** 67–74 (2006).

67. MacGregor, A. W., O'Dell, L. A. & Schurko, R. W. New methods for the acquisition of ultra-wideline solid-state NMR spectra of spin-1/2 nuclides. *J. Magn. Reson.* **208,** 103–113 (2011).

68. Gilardi, G., Abis, L. & Cass, A. E. G. Wide-line solid-state NMR of wood: proton relaxation time measurements on cell walls biodegraded by white-rot and brown-rot fungi. *Enzyme Microb. Technol.* **16,** 676–682 (1994).

69. Duer, M. J. *Introduction to solid-state NMR spectroscopy*. (Blackwell Publishing Ltd, 2004).

70. Ricardo, N. M. P. S., Lahtinen, M., Price, C. & Heatley, F. Blends of natural rubber and polyurethane latices studied by H-1 wideline and C-13 MAS solid-state NMR. *Polym. Int.* **51,** 627–634 (2002).

71. Butler, J. H., Joy, D. C., Bradley, G. F. & Krause, S. J. Low-voltage scanning electron microscopy of polymers. *Polymer (Guildf).* **36,** 1781–1790 (1995).

72. Vezie, D. L., Thomas, E. L. & Adams, W. W. Low-voltage, high-resolution scanning electron microscopy: a new characterization technique for polymer morphology. *Polymer (Guildf).* **36,** 1761–1779 (1995).

73. Sawyer, L. C., Grubb, D. T. & Meyers, G. F. Fundamentals of microscopy. in *Polymer Microscopy* 42–43 (Springer Netherlands, 1996). doi:10.1007/978-94-015-8595-8_6

74. Sands, D. E. *Introduction to crystallography*. (W. A. Benjamin, Inc., 1969).

75. Alexander, L. E. *X-ray diffraction methods in polymer science*. (Wiley-Interscience, 1969).

76. Van Reenen, A., Rohwer, E., Walters, P., Lutz, M. & Brand, M. Development and use of a turbidity analyzer for studying the solution crystallization of polyolefins. *J. Appl. Polym. Sci.* **109,** 3238–3243 (2008).

77. Shan, C. L. P., Degroot, W. A., Hazlitt, L. G. & Gillespie, D. A new turbidimetric approach to measuring polyethylene short chain branching distributions. *Polymer (Guildf).* **46,** 11755–11767 (2005).

78. Robertson, D. D., Neppalli, R. & van Reenen, A. J. Solution crystallization analysis of poly(lactic acid) by Scalls: a facile approach for thermal analysis of polymers in solution. *Polym. Test.* **40,** 79–87 (2014).

79. Van Reenen, A., Brand, M., Rohwer, E. & Walters, P. Solution crystallization analysis by laser light scattering (SCALLS). *Macromol. Symp.* **282,** 25–32 (2009).

Chapter 3: Experimental methods

3.1 Introduction

A variety of LLDPEs and a single grade of LDPE was obtained from commercial sources and solution blended. For the sake of comparison of blending processes, LLDPEs of different co-monomer structures and concentrations were reactor blended with the same commercial LDPE. These blends were characterised by solution crystallisation by laser light scattering (Scalls), preparative temperature rising elution fractionation (TREF), differential scanning calorimetry (DSC), high temperature size exclusion chromatography (HT-SEC), both scanning electron microscopy (SEM) and fluorescence microscopy as well as nuclear magnetic resonance (NMR). Preliminary work was conducted on the blend ratios at which these LLDPEs and LDPEs exhibit compatibility.

3.2 Materials

3.2.1 Commercial materials

LLDPE polymers were obtained from Sasol Polymers (South Africa) with the following specifications:

Table 3. 1 Specifications of LLDPEs obtained from Sasol Polymers

Grade	MFI (g/10 min)	Density (g/cm^3)
HF101	0.8	0.923
HF120	1.0	0.920
HF140	2.0	0.920
HR477	5.0	0.939

3.3 Blending procedures

3.3.1 Melt blending

The melt blending process was synonymous with film pressing. The polymer powders were weighed off according to the desired blend ratios and dry mixed by stirring. The mixture was then sandwiched between two square Teflon sheets and placed in a Graseby Specac melt press. The sample was heated to 130 °C between two aluminium blocks for two minutes, where after two tons of pressure was applied at one minute intervals for seven minutes. Once removed from between the aluminium blocks the film was left to cool to room temperature between the Teflon sheets.

3.3.2 Solution blending

Blends were prepared by dissolving both LLDPEs and LDPE in *p*-xylene (5% w/v) at 130 °C for two hours. The blends were then precipitated into methanol, filtered and dried at 40 °C in air. Blends of LLDPE contents of 10, 50 and 80 wt % were prepared.

3.4 Analytical procedures

3.4.1 Solution crystallisation analysis by laser light scattering

Solutions for SCALLS analysis were prepared by dissolving 20 mg of polymer in 20 mL *ortho*-dichlorobenzene (o-DCB) in a quartz vial. The dissolution process during the analysis was performed from 30 °C to 130 °C at a heating rate of 0.5 °C/min followed by a cooling step to 30 °C at 1 °C/min and another dissolution step to 130 °C at 1 °C/min.

3.4.2 Preparative temperature rising elution fractionation

The TREF procedure occurs in two stages. During the crystallisation stage 3 g of polymer was dissolved in 300 mL xylene with 2 wt% Irganox 1010 stabiliser at 130 °C for two hours. Upon complete dissolution, heated quartz sea sand (Sigma Aldrich, 50-70 mesh particle size) was added to just above the level of the solution. The reactor was then placed in an oil bath to cool from 130 °C to 30 °C at a rate of 1 °C/hour. During this stage the polymer crystallised onto the sand support.

Once cooled, the sand was transferred to a steel column with an inlet through which xylene is pumped (FMI Q pump model) and an outlet through which the fractions were eluted. The pump flow rate was 40 mL/min. The column was placed into an oven and fractions were collected by increasing the temperature of the oven from 30 °C to 130 °C. The solvent was removed from the fractions by rotary evaporator and further drying occurred under vacuum at 40 °C overnight.

3.4.3 Differential scanning calorimetry

A TA Instruments Q100 DSC was used to analyse sample crystallinity. The instrument was calibrated using indium standards. The standard cooling and heating rate was 10 °C/min, however rates of 5 °C/min and 20 °C/min were also used during co-crystallisation studies. DSC was normally run with three cycles, the first cycle being to erase thermal history. Samples of 4 mg were prepared for analysis in aluminium pans.

SSA fractionation was performed on the same calorimeter in the temperature range 0 °C to 150 °C. Samples of 2 mg were prepared in aluminium pans. Samples were first heated to 150 °C and held isothermally for five minutes before cooling to 0 °C and re-heating to an annealing temperature. This step was repeated for stepwise decreasing annealing temperatures. The heating rate was maintained at 10 °C/min.

3.4.4 High temperature size exclusion chromatography

Molecular weight and molecular weight distributions were determined by high temperature size exclusion chromatography. A PL-GPC 220 (Polymer Laboratories) instrument coupled to a refractive index detector was used. A flow rate of 1.0 mL/min was applied on a column measuring 300 mm by 7.5 mm. The column was packed with styrene-divinylbenzene copolymer of particle size 10 µm. Samples were dissolved in 1,2,4- trichlorobenzene and stabilised with 0.0125% BHT. Monodisperse polystyrene standards (Polymer Laboratories) were used to calibrate the system.

3.4.5 Microscopy

3.4.5.1 Scanning electron microscopy

In order to see crystallites by SEM, polymers should first be etched to remove amorphous regions. In this case the etchant used was permanganic etching based on the method of Olley and Basset.[1] Samples of constant thickness were prepared by injection moulding followed by thermal annealing at 130 °C and slow cooling. Potassium permanganate (2 % w/v) was dissolved in concentrated sulphuric acid for one hour. Samples were immersed in the etchant for one to two hours depending on the sample crystallinity. After the completion of the etching time the samples were rinsed with a cold solution of 25% (v/v) sulphuric acid in water, followed by a hydrogen peroxide rinse to reduce the manganese dioxide which formed during the formation of the etchant. Finally the samples were rinsed with acetone.

Before SEM analysis samples were placed onto carbon tape on stainless steel stubs. Additional carbon tape was placed along an edge of the sample to prevent sample charging. The samples were then coated with a gold layer before analysis.

3.4.5.2 Confocal fluorescence microscopy

In order to monitor the motion of chains from regions of individual polymers to blended regions the aid of fluorescent markers was used. A method was developed within our group[2] for the marking of polyolefins using cellulose nanowhiskers containing a fluorescent marker, either fluorescein-5'-isothiocyanate (FITC) or Rhodamine B (RhB). The synthesis of the cellulose nanowhiskers and the bonding of the fluorescent markers is described elsewehere.[2]

The procedure involves dissolving 0.5 g polymer and 2 wt% Irganox 1010 stabiliser in 20 mL xylene at 130 °C. Cellulose nanowhiskers with fluorescent markers (4 wt% for FITC, 6 wt% for RhB) were dispersed in 15 mL hot xylene separately and dispersed using ultrasound for ten minutes to prevent aggregation. The nanowhiskers solution was then added to the dissolved polymer and again dispersed using ultrasonication for ten minutes. The mixture was placed in a petri dish and the solvent allowed to evaporate in air to form a solvent cast film.

3.4.5.3 Polarised optical microscopy

An Axio optical microscope fitted with polarising lenses was used to generate images of tensile tested samples. Stress fringes could only be observed with lenses at a 45° angle to one another. Due to the irregularity of the surface of the tensile tested samples due to stretching, full area focused images were difficult to obtain. Focused images of the left and right side of a single area were blended together using PhotoShop™ software.

3.4.6 Solid state nuclear magnetic resonance

Solid state NMR analysis was performed in solution on a Varian VNMRS 500 MHz NMR spectrometer equipped with two channels and a 4 mm Chemagnetics T3 HX MAS probe. Samples were prepared by packing powdered samples into 4 mm zirconia rotors. Static ^{1}H experiments were performed at room temperature (25°C) through a 90° excitation in the proton channel. Spin-spin relaxation times were determined through the spin echo technique in the proton channel.

^{13}C experiments were also performed at room temperature either through cross-polarisation or direct pulse both in combination with MAS of 5 kHz and dipolar decoupling. All MAS experiments were performed using adamantane as an external chemical shift standard. Optimisation was done according to the Hartmann-Hahn match with RF fields of $\gamma_C B_{13C} = \gamma_H B_{1H} \approx 57$ kHz. Contact time was maintained at 1.0 ms, except during variable contact time experiments where contact times were varied at 0.1 ms, 1.0 ms, 2.0 ms, 5.0 ms and 8.0 ms.

3.4.7 X-ray diffraction

Crystal structures were determined by XRD. Samples were prepared by thermally annealing at 100 °C for one hour and allowing the sample to cool to room temperature. Analysis was performed on a Bruker D2 Phaser X-Ray diffractometer. Analysis was done at room temperature. A continuous scan was done with 2θ angles ranging from 5 – 60° and Kα_1 wavelength of 1.54184.

3.4.8 Tensile testing

Tensile tests were conducted on an LRX Plus Series tensile tester. A load cell of 50 kN was used with a strain rate of 50 mm/min. Sample specification can be seen in Figure 3.1 below.

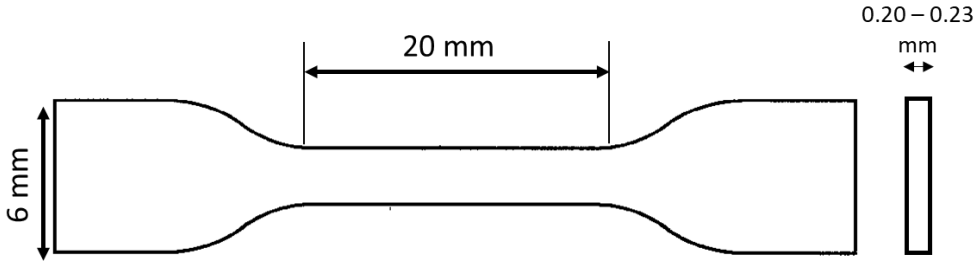

Figure 3. 1 Tensile sample specifications

3.5 References

1. Olley, R. H. & Bassett, D. C. An improved permanganic etchant for polyolefines. *Polym. Commun.* **23,** 1707–1710 (1982).

2. Le Grange, M. The use of fluorescence to probe the morphology changes in complex polymers (MSc). (Stellenbosch University, 2015).

Chapter 4: Characterisation of neat LDPE and LLDPE

Summary

The characterisation of the LDPE and LLDPE neat (unfractionated) polymers is discussed. Before the microstructure of the blends can be understood it is important to comprehend the composition and behaviour of the neat polymers under various conditions. A full understanding of the polymers can only be gained through thorough analysis of the polymer components, thus this chapter highlights the process of fractionation and provides insight into the composition of the fractions of the neat polymers.

4.1 General characteristics

4.1.1 Molar mass

The molar mass data of the neat polymers is presented in Table 4.1. The LLDPEs were all of higher molar mass than the LDPE. The molar mass of the HR477 grade was the most similar to that of the LDPE. The dispersity values were fairly high, as would be expected. This indicates a considerable amount of heterogeneity in terms of chain length for all of the neat polymers. The LDPE displayed the highest dispersity index and therefore the greatest amount of heterogeneity, which was expected since LDPEs in general are produced by free radical polymerisation leading to a large amount of chain variations in the degree of polymerisation.[1]

Table 4. 1 Molar mass parameters of neat polymers

Grade	M_w[a] (g/mol)	M_n[b] (g/mol)	Đ[c]
LDPE	165 928	34 323	4.83
HF101	279 108	75 282	3.70
HF120	295 862	59 984	4.93
HF140	282 698	68 723	4.11
HR477	176 161	42 036	4.19

Figure 4.1 displays the molar mass plots for the neat polymers. All of the polymers show a unimodal molar mass distribution. The LDPE and the HR477 grade LLDPE had similar distributions while the HF101 and HF140 grades showed similarities in their distributions. As could be inferred from the dispersity indices the HF101 displayed the narrowest distribution and the LDPE the broadest distribution. According to the shape of the molar mass distributions in Figure 4.1, the LDPE possessed the highest quantity of lower molar mass chains, followed by HR477, HF120, HF140 and HF101. It is important to note that these LLDPEs were synthesised using Ziegler Natta catalysts which is known to produce both linear and branched polymers with heterogeneous branching and chain length distributions.[1,2] The HR477 grade LLDPE was designed for rotational and injection moulding purposes while the other grades were designed for heavy duty film production. Therefore the lower average molar mass of HR477 relative to the other grades was intentionally done through the addition of a terminating agent such as hydrogen gas.[3]

[a] Weight average molar mass
[b] Number average molar mass
[c] Dispersity Index

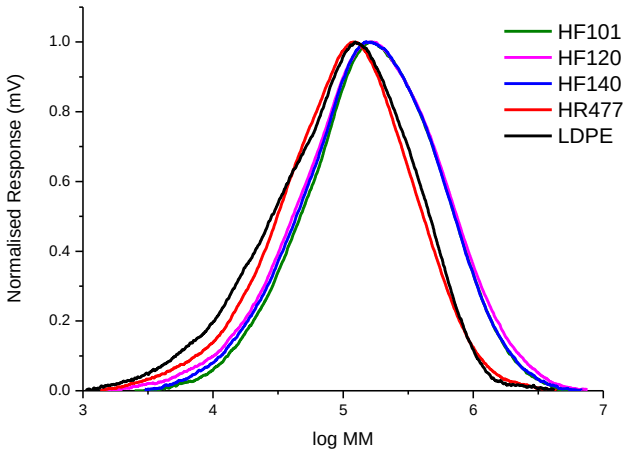

Figure 4. 1 Molar mass distributions of neat polymers

4.1.2 Solid state crystallinity

Crystallinity and melting behaviour of the neat polymers was determined by DSC and the resultant DSC thermograms are shown in Figure 4.2. The thermograms shown in Figure 4.2 display broad melting endotherms and crystallisation exotherms for all neat polymers. The polymers apparently contain a broad distribution of crystalline structures, as for all neat polymers the melting event begins more than 50 °C before the peak melting temperature. It was clear that the polymers contained both small and large crystallites, with the smaller crystallites resulting in the broad build-up to the larger melting event where the larger crystallites melt. The large quantities of these smaller crystallites were indicative of the heterogeneous branching distribution.

The LLDPEs possessed similar melting and crystallisation temperatures, with the HR477 having the highest melting and crystallisation temperature. From the enthalpy values in Table 4.2 it can be seen that the LLDPEs all displayed a higher degree of crystallinity than the LDPE, with the HR477 grade being the most crystalline. The HF101 and HF140 displayed similar degrees of crystallinity while the HF120 was the least crystalline of the LLDPEs.

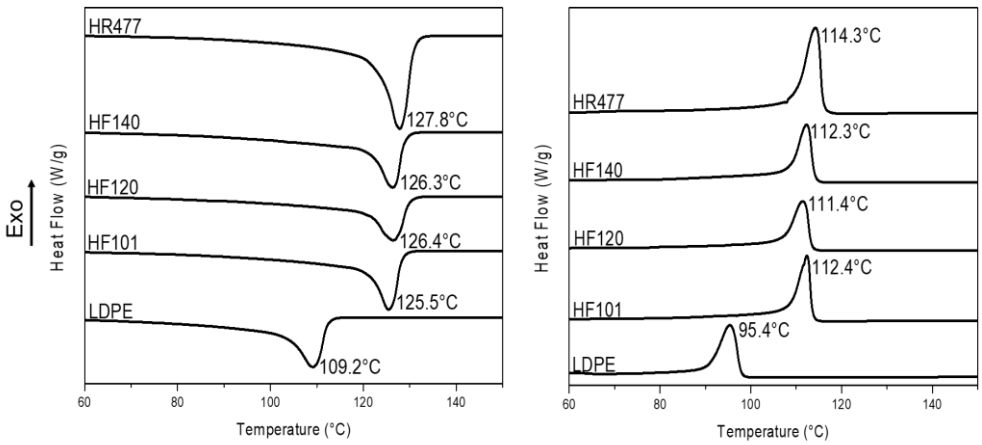

Figure 4. 2 DSC thermograms of second heating cycle and crystallisation cycle of neat polymers

Table 4. 2 Thermal parameters of neat polymers determined by DSC

Grade	Peak melting temperature (°C)	Peak crystallisation temperature (°C)	Melting enthalpy (J/g)
LDPE	109.2	95.4	114.9
HF101	125.5	112.4	131.3
HF120	126.4	111.4	120.3
HF140	126.3	112.3	130.7
HR477	127.8	114.3	172.9

4.1.3 Solution crystallinity

The SCALLS dissolution and crystallisation profiles of the neat polymers using the 405 nm wavelength laser are shown in Figures 4.3 and 4.4 respectively. The heat transfer is also better in solution than in the bulk sample. This undercooling effect is also seen in Crystaf.

The solution crystallinity behaviour of the LLDPEs was found to be highly similar in terms of peak temperatures. All LLDPEs displayed low quantities of lower crystallinity material with the HF120 grade showing the most significant amounts of material dissolving and crystallising at lower temperatures. This was in agreement with the DSC heating scans in Figure 4.2 which showed that melting was initiated long before the peak melting event. As expected, the dissolution and crystallisation temperature ranges were different for the LDPE compared to the LLDPE. The HF101 LLDPE appeared to have the narrowest peak dissolution and crystallisation events while the other neat polymers showed a fair amount of tailing. Interestingly, from the solution behaviour it would appear that the LLDPEs were more heterogeneous than the LDPE as the LDPE displayed no detectable crystallisation events at lower temperatures. The dissolution behaviour of the LDPE contradicts the broadness of the DSC melting endotherm in Figure 4.2 which suggests significant amounts of material melting at lower temperatures. In an attempt to understand this contradiction the crystallisation kinetics both in solution and the solid state was investigated and will be discussed in Section 4.3.

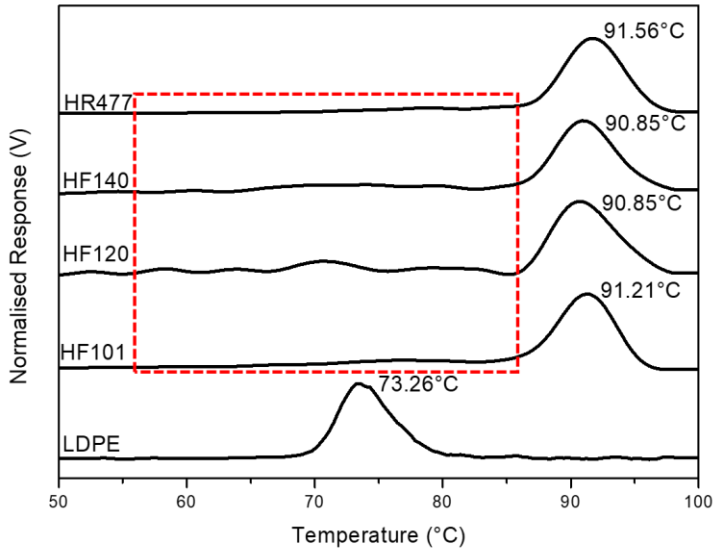

Figure 4. 3 SCALLS dissolution profiles of neat polymers (405 nm). Area inside red outline indicates material dissolving at lower temperatures.

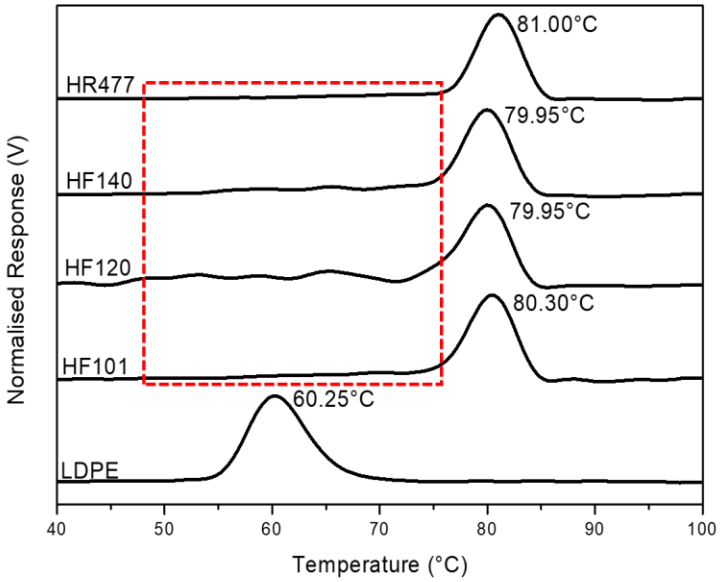

Figure 4. 4 SCALLS crystallisation profiles of neat polymers (405 nm). Area inside red outline indicates material crystallising at lower temperatures.

4.2 Crystalline structure and morphology

The SEM images of the neat polymers after permanganic etching are shown in Figure 4.5. Figure 4.5 shows that all the LLDPEs crystallise in a spherulitic morphology as the characteristic spherulites patterns could be seen. The LDPE possessed a fairly flat crystal profile which suggests the presence of two dimensional spherulites, or axialites.

Due to the inherent properties of the polyethylene the samples were fairly difficult to image due to high amounts of charge build up under the electron beam. The images were also highly dependent on the etching process and etching time. It is likely that some of the smaller crystals may also have been etched away along with the amorphous areas.

The images in Figure 4.5 focus specifically on regions where crystals occurred. For the LLDPEs the crystalline regions were fairly evenly distributed across the surface whereas in the LDPE the axialites were found in localised clusters.

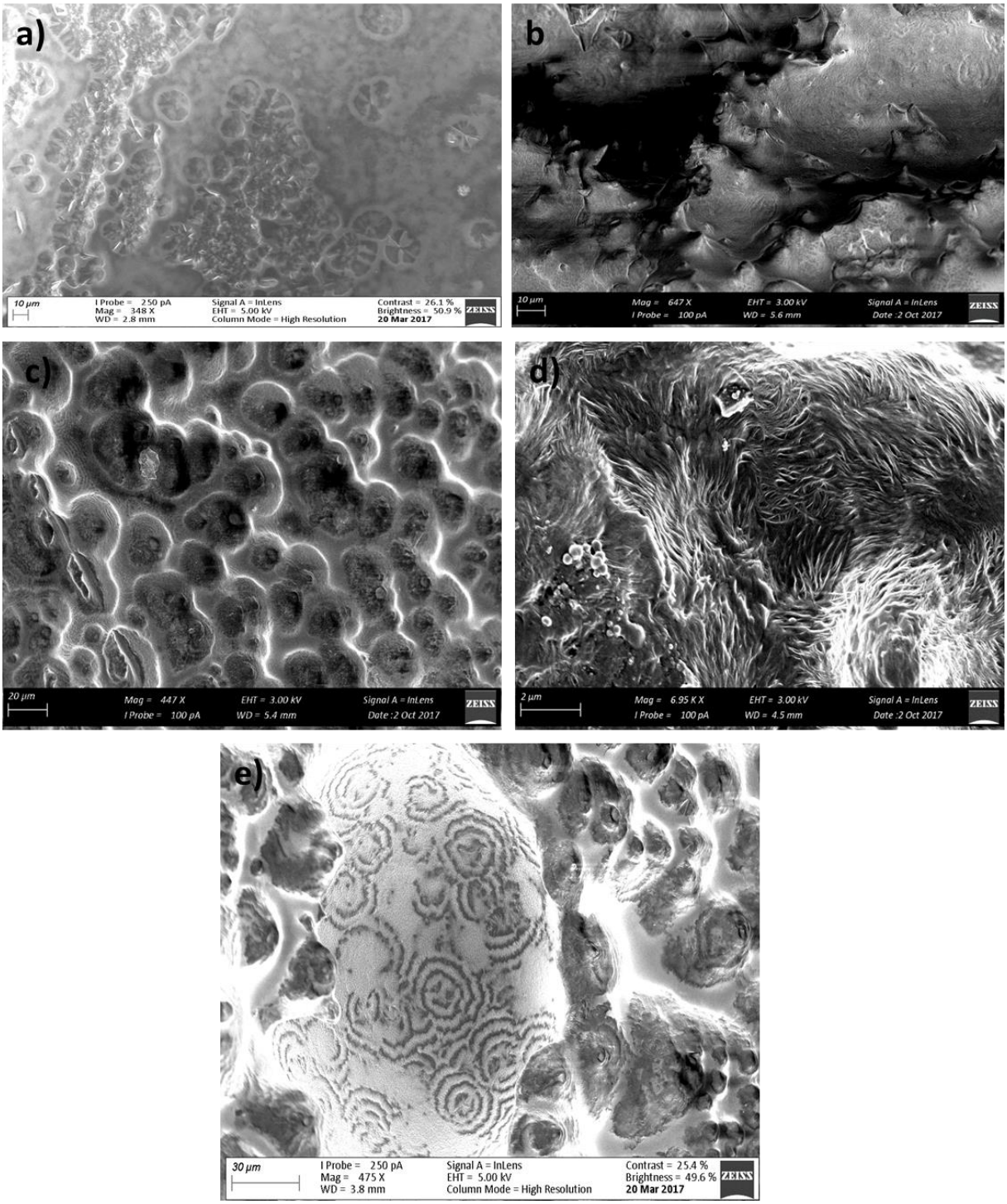

Figure 4. 5 Crystal morphology by SEM for a) LDPE b) HF101 c) HF120 d) HF140 and e) HR477

Figure 4.6 shows the X-ray diffraction patterns of the neat polymers. Similar patters could be seen for all neat polymers indicating that they all possessed the same crystal structure. The peaks were assigned using the results of Walter and Reding[4]. The peaks could accordingly be classified as representing the orthorhombic crystalline structure. All of the diffraction patterns in Figure 4.6 display a small shoulder at $2\theta = 19.66$ which could be attributed to the 010 plane of the triclinic crystal structure.[5] The diffraction patterns therefore suggest that the neat polymers crystallise into two crystal structures with the orthorhombic being the most common and the triclinic occurring to a lesser degree. This assumption is deduced from the intensity differences of the peaks. Further classification of the triclinic structure was not

possible as the major peaks occur at $2\theta = 23.39$ and 25.10[5] which overlap with the peaks of the orthorhombic structure at $2\theta = 21.57$ and 24.00 as shown in Figure 4.6.

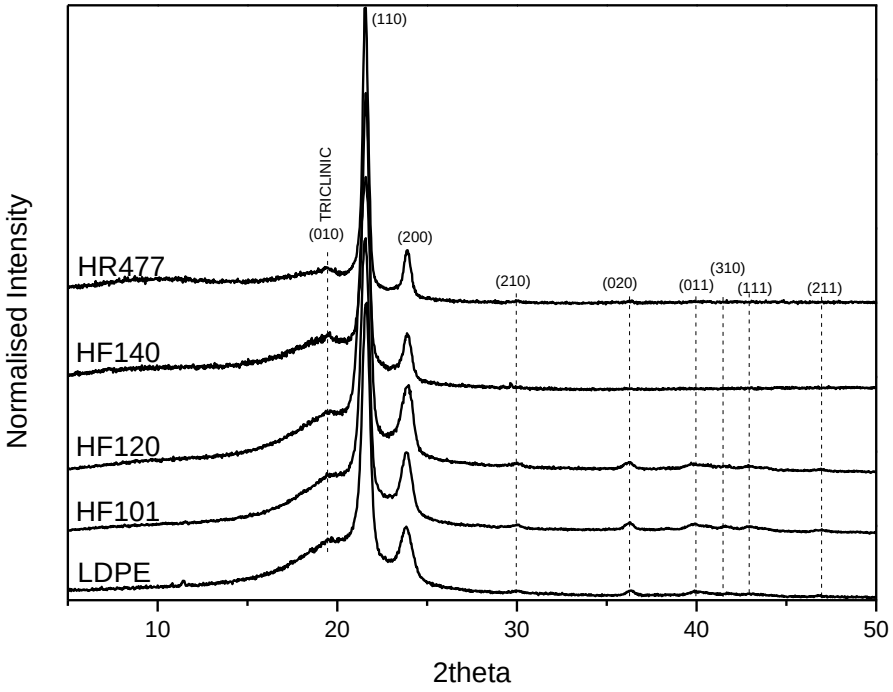

Figure 4. 6 X-ray diffraction patterns of neat polymers

4.3 Crystallisation kinetics

4.3.1 Isothermal crystallisation

DSC was used to determine the kinetic parameters of the neat polymers after isothermal crystallisation. Avrami fitting was in all cases performed in the relative crystalline conversion range of 5 – 35%. Avrami fitting was performed using an Origin plugin developed by Lorenzo and Müller.[6] Table 4.3 lists the kinetic parameters for the neat polymers at different crystallisation temperature values. The values for the Avrami index (*n*) varied between 2.21 and 3.20 at different values of crystallisation temperature (T_c) which suggests similar crystallisation mechanisms at different levels of undercooling.[7] For LDPE the *n* value varied between 2.25 and 2.51, which suggested either sporadic growth in one dimension or simultaneous growth in two dimensions. Although the samples prepared for SEM were not crystallised under isothermal conditions the images can still provide an idea of the likely morphologies possible for a specific sample. As the SEM images for the LDPE did not show any rod-like structures the scenario of simultaneous growth in two dimensions can be regarded as the most likely. The HF101 LLDPE had *n* values ranging from 2.67 to 3.05, which was approximated to 3. An *n* value of 3 corresponds to sporadic growth in two dimensions or simultaneous growth in three dimensions. The SEM images in Figure 4.5 displayed spherulitic structures indicating that three dimensional growth occurred. Simultaneous nucleation with three dimensional growth was therefore the most probable case for crystallisation. This was also the case for the HF120 and HF140 LLDPE. The HR477 grade had slightly lower *n* values which could not be approximated to a value of 3.

The *n* values were also too high to be approximated to 2 as in the case of the LDPE. It has been reported that a value of 0.5 can be obtained for the time dependent component of the *n* value representing a nucleation that is intermediate between instantaneous and sporadic growth.[6] For an *n* value of 2.5 and intermediate nucleation the dimensionality should then be 2. This contradicts the SEM images in Figure 4.5 which appeared to show three dimensional structures.

The crystallisation rate constant (K) showed significant variations when the polymers are compared. Due to the dependence of K on *n* (which varied slightly for every sample and T_c) the crystallisation rate can be inferred from the value of the crystallisation half-time ($t_{0.5}$).[7] The $t_{0.5}$ values showed a general decrease with decreasing T_c, which was expected since the larger undercooling means that crystallisation should proceed faster at values further away from the melting temperature.

Table 4. 3 Avrami parameters of neat polymers at various crystallisation temperature (T_c) values

Grade	T_c (°C)	*n*	K (min^{-n})	$t_{0.5}$ (min)
LDPE	101.0	2.45	8.18×10^{-3}	6.41
	100.5	2.30	1.62×10^{-3}	5.31
	100.0	2.25	2.67×10^{-2}	4.37
	99.5	2.51	2.71×10^{-2}	3.77
HF101	119.0	2.71	6.32×10^{-3}	5.75
	118.5	2.67	1.24×10^{-2}	4.59
	118.0	2.81	1.95×10^{-2}	3.64
	117.5	3.05	2.52×10^{-2}	3.06
HF120	119.0	2.47	9.89×10^{-3}	5.48
	118.5	2.65	7.23×10^{-3}	5.72
	118.0	3.20	4.16×10^{-3}	5.18
	117.5	3.18	1.57×10^{-2}	3.42
HF140	119.0	2.47	1.51×10^{-2}	4.82
	118.5	3.17	7.11×10^{-3}	4.40
	118.0	2.77	2.60×10^{-2}	3.35
	117.5	2.73	5.43×10^{-2}	2.62
HR477	119.0	2.21	9.67×10^{-2}	2.69
	118.5	2.52	1.26×10^{-1}	2.15
	118.0	2.46	2.96×10^{-1}	1.52
	117.5	2.44	5.92×10^{-1}	1.12

Although fairly straight lines were obtained for the Avrami plots (shown in Figure 4.7 a-e), for the Avrami method to successfully describe the system the plots also need to be parallel to one another. In none of the Avrami plots in Figure 4.7 are the plots equal distances apart, and in most cases some overlap of the Avrami plots at different crystallisation temperatures occurred. Therefore the Avrami method does not quite accurately describe crystallisation event in the neat polymers.

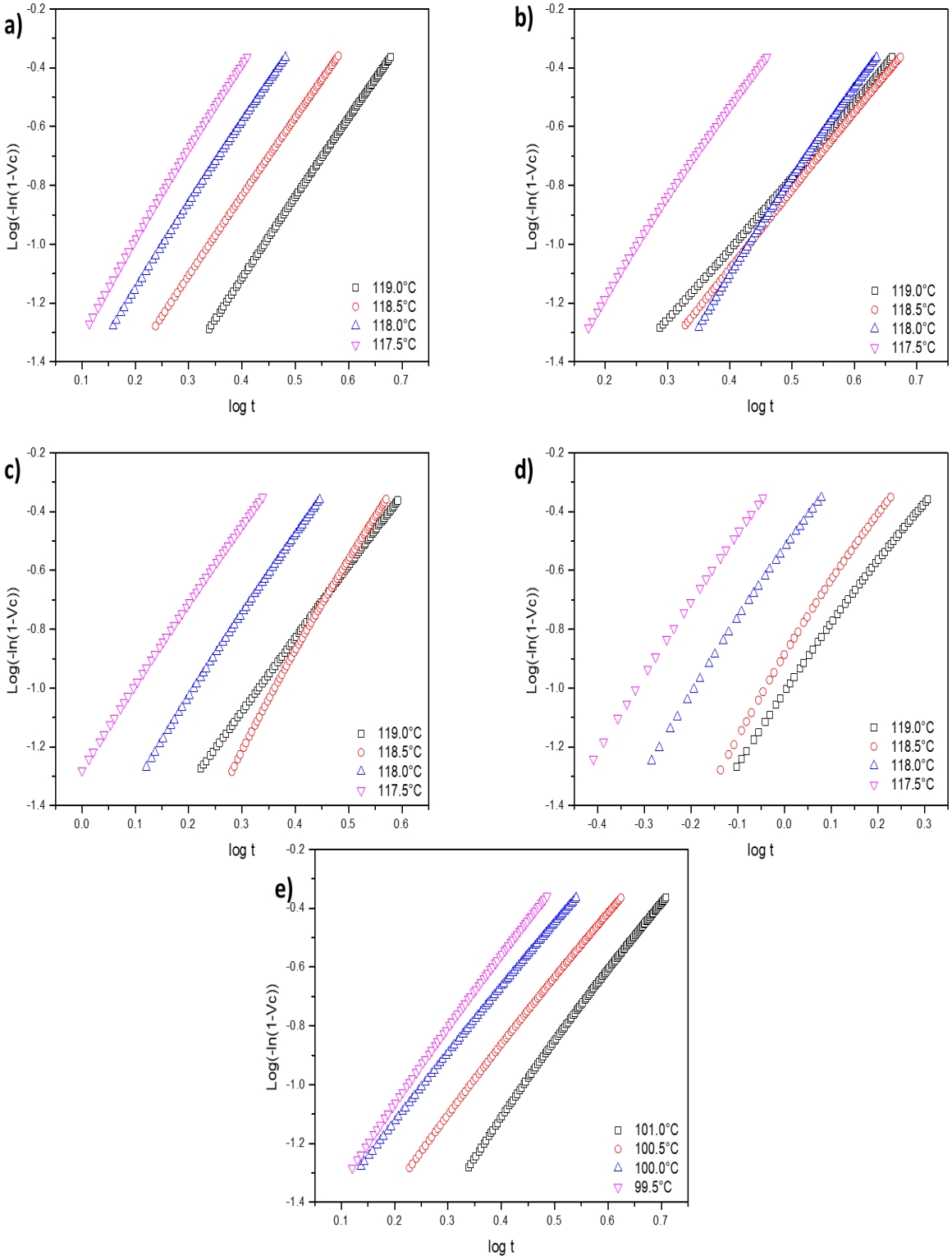

Figure 4. 7 Avrami plots of a) HF101 b) HF120 c) HF140 d) HR477 and e) LDPE at different crystallisation temperatures

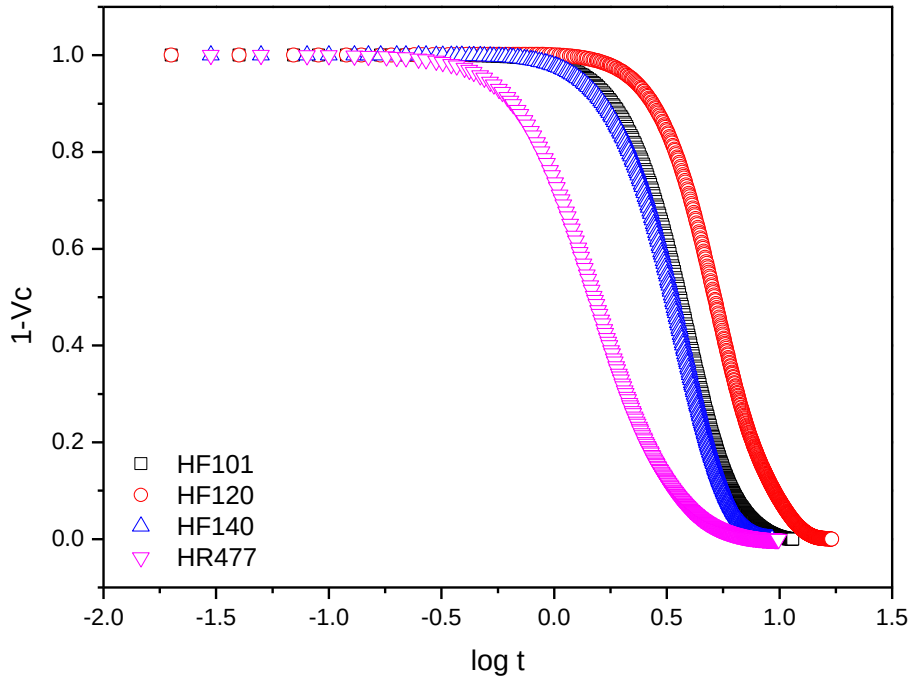

Figure 4. 8 Change in relative amorphous fraction with time for LLDPEs at 118 °C

The crystallisability of a polymer can be inferred from the rate at which the relative amorphous content decreases (conversely, the rate at which the relative crystalline content increases) when the temperature is maintained at a constant value of T_c. Figure 4.8 displays the rate of decrease of the relative amorphous fraction within the LLDPE samples at 118 °C. The sigmoidal curve shape indicates the rapid crystallisation from the melt during primary crystallisation which later plateaus as primary crystallisation ends. As expected the curves follow the same crystallinity trend as indicated by the melt enthalpy values in Table 4.2. The most crystalline LLDPE, the HR477 grade, had the fastest rate of decrease in amorphous fraction while the HF120 grade, which has the lowest crystallinity of the LLDPEs had the slowest rate of decrease in relative amorphous fraction. The HF101 and HF140 have similar values for melt enthalpy and thus in Figure 4.8 they have very similar rates of decrease of their relative amorphous fractions.

4.3.2 Non-isothermal crystallisation

The first method applied for the analysis of the non-isothermal crystallisation of the neat polymers was the simplest; that of Nadkarni which produces a linear plot.[8] The undercooling, ΔT_c was plotted as a function of the cooling rate, χ, and the slope and intercept correspond to the *P* and ΔT_c^0 values respectively. The Nadkarni plots for the neat polymers are shown in Figure 4.9 a-e. In each case the value of ΔT_c^0 was 10 ± 0.5 °C which suggested similarity in nucleation densities.[8] The *P* values were also very similar and relatively low across all the samples indicating that the rate of crystallisation was generally not highly sensitive to the cooling rate.[8] The R^2 values indicate that the fitting, although adequate, was not quite successful as perfectly linear plots could not be obtained.

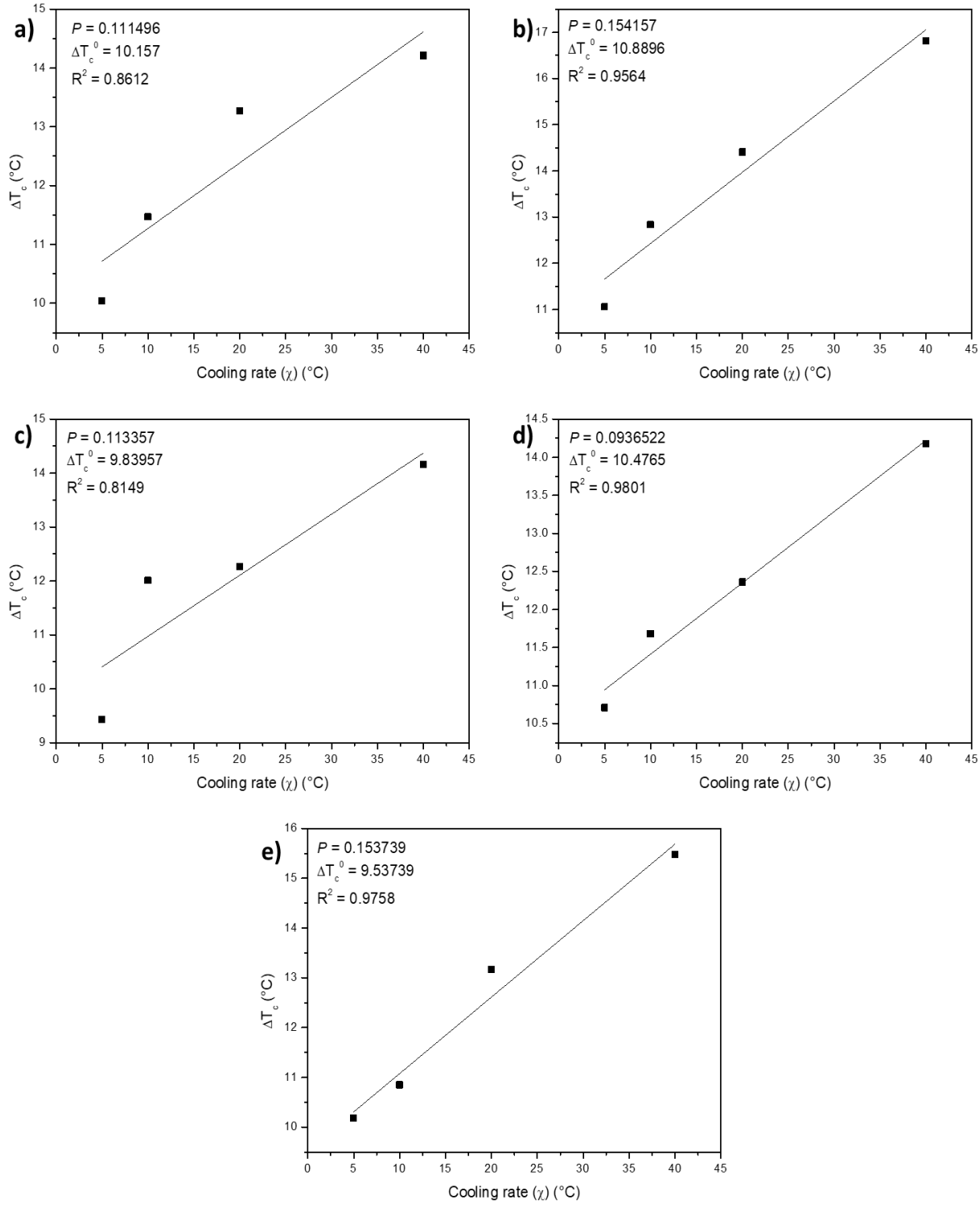

Figure 4. 9 Nadkarni plots for a) HF101 b) HF120 c) HF140 d) HR477 and e) LDPE

The second, more popular, method of analysing non-isothermal crystallisation kinetics is that of Ozawa[9], which is applicable for non-isothermal crystallisation at a constant cooling rate. In Figure 4.10 a-e the double logarithm of the relative amorphous fraction was plotted as a function of the logarithm of the cooling rate (χ) and the resultant slope is the Avrami index (n) while the intercept is known as the cooling crystallisation function (K*).[9]

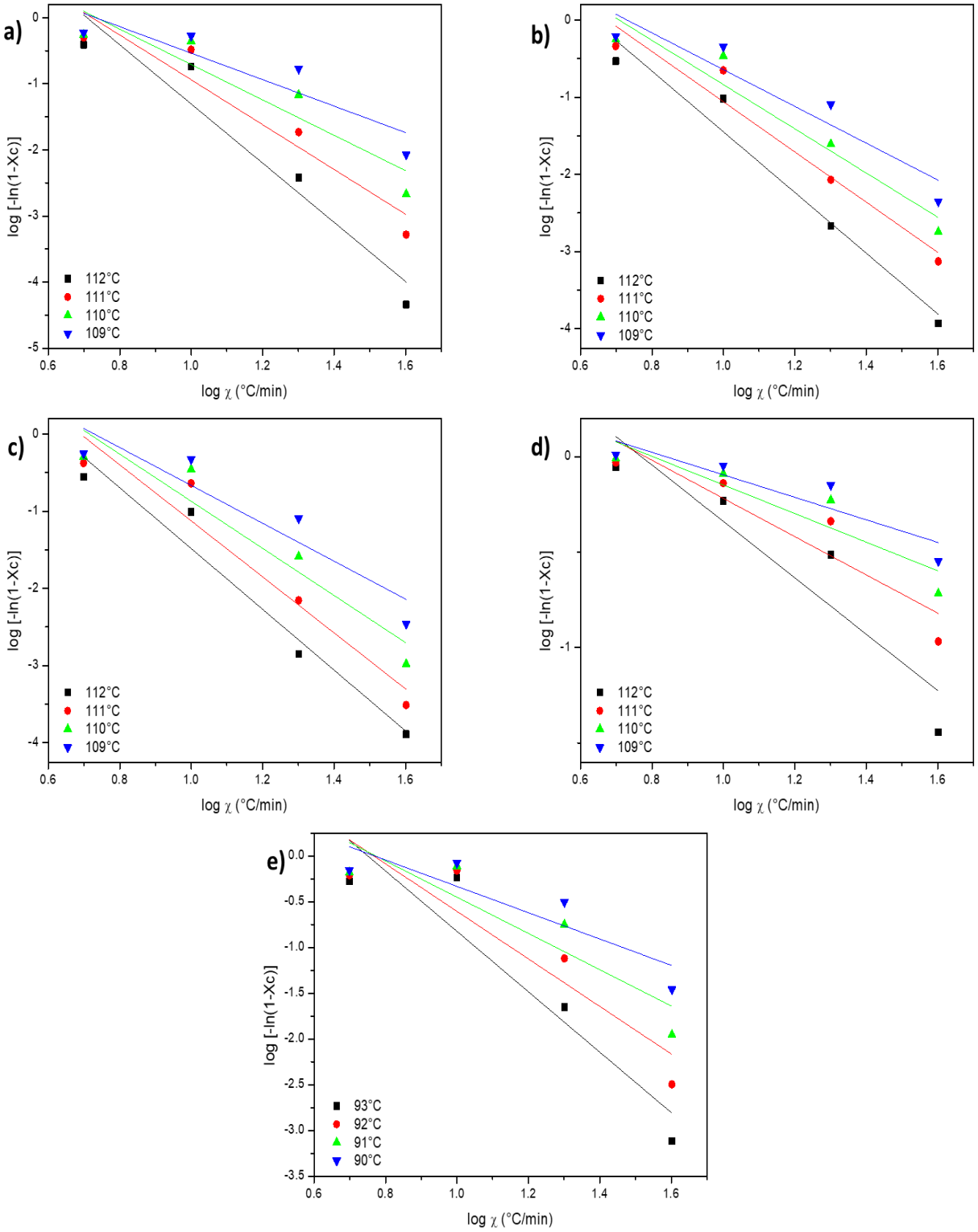

Figure 4. 10 Ozawa plots for a) HF101 b) HF120 c) HF140 d) HR477 and e) LDPE

Table 4. 4 Ozawa fitting parameters for neat polymers

Sample	Temperature (°C)	*n*	K* (°C.min)	R^2
HF101	112	4.48	3.17	0.93
	111	3.39	2.45	0.91
	110	2.68	1.97	0.87
	109	2.00	1.47	0.82
HF120	112	3.93	2.48	0.96
	111	3.25	2.19	0.95
	110	2.86	2.03	0.94
	109	2.38	1.74	0.89
HF140	112	3.93	2.45	0.96
	111	3.63	2.50	0.94
	110	3.05	2.18	0.91
	109	2.45	1.78	0.87
HR477	112	1.48	1.14	0.86
	111	1.00	0.78	0.86
	110	0.75	0.60	0.85
	109	0.59	0.49	0.83
LDPE	93	3.30	2.48	0.88
	92	2.60	1.99	0.85
	91	1.98	1.53	0.81
	90	1.44	1.11	0.78

The Avrami indices in Table 4.4 for the HF101, HF120 and HF140 indicate that the crystals grow sporadically in three dimensions above 112 °C. Between 111 and 110 °C the *n* value changes to approximately 3, suggesting simultaneous growth in three dimensions.[10] This was in agreement with the SEM images in Figure 4.5 which showed spherulitic structures for these grades of LLDPE. At 109 °C the *n* value decreased to 2, suggesting simultaneous growth in two dimensions. Axialites were, however, not observed in the SEM images of the LLDPEs. For the LDPE the Avrami index at 93 °C suggested sporadic growth in two dimensions which agreed with the two dimensional axialites seen in Figure 4.5 a. At 92 °C the Avrami index can be approximated to 2.5, which was an indication of nucleation which was intermediate between sporadic and instantaneous and growth in two dimensions, which still agreed with the morphology as seen in the SEM image. Similarly the *n* value of 2 suggested instantaneous growth in two dimensions. At 90 °C the *n* value could be approximated to 1.5 which is indicative of rod-like structures. This did not agree with the SEM image in Figure 4.5, which suggests that a temperature limit exists in which the Ozawa method is effective. This is validated by the decrease in R^2 with temperature in Table 4.4. This means that the range over which the Ozawa method is accurate is very limited and seems to be more effective at lower crystalline conversions. Since the *n* value contains information about nucleation the inability of the Avrami index to accurately describe the system at lower temperatures suggests that nucleation is not a dominant factor at lower temperatures. This is supported by the Keith-Padden theory which implies that low temperature crystallisation is dominated by diffusion while at high temperatures the nucleation rate is the more important factor.[10]

For the HR477 grade LLDPE none of the Avrami indices (which were all below 2) agreed with the spherulitic morphology observed by SEM. Due to the high crystallinity of the HR477 grade it was likely that the ideal temperature range in which the Ozawa method was valid had already been exceeded. Therefore the analysis was repeated using higher temperatures

as shown in Figure 4.11. The R^2 values for the HR477 fitting in Table 4.5 are slightly higher than those in Table 4.4 which suggested a better fit was obtained at higher temperatures or lower crystalline conversions. This supported the idea of a very narrow temperature range over which the Ozawa method could be applied.

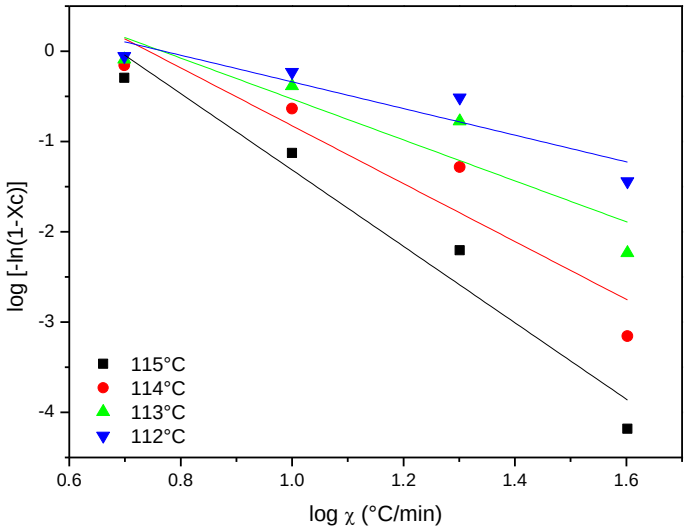

Figure 4. 11 HR477 Ozawa plot at higher temperatures

Table 4. 5 Ozawa fitting parameters for HR477 grade LLDPE

Temperature (°C)	*n*	K* (°C.min)	R^2
115	4.23	2.92	0.96
114	3.21	2.38	0.90
113	2.27	1.74	0.86
112	1.48	1.14	0.86

The non-isothermal crystallisation analysis appeared to be in good agreement with the SEM images shown in Figure 4.5, since the samples were not crystallised under isothermal conditions. Another reason for the better agreement between the Ozawa model and the experimental results than the Avrami model could also be the insignificance of the slower process of secondary crystallisation under non-isothermal conditions.[9] Under isothermal conditions secondary crystallisation plays a larger role and is not considered by the Avrami equation. This was possibly why the Avrami model could not effectively describe the neat polymers under isothermal conditions.

Another method which aided in understanding the non-isothermal kinetics of the neat polymers was the Scalls method introduced in Section 4.1.3. The Scalls method with the response from all three laser wavelengths was used to provide insight into the rate of dissolution of LDPE, this is shown in Figure 4.12. Since interaction between the laser light and the crystallites can only occur when the size of the crystallites are of the same order as the wavelength of the light, it follows that during dissolution the crystals begin as large particles which were first detected by the red laser. As the crystals became smaller in size the response of the lower wavelengths became more dominant from green to blue. The shifts in the dissolution events for the different laser wavelengths is therefore an indication of the dissolution rate. The inclusion of all three wavelengths of laser light explained the

contradiction of LDPE complexity in the melt and simplicity in solution; since the heterogeneity of the LDPE was mostly detected by the 635 nm wavelength whereas the dissolution profiles in Figures 4.3-4.4 compared only responses from the 405 nm wavelength. This indicated that the heterogeneity in the LDPE occurred on a larger scale than the heterogeneity in the LLDPEs.

From Figure 4.12 it appears that the crystals remain large until approximately 65 °C as there was a measurable response from the red laser but the green and blue lasers remained saturated as a result of large crystal sizes being greater than the limit of detection for the lower wavelength lasers. After 65 °C dissolution occurred rapidly in the range of 60 – 80 °C, as was indicated by the proximity of the blue dissolution peak to the green dissolution peak. In comparison, the signals from the three wavelengths overlap for all of the LLDPE polymers (Figure 4.13) indicating that the dissolution event occurs so rapidly that there is no detectable lag in the responses of the different wavelengths. The crystallisation kinetics of the LLDPEs is therefore much more rapid than that of the LDPE which is likely to have a significant effect on the miscibility of the blends.

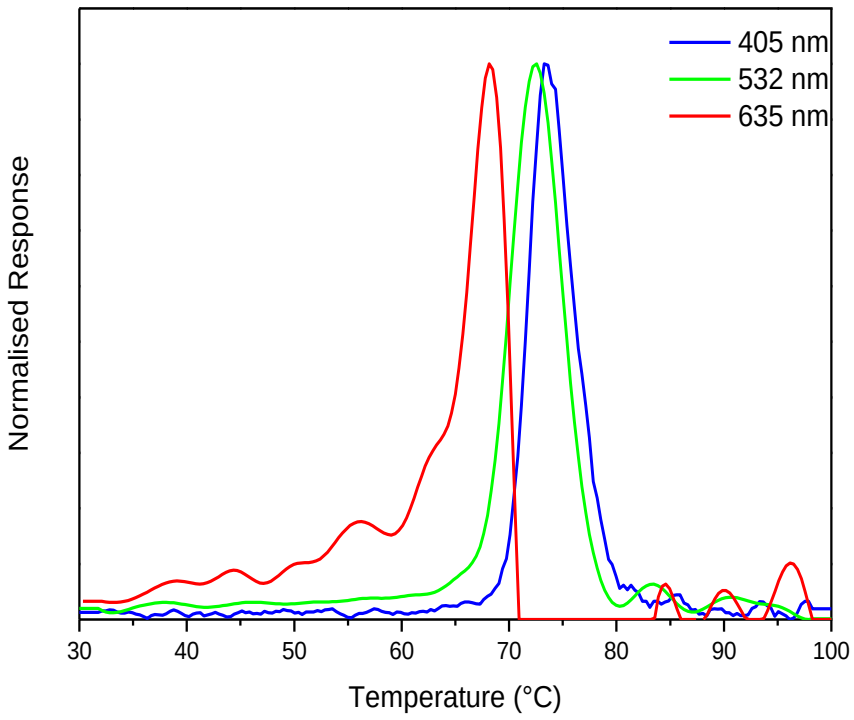

Figure 4. 12 SCALLS dissolution profile of LDPE at three different laser wavelengths (405 nm, 532 nm and 635 nm)

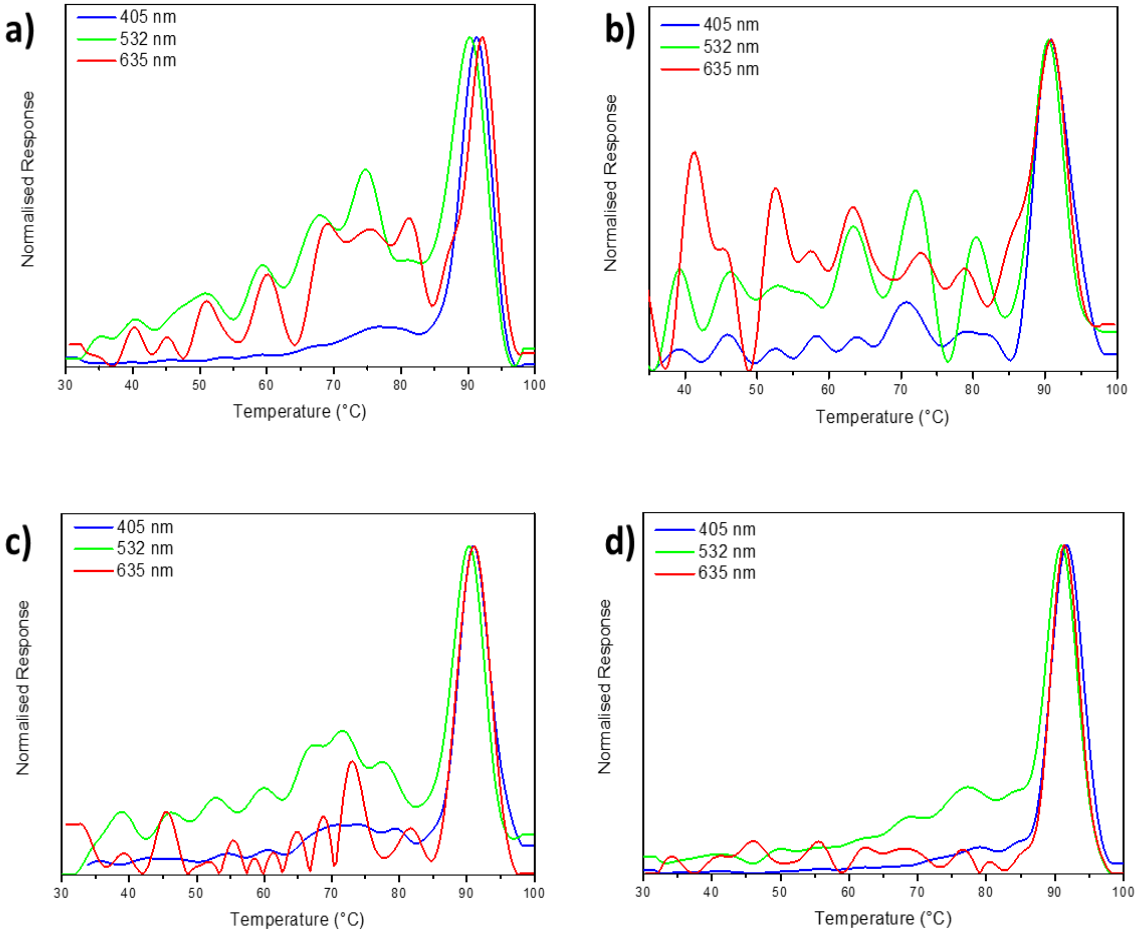

Figure 4. 13 Scalls dissolution profiles of a) HF101 b) HF120 c) HF140 and d) HR477

4.4 Fractionation

Figure 4.14 shows the TREF profiles for the neat polymers. It was clear that for all polymers the higher crystallinity fractions made up the major components. For all grades of LLDPE the 80 °C and 100 °C fractions contributed more than 76 wt% of the polymer. The contributions of the various fractions is summarised in Table 4.6. These results suggested that the neat polymers consist largely of highly crystalline material. This was confirmed by the DSC curves of the TREF fractions, shown in Figure 4.15 and Figure 4.16. The DSC thermograms of the LDPE fractions show that the fraction eluting at 30 °C contains a fair amount of crystalline material which is greater than what can be explained by the very slow cooling process of TREF. The ability to crystallise suggests that this fraction contains chains with a lower branching density and a low molar mass. This agrees with the amount of low molar mass material seen in the SEC chromatogram of LDPE relative to the LLDPEs. In addition to the slow cooling effects of the prep-TREF process, fractionated materials will also behave differently from the bulk material simply because they are fractionated. Due to the differences in the chemical environments for an isolated fraction compared to the multiple effects at play in the bulk sample differences in crystallinity are inevitable. This implies that measured properties of the bulk material is not simply a summation of the measured properties of the fractions.

Table 4. 6 Percentage composition of various fractions within neat polymers obtained by TREF

Elution Temperature (°C)	Percentage composition (wt %)				
Grade	LDPE	HF101	HF120	HF140	HR477
30	1.4	3.9	6.1	3.3	0.4
60	20.8	13.2	14.0	12.8	4.6
80	76.6	30.8	38.9	32.3	22.4
100	0.8	46.8	37.4	44	66.2
130	0.3	5.3	3.6	7.6	6.5

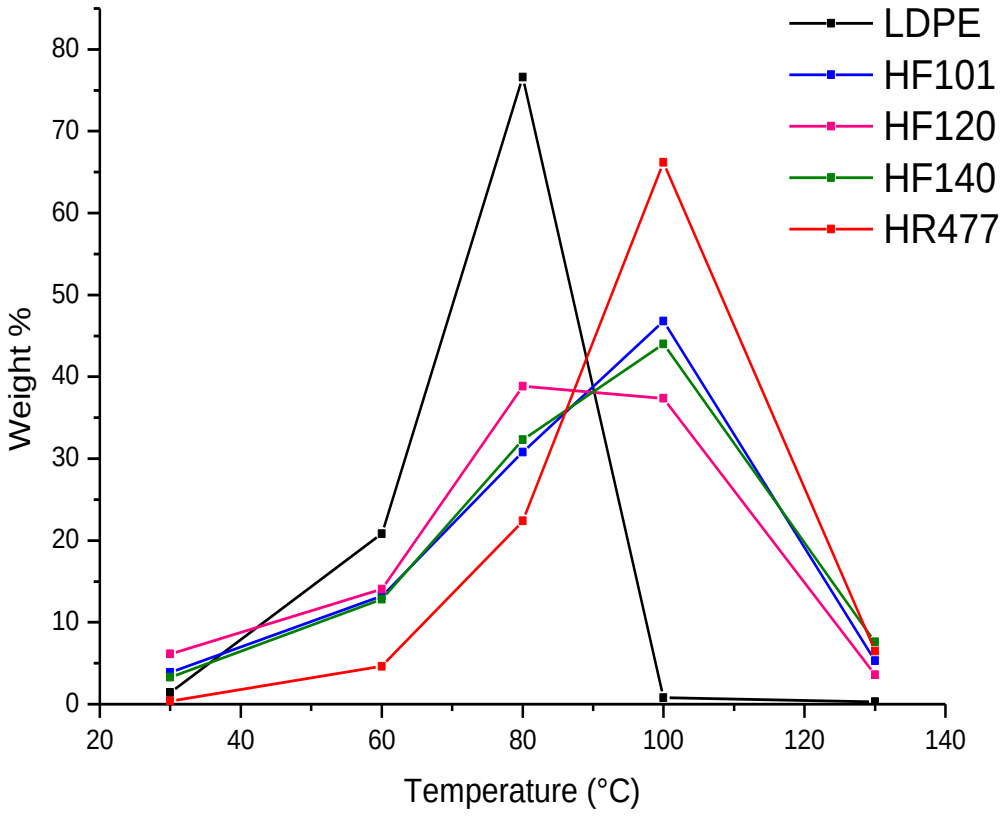

Figure 4. 14 TREF profiles of neat polymers

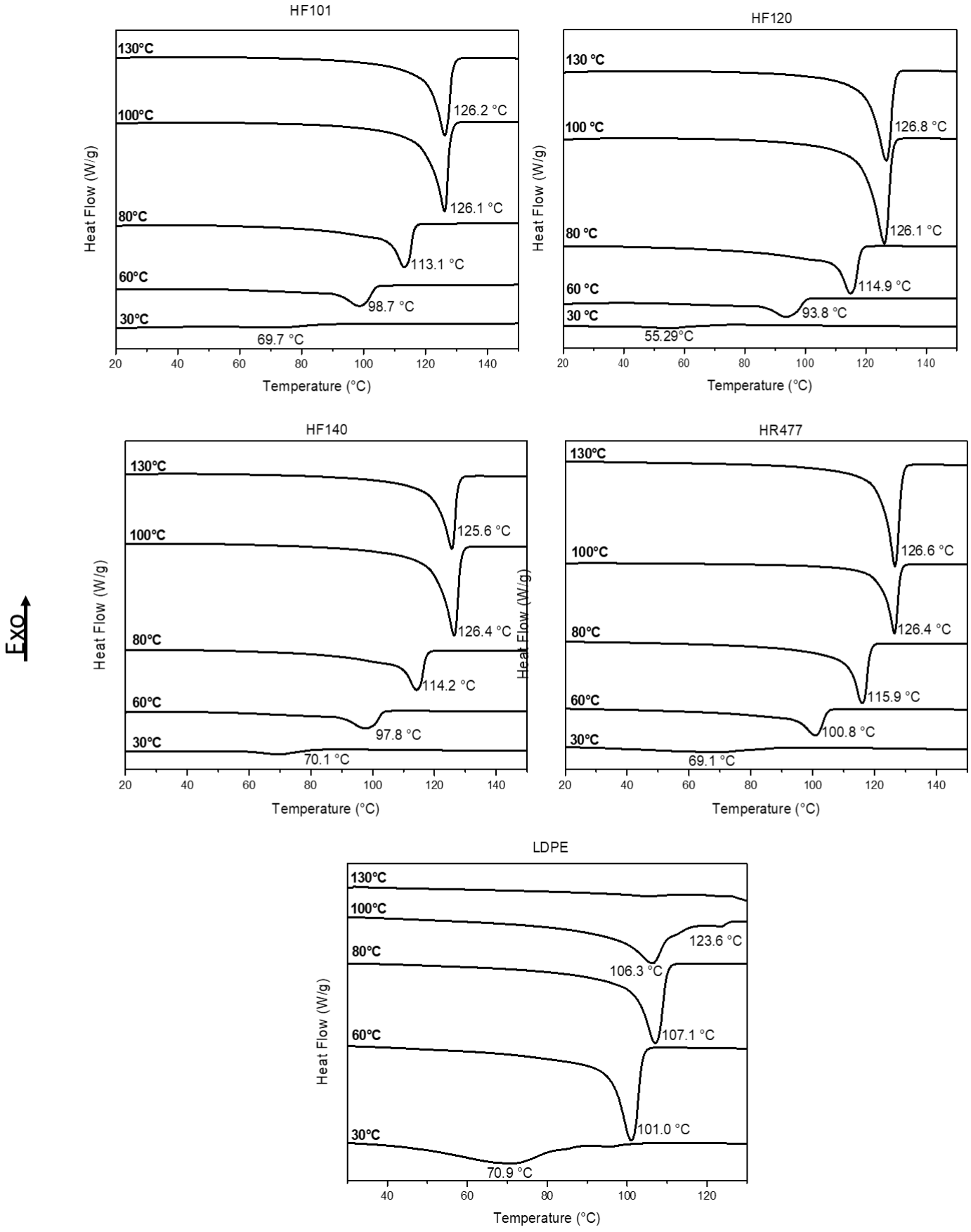

Figure 4. 15 DSC second heating cycle of neat polymer TREF fractions

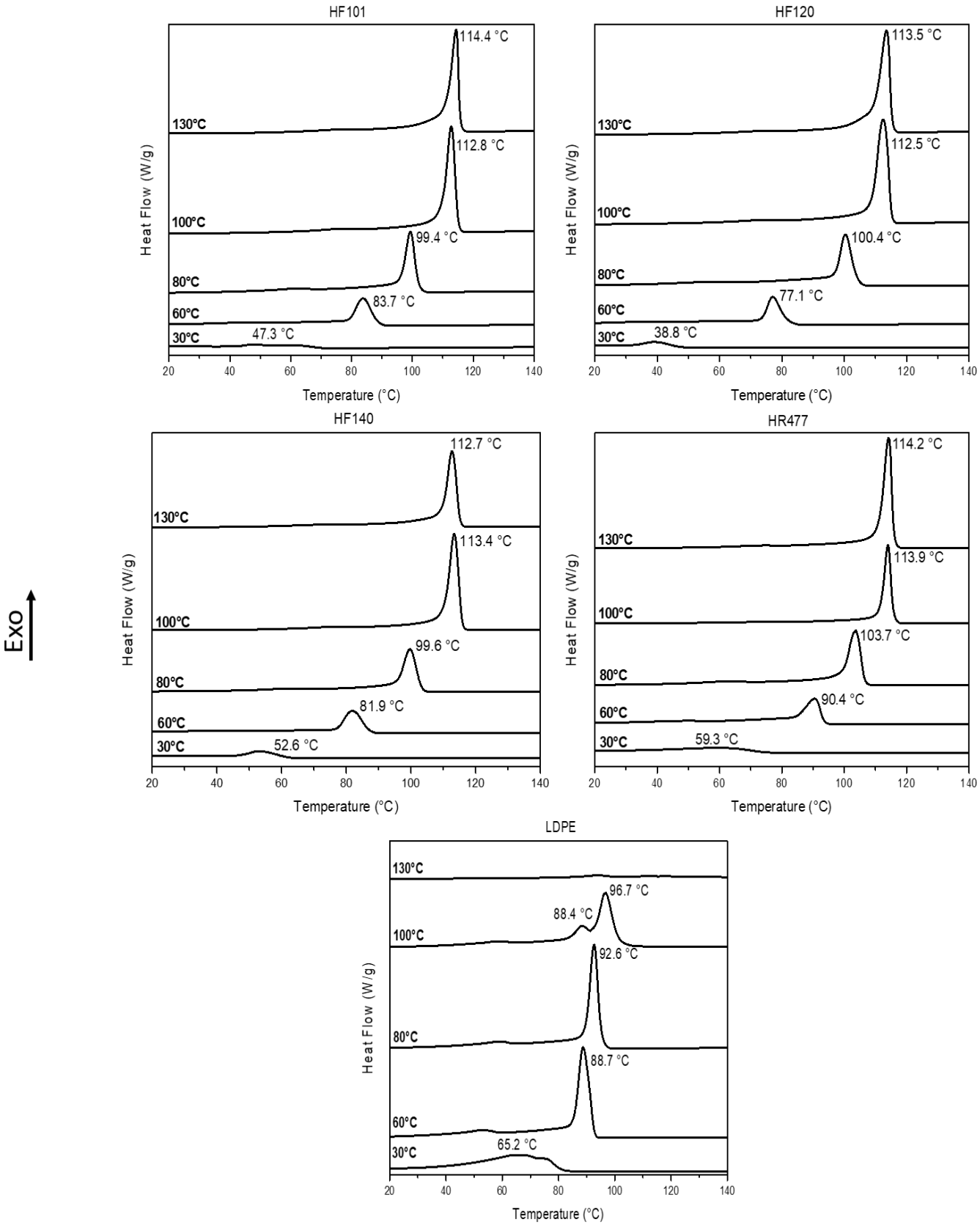

Figure 4. 16 DSC crystallisation cycle of neat polymers TREF fractions

The fractionation data of the LDPE polymer suggested that the full picture cannot be seen with the current number of fractions. Approximately 97 wt% of the polymer was contained within the 60 °C and 80 °C fractions. For this reason the LDPE TREF was repeated to obtain a greater number of fractions and greater insight into the composition of the 60 °C and 80 °C fractions. The contributions of the various fractions is summarised in Table 4.7 and the new TREF profile displayed in Figure 4.17. The 60 °C fraction appeared to be a true 60 °C fraction, contributing approximately 66% to the original 60 °C fraction. The original 80 °C fraction consisted mainly of a 70 °C fraction which also contains the majority of the LDPE polymer.

The DSC thermograms of the fractions in Figure 4.18 still display broad peaks. In addition, the fraction eluting at 90 °C contained two distinct components which are believed to have similar crystallinities but varying degrees of branching. This suggests that TREF alone is not an effective method for fractionating LDPE.

Table 4. 7 Percentage composition of LDPE obtained by TREF

Elution Temperature (°C)	Percentage Composition (wt %)
30	0.78
40	0.98
50	3.08
60	13.17
70	57.21
80	24.25
90	0.40
100	0.13

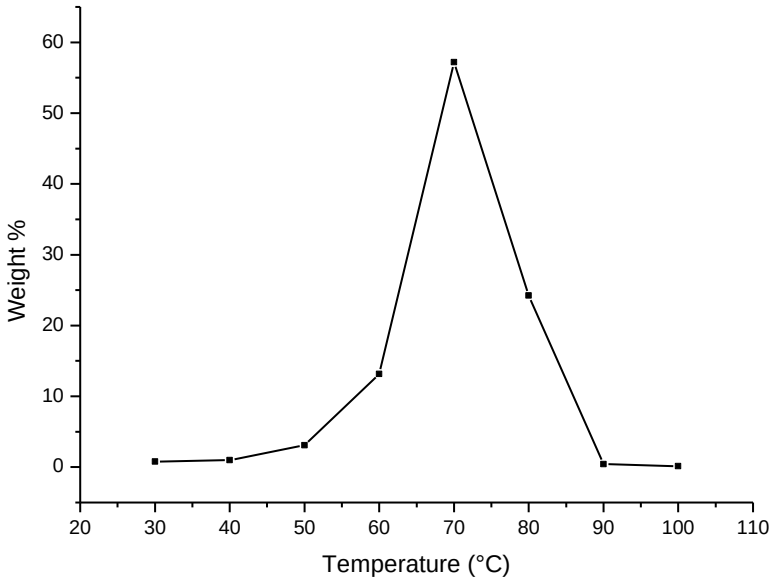

Figure 4. 17 TREF profile of LDPE with increased number of fractions

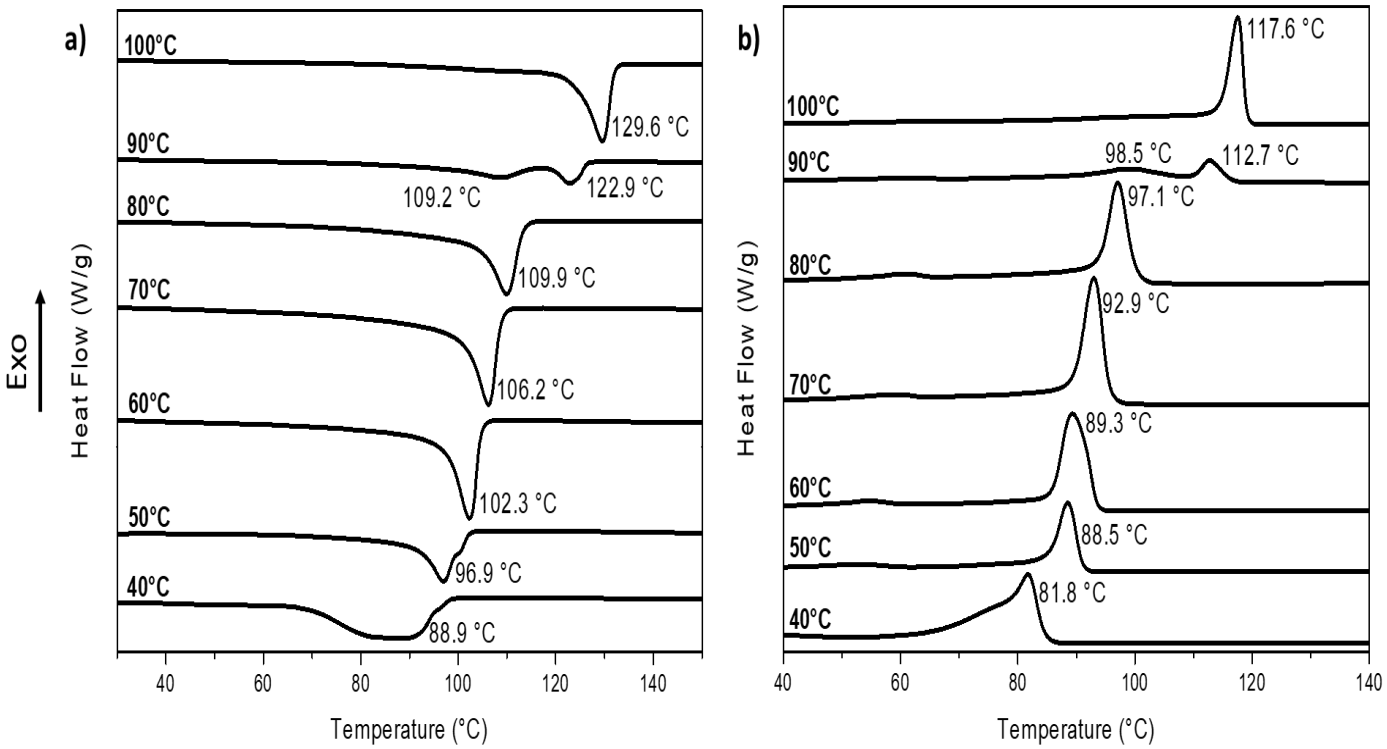

Figure 4. 18 DSC thermograms of a) second heating and b) crystallisation cycles of LDPE TREF fractions

Figure 4.19 displays the molar mass distributions of the LDPE TREF fractions obtained by SEC. The molar mass appeared to increase with elution temperature, excepting the fractions which eluted at 70 °C and 80 °C which had very similar distributions. The molar mass distributions for all fractions were fairly broad. The fractions eluting at 30 °C, 90 °C and 100 °C displayed bimodal distributions to increasing degrees with the 100 °C fraction possibly containing three regions of interest. The molar mass distributions of the fractions eluting at both 90 °C and 100 °C displayed significant similarities with the distributions of the fractions eluting at lower temperatures. The highest molar mass and the broadest distribution could be found in the fraction eluting at 100 °C. Table 4.8 also confirms the increase in molar mass and dispersity with increasing elution temperature, excepting the 80 °C fraction which had a lower dispersity index than the 70 °C fraction indicating a narrower molar mass distribution.

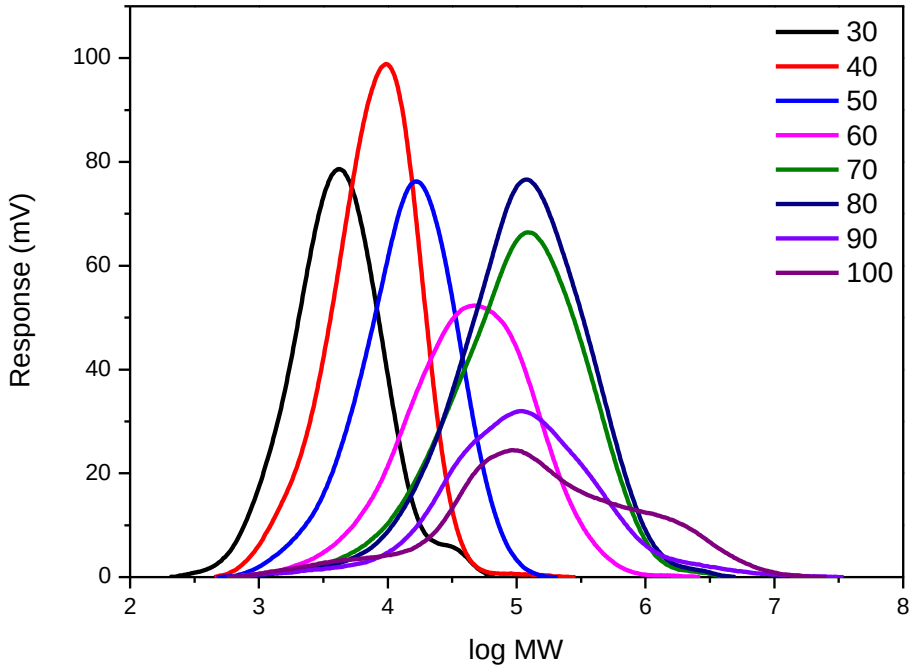

Figure 4. 19 Molar mass distributions of LDPE TREF fractions

Table 4. 8 Molar mass parameters of LDPE TREF fractions

Elution Temperature (°C)	M_w (g/mol)	M_n (g/mol)	Đ
30	6 149	3 130	1.96
40	10 611	5 858	1.81
50	20 267	9 871	2.05
60	75 120	22 226	3.38
70	173 895	41 195	4.22
80	185 027	47 942	3.86
90	269 720	38 385	7.03
100	499 928	33 364	14.98

From TREF it was clear that the neat polymers were heterogeneous in terms of crystallisable material. The TREF process is a solution based technique and since variations do exist for polymers between their solution and solid state behaviour it was important to compare the fractions obtained by a solid state fractionation technique. For solid state fractionation SSA was highly effective. The DSC heating scans following SSA fractionation for the neat polymers is shown in Figure 4.20. It is clear that the LLDPEs display less heterogeneity than the LDPE in terms of crystallinity as the LDPE thermogram showed multiple large melting peaks. Each melting peak in SSA is indicative of a group of similar methylene sequence lengths[11] (MSLs). The MSL distribution within each TREF fraction was determined according to the method of Zhang and Wanke[12] and is explained in Chapter 2. The MSL distributions of the neat polymers is shown in Figure 4.21. Despite the small contributions of the lower melting peaks, the LLDPEs do display broad ranges of MSLs from 40 to 194, indicating heterogeneous branching distributions. The LDPE appears to have the most limited range of MSLs however the relative contributions of the lower temperature LDPE fractions was

greater than the contributions of the lower temperature fractions of the LLDPEs. The SSA of the bulk LDPE polymer did not suggest as much heterogeneity as was suggested from the analysis of the TREF fractions. This was most likely due to the effect of the TREF process itself. As mentioned before, TREF is a fractionation process which occurs in solution while SSA is a solid state fractionation technique. The differences in degrees of mobility is vastly different between these two processes. In addition the cooling rate during the TREF process was approximately 600 times slower than the cooling process in SSA which allows most of the material to crystallise which would not do so under normal conditions.

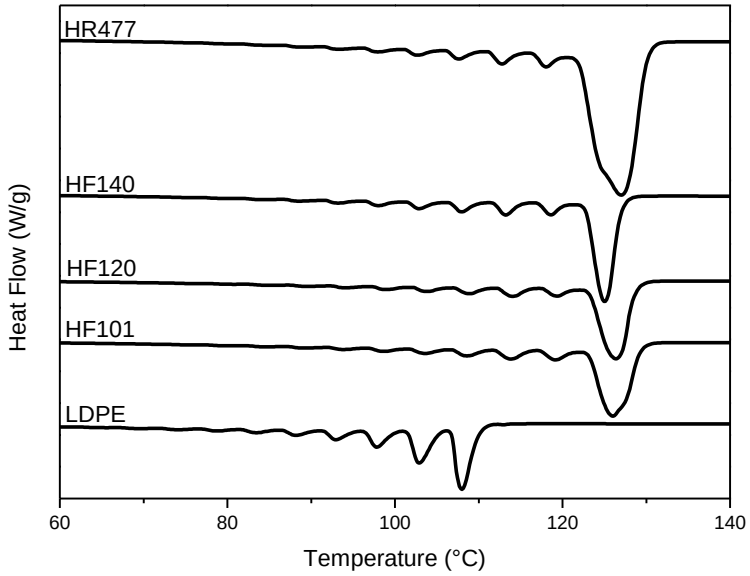

Figure 4. 20 DSC heating scans of neat polymers after SSA fractionation

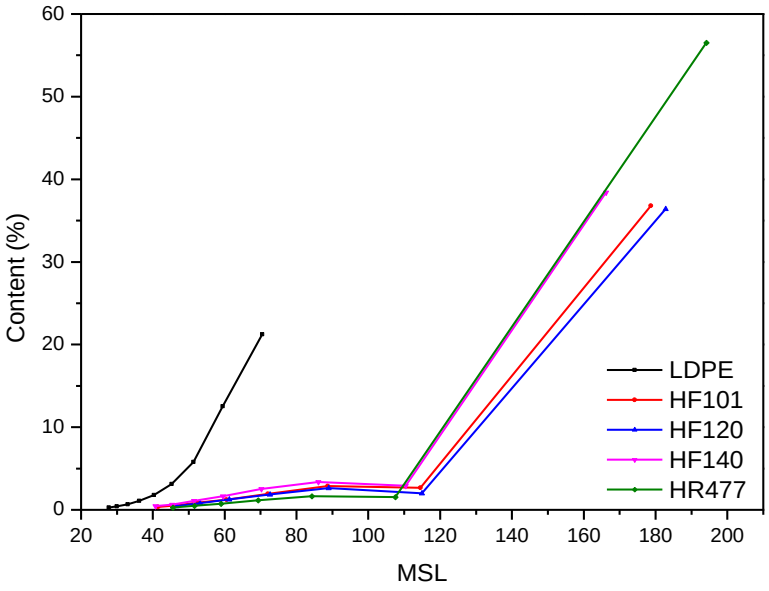

Figure 4. 21 Methylene sequence length distributions of neat polymers

Due to the greater heterogeneity of the LDPE polymer relative to the LLDPEs, SSA was also performed on the TREF fractions, which yielded more insight than performing SSA on the bulk material. The heating cycle after SSA fractionation for the various TREF fractions is shown in Figure 4.22. All LDPE fractions below 100 °C displayed broad melting endotherms and multiple melting peaks indicating significant amounts of different MSLs. The MSL distributions can be seen in Figure 4.23. In Figure 4.23 the span of the distribution increases with increasing elution temperature of the LDPE fractions. Despite the difference in the distribution profiles the 40 °C, 50 °C and 60 °C TREF fractions span a similar amount of MSLs. The MSL of the 40 °C fraction ranges from 23 to 50 with peak MSL at 36. The 50 °C fractions contains MSL in the region of 30 to 58 and peaks at MSL of 45 while the 60 °C fraction ranges from MSL of 36 to 59 and peaks at 59. The 50° C and 60 °C fractions were thus very similar in their MSLs and only varied in the relative contributions of those MSLs. The broadest distribution of MSLs was found within the 100 °C fraction with MSL varying from 52 to 271, with 271 comprising 57% of the fraction. The effect of the TREF process was again visible in the difference between the MSL maxima of the isolated TREF fractions compared to the maximum MSL obtained in the bulk material. In Figure 4.21 the maximum MSL in LDPE was 70, however after fractionation MSLs of above 200 were obtained (Figure 4.23). Apart from the effect of the TREF process it is also possible that the difference in MSL was due to interactions between the less crystalline and more crystalline components. By separating those components during fractionation the interactions would be eliminated and the crystalline material is left to crystallise to a greater extent. This idea was supported by the molar mass distributions given in Figure 4.19 which shows that the molar mass distribution of the 100 °C fraction overlapped with those of all the fractions eluting at lower temperatures. In addition, the molar mass range of the TREF fractions (~316 – 22 980 000 g/mol) was broader than that of the unfractionated LDPE (~1000 – 390 000 g/mol) which suggested that these interactions even prevented complete molar mass fractionation during SEC.

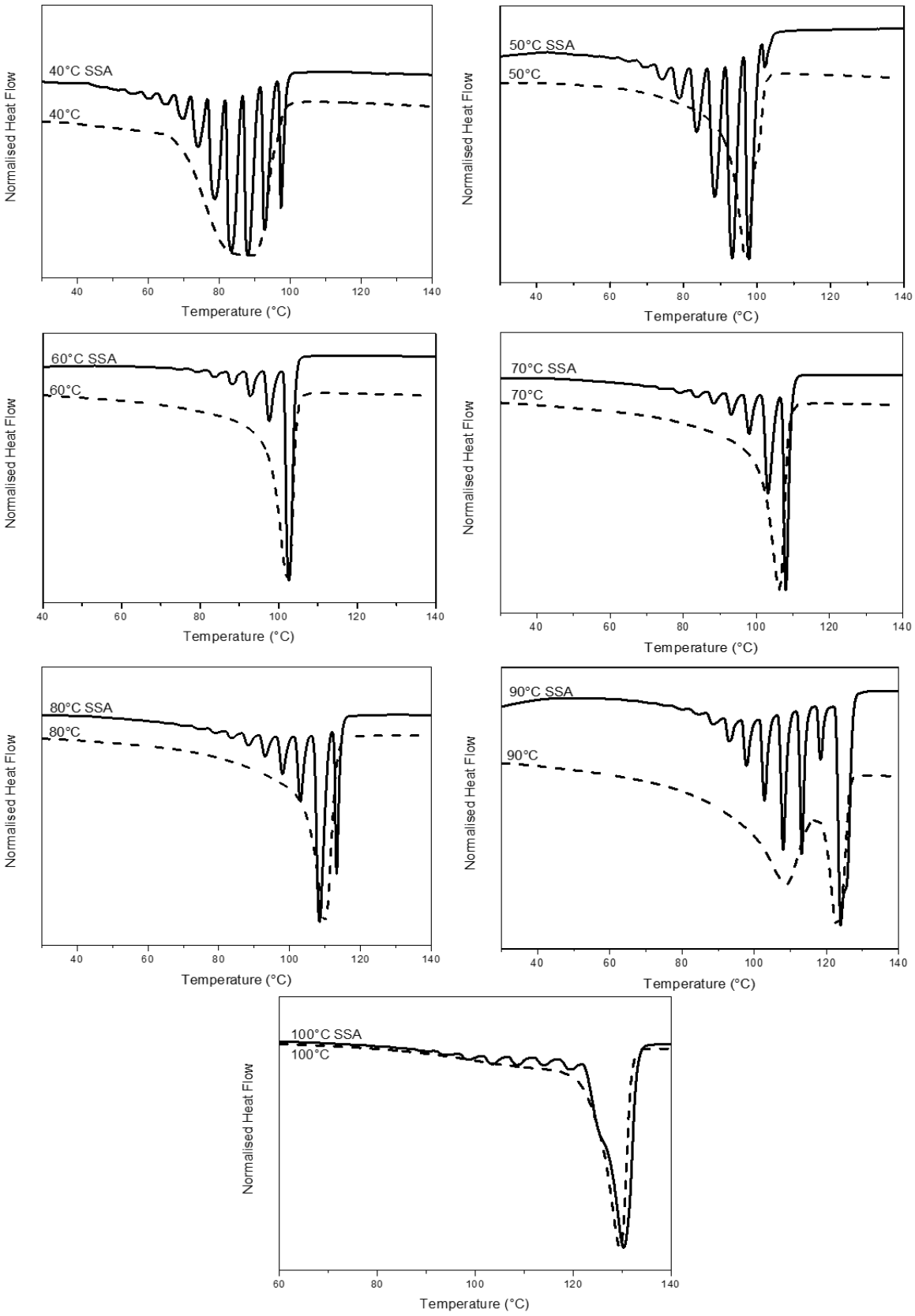

Figure 4. 22 Comparison of DSC second heating cycle of LDPE TREF fractions to heating cycle after SSA fractionation

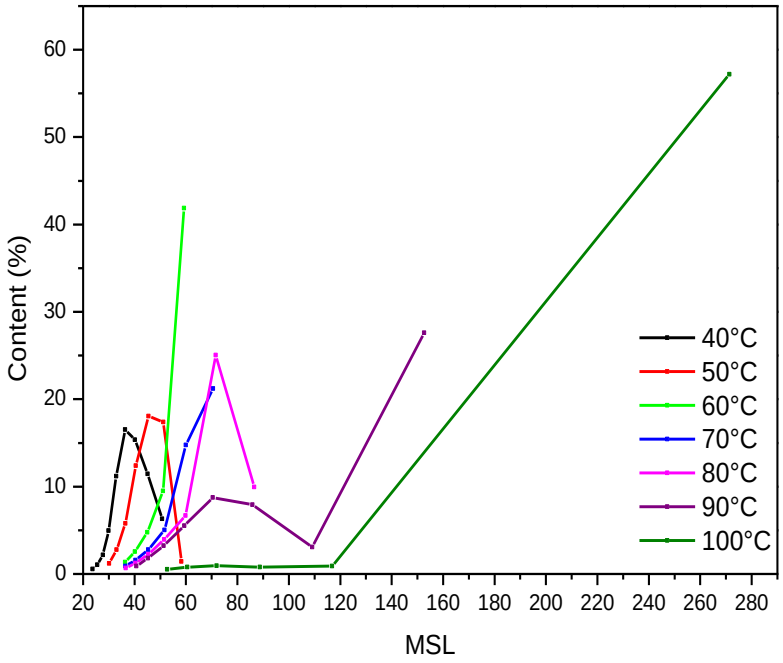

Figure 4. 23 Methylene sequence length distributions for LDPE TREF fractions

4.5 Mechanical Properties

The average tensile modulus for the neat polymers is listed in Table 4.9. The average tensile modulus was much greater for the LLDPEs than the LDPE. This was expected as LLDPE is commonly added to LDPE to increase the strength of the LDPE films.[13] Tensile moduli appeared to correlate with crystallinity as determined by DSC (see Figure 4.24), excepting the HF120 grade LLDPE which showed a greater modulus than was expected for its degree of crystallinity.

Table 4. 9 Average tensile modulus of neat polymers

Grade	Average modulus (MPa)
LDPE	148.71
HF101	275.07
HF120	270.99
HF140	239.21
HR477	321.97

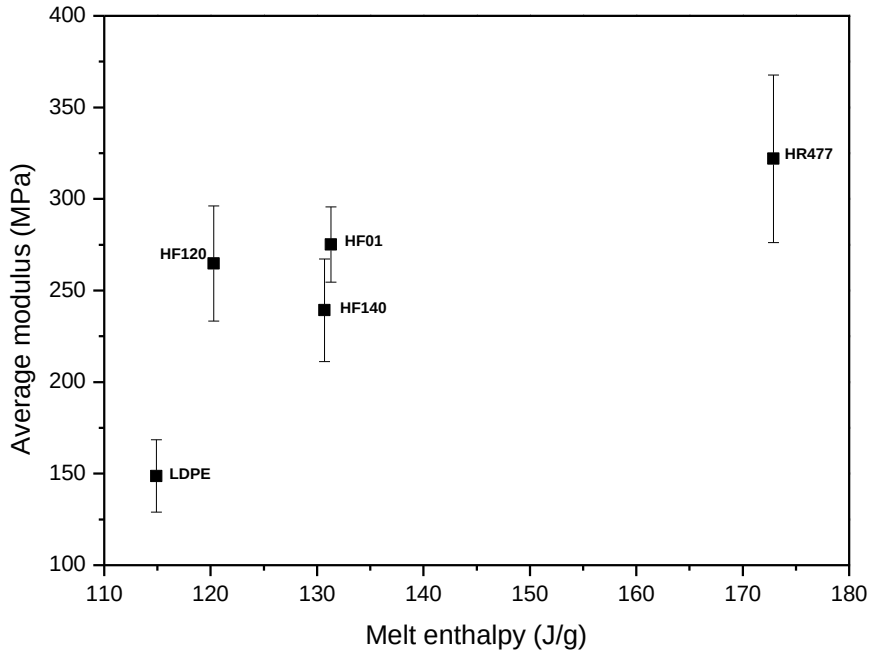

Figure 4. 24 Relationship between tensile modulus and crystallinity for neat polymers

The exception that the HF120 grade presented suggested that crystallinity was not the only parameter affecting the tensile properties. Thus the effect of molar mass on the tensile modulus was also considered and is shown in Figure 4.25. From Figure 4.24 it appeared that the modulus mostly follows the crystallinity trend. As mentioned, the HF120 was an outlier. The HF120 also had the largest value for molar mass which suggests the possibility of molar mass limits. It may be that at lower molar mass crystallinity plays a dominant role in the tensile properties while above a certain high molar mass limit the molar mass then becomes the dominant effect. In contrast, the stress at maximum load did not follow a clear crystallinity trend but rather showed an almost linear correlation with molar mass (Figure 4.26). It therefore seemed that the dominance between crystallinity and molar mass not only displayed a molar mass dependence but was also dependent on the extension of the tensile sample.

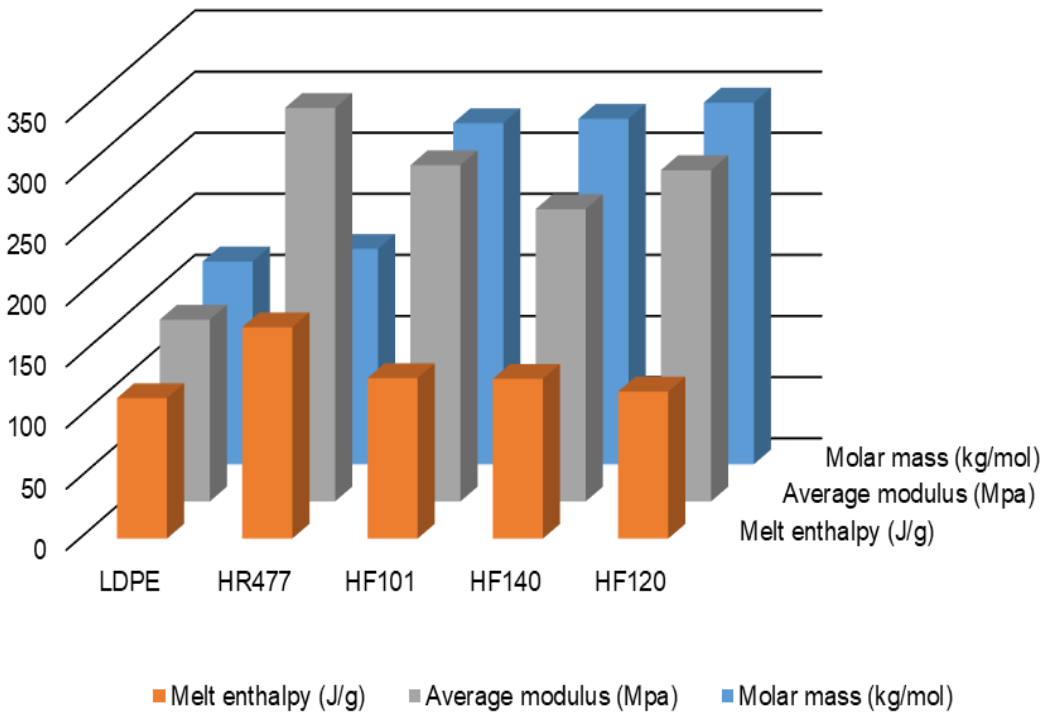

Figure 4. 25 Relationship between crystallinity, average tensile modulus and molar mass for neat polymers

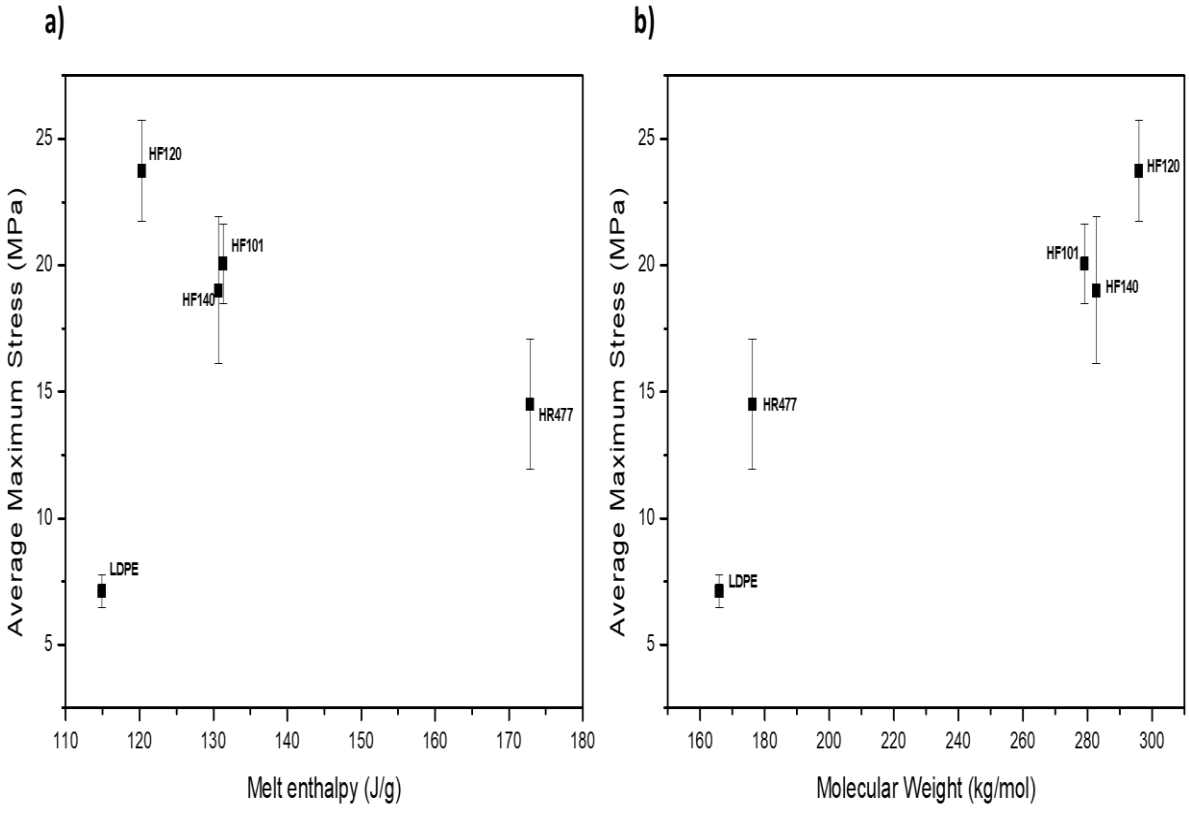

Figure 4. 26 Stress at maximum load as a function of a) crystallinity and b) molar mass

In addition to the absolute values for mechanical strength, it was also important to discern the mechanism through which stress is dissipated within the polymer. Polymers usually exhibit two possible yielding mechanisms known as shear yielding and crazing. Although crazing occurs mainly in polymers which display brittle fracture and shear yielding is common to those which fracture in a ductile fashion it is not necessary for these processes to occur exclusively.[14] The polyethylenes in this study displayed shear yielding, which could be characterised by the formation of a necked region beyond the yield point (Figure 4.27).

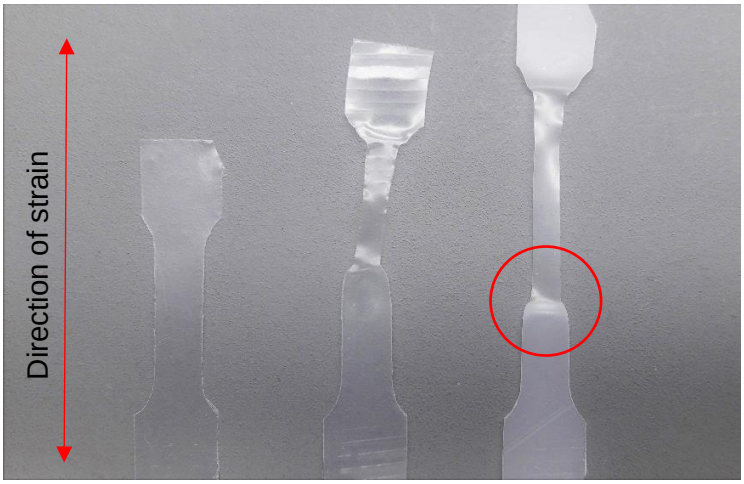

Figure 4. 27 Example of tensile samples at varying degrees of extension

Another characteristic of shear yielding is the formation of shear bands which are oriented in the direction of the highest shear stress.[14] Interestingly, this can be monitored by polarised optical microscopy (POM), as shown in Figures 4.28 – 4.30. For analysis by POM all tensile samples were drawn to 50% extension an example of which is shown on the far right in Figure 4.27. The circled region in Figure 4.27 indicates what is referred to as the transition zone.

The technique of photo elasticity allows the measurement of stress and strain through the birefringence of materials which can be viewed under polarised light. This technique is widely used in the engineering of various machine components by modelling where the greatest stress would occur in a material by applying a similar load to a photo elastic coating which demonstrates birefringence under polarised light, allowing the engineers to compensate for regions of high stress or save material in regions of low stress.[15] The birefringence pattern, which occurs as a series of successive colourful bands which occur as a result of the varying degrees of birefringence in the sample, yields a wealth of information through what is known as the 'fringe order' (*N*)which is related to both the Young's modulus (*E*) and the stress (σ) through the stress-optic law:[16]

$$\sigma = \frac{E}{1+\nu}\frac{N\lambda}{h\kappa} \tag{4.1}$$

where ν is the Poisson ratio, λ is the wavelength of the light and *h* and κ are the sample thickness and the strain-optic coefficient respectively.

A diagram illustrating the relationship between the fringe order and stress is shown in Figure 4.28.

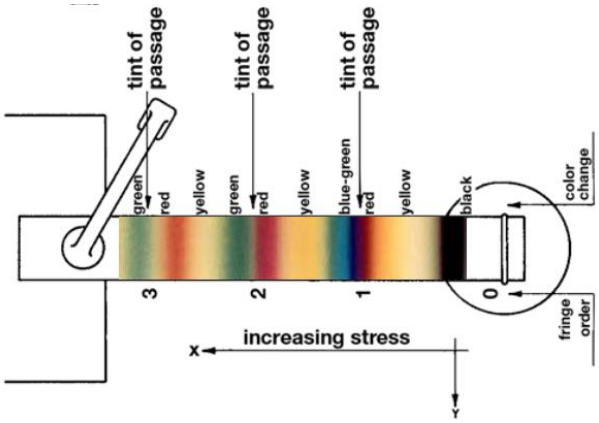

Figure 4. 28 Relationship between fringe order and stress[17]

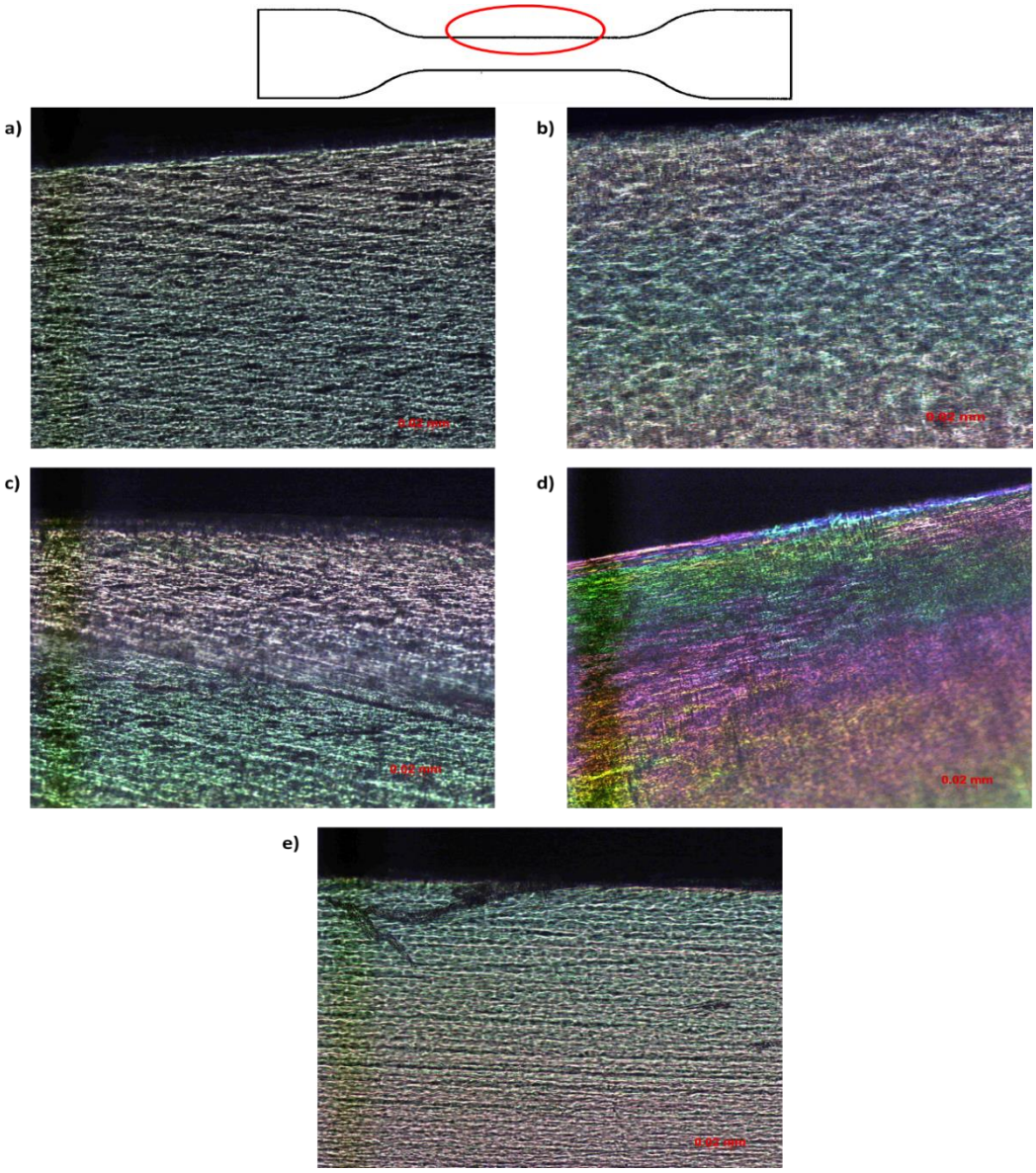

Figure 4. 29 Polarised optical microscopy images of edge of centre of necked region of tensile samples for a) HF101 b) HF120 c) HF140 d) HR477 and e) LDPE

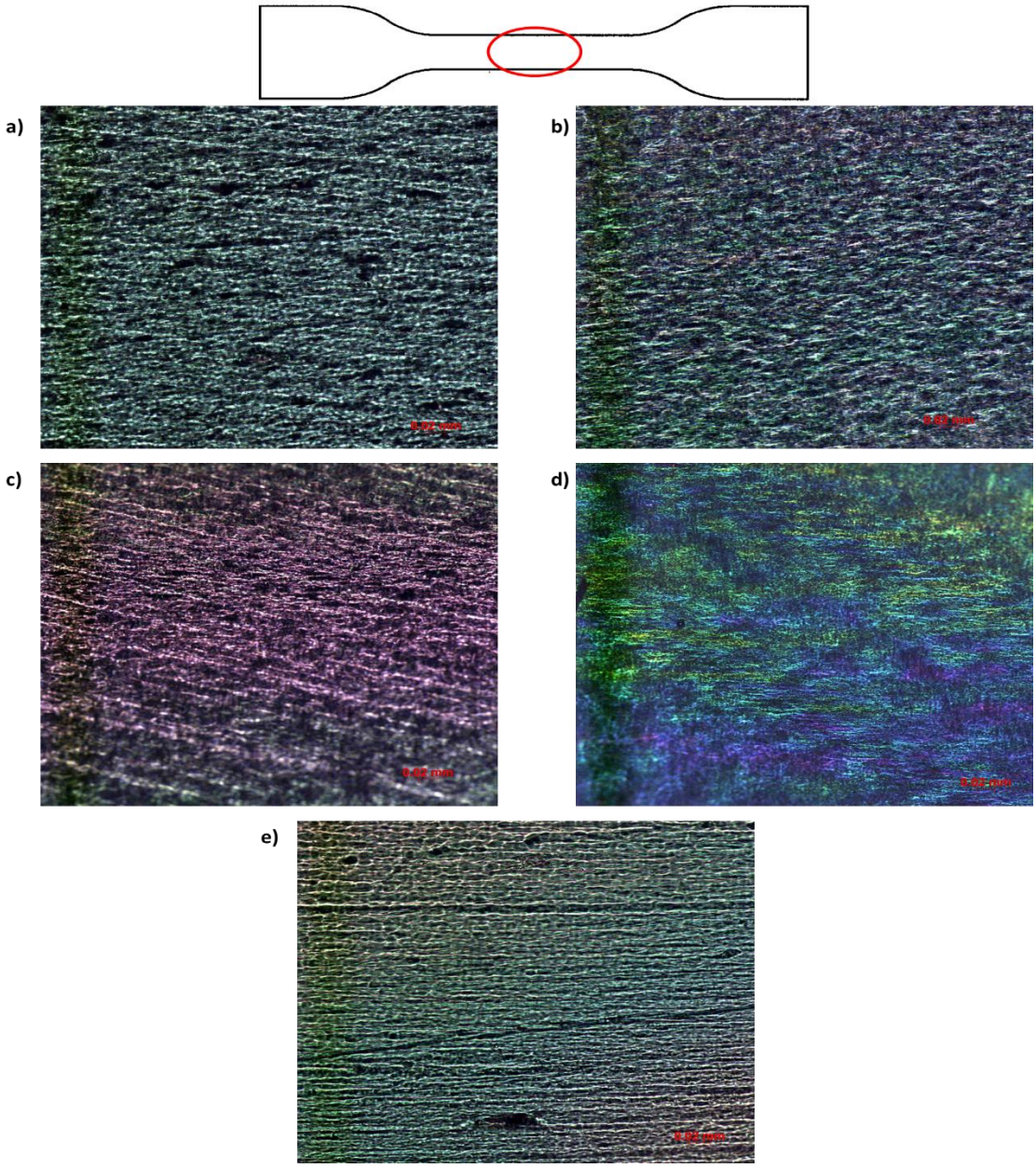

Figure 4. 30 Polarised optical microscopy images of centre of necked region of tensile samples for a) HF101 b) HF120 c) HF140 d) HR477 and e) LDPE

It appeared, from Figures 4.28 – 4.30, that different regions within the sample experienced varying levels of stress which caused variations in the extent of orientation in different regions of the sample during cold drawing. These differences could be visualised in the different colours seen by POM. It has been shown that the birefringence of polyethylene films is due to orientation of the crystalline regions geometrically and not due to stress deformations.[18,19] For this reason the unstressed films in Figure 4.31, which were unoriented, did not display the same extent of birefringence as the tensile tested samples.

In Figure 4.28 a, b, c and e the tensile sample displayed a transition from a dull red colour to a blue colour which indicated low stress concentrations since isochromatic fringes were not present. Figure 4.28 d shows a rainbow-like region which could be related to isochromatic fringe patterns indicating a greater degree of orientation.

The fringe pattern regions in Figure 4.31 were much more defined than in Figure 4.28 d and was most likely an indication of the shear banding which occurred during the tensile test and were usually located around the base of the necked region as illustrated by the diagram in Figure 4.31. Since shear bands are orientated in the direction of highest stress it was apparent from Figure 4.30 that the stress which the sample experienced was largely in the transverse direction to the applied force. Isochromatic fringes can be clearly seen in Figure 4.31 a, c and e in which both first and second order fringes can be seen according to the diagram in Figure 4.28.

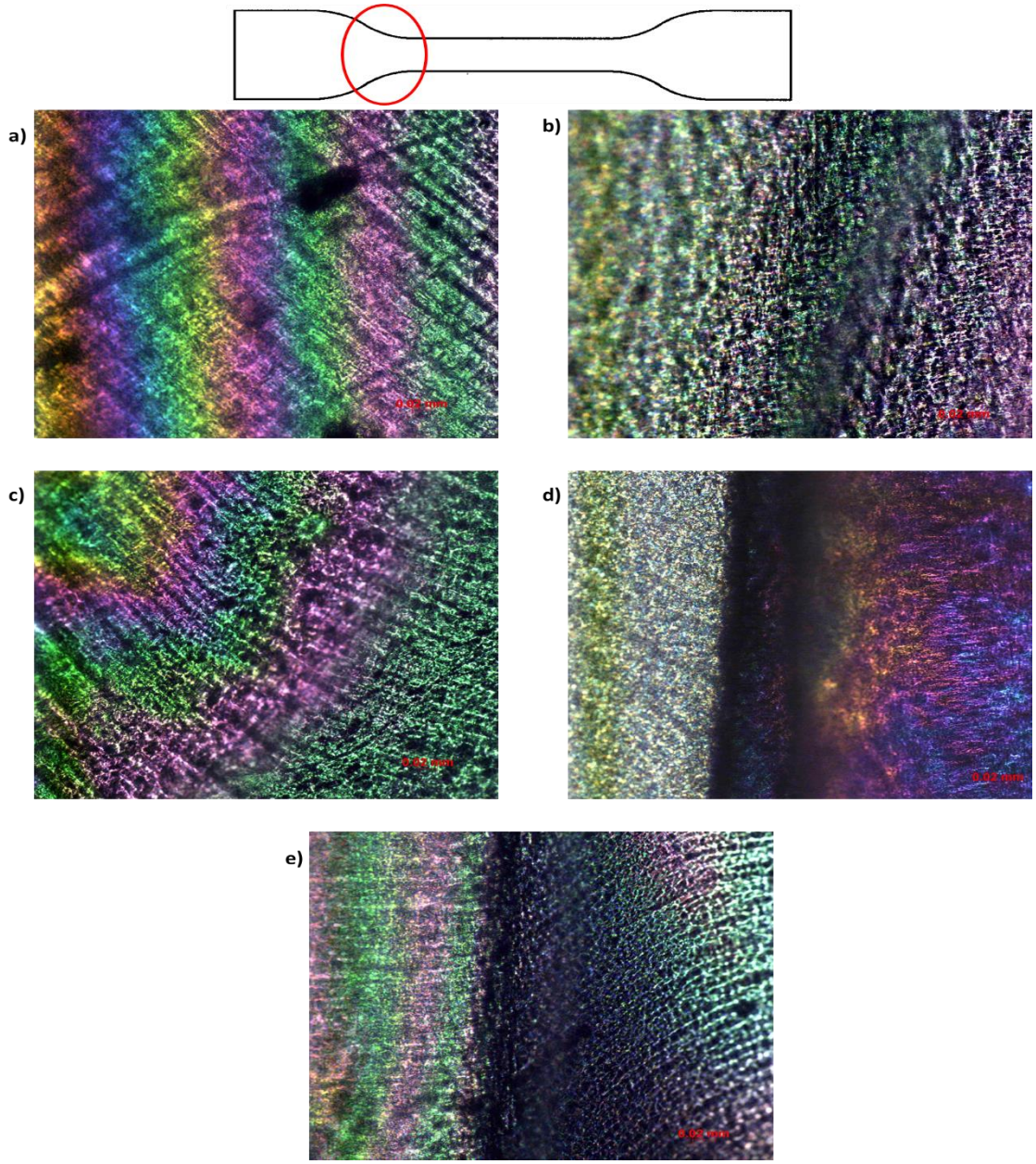

Figure 4. 31 Polarised optical microscopy images of unstressed-necked transition zone of tensile samples for a) HF101 b) HF120 c) HF140 d) HR477 and e) LDPE

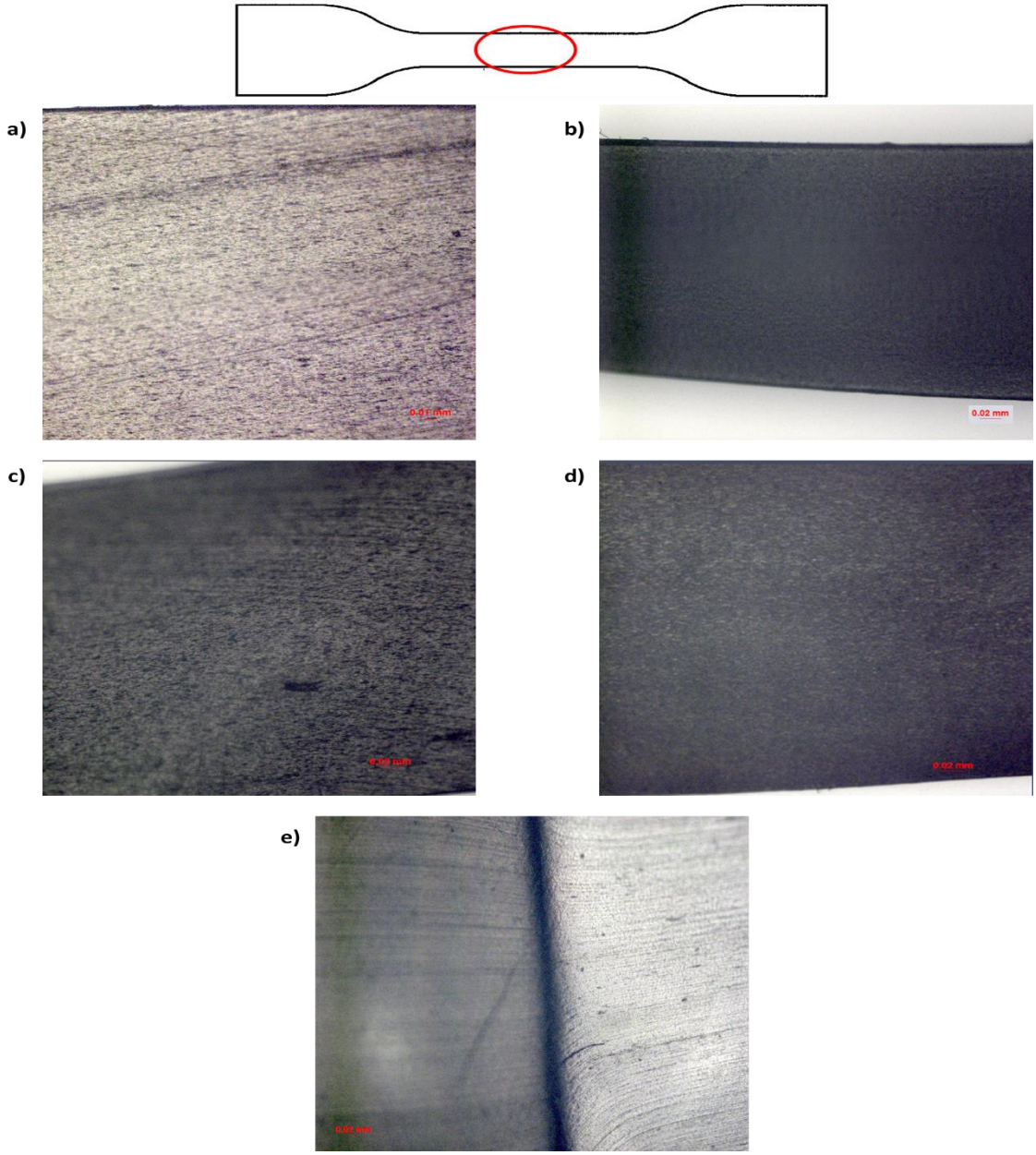

Figure 4. 32 Polarised optical microscopy images of centre of unstressed tensile samples for a) HF101 b) HF120 c) HF140 d) HR477 and e) LDPE

Differences could also be seen by FTIR spectroscopy as shown in Figure 4.33. The spectra in Figure 4.33 are focussed on the lower wavenumbers, specifically the methylene scissoring mode[20] at approximately 1460 cm^{-1} as well as the methylene rocking of crystalline regions at approximately 720 cm^{-1} and the shoulder on this peak at approximately 730 cm^{-1} which corresponds to the methylene rocking of ethyl branches.[21] The crystalline regions contribute equally to both the 720 and 730 cm^{-1} peaks while the amorphous regions only contribute to the peak at 720 cm^{-1}.[19] In Figure 4.33 a-d the shoulder on the 720 cm^{-1} peak appeared to decrease from the unstressed sample through the transition zone above the neck to the necked region of the tensile sample. This suggested that sample crystallinity was at maximum before any load was applied and decreased during the necking process with increasing strain. Importantly, the samples analysed by FTIR spectroscopy were samples which had completed an entire tensile cycle, meaning the FTIR spectroscopy analysis was done after the sample failure which was well beyond 100% extension. It was therefore likely that orientation of the samples due to drawing had occurred as well as chain slippage

beyond this point. The chain slippage out of the crystal structures and the further reliance of the system on amorphous chain entanglements[22] would explain the decrease in the crystalline contribution at 730 cm^{-1} in the FTIR spectroscopy.

In Figure 4.33e, the LDPE tensile sample displayed the most intense 730 cm^{-1} peak in the transition zone. Since the long chain branching present in the LDPE makes it difficult for crystals to form during the crystallisation process the orientation of the LDPE under normal conditions is relatively low. This was confirmed by the crystallinity values calculated from DSC in Section 4.1.2. Since the drawing process after the yield point increases chain orientation the crystallinity would appear to be greater relative to the unstressed state. Once again the chain slippage seemed to occur from the centre of the sample meaning that the transition zone which was further outwards from the centre retained some of that orientation.

The splitting of the 1472-1461 cm^{-1} peaks did not follow a clear trend across all the polymers except for a tendency to collapse into a single peak at the centre of the drawn region.

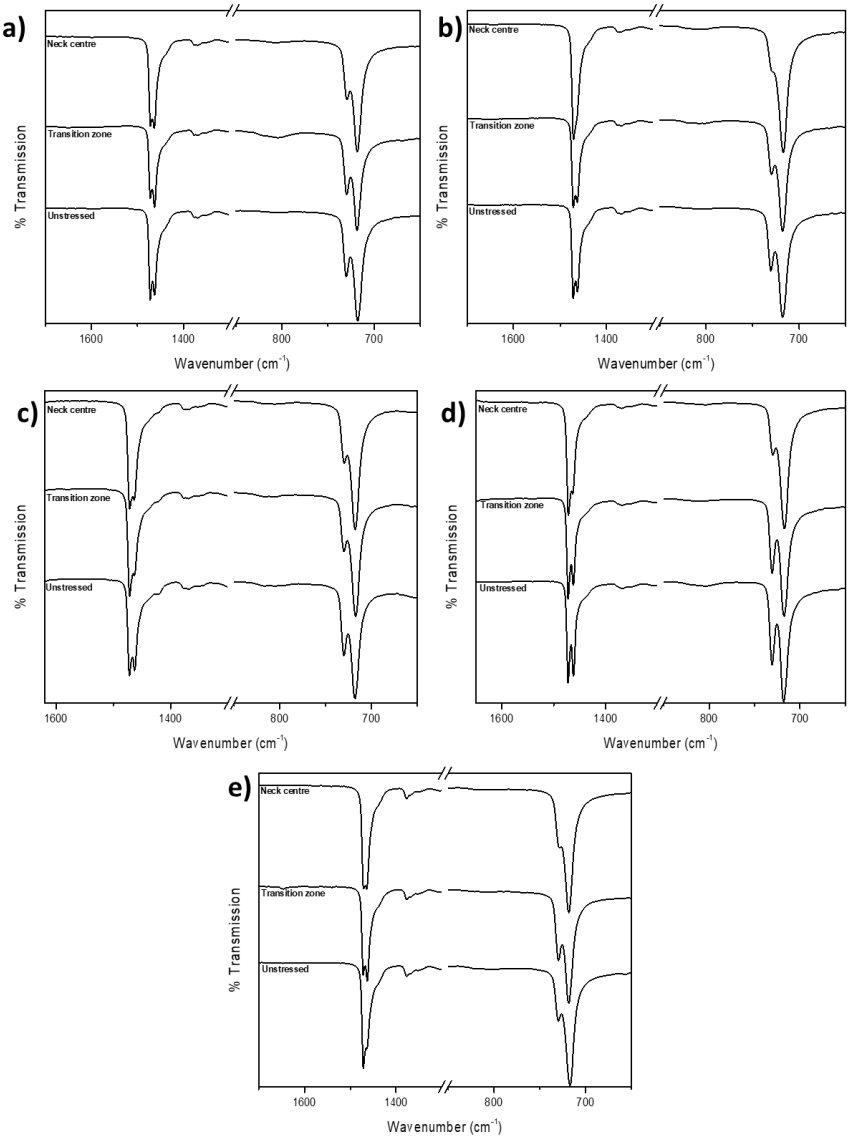

Figure 4. 33 FTIR spectra of tensile samples at different sample areas for a) HF101 b) HF120 c) HF140 d) HR477 and e) LDPE

4.6 References

1. Hussein, I. A., Hameed, T., Sharkh, B. F. A. & Mezghani, K. Miscibility of hexene-LLDPE and LDPE blends: influence of branch content and composition distribution. *Polymer (Guildf).* **44,** 4665–4672 (2003).

2. Hussein, I. A. Influence of composition distribution and branch content on the miscibility of m-LLDPE and HDPE blends: rheological investigation. *Macromolecules* **36,** 2024–2031 (2003).

3. Huang, J. & Rempel, G. L. Ziegler-Natta catalysts for olefin polymerization: mechanistic insights from metallocene systems. *Prog. Polym. Sci.* **20,** 459–526 (1995).

4. Walter, E. R. & Reding, F. P. Variations in unit cell dimensions in polyethylene. *J. Polym. Sci.* **21,** 561–562 (1956).

5. Turner-Jones, A. The triclinic crystal form of polymethylenes and polyethylenes. *J. Polym. Sci.* **62,** 53–56 (1962).

6. Lorenzo, A. T., Arnal, M. L., Albuerne, J. & Müller, A. J. DSC isothermal polymer crystallisation kinetics measurements and the use of the Avrami equation to fit the data: guidelines to avoid common problems. *Polym. Test.* **26,** 222–231 (2007).

7. Wang, G. Y. & Qiu, Z. Bin. Crystalline morphology and crystallisation kinetics of melt-miscible crystalline/crystalline polymer blends of poly(vinylidene fluoride) and poly(butylene succinate-co-24mol% hexamethylene succinate). *Chinese J. Polym. Sci. (English Ed.* **32,** 1139–1148 (2014).

8. Krishnaswamy, R. K., Yang, Q., Fernandez-Ballester, L. & Kornfield, J. A. Effect of the distribution of short-chain branches on crystallisation kinetics and mechanical properties of high-density polyethylene. *Macromolecules* **41,** 1693–1704 (2008).

9. Ozawa, T. Kinetics of non-isothermal crystallisation. *Polymer (Guildf).* **12,** 150–158 (1971).

10. Sperling, L. H. *Introduction to physical polymer science*. (John Wiley & Sons, 2006).

11. Xue, Y., Fan, Y., Bo, S. & Ji, X. Microstructure characterization of a complex branched low-density. *Chinese J. Polym. Sci.* **33,** 508–522 (2015).

12. Zhang, M. & Wanke, S. E. Branching content and distribution in commercial polyethylenes by thermally fractionated differential scanning calorimetry. *Polym. Eng. Sci.* **43,** 1878–1888 (2003).

13. Ajji, A., Sammut, P. & Huneault, M. A. Elongational rheology of LLDPE / LDPE blends. *J. Appl. Polym. Sci.* **88,** 3070–3077 (2003).

14. Strobl, G. R. *The physics of polymers : concepts for understanding their structures and behavior*. (Springer, 2007).

15. Blum, A. E. The use and understanding of photoelastic coatings. *Strain* **13,** 96–101 (1977).

16. Fernández, M. S. B., Calderón, J. M. A., Díez, P. M. B. & Segura, I. I. C. Stress-separation techniques in photoelasticity: A review. *J. Strain Anal. Eng. Des.* **45,** 1–17 (2010).

17. Inc, V. P. G. *Introduction to stress analysis by the PhotoStress ® method by TN-702-2 the PhotoStress*. (2005). doi:11212

18. Crawford, S. M. & Kolsky, H. Stress birefringence in polyethylene. *Proc. Phys. Soc. Sect. B* **64,** 119–125 (1951).

19. Stein, R. S. & Norris, F. H. The x-ray diffraction, birefringence, and infrared dichroism of stretched polyethylene. *J. Polym. Sci.* **21,** 381–396 (1956).

20. Hagemann, H., Snyder, R. G., Peacock, A. J. & Mandelkern, L. Quantitative infrared methods for the measurement of crystallinity and its temperature dependence. Polyethylene. *Macromolecules* **22,** 3600–3606 (1989).

21. Blitz, J. P. & McFaddin, D. C. The characterization of short chain branching in polyethylene using fourier transform infrared spectroscopy. *J. Appl. Polym. Sci.* **51,** 13–20 (1994).

22. López-Barrón, C. R., Zeng, Y., Schaefer, J. J., Eberle, A. P. R., Lodge, T. P. & Bates, F. S. Molecular alignment in polyethylene during cold drawing using in-situ SANS and raman spectroscopy. *Macromolecules* **50,** 3627–3636 (2017).

Chapter 5: Crystallisation behaviour of solution blended LLDPE/ LDPE

Summary

Characterisation of blends of LDPE and LLDPE at various blend ratios form the bulk of this chapter. Solution blending is believed to encourage association between the blend components since the mobility is solution is higher than in the solid state and the solvent used for blending is a good solvent for both components. Blend morphology and the properties resulting from the morphology are analysed. Specifically, the cause and effect of co-crystallisation is investigated in order to rationalise the properties of the blends.

5.1 General characteristics

Blends nomenclature was determined by the weight percentage of the LLDPE in the blend as explained in Table 5.1.

Table 5. 1 Explanation of blend nomenclature

Blend name	Composition
HF10110	10 wt% HF101/ 90wt% LDPE
HF10150	50 wt% HF101/ 50wt% LDPE
HF10180	80 wt% HF101/ 20wt% LDPE

5.1.1 Molar mass

The molar mass data of the blends are shown in Tables 5.2 – 5.5. The molar mass of all blends appeared to be additive according to the various blend ratios. This could also be seen from the molar mass plots in Figure 5.1 a – d. In Figure 5.1 a – d a unimodal distribution could be seen for all blends.

Table 5. 2 Molar mass data of HF101/LDPE blends

Blend	M_w	M_n	Đ
LDPE	165 928	34 323	4.83
HF10110	163 672	38 828	4.21
HF10150	237 834	49 726	4.78
HF10180	261 579	60 390	4.33
HF101	279 108	75 282	3.70

Table 5. 3 Molar mass data of HF120/LDPE blends

Blend	M_w	M_n	Đ
LDPE	165 928	34 323	4.83
HF12010	153 991	33 313	4.62
HF12050	230 470	46 823	4.92
HF12080	250 853	40 235	6.23
HF120	295 862	59 984	4.93

Table 5. 4 Molar mass data of HF140/LDPE blends

Blend	M_w	M_n	Đ
LDPE	165 928	34 323	4.83
HF14010	170 198	38 336	4.44
HF14050	211 969	48 700	4.35
HF14080	266 716	66 239	4.03
HF140	282 698	68 723	4.11

Table 5. 5 Molar mass data of HR477/LDPE blends

Blend	M_w	M_n	Đ
LDPE	165 928	34 323	4.83
HR47710	154 277	32 044	4.81
HR47750	173 277	44 593	3.88
HR47780	176 349	38 252	4.61
HR477	176 161	42 036	4.19

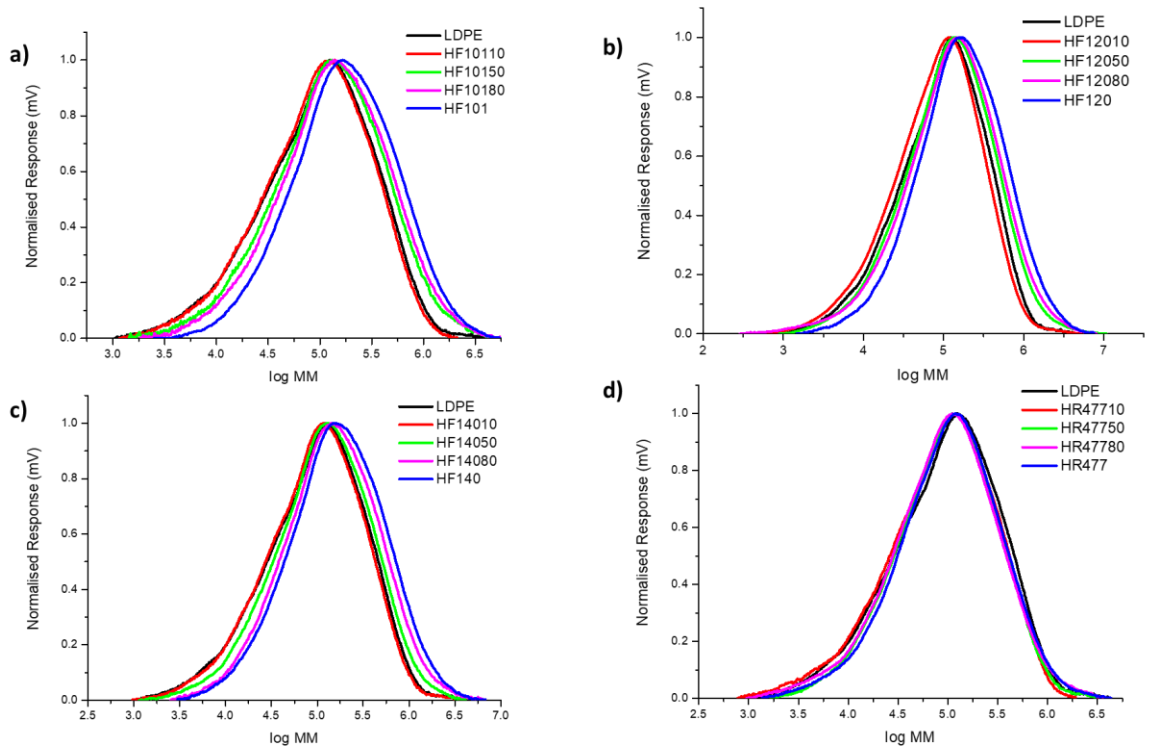

Figure 5. 1 Molar mass distribution of a) HF101 blends b) HF120 blends c) HF140 blends and d) HR477 blends

5.1.2 Solid state crystallinity

DSC was used to investigate the non-isothermal crystallisation behaviour of the blends. The DSC thermograms in Figure 5.2 display at least two melting events for all blends, with the 10 wt% LLDPE blends all displaying three melting events. This separation of melting events suggested separate crystallisation and therefore a degree of phase separation. It is not surprising that phase separation occurred considering that the individual components of the blends contain no specific functional groups to attract each other. The presence of the third

intermediate melting peak at 10 wt% LLDPE in Figure 5.2 does, however, suggest that some co-crystallisation may have occurred.

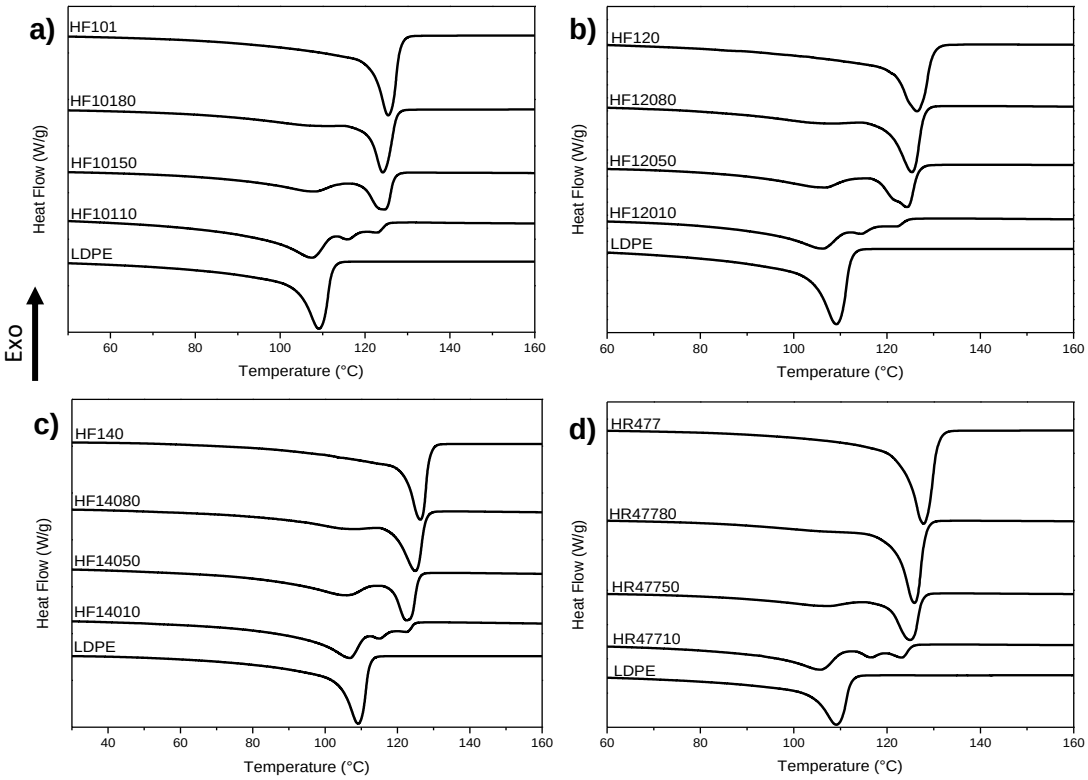

Figure 5. 2 DSC second heating cycles of a) HF101 blends b) HF120 blends c) HF140 blends and d) HR477 blends

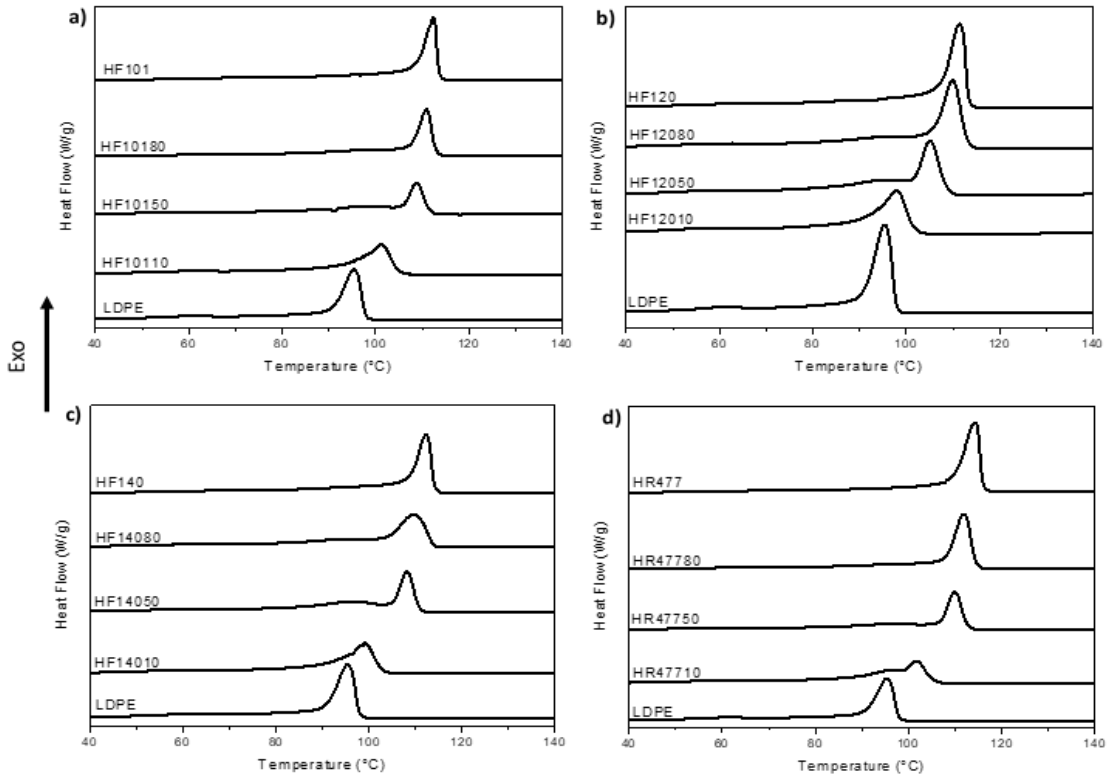

Figure 5. 3 DSC crystallisation cycles of a) HF101 blends b) HF120 blends c) HF140 blends d) HR477 blends

Separate melting events were observed for all blends, but Figure 5.3 shows no clear boundaries between crystallisation peaks for all blends. Although it was clear that more than one crystallisation event occurred the peaks appeared very close to each other, often appearing as a shoulder on the exotherm of the major component. This also suggested that some degree of association was occurring between the blend components. It is possible that the crystallisation events occurred separately within a similar temperature range, however the movement of the peaks with changing blend ratio still implied that the blends may not be completely incompatible. The most pronounced phase separation occurred at the 50/50 blend ratio for all blends. This could be inferred from the intensity and definition of the separate melting peaks and was confirmed by the difference between the peak melting temperatures shown in Tables 5.6 – 5.9.

From Table 5.6 the crystallinity was found to be the lowest for the HF10150 blend and remained low in the HF10180 despite the more crystalline HF101 being the dominant component. Possibly the presence of the LDPE inhibited the crystallisation of the HF101 even in low quantities. It has been suggested that the inclusion of some less branched LDPE segments into an LLDPE rich crystal may result in a lower thermal stability of the LLDPE crystals, effectively lessening the total attainable crystallinity.[1] According to Table 5.7 the least crystalline blend was the HF12010, the apparently co-crystallised blend. The HF12050 possessed a similarly low crystallinity while the crystallinity of the HF12080 appeared to approach that of the neat HF120. The HF140 blends displayed an almost linear increase in crystallinity, excepting the lower crystallinity for HF14010 while the HR477 blends followed the same trend as the HF101 blends, with HR47750 possessing the lowest crystallinity. These results are summarised in Figure 5.4, which shows that in most cases the increase in crystallinity from the less crystalline LDPE to the more crystalline LLDPE does not follow a simply linear increase. For the all of the blends, except the HF140 blends, the crystallinity was significantly restricted (in many cases below the crystallinity value of the LDPE) even to 80% LLDPE content. From this it was clear that each individual component interfered with the crystallisation of the other component. The almost linear increase in crystallinity for the HF140 blends indicated that the blends simply behaved in an additive manner and did not have significant interaction. It could also be expected from these results that the blend properties also will not follow an additive trend.

Table 5. 6 Thermal parameters of HF101/LDPE blends determined by DSC

Blend	T_c (°C)	T_{m1} (°C)	T_{m2} (°C)	T_{m3} (°C)	ΔH_f (J/g)
LDPE	95.4	109.2	-	-	115.1
HF10110	101.3	107.5	115.9	122.9	116.6
HF10150	108.7	106.8	-	124.7	94.9
HF10180	110.9	111.2	-	124.2	112.8
HF101	112.4	125.5	-	-	131.3

Table 5. 7 Thermal parameters of HF120/LDPE blends determined by DSC

Blend	T_c (°C)	T_{m1} (°C)	T_{m2} (°C)	T_{m3} (°C)	ΔH_f (J/g)
LDPE	95.4	109.2	-	-	115.1
HF12010	97.9	106.2	114.5	121.8	87.5
HF12050	105.1	106.8	-	124.3	99.8
HF12080	109.9	108.2	-	125.3	113.7
HF120	111.4	126.4	-	-	119.8

Table 5. 8 Thermal parameters of HF140/LDPE blends determined by DSC

Blend	T_c (°C)	T_{m1} (°C)	T_{m2} (°C)	T_{m3} (°C)	ΔH_f (J/g)
LDPE	95.4	109.2	-	-	115.1
HF14010	99.0	106.8	115.1	122.6	112.9
HF14050	108.1	106.2	-	122.5	122.2
HF14080	109.8	108.3	-	124.9	129.1
HF140	112.3	126.3	-	-	131.1

Table 5. 9 Thermal parameters of HR477/LDPE blends determined by DSC

Blend	T_c (°C)	T_{m1} (°C)	T_{m2} (°C)	T_{m3} (°C)	ΔH_f (J/g)
LDPE	95.4	109.2	-	-	115.1
HR47710	101.7	105.8	116.5	123.1	114.8
HR47750	109.9	107.5	-	124.9	113.2
HR47780	111.9	-	-	125.9	147.5
HR477	114.3	127.8	-	-	173.0

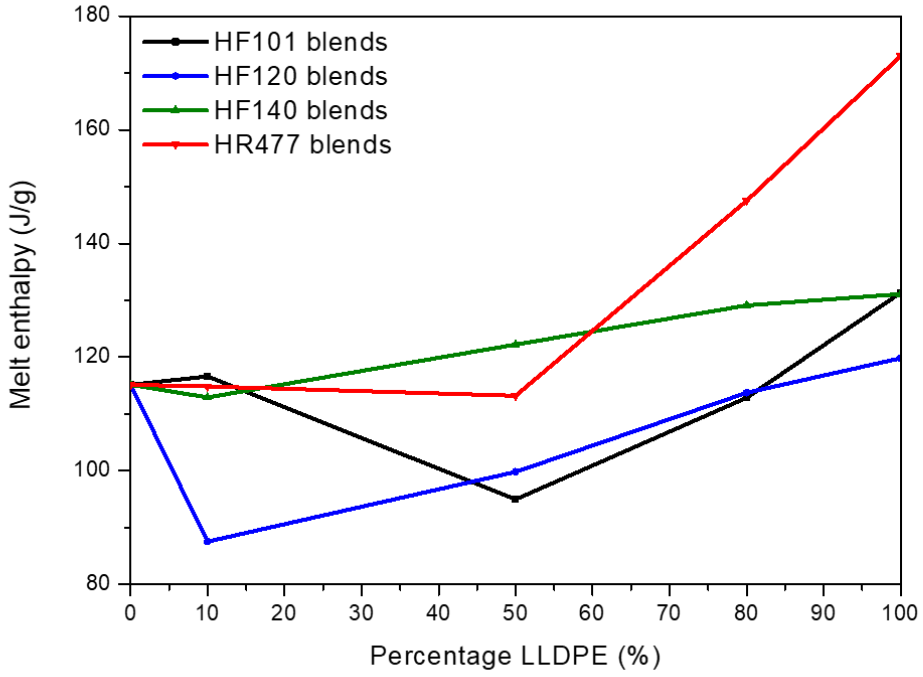

Figure 5. 4 Variation in crystallinity with blend composition

Figure 5.5 shows the variation in peak melting temperatures for the two separate major melting events. In Figure 5.5 a, the melting events occur furthest apart at a 50/50 blend ratio for the HF101 blends. For the HF120 blends in Figure 5.5 b, the difference between the melting temperatures was only slightly greater for the 50/50 blend ratio compared to the 20% LDPE blend ratio while the difference in melting temperatures decreased for the 90% LDPE blend ratio. For the HF140 blends in Figure 5.5 c the difference between the melting temperatures increased slightly with LDPE content. The HR477 blends in Figure 5.5 d showed a similar trend where the 80% HR477 blend displayed only a single melting event. It is believed that deductions about compatibility can be made from these observations. Large differences in

peak melting temperatures could indicate a large degree of incompatibility while smaller differences in peak melting temperatures may indicate greater interaction between the two neat components.

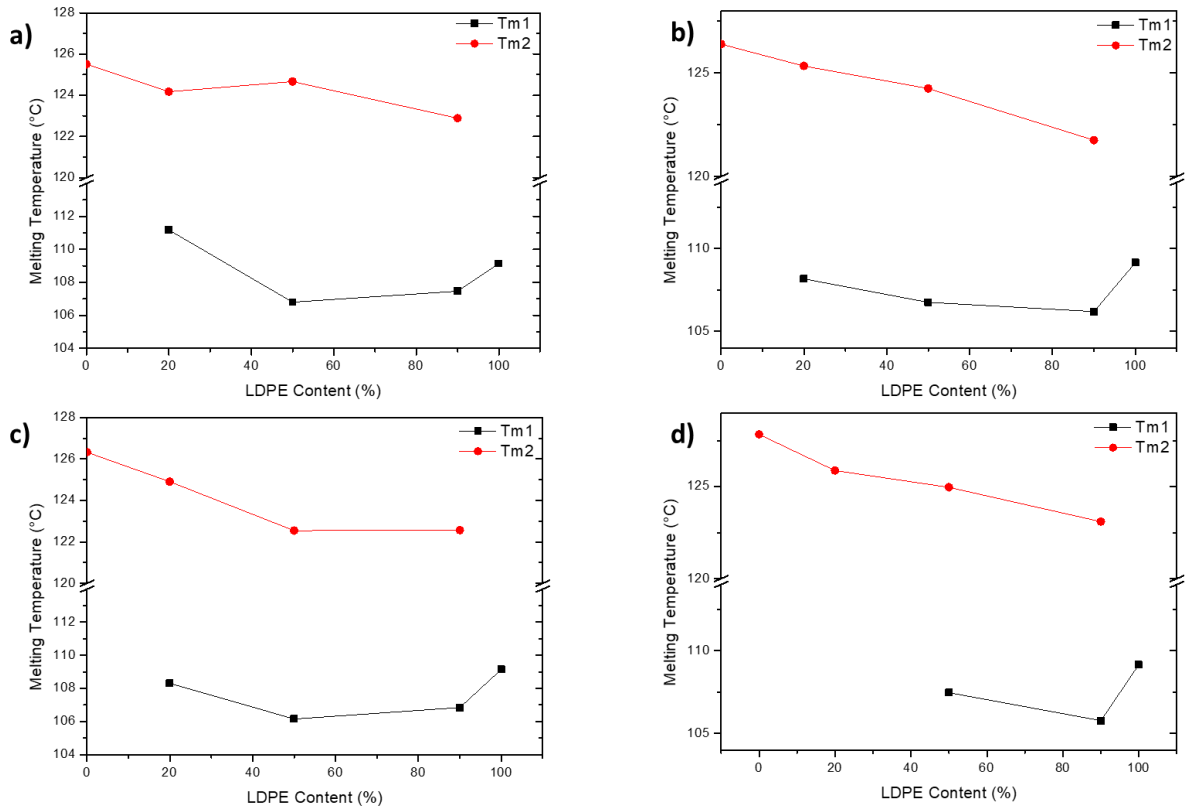

Figure 5. 5 Peak melting temperatures of two major melting events for a) HF101 blends b) HF120 blends c) HF140 blends and d) HR477 blends

5.1.3 Solution crystallinity

The solution crystallisation behaviour of the blends was monitored using the Scalls technique. Figure 5.6 a shows the dissolution of the HF101 blends. There was a clear shift in the peak dissolution temperatures for both the HF101 and the LDPE. The difference between the peak temperatures appeared to decrease with increasing LDPE content. Notably, the Scalls dissolution of the HF10110 blend did not display the same triple melting peaks that were observed by DSC. The crystallisation peaks in Figure 5.6 b displayed less significant shifts in peak temperatures between different blend ratios. In both crystallisation and dissolution two separate events occur for the LDPE and LLDPE indicating that complete co-crystallisation did not occur. The distinct dissolution and crystallisation events of both components as well as the absence of the third intermediate peak for the HF10110 blends was most likely due to the enhanced mobility in solution which facilitated the separation of the chains into their respective domains. The dissolution and crystallisation of the HF120 blends (Figure 5.7) display a significant amount of material which dissolved and crystallised at lower temperatures. The dissolution behaviour suggested co-crystallisation as only a single peak could be identified at similar peak temperatures to that of LDPE. Increasing quantities of HF120 seemed to decrease the peak dissolution temperature of the blend to values below that of LDPE. For the crystallisation two separate events could once again be observed for the HF12080 and HF12050 blends. It appeared that the solvent enhanced the compatibility of the HF120 and the LDPE as these blends demonstrated less interactions in the solid state.

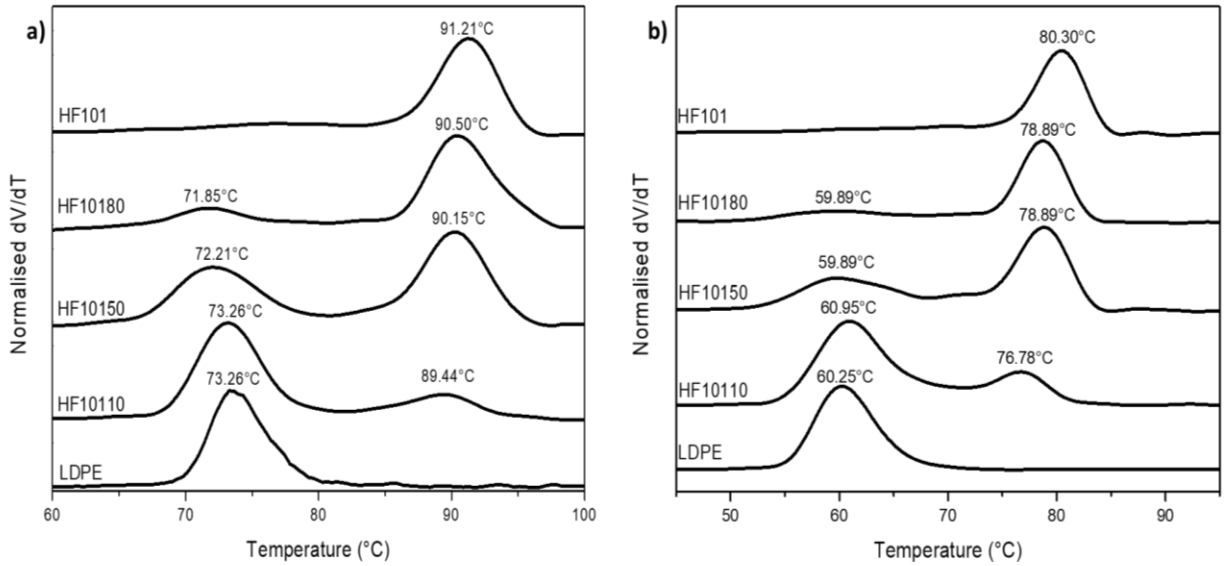

Figure 5. 6 Scalls profiles of HF101/LDPE blends a) dissolution and b) crystallisation at 405 nm

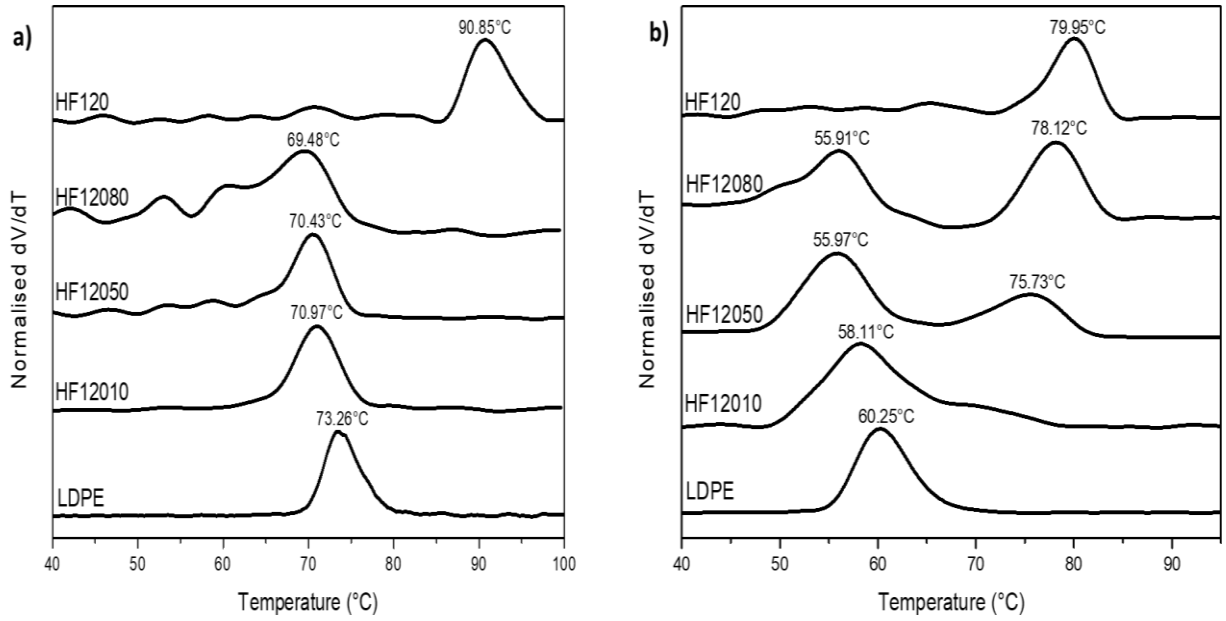

Figure 5. 7 Scalls profiles of HF120/LDPE blends: a) dissolution and b) crystallisation at 405 nm

The Scalls profiles of the HF140 blends are shown in Figures 5.8 a and b. The HF140 blends showed a similar trend to the HF101 blends with difference between peak dissolution temperatures decreasing with increasing LDPE content. The Scalls profiles of the HR477 blends in Figure 5.9 a displayed an almost constant difference in peak dissolution temperatures until the HR47710 where a decrease between peak dissolution temperatures was observed. For all blends the peak temperatures of both LLDPE and LDPE crystallisation and dissolution displayed a general decrease, not simply towards the value of the LDPE peak temperature but below this value. This suggested that both components inhibit the crystallisation of the other.

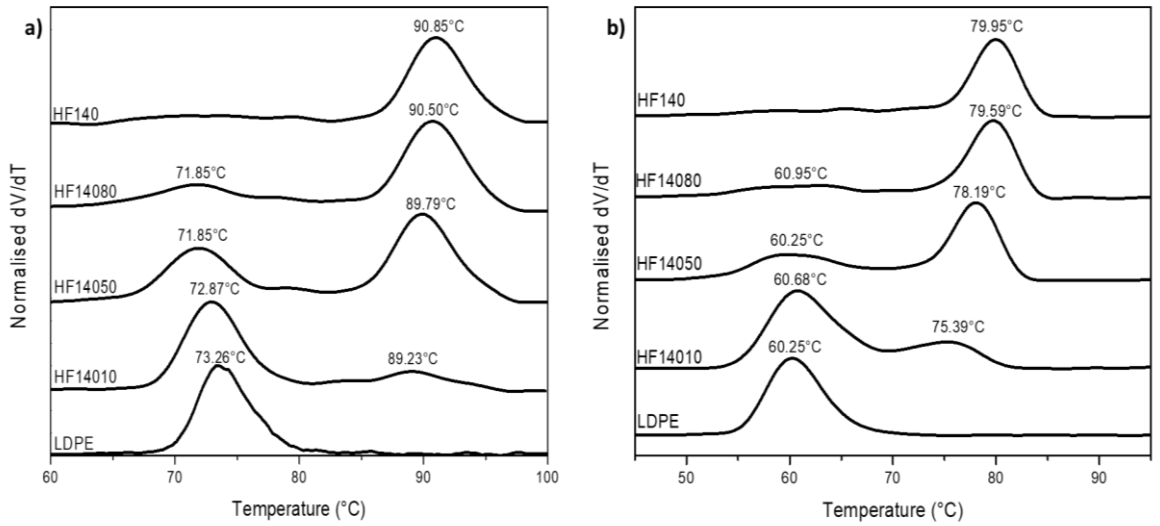

Figure 5. 8 Scalls profiles of HF140/LDPE blends a) dissolution and b) crystallisation at 405 nm

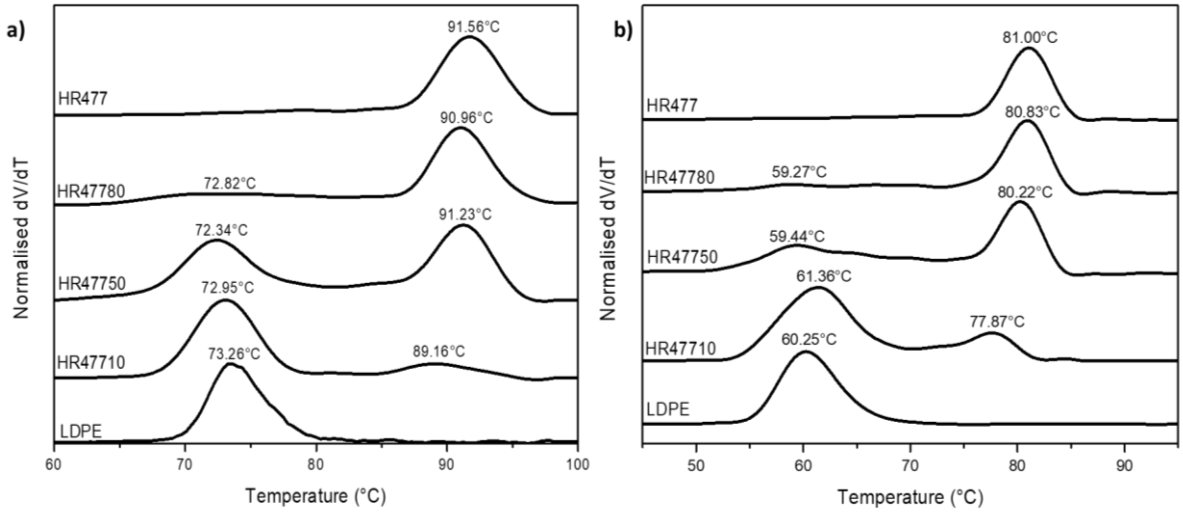

Figure 5. 9 Scalls profiles of HR477/LDPE blends a) dissolution and b) crystallisation at 405 nm

5.2 Crystallisation kinetics

5.2.1 Isothermal crystallisation

Table 5.10 lists the Avrami parameters of all blends at different crystallisation temperatures. The Avrami indices vary between 1.25 and 3.29 depending on the blend ratio and crystallisation temperature. The *n* value was indicative of rod-like structures or two-dimensional axialites. Avrami indices appeared to decrease with blend ratio, suggesting that the changes in growth dimensions occurred due to addition of LDPE to the LLDPE.[2] This was in agreement with reported theories about the unlikelihood of highly branched polyethylenes, such as LDPE, forming three-dimensional spherulites.[2]

The Avrami plots for the blends are shown in Figures 5.10 – 5.13. As pure LDPE cannot crystallise in the temperature range which was used to study the kinetics of the blends and therefore only the LLDPEs could be used for comparison. For the HF101 blends a similarity in the kinetics could be observed between the neat HF101 and the HF10180 blends at all crystallisation temperatures. Although the kinetics of the HF10110 blend was relatively constant for varying values of T_c, the kinetics was vastly different from that of the neat HF101 and HF10180 blend. The HF10150 blend was most dependent on the crystallisation

temperature. At high values of T_c the kinetics was similar to that of the HF10110 blend, however with decreasing T_c the plot shifted towards the range of the HF10180. Similar behaviour was observed for the HF120 and HR477 blends. The HF12080 and HR47780 blends also showed a crystallisation temperature dependency similar to that of the 50/50 blend ratio. The HF14080 blend appeared to crystallise faster than the neat HF140 at most values of T_c, however all blend ratios excluding HF14010 displayed a crystallisation temperature dependency.

Table 5. 10 Avrami parameters of blends with varying values of T_c

Sample	T_c (°C)	*n*	K (min^{-n})	$t_{0.5}$ (min)
HF10180	119.0	2.15	1.05×10^{-2}	6.84
	118.5	2.48	1.20×10^{-2}	5.04
	118.0	2.57	2.19×10^{-2}	3.85
	117.5	2.65	4.46×10^{-2}	2.82
HF10150	119.0	2.03	1.59×10^{-3}	22.27
	118.5	1.82	4.40×10^{-3}	20.05
	118.0	2.38	6.16×10^{-3}	7.35
	117.5	2.52	9.11×10^{-3}	5.63
HF10110	119.0	1.25	7.61×10^{-3}	36.55
	118.5	1.26	7.44×10^{-3}	36.49
	118.0	1.26	7.55×10^{-3}	35.88
	117.5	1.31	6.45×10^{-3}	35.89
HF12080	119.0	2.12	2.84×10^{-3}	15.43
	118.5	2.25	6.93×10^{-3}	8.10
	118.0	2.93	4.57×10^{-3}	5.84
	117.5	2.21	3.44×10^{-2}	3.96
HF12050	119.0	1.62	3.25×10^{-3}	27.69
	118.5	1.67	4.06×10^{-3}	23.18
	118.0	1.84	3.42×10^{-3}	21.33
	117.5	1.90	4.13×10^{-3}	19.92
HF12010	119.0	1.43	4.19×10^{-3}	36.04
	118.5	1.29	7.20×10^{-3}	33.89
	118.0	1.29	7.77×10^{-3}	32.19
	117.5	1.36	5.93×10^{-3}	33.46
HF14080	119.0	2.89	2.00×10^{-2}	3.68
	118.5	2.49	4.27×10^{-2}	3.26
	118.0	2.22	9.51×10^{-2}	2.56
	117.5	2.30	1.47×10^{-1}	2.06
HF14050	119.0	2.50	3.44×10^{-3}	8.35
	118.5	2.34	1.04×10^{-2}	5.94
	118.0	3.24	4.30×10^{-3}	4.92
	117.5	3.29	9.77×10^{-3}	3.75
HF14010	119.0	1.30	6.07×10^{-3}	37.89
	118.5	1.32	6.53×10^{-3}	34.24
	118.0	1.34	6.44×10^{-3}	33.29
	117.5	1.32	6.89×10^{-3}	32.85
HR47780	119.0	2.62	4.29×10^{-2}	2.92
	118.5	2.98	5.52×10^{-2}	2.41
	118.0	2.57	2.43×10^{-1}	1.55
	117.5	2.61	4.45×10^{-1}	1.22
HR47750	119.0	2.21	1.14×10^{-2}	6.36
	118.5	2.22	2.26×10^{-2}	4.62
	118.0	2.34	3.89×10^{-2}	3.43
	117.5	2.49	6.15×10^{-2}	2.70
HR47710	119.0	1.44	4.56×10^{-3}	33.72
	118.5	1.28	9.45×10^{-3}	30.71
	118.0	1.35	6.05×10^{-3}	33.82
	117.5	1.34	7.02×10^{-3}	32.05

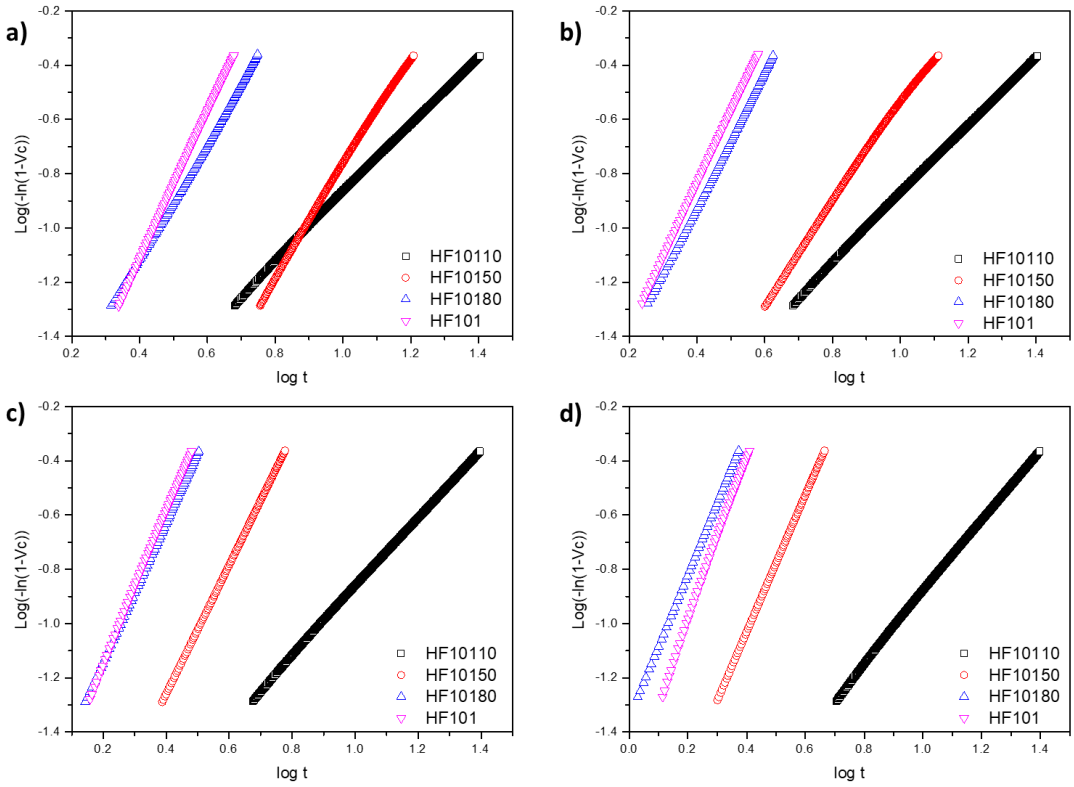

Figure 5. 10 Avrami plots of HF101 blends at a) 119 °C b) 118.5 °C c) 118 °C and d) 117.5 °C

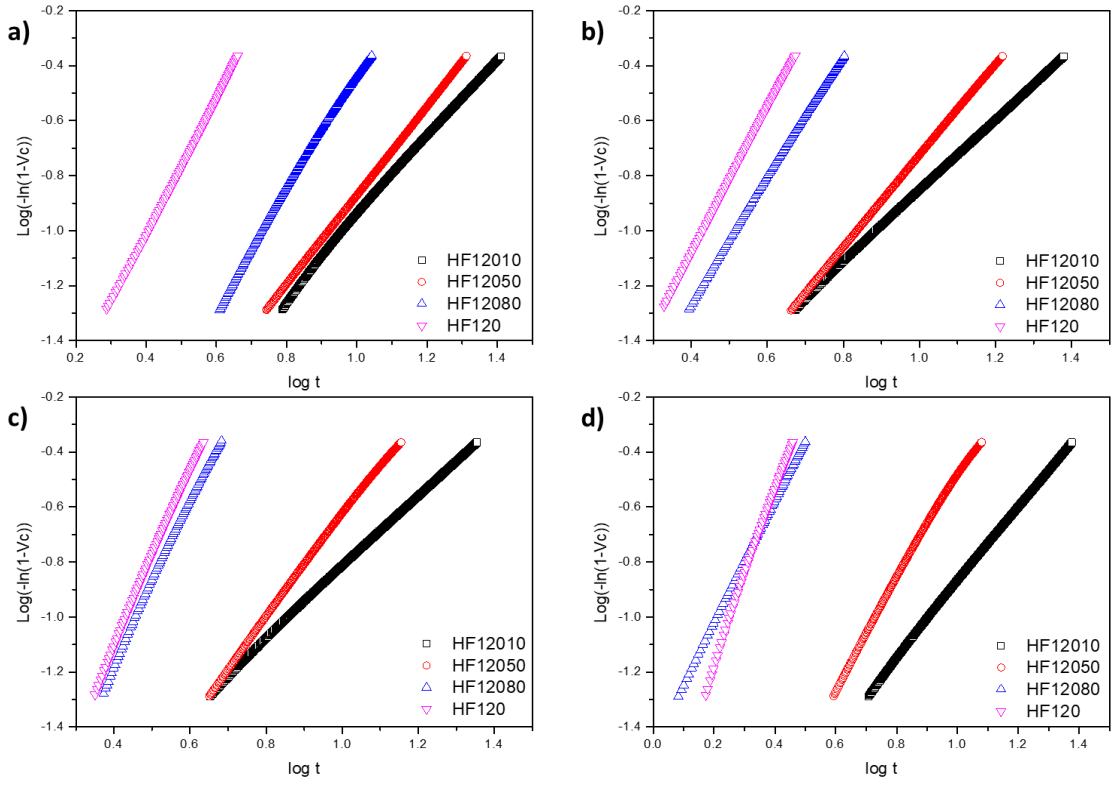

Figure 5. 11 Avrami plots of HF120 blends at a) 119 °C b) 118.5 °C c) 118 °C and d) 117.5 °C

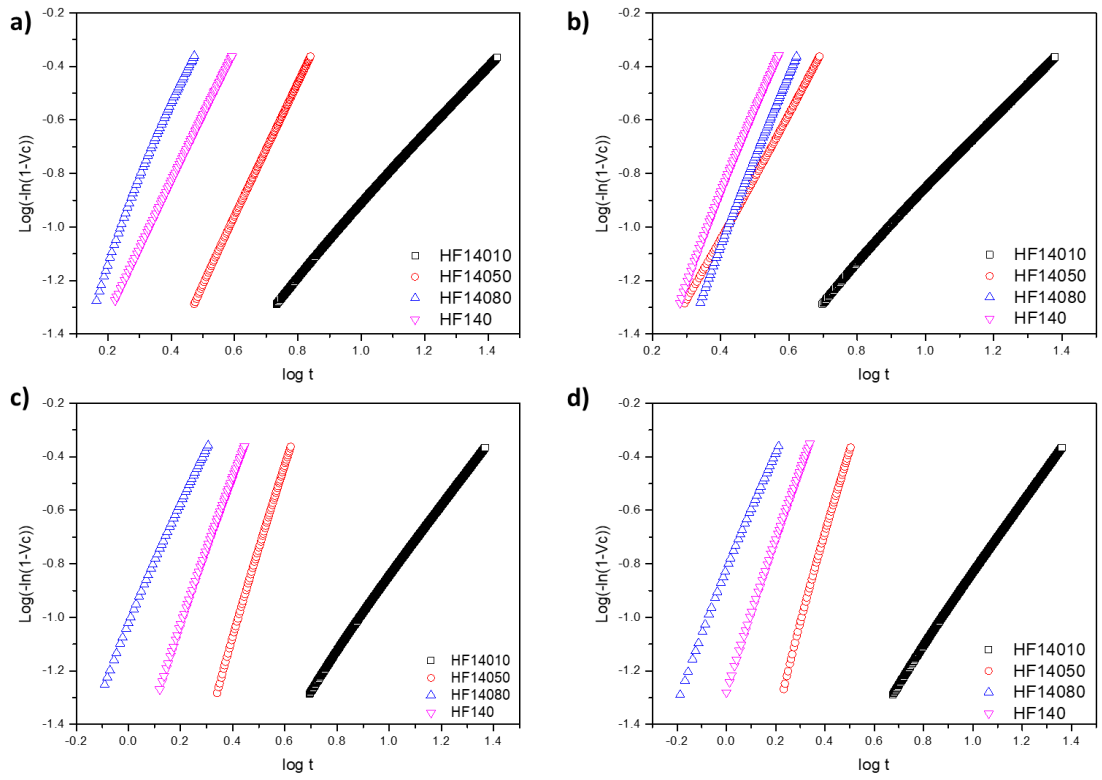

Figure 5. 12 Avrami plots of HF140 blends at a) 119 °C b) 118.5 °C c) 118 °C and d) 117.5 °C

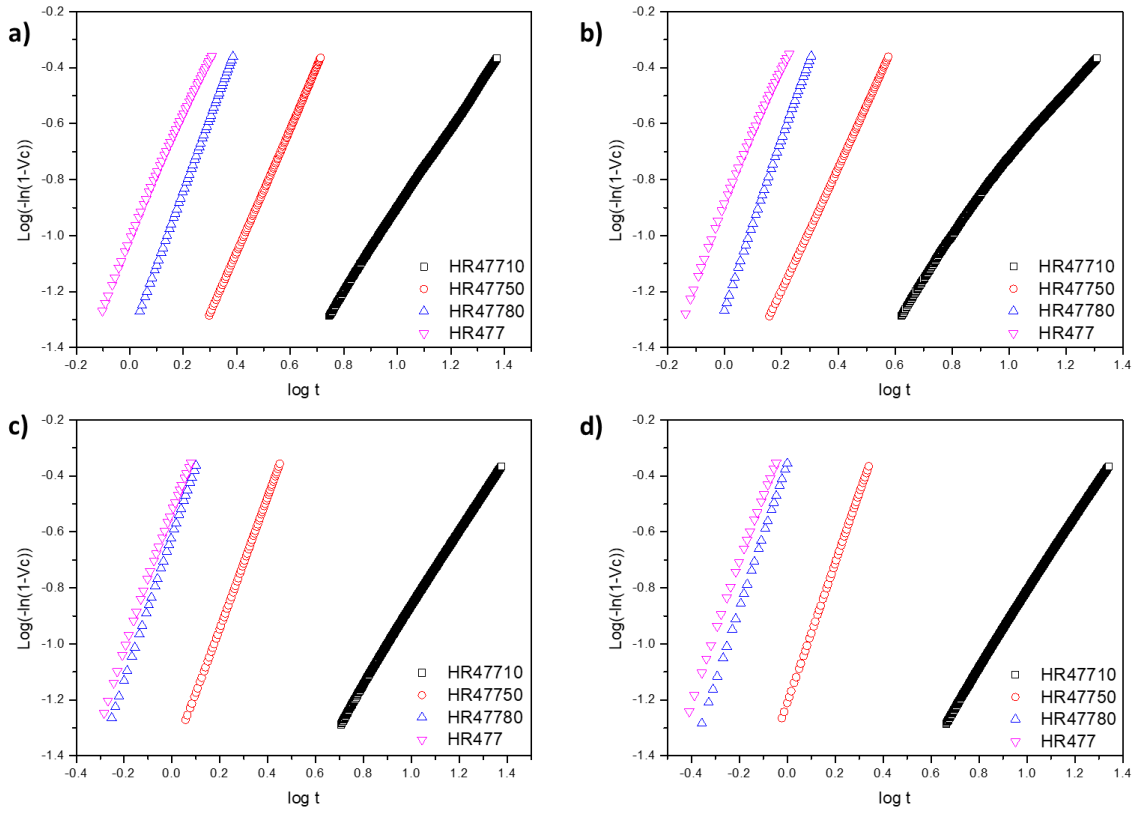

Figure 5. 13 Avrami plots of HR477 blends at a) 119 °C b) 118.5 °C c) 118 °C and d) 117.5 °C

Figure 5.14 shows the variation in the time required to reach 50% of the total crystallinity ($t_{0.5}$) with LLDPE content. In all cases the neat LLDPE displayed the fastest rate of crystallisation and the rate gradually decreased with increasing LDPE content. This was expected due to the high branching content of LDPE which would inhibit crystallisation of the blends. In the case of the HF101 blends it appeared that the ability of the LDPE to hinder the crystallisation of the HF101 was enhanced at higher temperature and therefore displayed a T_c dependence. The HF120 blends displayed a similar effect to a lesser degree. In the case of the HF140 and HR477 blends the crystallisation rate increased significantly between 10 and 50% LLDPE. The behaviour observed in the HF140 and HR477 blends did not display a significant T_c dependence.

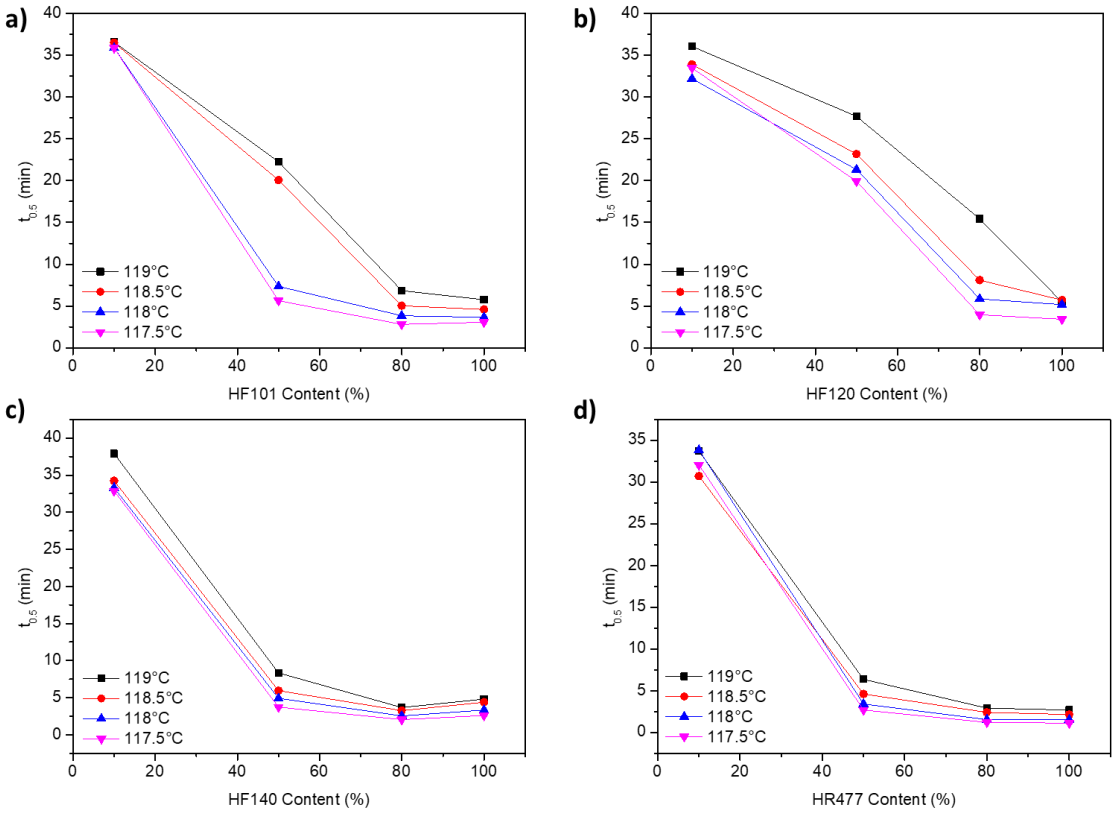

Figure 5. 14 Crystallisation half time for isothermally crystallised a) HF101 b) HF120 c) HF140 and d) HR477 blends

The rate of decrease of the amorphous fraction at 118°C for all blends is shown in Figure 5.15. Figure 5.15 a – c shows that the rate of decrease of the amorphous content was very similar for the neat LLDPE and their corresponding 80% blend. Between the HF10150 and HF10110 blend ratios the rate of decrease of the amorphous fraction was dramatically slowed. For the rate of decrease of the relative amorphous fraction of the HF120 blends shown in Figure 5.15 b the difference between the rates of decrease of the relative amorphous fraction of the HF12050 and HF12010 was not as great as in the case of the HF101 blends. The rate of decrease of the relative amorphous fraction of the HR47780 blend in Figure 5.15 d had a two-step decrease which suggested a two-phase system. It has also been proposed that the formation of crystalline regions can decrease the mobility of the remaining uncrystallised chains, dubbed the 'confining effect'.[3] This effect was reported to result in a decrease in the rate of crystallisation after the initial crystallisation process had already begun. Why this would only occur for these specific blend ratios is still unclear.

The HF14080 blend appeared to crystallise even faster than the neat HF140. As the HF140 is one of the lower crystallinity LLDPEs this enhanced rate was possibly a molar mass effect. Since the HF140 displayed the second highest molar mass the addition of the long-chain branched LDPE may have reduced the viscosity and enhanced segmental diffusion towards the crystal growth fronts.[4] The reason behind the occurrence of this phenomenon only for this specific blend was uncertain.

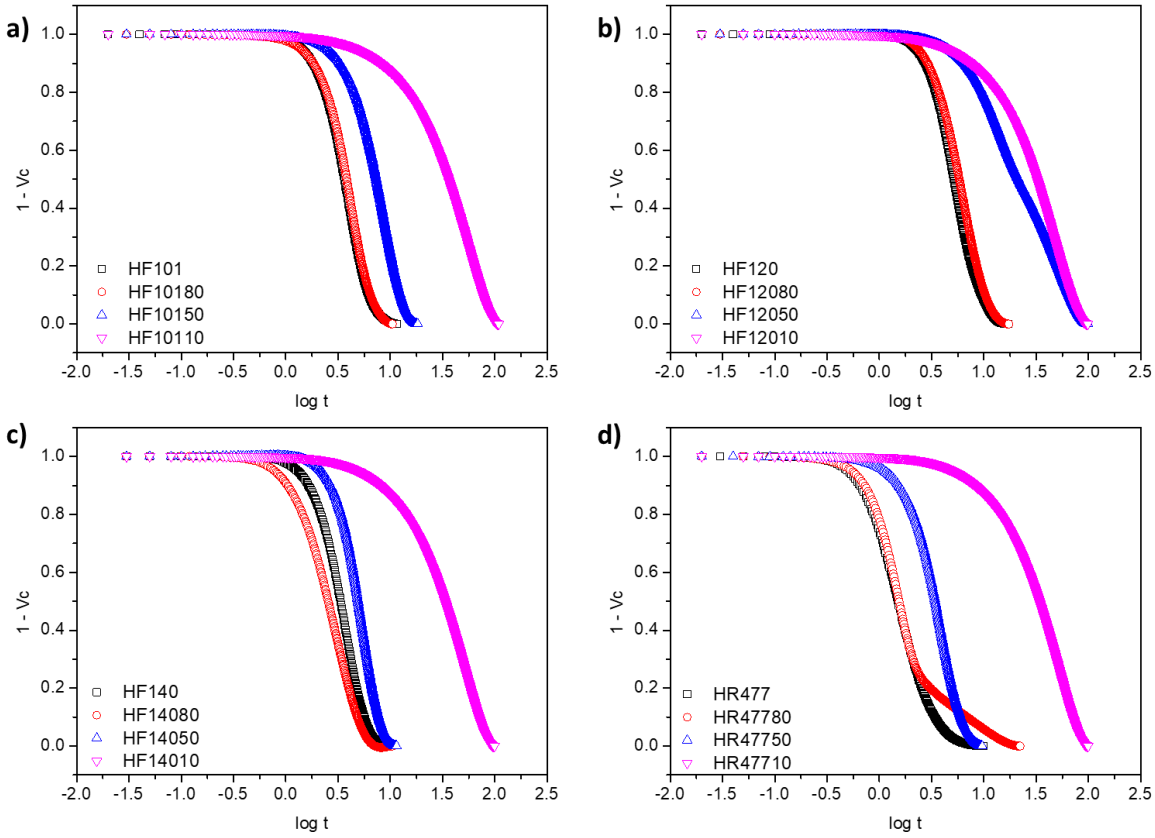

Figure 5. 15 Relative amorphous fractions of a) HF101 b) HF120 c) HF140 and d) HR477 blends at 118 °C

5.2.2 Non-isothermal crystallisation

The Nadkarni plots of the blends are shown in Figure 5.16 and their fitting parameters in Table 5.11. The fairly high correlation coefficient values indicated that the Nadkarni model could be successfully applied to these blend systems.

The value of ΔT_c^0 varied between blend ratios which indicated changes in nucleation densities at different blend ratios. The Nadkarni plots of the HF14010 and HF10110 blends in Figure 5.16 c and a demonstrated the greatest difference in the non-isothermal kinetics compared to the other blend ratios. The HF140 and HR477 50% and 80% blends displayed the greatest similarity relative to the neat LLDPEs in their Nadkarni plots (Figure 5.16 c and d). This indicated a similarity between the kinetics of these blend ratios and that of the neat LLDPEs under non-isothermal conditions. The HF120 blends displayed the most gradual change in non-isothermal kinetics with blend ratio. The *P* values decreased with increasing LLDPE content which showed the sensitivity of the blends to different cooling rates.

Table 5. 11 Nadkarni parameters of LDPE/LLDPE blends

Sample	*P*	ΔT_c	R^2
HF10110	0.2272	14.21	0.94100
HF10150	0.17454	10.42739	0.90673
HF10180	0.14099	9.92391	0.98485
HF12010	0.22419	13.24391	0.94172
HF12050	0.18687	11.5887	0.87573
HF12080	0.15416	10.88957	0.95637
HF14010	0.23882	14.00217	0.94804
HF14050	0.19042	8.60217	0.96257
HF14080	0.12525	9.10652	0.94121
HR47710	0.19812	11.99522	0.96726
HR47750	0.14499	9.78391	0.89795
HR47780	0.11643	9.84435	0.94279

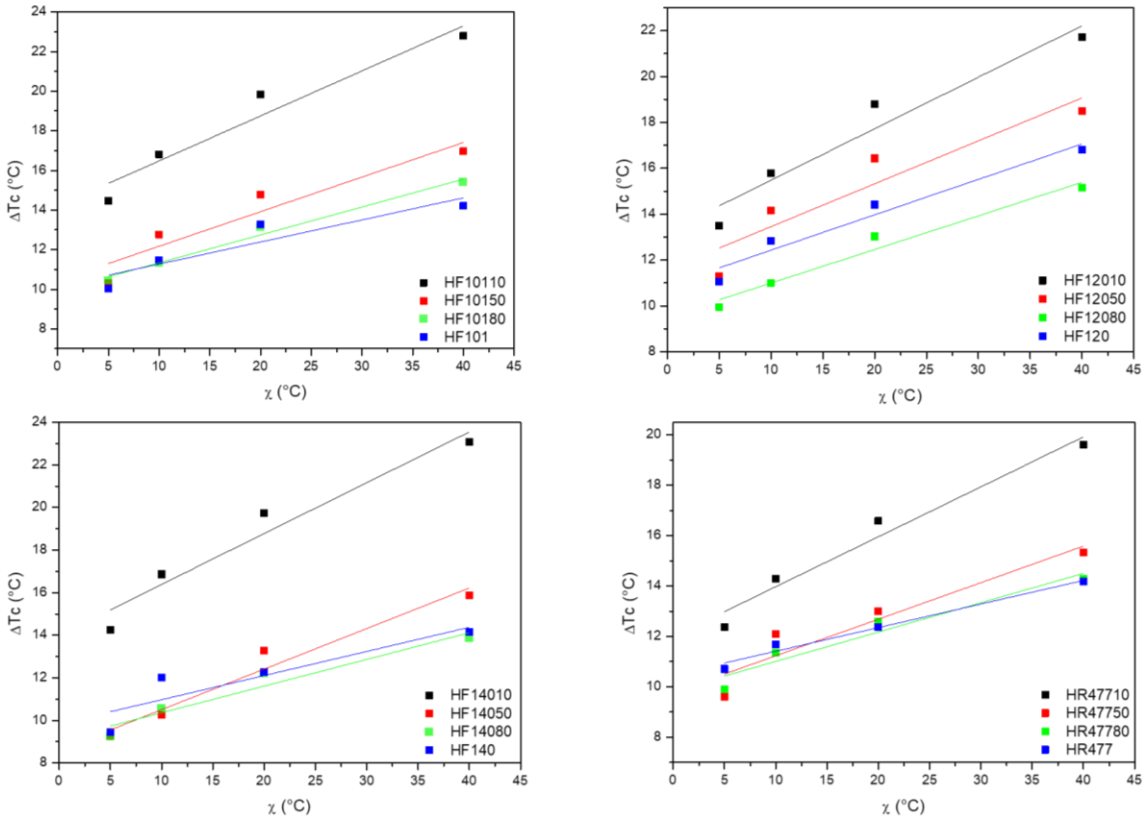

Figure 5. 16 Nadkarni plots of a) HF101 blends b) HF120 blends c) HF140 blends and d) HR477 blends

The results obtained using the Nadkarni model were compared to those from the Ozawa model. The Ozawa plots of the blends at various temperatures can be found in Figures 5.17 – 5.20 a – e. Once again it was clear from Figures 5.17 – 5.20 that the non-isothermal kinetics of the 10% LLDPE blends was different to that of the other blend ratios. The correlation coefficients in Tables 12 – 14 also indicated that the fit for the 10% LLDPE blends was very poor. It is likely that the HF10110, HF12010 and HF14010 blends may display better fitting if tested at the same temperatures as the LDPE. The highly crystalline HR477 blends displayed good fitting at the chosen temperatures, including the HR47710 blends. It was still clear from Figure 5.20 that the HR47710 crystallised slower than the other blend ratios.

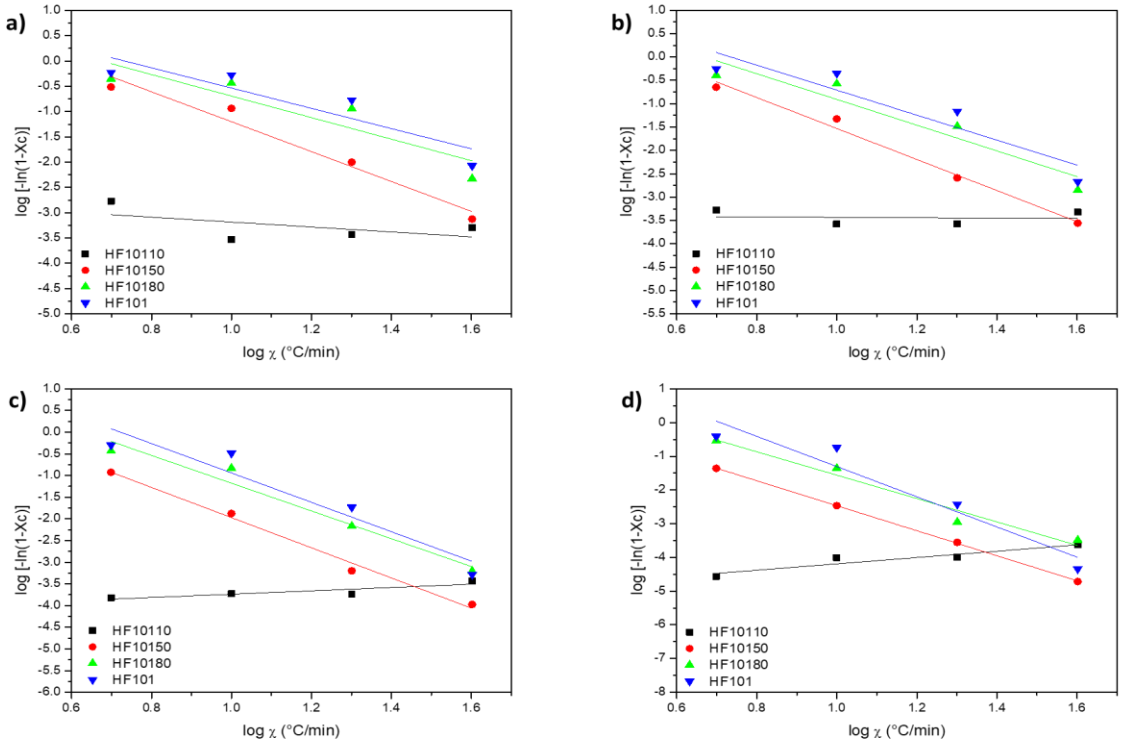

Figure 5. 17 Ozawa plots of HF101 blends at a) 109 °C b) 110 °C c) 111 °C and d) 112 °C

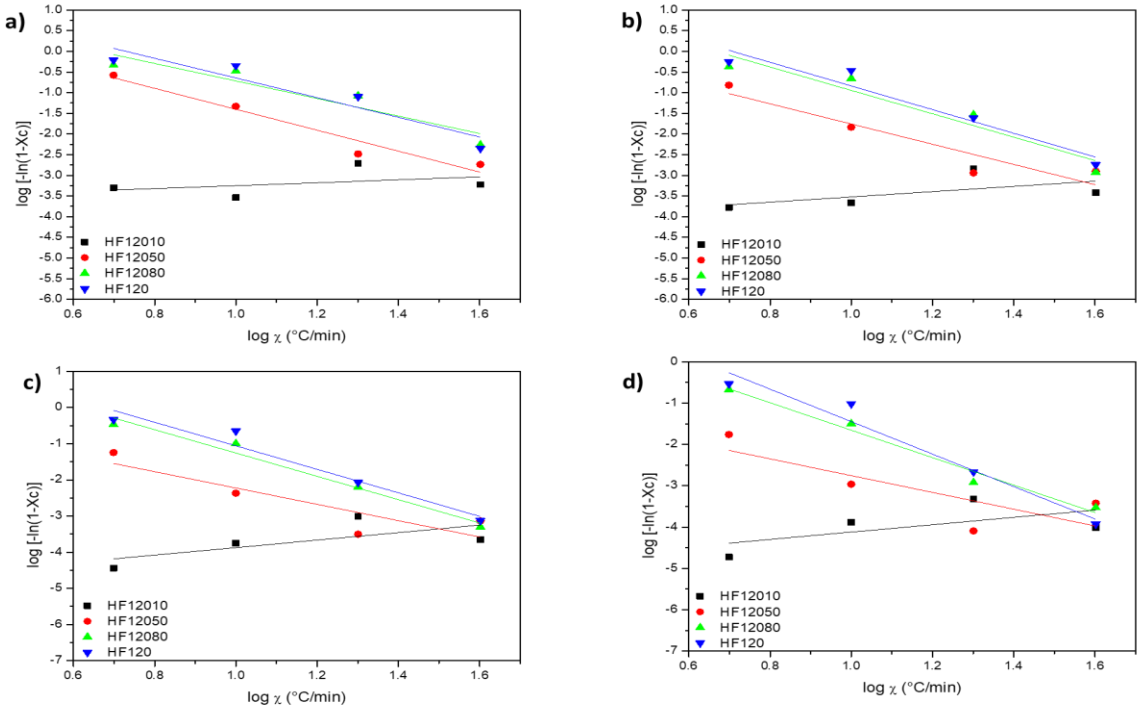

Figure 5. 18 Ozawa plots of HF120 blends at a) 109 °C b) 110 °C c) 111 °C and d) 112 °C

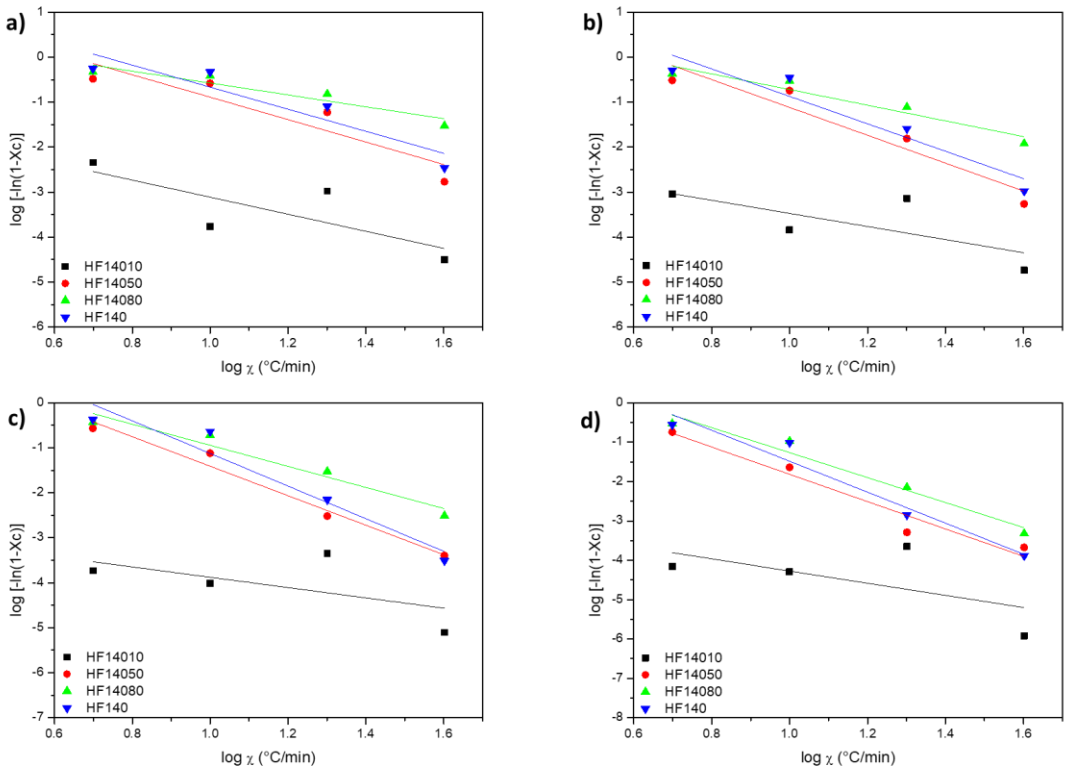

Figure 5. 19 Ozawa plots of HF140 blends at a) 109 °C b) 110 °C c) 111 °C and d) 112 °C

The Ozawa plots also displayed very similar behaviour for all 50% and 80% LLDPE blends under non-isothermal conditions when compared to the neat LLDPE. This was in agreement with the observations according to the Nadkarni model from which it was proposed that at blend ratios above 50% LLDPE content the LLDPE concentration does not significantly vary the kinetics under non-isothermal conditions.

The values for the Avrami indices in Tables 5.12 – 5.15 according to the Ozawa model were all within the feasible range for polyethylenes[5,6] excepting the *n* values of the 10% LLDPE blends. The *n* values range between 4 and 1 and once again displayed a decrease with temperature. It was not clear whether the Avrami index displayed a compositional variation.

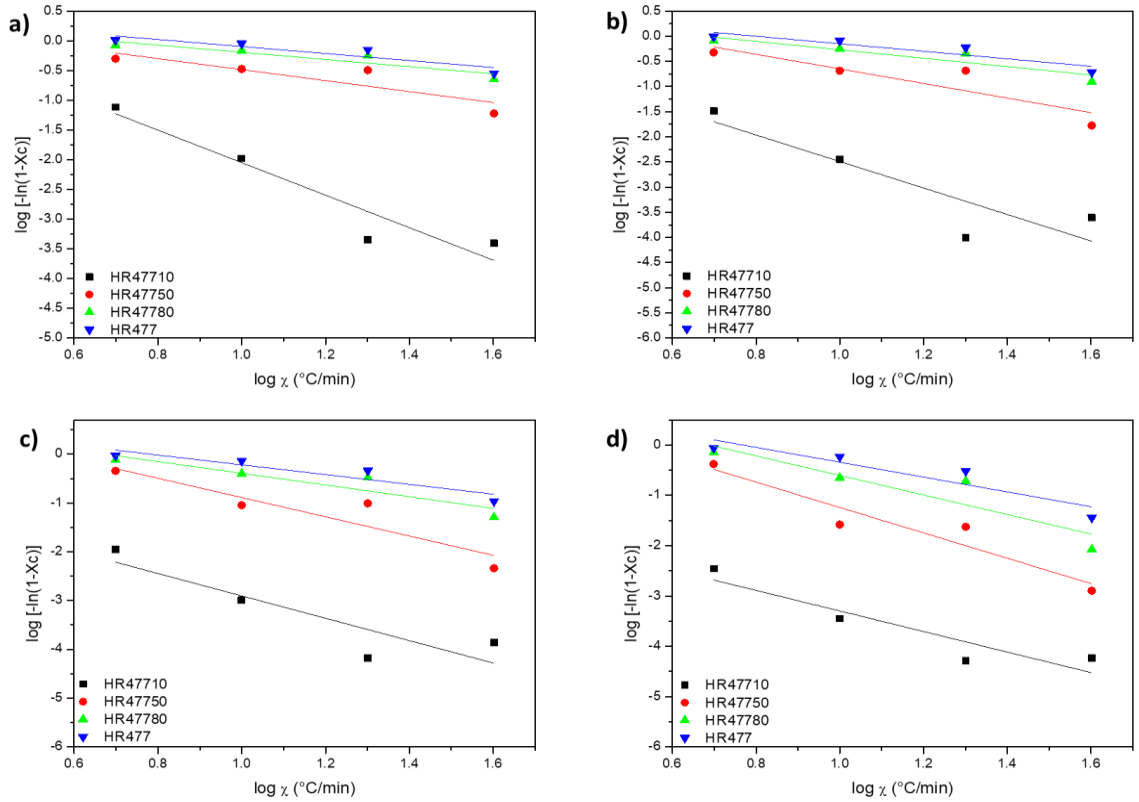

Figure 5. 20 Ozawa plots of HR477 blends at a) 109 °C b) 110 °C c) 111 °C and d) 112 °C

Table 5. 12 Ozawa fitting parameters for HF101 blends

Sample	Temperature (°C)	*n*	K* (°C.min)	R^2
HF101	112	4.48	3.17	0.93
	111	3.39	2.45	0.91
	110	2.68	1.97	0.87
	109	2.00	1.47	0.82
HF10110	112	0.94	5.13	0.89
	111	0.38	4.12	0.76
	110	0.04	3.39	0.01
	109	0.49	2.70	0.31
HF10150	112	3.71	1.24	0.99
	111	3.48	1.51	0.99
	110	3.32	1.79	0.99
	109	2.96	1.75	0.97
HF10180	112	3.47	1.90	0.97
	111	3.20	2.03	0.96
	110	2.75	1.85	0.91
	109	2.13	1.43	0.83

Table 5. 13 Ozawa fitting parameters for HF120 blends

Sample	Temperature (°C)	*n*	K* (°C.min)	R^2
HF120	112	3.93	2.48	0.96
	111	3.25	2.19	0.95
	110	2.86	2.03	0.94
	109	2.38	1.74	0.89
HF12010	112	0.89	5.01	0.36
	111	1.04	4.91	0.47
	110	0.63	4.16	0.34
	109	0.36	3.61	0.16
HF12050	112	2.03	0.73	0.66
	111	2.26	0.03	0.77
	110	2.45	0.69	0.89
	109	2.53	1.13	0.95
HF12080	112	3.32	1.67	0.98
	111	3.23	1.97	0.98
	110	2.83	1.89	0.92
	109	2.12	1.40	0.88

Table 5. 14 Ozawa fitting parameters for HF140 blends

Sample	Temperature (°C)	*n*	K* (°C.min)	R^2
HF140	112	3.93	2.45	0.96
	111	3.63	2.50	0.94
	110	3.05	2.18	0.91
	109	2.45	1.78	0.87
HF14010	112	1.54	2.73	0.37
	111	1.15	2.73	0.35
	110	1.46	2.02	0.52
	109	1.90	1.22	0.61
HF14050	112	3.47	1.65	0.95
	111	3.28	1.87	0.98
	110	3.10	1.98	0.92
	109	2.49	1.60	0.84
HF14080	112	3.17	1.91	0.97
	111	2.34	1.40	0.95
	110	1.74	1.02	0.93
	109	1.32	0.74	0.89

Table 5. 15 Ozawa fitting parameters for HR477 blends

Sample	Temperature (°C)	*n*	K* (°C.min)	R^2
HR477	112	1.48	1.14	0.86
	111	1.00	0.78	0.86
	110	0.75	0.60	0.85
	109	0.59	0.49	0.83
HR47710	112	2.06	1.25	0.86
	111	2.29	0.61	0.80
	110	2.63	0.14	0.80
	109	2.74	0.69	0.91
HR47750	112	2.52	1.28	0.91
	111	1.97	1.09	0.85
	110	1.45	0.80	0.80
	109	0.93	0.44	0.77
HR47780	112	1.94	1.34	0.84
	111	1.20	0.81	0.85
	110	0.84	0.57	0.85
	109	0.60	0.41	0.85

5.3 Co-crystallisation

Although it was assumed that the intermediate peak observed in 90% LDPE blends by DSC was due to co-crystallisation, it was difficult to prove this directly as the co-crystallisation was not observed in solution and the resultant structures could therefore not be isolated by prep-TREF. An initial check is to test whether the neat polymers meet the criteria for co-crystallisation. These criteria are similarity in chemical structure, similarity in crystal structure and miscibility or partial miscibility in the melt.[7] LDPE and LLDPE, although possessing the same chemical units, do have significant differences in their chemical structures in terms of branching length. As the LLDPEs were produced by the Ziegler-Natta catalysis method the branching distribution is also random as is the case for LDPE. These differences did not affect the crystal structure, which was orthorhombic in both cases, as was shown in Chapter 4.

5.3.1 Similarity in crystal structure

The crystal structures of the blends also showed no change from that of the neat polymers. The X-ray diffraction patterns shown in Figure 5.21 display all the main peaks from the diffraction patterns of the neat polymers present at all blend ratios, including the blend ratio where co-crystallisation was observed by DSC. It appeared that blending of the LDPE with any grade of LLDPE did not result in a change in the overall crystal system at any blend ratio. This was as expected since all the neat polymers possess the same crystal system and although blending can affect the extent of crystallisation, the crystalline system remained orthorhombic.

Small changes were observed in the shape of the diffraction patterns, specifically the crystal spacings at (110) and (200) which indicated defects within the crystal structure. It has also been suggested that changes in the XRD diffraction pattern could be indicative of blend miscibility or interactions between blend components.[8,9]

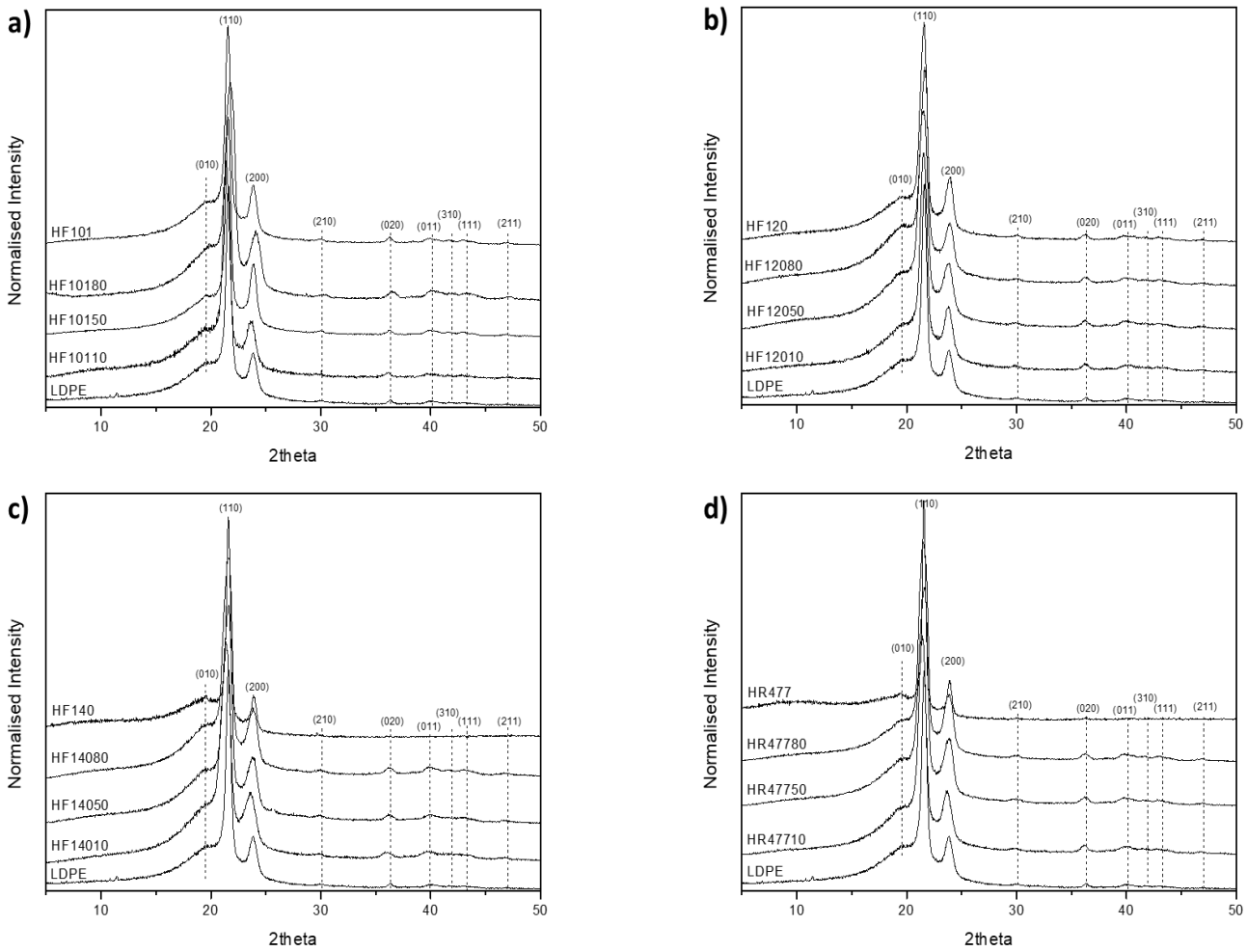

Figure 5. 21 X-Ray diffraction patterns of a) HF101 blends b) HF120 blends c) HF140 blends and d) HR477 blends

5.3.2 Miscibility/partial miscibility in the melt

The remaining criterion is the miscibility or partial miscibility of the blends in the molten state. Although the DSC thermograms show that phase separation occurs upon cooling, the microstructure of the melt cannot be inferred from this. For this reason an alternative method was used to investigate melt miscibility.

It has been shown in our group that polyolefins can be marked with fluorescent cellulose nanowhiskers[10] which are dispersed in the melt and trapped within the polymer due to the high relative viscosity of the polymer solution. The movement of the polyolefin can then be studied by fluorescence microscopy. Cellulose nanowhiskers containing the red fluorescing Rhodamine B were dispersed in an LDPE matrix while cellulose nanowhiskers containing green fluorescent FITC were dispersed within an LLDPE matrix. The fluorescence microscopy images in Figure 5.22 – 5.26 showed that the whiskers were fairly evenly dispersed throughout the LDPE and LLDPE films with very little aggregation occurring.

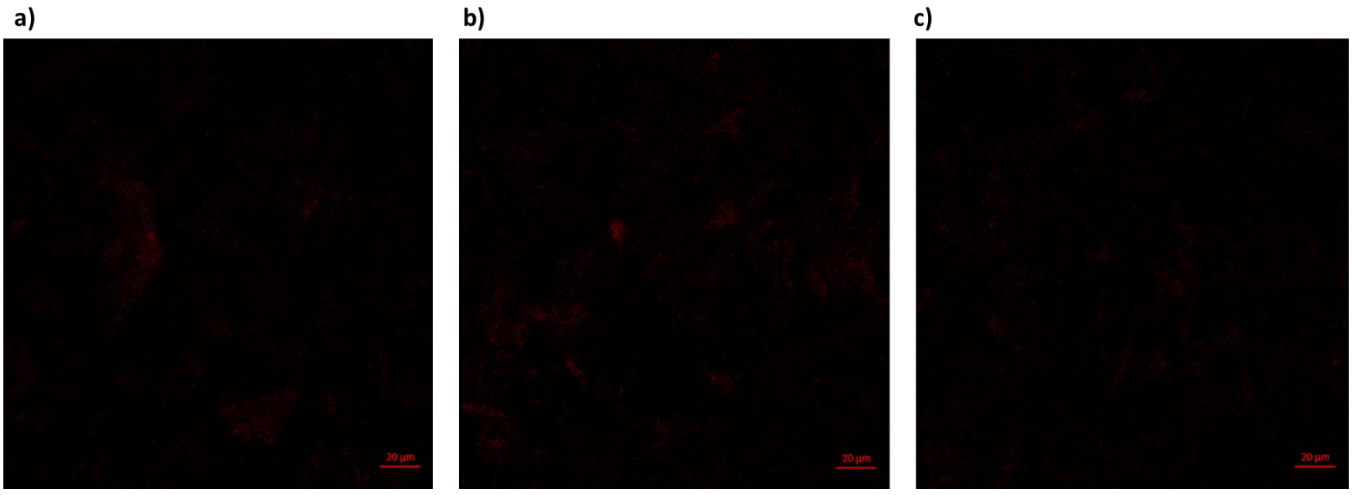

Figure 5. 22 Confocal fluorescence microscopy images of LDPE containing cellulose nanowhiskers tagged with Rhodamine B where a, b and c are different areas of the same film

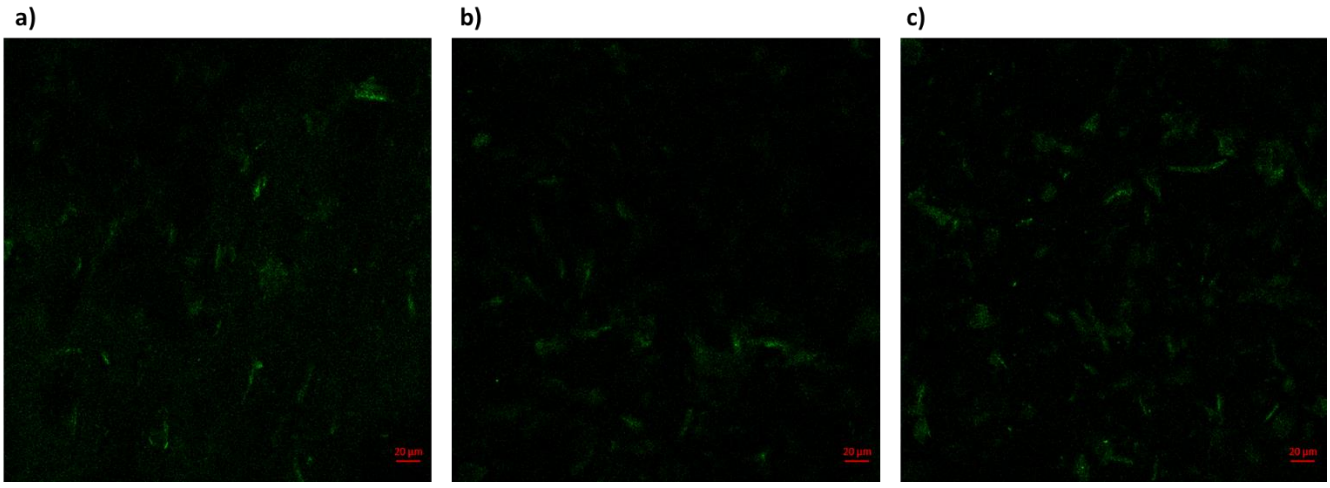

Figure 5. 23 Confocal fluorescence microscopy images of HF101 containing cellulose nanowhiskers tagged with FITC where a, b and c are different areas of the same film

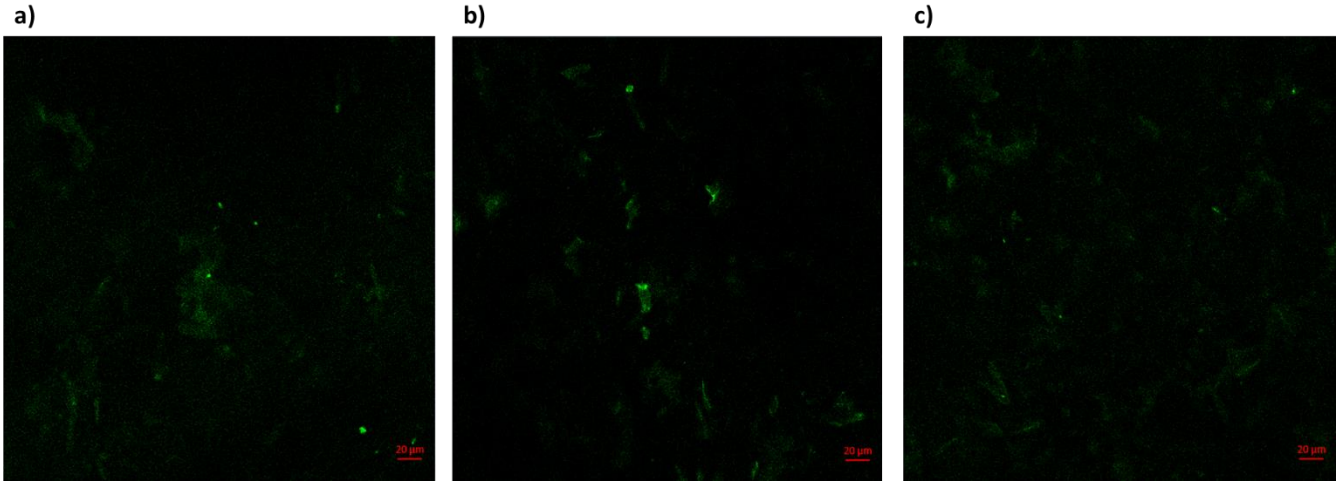

Figure 5. 24 Confocal fluorescence microscopy images of HF120 containing cellulose nanowhiskers tagged with FITC where a, b and c are different areas of the same film

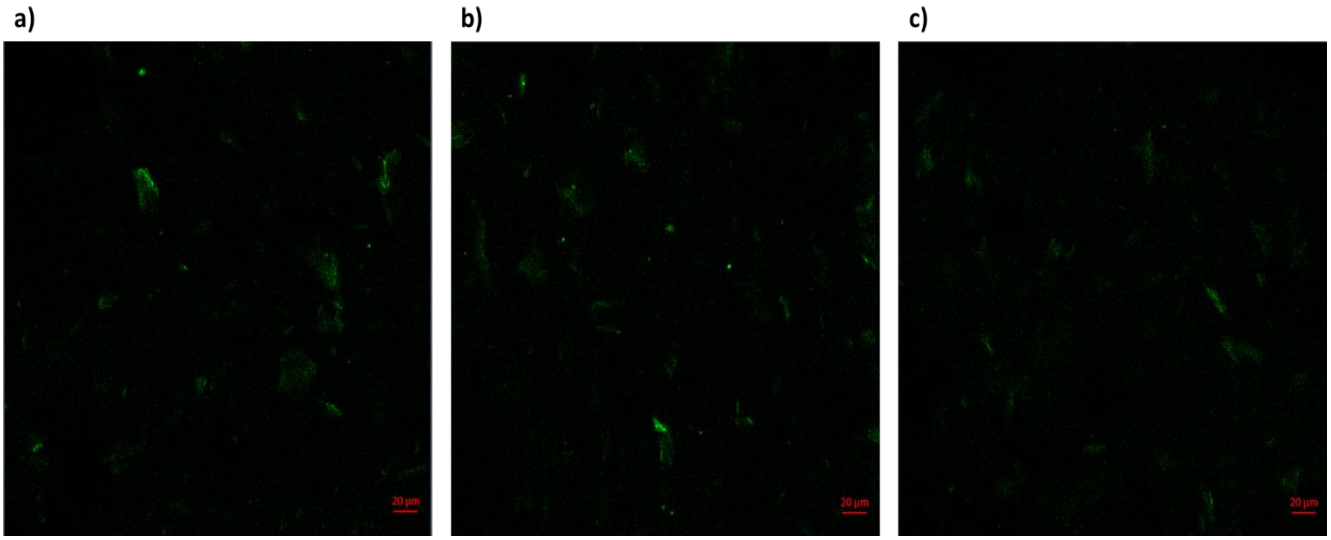

Figure 5. 25 Confocal fluorescence microscopy images of HF140 containing cellulose nanowhiskers tagged with FITC where a, b and c are different areas of the same film

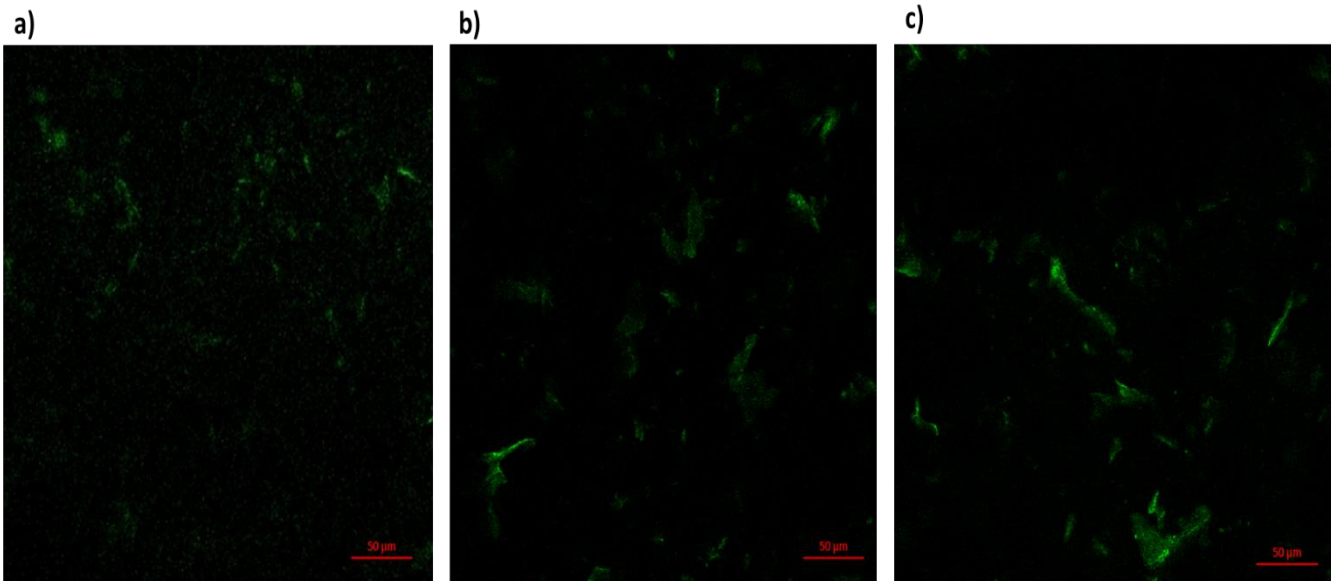

Figure 5. 26 Confocal fluorescence microscopy images of HR477 containing cellulose nanowhiskers tagged with FITC where a, b and c are different areas of the same film

These films containing the fluorescent tags were then melt blended. One tagged LLDPE segment of film and one tagged LDPE film segment were placed adjacent to each other between two sheets of Teflon. Heat was applied to the centre between the two film segments to form the blended region.

If the blends were immiscible in the melt the fluorescence should be separated into domains. Figures 5.27, 5.29, 5.31 and 5.33 do not display any isolated domains, indicating melt miscibility. Although FITC generally appears brighter than Rhodamine B the slight orange tinge to the green fluorescence of the FITC at the centre of the blend was indicative of the presence of Rhodamine B. To confirm this Figure 5.28, 5.30, 5.32, 5.34 shows a depth profile of the (b) region from Figures 5.27, 5.29, 5.31, 5.33. The highest concentration of whiskers occurs in the centre of the film, proving that the nanowhiskers are not simply accumulated onto the surface of the film. More equal contributions from both FITC and Rhodamine B at the centre of the blend occurred for the HF101 and HR477 blends while the remaining blends displayed a dominance of FITC. It is possible that this could indicate the degree of melt miscibility and

would then correspond with the DSC results in Figure 5.2 which indicated that HR477 blends with LDPE were more miscible that HF120 and HF140. Thus this study confirmed the melt miscibility of the LDPE/LLDPE blends.

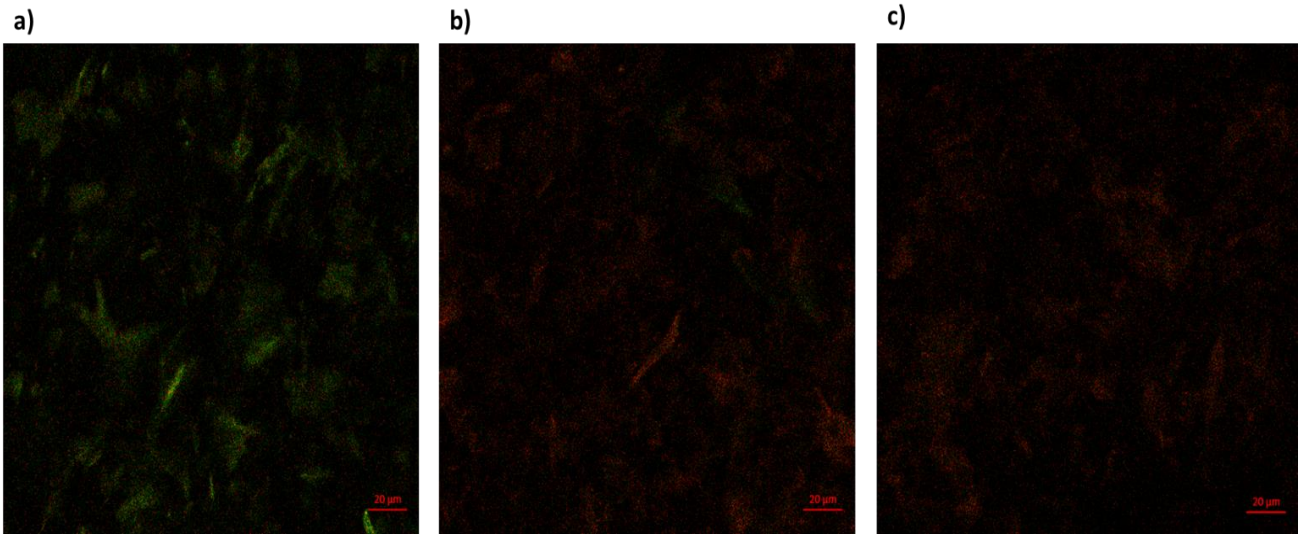

Figure 5. 27 Confocal fluorescence microscopy images of melt blended LDPE and HF101 containing fluorescent cellulose nanowhiskers where the different areas represent a) the HF101 edge containing FITC b) the centre of the blended region c) the LDPE edge containing RhB

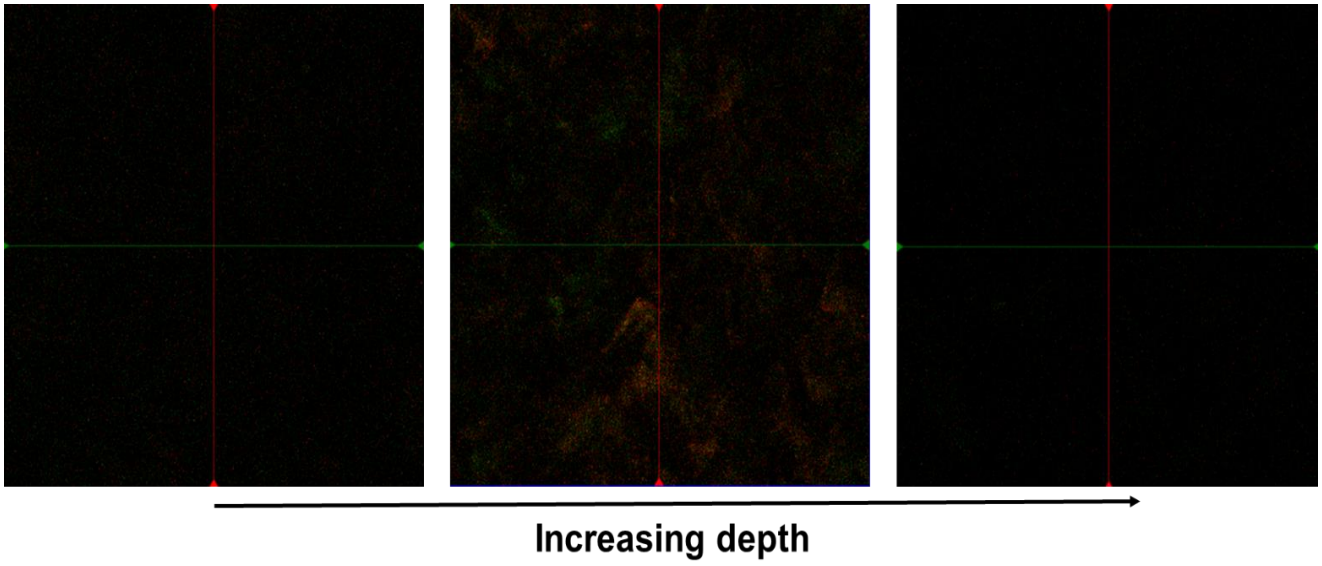

Figure 5. 28 Confocal fluorescence microscopy depth profile of melt blended LDPE and HF101 containing fluorescent cellulose nanowhiskers

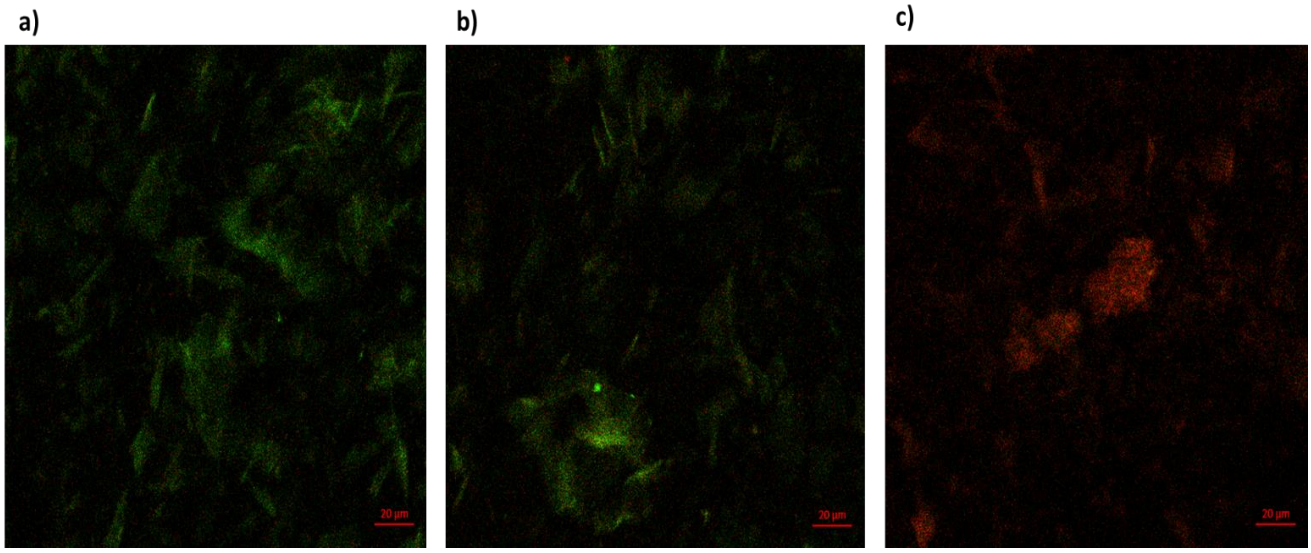

Figure 5. 29 Confocal fluorescence microscopy images of melt blended LDPE and HF120 containing fluorescent cellulose nanowhiskers where the different areas represent a) the HF120 edge containing FITC b) the centre of the blended region c) the LDPE edge containing RhB

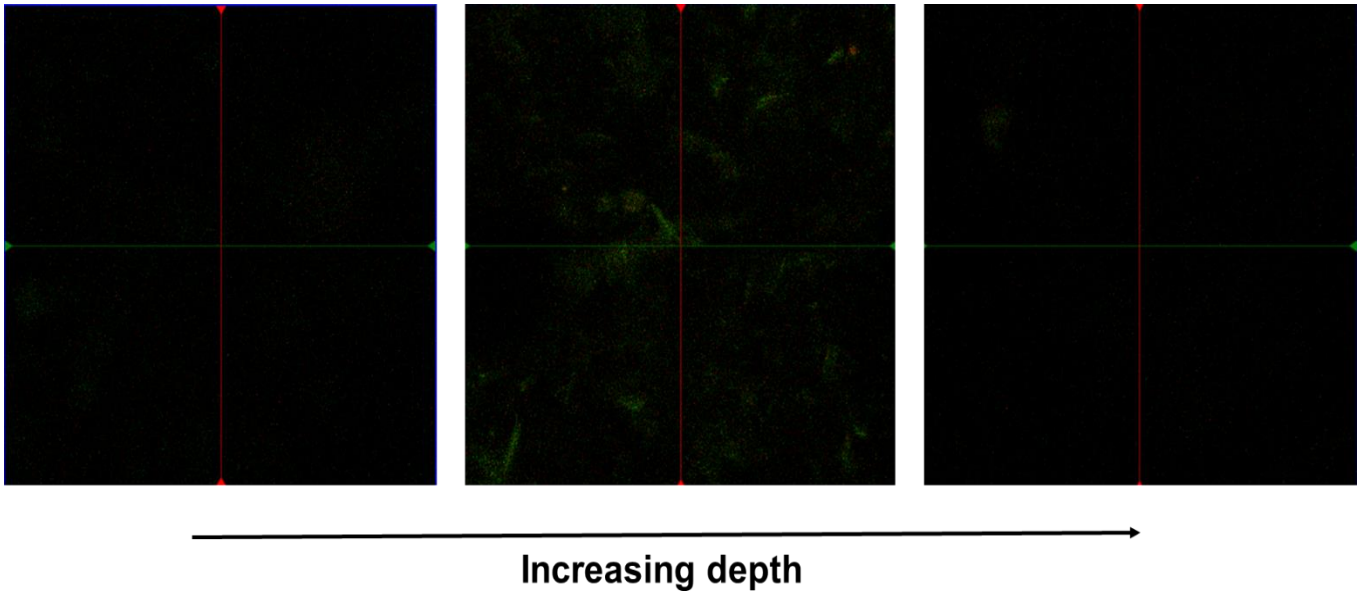

Figure 5. 30 Confocal fluorescence microscopy depth profile of melt blended LDPE and HF120 containing fluorescent cellulose nanowhiskers

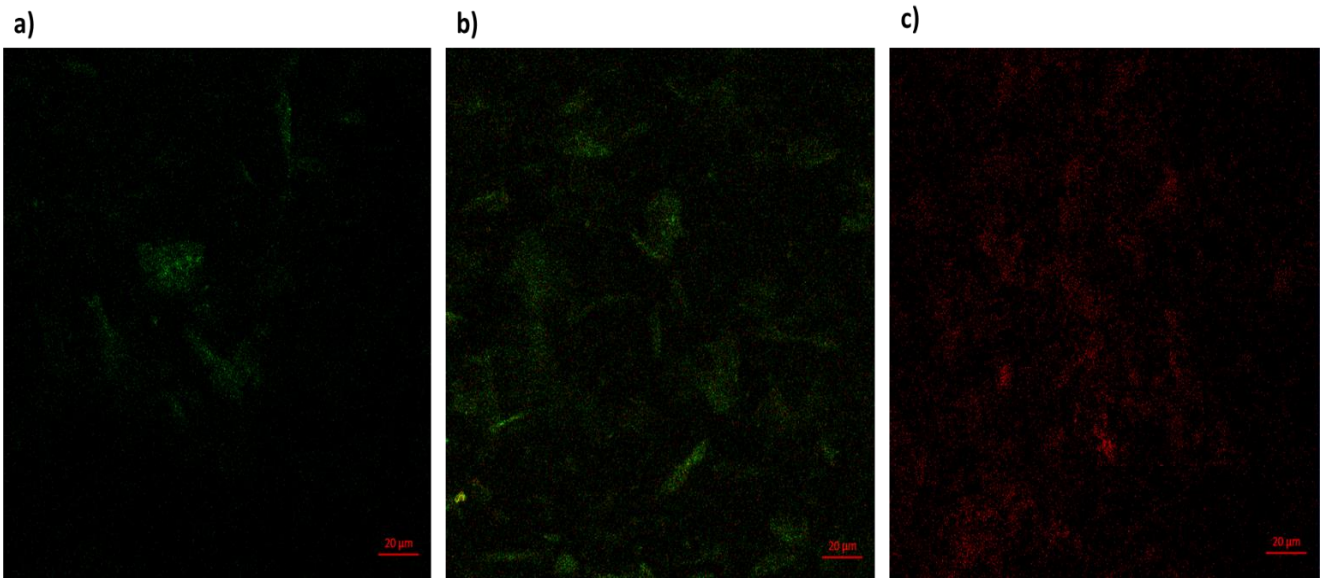

Figure 5. 31 Confocal fluorescence microscopy images of melt blended LDPE and HF140 containing fluorescent cellulose nanowhiskers where the different areas represent a) the HF140 edge containing FITC b) the centre of the blended region c) the LDPE edge containing RhB

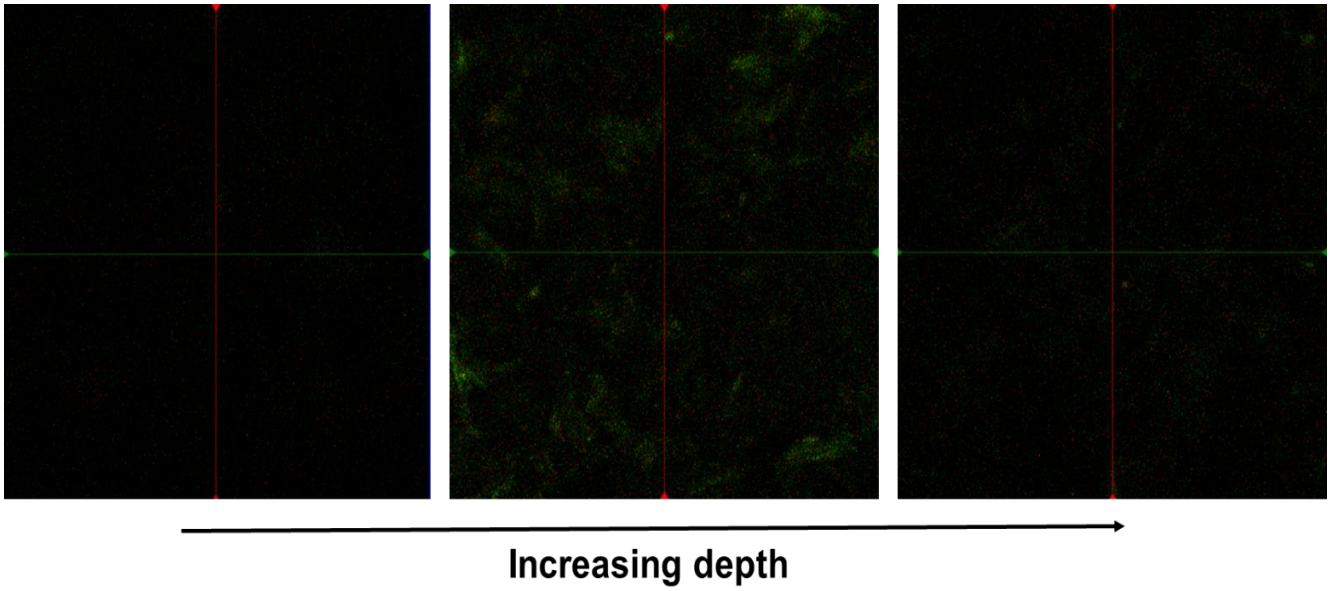

Figure 5. 32 Confocal fluorescence microscopy depth profile of melt blended LDPE and HF140 containing fluorescent cellulose nanowhiskers

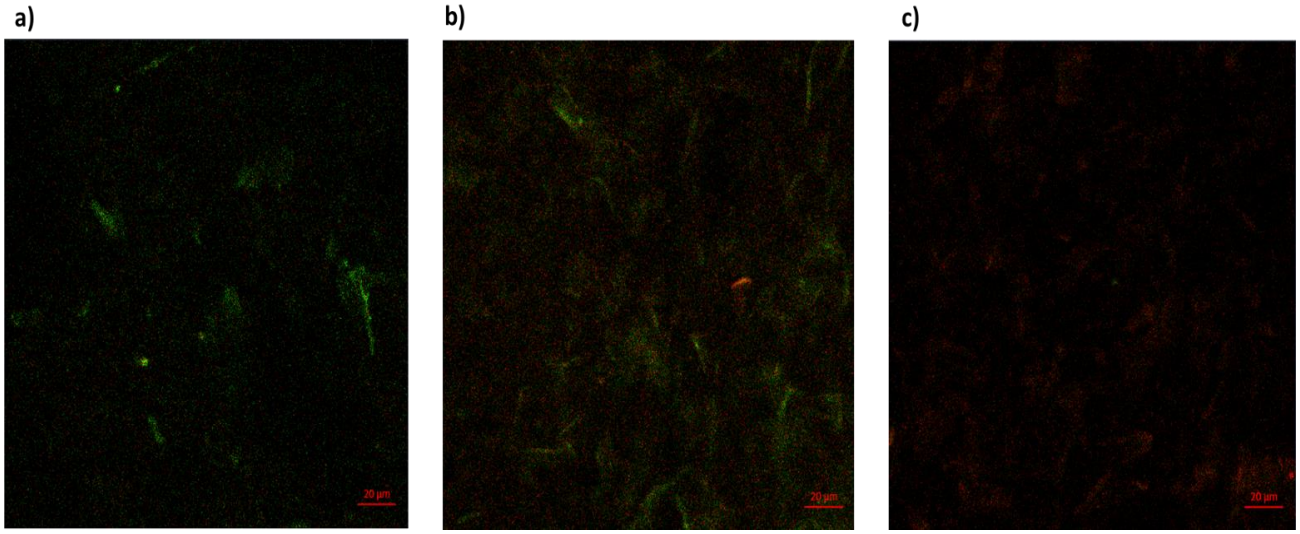

Figure 5. 33 Confocal fluorescence microscopy images of melt blended LDPE and HR477 containing fluorescent cellulose nanowhiskers where the different areas represent a) the HR477 edge containing FITC b) the centre of the blended region c) the LDPE edge containing RhB

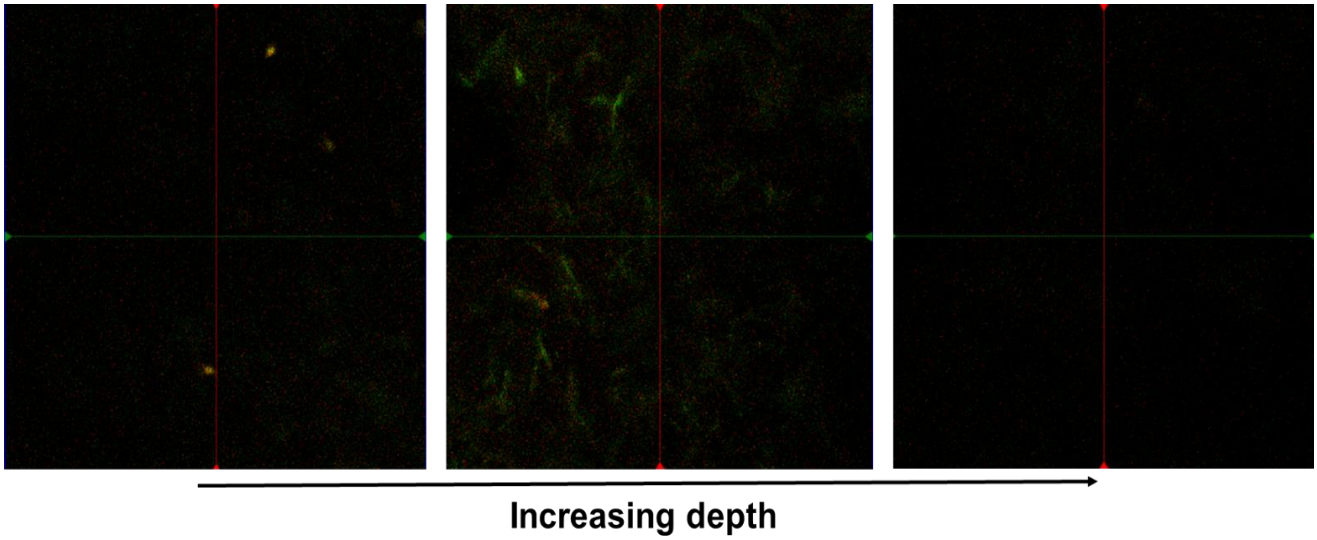

Figure 5. 34 Confocal fluorescence microscopy depth profile of melt blended LDPE and HR477 containing fluorescent cellulose nanowhiskers

The melt miscibility was also evaluated by DSC after quenching the 50/50 blends (the most incompatible blend ratio) from the melt. Figure 5.35 shows the first heating cycle after the quenching. Although the melting event begins at approximately 60 °C for all the quenched blends, only a single melting peak was observed. This, together with the fluorescence study, confirmed the melt miscibility of these blends.

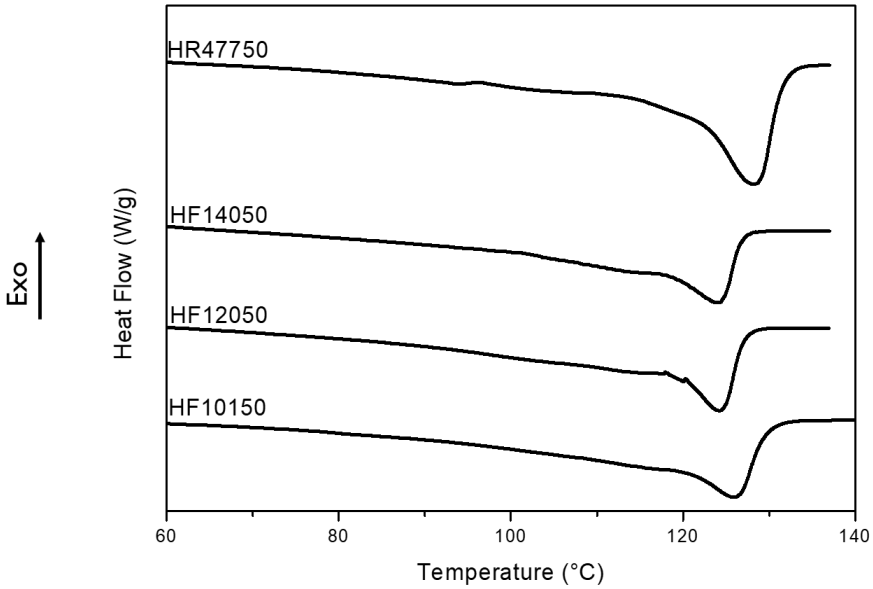

Figure 5. 35 DSC first heating cycle of 50/50 blends after quenching from the melt

5.3.3 Identification of compatibilising component

It is now established that the intermediate melting event observed for 90% LDPE blends could be attributed to co-crystallisation, yet it is still unclear why this apparent co-crystallisation occurred for these specific blends and why it would only occur at the specific blend ratio of 90% LDPE and 10% LLDPE. To understand this phenomenon the LDPE fractions obtained by prep-TREF and discussed in Chapter 4 were used to identify the key component which causes the interaction in these blends.

The majority fraction of the LDPE was the fraction eluting at 70 °C which composed 57.21% of the polymer. This fraction was blended with the LLDPEs in a 90% 70 fraction and 10% LLDPE ratio, the same blend ratio at which co-crystallisation was observed for unfractionated blends. The DSC results of these blends in Figure 5.36 shows that no intermediate melting peak was observed in any of the blends, indicating that no co-crystallisation had occurred. The DSC curves of the LDPE TREF fractions in Figure 4.18 showed a peak melting temperature of 106.2 °C for the LDPE 70 °C fraction. In Figure 5.36 all of the peak melting temperatures of the lowest melting component were below 106.2 °C. This suggests a negative interaction between the LDPE 70 °C fraction and each of the LLDPEs. In other words, the components of the blends are pushing each other away in order to minimise interactions.

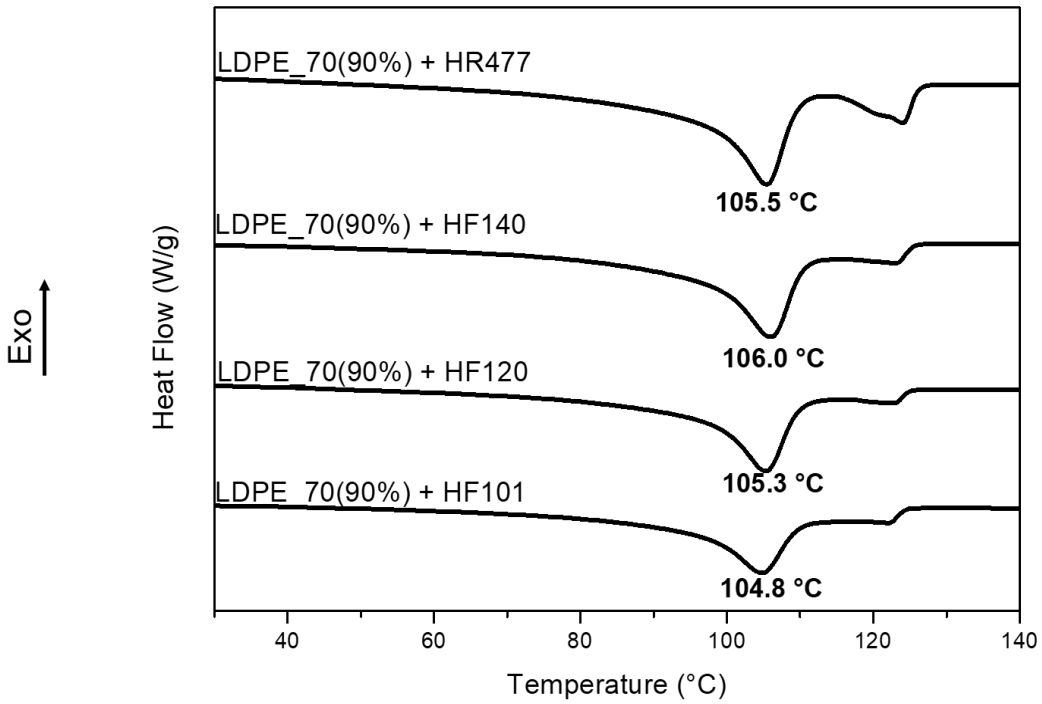

Figure 5. 36 DSC second heating cycles of 90% LDPE 70 fraction with 10% LLDPE blends

As the fraction eluting at 70 °C was not the binding component it was then decided to follow a systematic approach by blending each of the other fractions with the LLDPEs in a 90/10 ratio. Due to a shortage of material obtained from TREF, it was necessary to use the unfractionated 60 °C fraction for blending. Should the triplicate melting peaks be observed we could identify either the 60 °C, 50 °C or 40 °C fractions as the binding component. Figure 5.37 shows the DSC curves of these blends. Once again, the triplicate melting peaks were not observed. The peak melting temperature of the pure unfractionated 60 °C fraction was 101 °C as shown in Figure 4.15 in Chapter 4. In this case the peak melting temperatures of the lower melting component in the blends were slightly higher than that of the pure fraction. This indicated a positive, or associative, interaction. The HF101 and HF120 melting peaks also seemed to disappear in Figure 5.37, which was an indication of co-crystallisation.

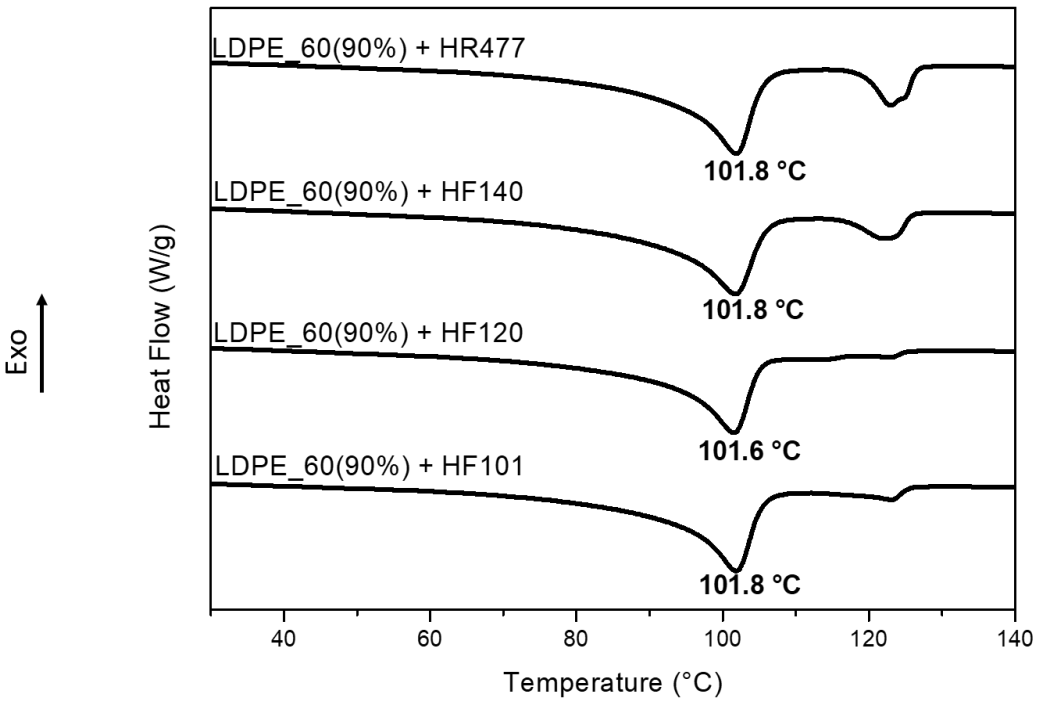

Figure 5. 37 DSC second heating cycles of 90% LDPE 60 fraction with 10% LLDPE blends

It seemed that moving towards the lower eluting fractions was thus a step in the right direction towards finding the binding component. The only fraction below the fraction eluting at 40 °C was the soluble fraction which was eluted at room temperature i.e. 30 °C. The 30 °C fraction was therefore blended with the LLDPEs in a 90/10 blend ratio. Figure 5.38 shows the DSC melting curves of the resultant blends as well as that of the pure 30 °C fraction for comparison. In Figure 5.38 three melting events can be seen per blend melting curve; that of the 30 °C fraction at approximately 72 °C and the melting peaks of the LLDPE component which appeared to have split into two melting peaks. The peaks were not clear for the HF12010 blend due to low quantities of material obtained. The binding component between blends of LDPE and LLDPE could therefore be identified as the LDPE 30 °C fraction. Fractions eluting at 30 °C typically contain a large amount of amorphous material resulting in a significantly lower crystallisation temperature than that of the LLDPEs. The 30 °C fraction should thus still be molten while the LLDPE blend component is crystallising. The highly amorphous nature of the 30 °C fraction even makes nucleation by the crystallised LLDPEs unlikely at the temperature at which the intermediate peak was found. The more likely explanation is that the LDPE soluble fraction associates with a certain component within the LLDPEs, preventing that component from crystallising with the bulk crystalline material. It appeared that below a certain temperature the association between that component and the 30 °C fraction is outweighed by the thermodynamic need of the chains to crystallise.

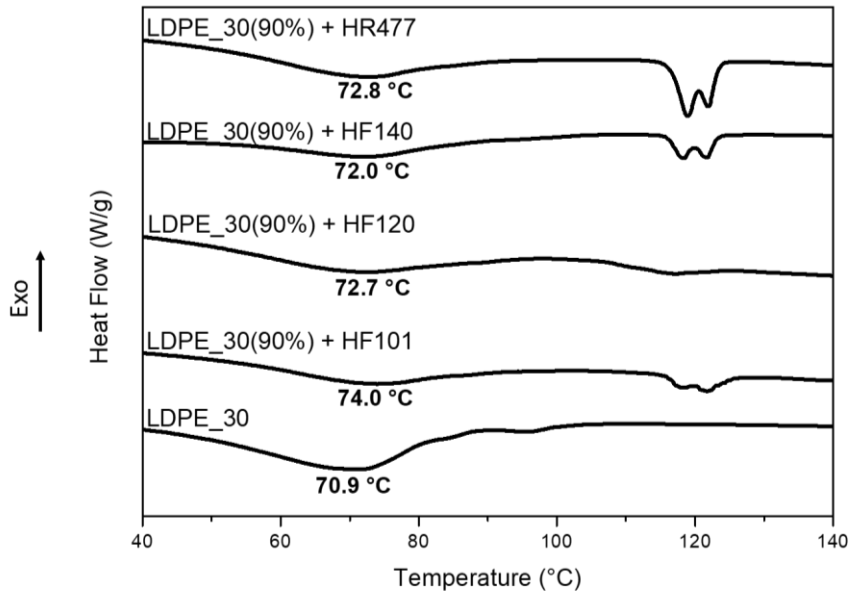

Figure 5. 38 DSC second heating cycles of 90% LDPE 30 fraction with 10% LLDPE blends

Due to the shortage of material eluting at 30 °C obtained by prep-TREF these blends were attempted to be reproduced using the soluble fraction remaining after recrystallizing pure LDPE in xylene. This room temperature fraction isolated by solvent extraction displayed a slightly different composition to that of the 30 °C fraction obtained by prep-TREF in that it contained residue which melted at a peak temperature of 100 °C in the DSC, in addition to the broad melting event at approximately 70° C, which could be attributed to the 60 °C fraction of the LDPE if we look at the results shown in Figure 4.18. It is believed that this 60 °C fraction was also present in the 30 °C fraction obtained by prep-TREF although in smaller quantities, as the molar mass distribution shown in Figure 4.19 displayed a small shoulder at higher molar mass. This was comparable to the molar mass distribution of the solvent extracted 30 °C fraction shown in Figure 5.39.

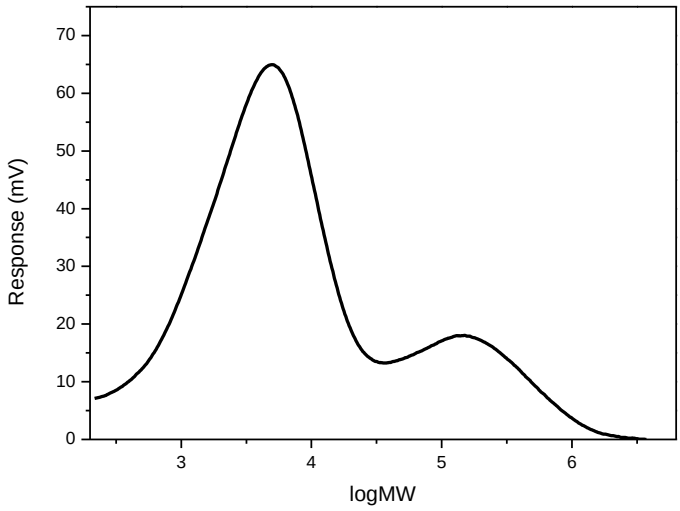

Figure 5. 39 Molar mass distribution of solvent extracted LDPE 30 °C fraction

Nonetheless, the multiple melting events at approximately 120 °C could still be observed when this solvent extracted room temperature fraction was combined with the LLDPEs in a 90/10

blend ratio. The DSC second heating cycles of the solvent extracted room temperature fraction (hereafter denoted SE) and its blends are shown in Figure 5.40. What was also of interest was the extent to which the residual 60 °C fraction interacted with the various LLDPEs in Figure 5.40. A similar trend to that of Figure 5.37 could be seen in that the greatest interaction with the 60 °C fraction occurred for the HF101 and HF120 LLDPE. The interaction demonstrated by the 60 °C fraction with the LLDPEs and the fact that the 30 °C fraction could not be isolated from the 60 °C fraction by solvent extraction suggested a similarity between these fractions.

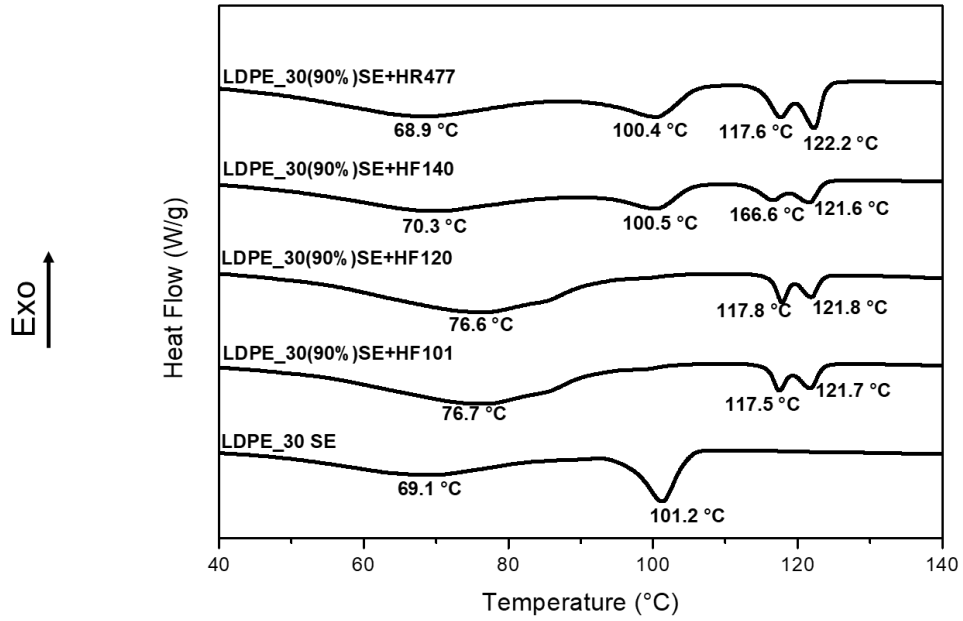

Figure 5. 40: DSC second heating cycles of 90% solvent extracted LDPE room temperature fraction (LDPE SE) and 10% LLDPE blends

Proton wideline spectra obtained from solid state NMR can provide great insight into sample rigidity. By understanding the sample properties as determined by other techniques such as DSC and XRD, wideline spectra can be used as a tool to make deductions about crystallinity variations. In general wideline spectra of semi-crystalline polymers can be separated into two components; a broad base which represents the highly crystalline component and a sharp peak representing the highly mobile components. The causes for the shapes of these components has been discussed in Chapter 2.

In Figure 5.41 a the proton wideline spectrum of LDPE SE shows a narrow peak which indicated high mobility, however the slightly wider base of the narrow peak indicated that the LDPE SE also contained a more rigid component. This was in agreement with the DSC melting endotherms showing a more crystalline component melting at approximately 101 °C present within the LDPE SE sample. The HF101 grade LLDPE displayed a fairly narrow wideline spectrum in Figure 5.41 c, which suggested a relatively high mobility. The percentage area for the broad components at the base of the spectra in a, b and c was 58.1%, 51.4% and 76.7% respectively. It should be noted that the percentage area of the blend was the lowest of the three and similar to that of the LDPE SE.

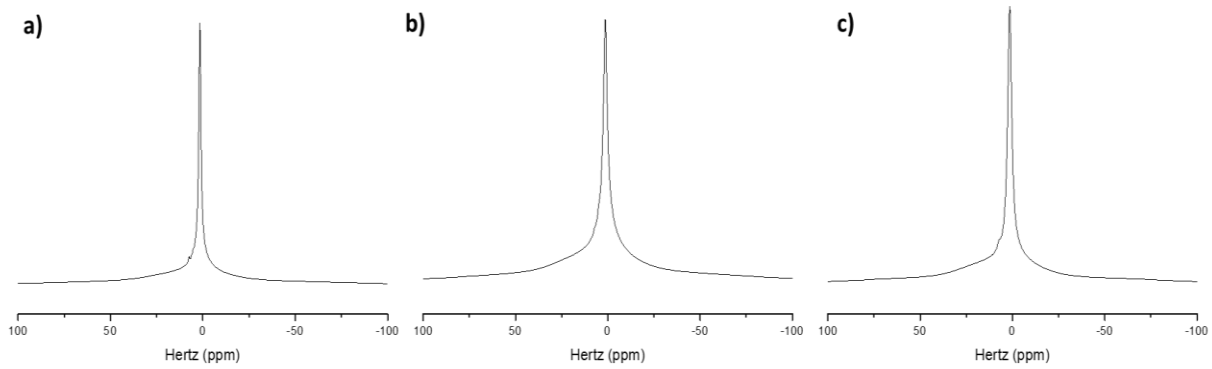

Figure 5. 41 ^{1}H wideline spectra of a) LDPE SE b) 90% LDPE SE 10% HF101 blend and c) HF101 LLDPE

The HF120 LLDPE showed a significantly more rigid wideline spectrum than the HF101, in Figure 5.42 c. In contrast, from Table 4.2 in Chapter 4, the DSC melt enthalpy showed that the HF120 grade possessed the lowest crystallinity of the LLDPEs. Conversely the HF120 possessed the highest average molar mass of the LLDPEs, suggesting that the reptation of the chains were dramatically slowed due to the weight of the chains. The high rigidity observed in the proton wideline spectrum can therefore possibly be attributed to the high molar mass of the HF120 LLDPE. The percentage area for the broad components at the base of the spectra in a, b and c was 58.1%, 76.4% and 72.2% respectively.

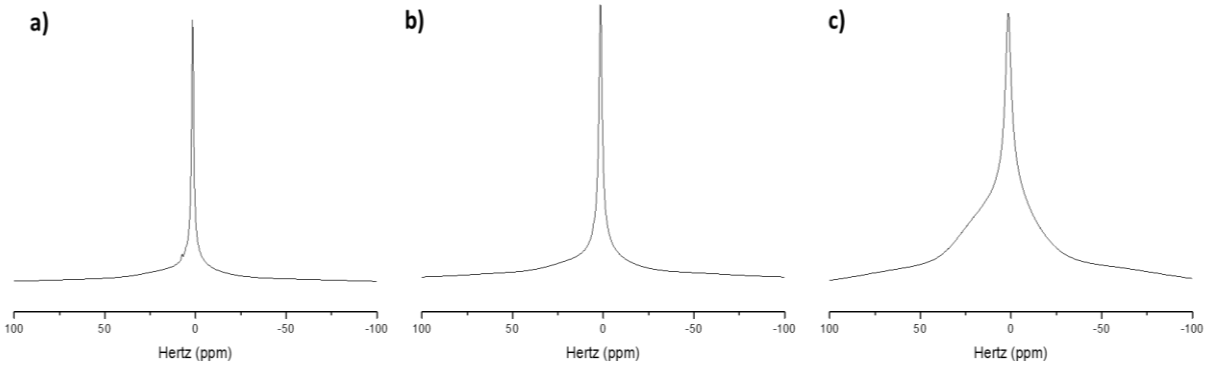

Figure 5. 42 ^{1}H wideline spectra of a) LDPE SE b) 90% LDPE SE 10% HF120 blend and c) HF120 LLDPE

The HF140 grade LLDPE in Figure 5.43 c displayed a similar wideline spectrum to that of the HF120 LLDPE, however in this case the broad base of the spectrum was a result of rigidity due to crystallinity. The blend shown in Figure 5.43 b displayed a second narrow peak which suggested to mobile phases. The DSC data also showed that this blend seemed to be the most incompatible of the four blends and it is likely that this incompatibility resulted in phase separation. What was interesting to observe was that the phase separation seems to have occurred within the mobile phase and not the crystalline phase. The percentage area of the broad components at the base of the spectra in a, b and c was 58.1%, 76.5% and 74.0% respectively. The high crystallinity in the blend once again indicated that the phase separation occurred within the mobile phase.

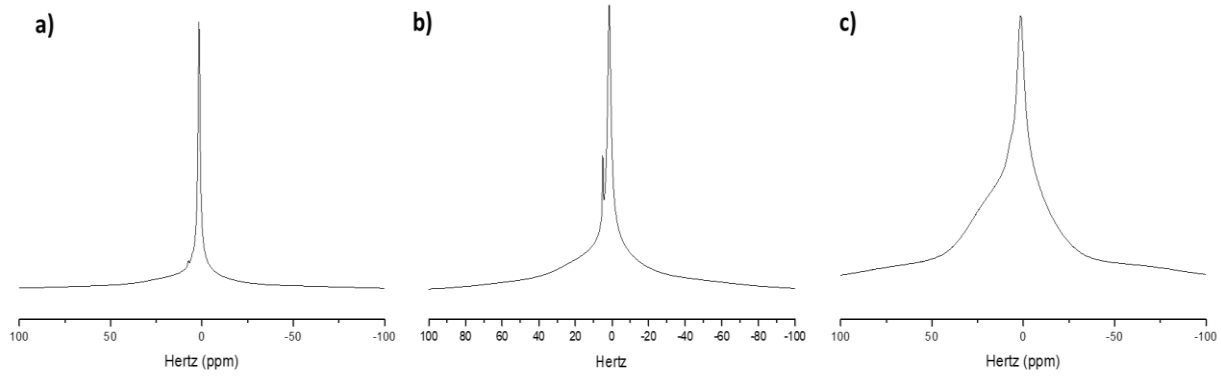

Figure 5. 43 ^{1}H wideline spectra of a) LDPE SE b) 90% LDPE SE 10% HF140 blend and c) HF140 LLDPE

As was expected for the most crystalline grade of LLDPE, the HR477 displayed a broad wideline spectrum in Figure 5.44 c, indicating significant rigidity. The percentage area for the broad components at the base of the spectra in a, b and c was 58.1%, 56.9% and 91.6% respectively.

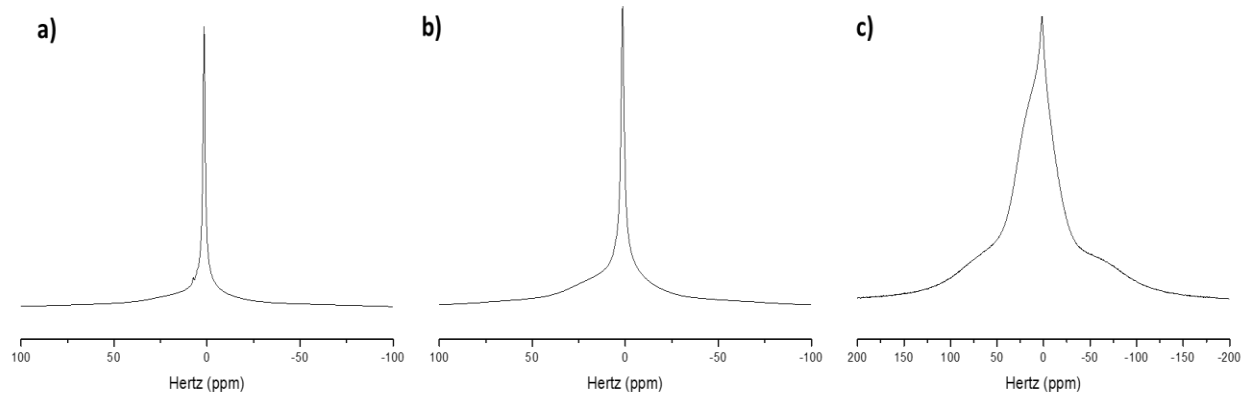

Figure 5. 44 ^{1}H wideline spectra of a) LDPE SE b) 90% LDPE SE 10% HR477 blend and c) HR477 LLDPE

The ^{13}C CP MAS spectra with dipolar decoupling (DD) of the LDPE SE and neat polymers with variable contact times are shown in Figures 5.45 – 5.46 focusing specifically on the internal chain methylene carbon region around 30-33 ppm. The variation in the spectra at different contact times is attained when the components contributing to the signal have differences in the rates at which they are cross-polarised.[11] This means that resonances due to more rigid components will be visible at short contact times while more mobile components which are less strongly coupled will only be visible at longer contact times.

The methylene resonance in the ^{13}C CP MAS DD spectra was split into two regions; a peak at approximately 33 ppm due to the carbons in an all-trans conformation giving rise to the orthorhombic crystalline structure and a lesser peak at approximately 30 ppm due to methylene sequences containing more gauche conformations leading to a more amorphous environment.[12]

In Figure 5.45 it is clear that the LDPE SE contains a significant crystalline component, while at 5 and 8 ms (when only mobile components should be visible) the peak at 32.61 ppm was still present. This indicated that within the crystalline domain there exists substantial mobility.

The ^{13}C CP MAS DD of the blends in Figure 5.46 a-d shows that the peak due to methylene carbons in the amorphous regions was significantly smaller than that of the LDPE. The majority of the methylene carbons were therefore in a crystalline environment. This was expected as it was known that the LLDPEs crystallise to a greater extent than the LDPE sample. Similarly to the ^{13}C CP MAS DD of the LDPE SE the resonance due to the methylene carbons in the orthorhombic crystalline domains also displayed significant mobility. This can again be seen by the visibility of the crystalline peak at a contact time of 5 ms and 8 ms in Figure 5.46 a-d.

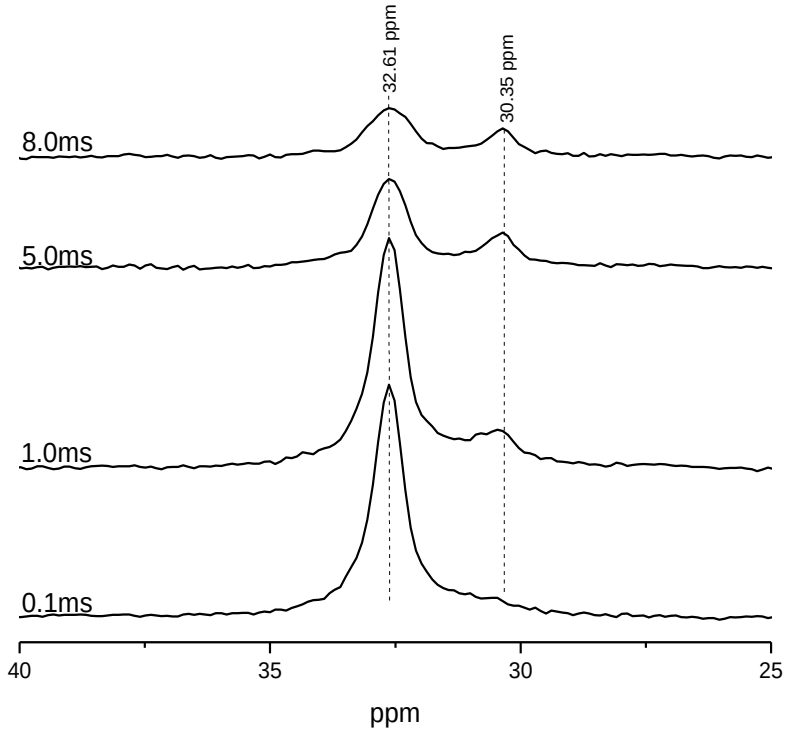

Figure 5. 45 ^{13}C CP MAS spectra of LDPE SE at various contact times

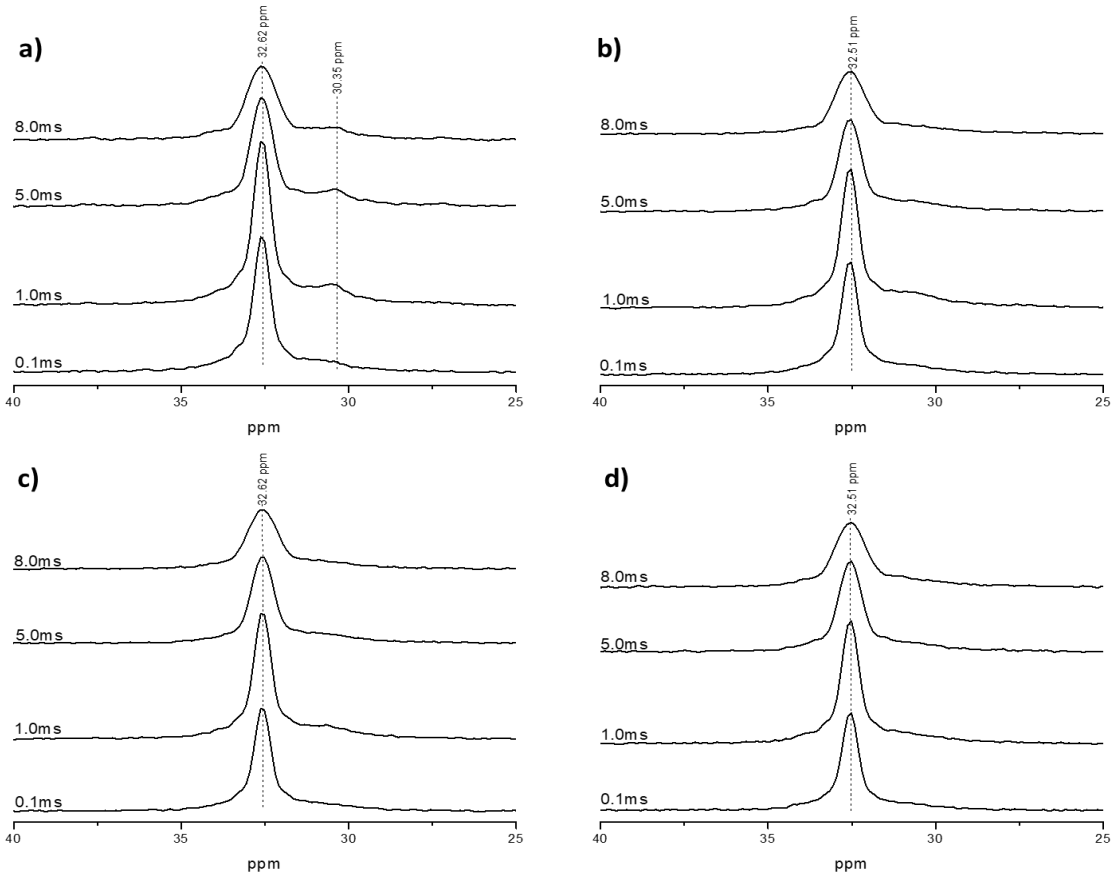

Figure 5. 46 ^{13}C CP MAS spectra for a) HF101 b) HF120 c) HF140 and d) HR477 LLDPEs at various contact times

Figure 5.47 a-d shows the ^{13}C CP MAS DD spectra of the blends at various contact times. It is immediately noticeable that the peak at approximately 30 ppm due to the methylene carbons in the amorphous areas has increased relative to that of the LLDPE spectra shown in Figure 5.46 a-d. It also appeared that the area under the crystalline peak at a contact time of 8 ms had decreased in all cases from a-d. This implied that fewer of the methylene carbons in the blends were in a more mobile crystalline phase than had been in the case of the neat LLDPEs. This was most likely due to the presence of the LDPE SE which enhanced the blend mobility.

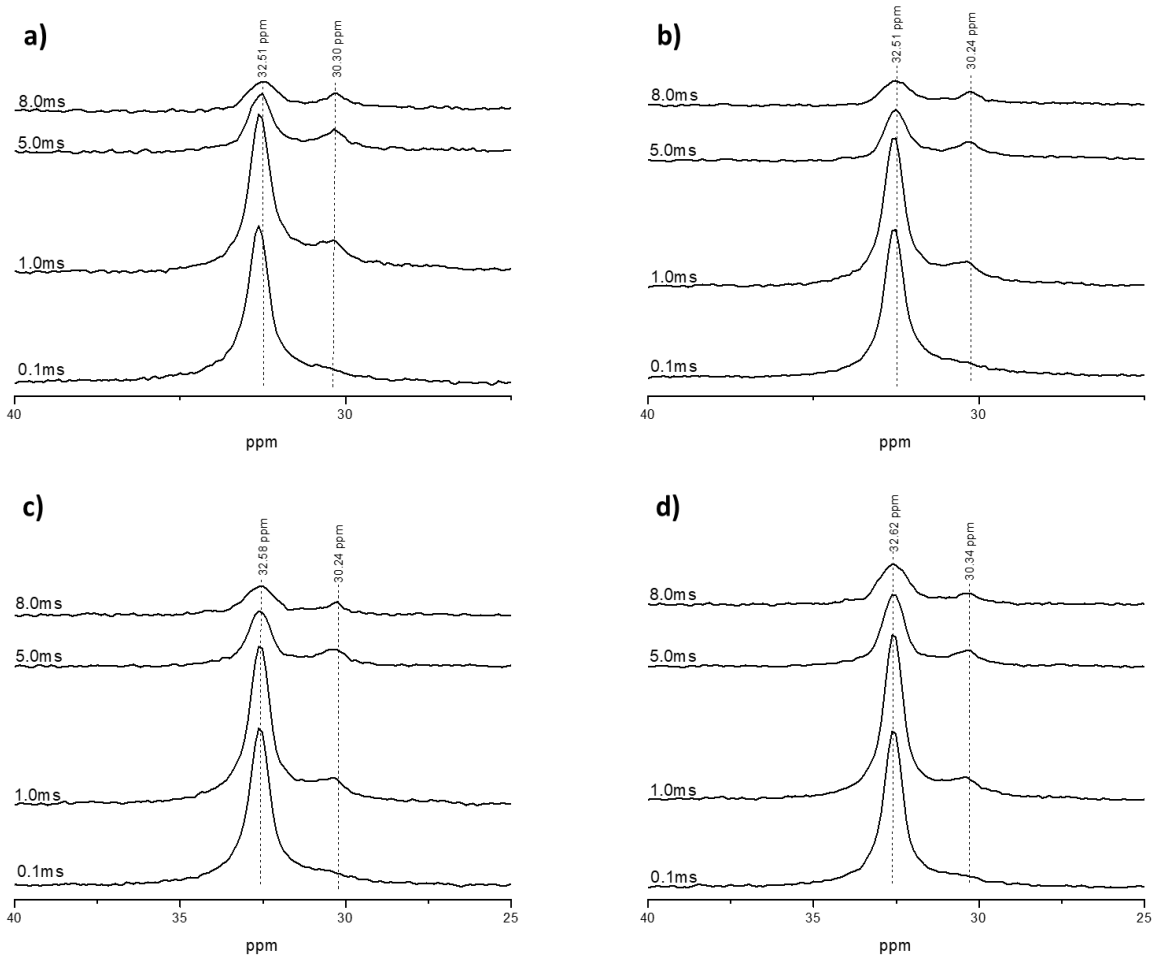

Figure 5. 47 ^{13}C CP MAS spectra for a) 90% LDPE SE 10% HF101 b) 90% LDPE SE 10% HF120 c) 90% LDPE SE 10% HF140 and d) 90% LDPE SE 10% HR477 blends at various contact times

While CP MAS NMR spectra can demonstrate a slight bias towards more rigid components the SPE excitation (SPE) experiment, in contrast, has a bias towards more mobile components. By increasing the duration of the SPE experiment this bias can be reduced to obtain a more representative spectrum than could be obtained by CP MAS. For this reason the SPE experiments have been the subject of quantitative analysis as opposed to the CP MAS spectra.

In Figure 5.49 the methylene region obtained by the SPE experiment of the LDPE SE sample can be seen. Once again the methylene region contains multiple components; a peak at approximately 30 ppm due to the methylene carbons in the amorphous regions (designated ‘a’) as well as the peak at approximately 32.5 ppm due to methylene carbons in crystalline domains (designated ‘c’). The origin of the shoulder at approximately 34 ppm (peak ‘d’) has been the source of some debate. Some authors have proposed that the peak is due to a monoclinic crystalline structure and therefore forms part of the peak at 32.5 ppm.[13] Based on Grant and Paul empirical calculations the carbon in the γ position (see Figure 5.48) should display a peak at 34 ppm. In this case, no monoclinic crystalline phase was observed by XRD, which should occur at a 2θ of 19.4°.[14] In addition, the ^{13}C CP MAS (which has a rigidity bias) shows no shoulder at 34 ppm which it should have had another crystalline phase been present. The conclusion was therefore that the peak at 34 ppm observed in the SPE experiment could be attributed to the γ position on the chain backbone.

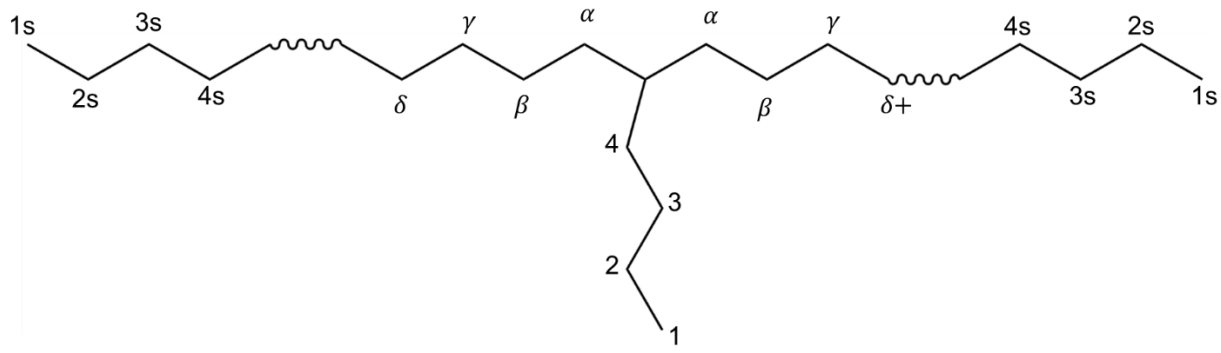

Figure 5. 48 Notation used for assignments of carbons in ethylene-1-hexene copolymers

The peak designated as ‘b’ can be interpreted as the methylene carbons which exist between the crystalline and amorphous phases; an interfacial region.[15] Of interest is how this interfacial region varies between blends. For the LDPE SE the interfacial region formed 44.7% of the methylene resonance (calculated by excluding the contribution of the γ carbon).The amorphous peak ‘a’ contributed 24.0% to the overall resonance while the crystalline peak ‘c’ contributed 31.2%.

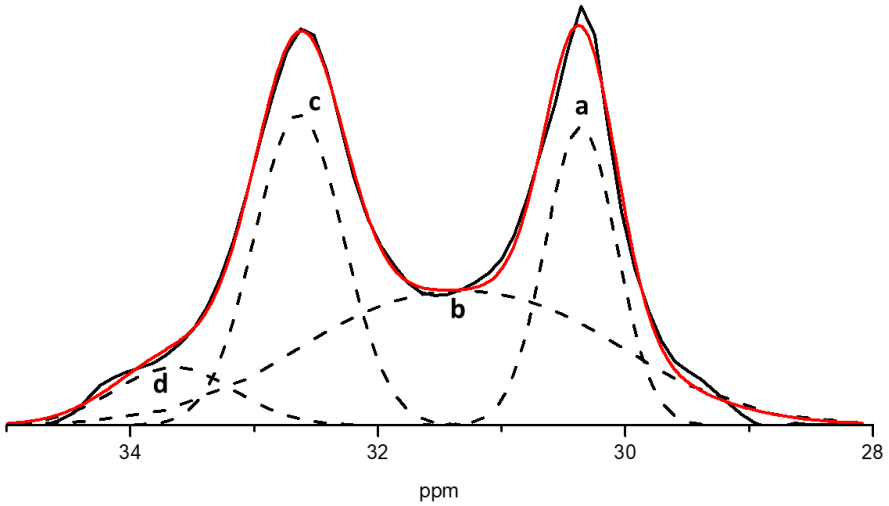

Figure 5. 49 Deconvolution of the methylene region of the LDPE SE ^{13}C SPE spectrum

Table 5. 16 Mass fractions obtained by deconvolution of LDPE SE SPE spectrum (R^2 = 99.5)

Peak	δ (ppm)	Fraction (%)	Fitting function
a	30.36	22.30	Gaussian
b	31.32	41.50	Gaussian Lorentzian Cross
c	32.64	28.99	Gaussian
d	33.64	7.18	Gaussian

Figure A.1 in Appendix A shows the SPE experiment of the HF101 LLDPE. The amorphous phase (peak ‘a’) contributed 12.7% to the total resonance while the crystalline phase (peak ‘c’) contributed 44.6%. As expected of the LLDPEs relative to the LDPE SE, the crystalline domain forms a much more significant contribution to the overall resonance. The interfacial region (peak ‘b’) contributed 42.6% to the total resonance. In this case the position of the interfacial region was shifted towards the amorphous peak position, indicating that this region

was more amorphous in character. This is not surprising as in many cases other researchers have allocated the interfacial region to a component within the amorphous peak.[15,13]

Table 5. 17 Mass fractions obtained by deconvolution of HF101 SPE spectrum (R^2 = 99.6)

Peak	δ (ppm)	Fraction (%)	Fitting function
a	30.37	11.91	Gaussian
b	30.42	39.73	Gaussian Lorentzian Cross
c	32.51	41.64	Gaussian Lorentzian Cross
d	33.96	6.72	Gaussian

Figure A.2 in Appendix A shows the SPE experiment of the HF120 LLDPE. In this case the deconvolution of the SPE resonance yielded five components. Peak ‘b’ due to the amorphous phase contributed 29.5% to the total resonance while peak ‘d’ due to the crystalline phase contributed 30.4%. The crystalline domain contributes less to the overall resonance than in the case of the HF101, which correlates to the DSC results which show a lower melt enthalpy for the HF120 then the HF101. The interfacial region (peak ‘c’) contributed 40.0% to the total resonance. The peak labelled ‘a’ was most likely due to a saturated chain end[16] (4s in Figure 5.48 above).

Table 5. 18 Mass fractions obtained by deconvolution of HF120 SPE spectrum (R^2 = 99.9)

Peak	δ (ppm)	Fraction (%)	Fitting function
a	29.39	10.81	Gaussian Lorentzian Cross
b	30.33	23.61	Gaussian
c	31.26	32.01	Gaussian
d	32.55	24.25	Gaussian
e	33.57	9.30	Gaussian

Figure A.3 in Appendix A shows the SPE experiment of the HF140 LLDPE. The deconvolution of the methylene region of this spectrum also yielded five components. Once again the backbone γ position and the saturated end group was visible as peaks ‘a’ and ‘e’. Peak ‘b’ due to the amorphous phase contributed 20.4% to the total resonance while peak ‘d’ due to the crystalline phase contributed 33.2%. The interfacial region (peak ‘c’) contributed 46.4% to the total resonance.

Table 5. 19 Mass fractions obtained by deconvolution of HF140 SPE spectrum (R^2 = 99.9)

Peak	δ (ppm)	Fraction (%)	Fitting function
a	29.50	12.31	Gaussian
b	30.34	16.88	Gaussian
c	31.16	38.28	Gaussian
d	32.56	27.37	Gaussian
e	33.58	5.14	Gaussian

The SPE experiment of the HR477 LLDPE is shown in Figure A.4 in Appendix A. The deconvolution of the methylene region of this spectrum yielded four components. It was clear from Figure A.4 that this grade of LLDPE was highly crystalline but the same sample also contains a high amorphous content, most likely due to the lower molar mass. Peak ‘a’ due to the amorphous phase contributed 45.0% to the total resonance while peak ‘d’ due to the

crystalline phase contributed 37.3%. Interestingly there appeared to be two interfacial regions; peaks ‘b’ and ‘c’ which each contributed 10.9% and 6.5% respectively. Interfacial peak ‘b’ seemed to be more amorphous in character while interfacial peak ‘c’ seemed to have the more conventional interfacial composition which is approximately equal parts crystalline and amorphous.

Table 5. 20 Mass fractions obtained by deconvolution of HR477 SPE spectrum (R^2 = 99.8)

Peak	δ (ppm)	Fraction (%)	Fitting function
a	30.31	45.00	Gaussian
b	30.89	10.88	Gaussian
c	31.56	6.47	Gaussian
d	32.47	37.63	Gaussian Lorentzian Cross

Table 5.21 summarises the contributions of the interfacial regions within the various neat polymers. The HF140 LLDPE possessed the largest interfacial region, closely followed by the LDPE SE and the HF101. The HR477 LLDPE possessed the lowest interfacial region at 17.4%.

Table 5. 21 Mass fractions of interfacial regions obtained by deconvolution of SPE spectra of neat polymers

Sample	Interfacial fraction (%)
LDPE SE	44.7
HF101	42.6
HF120	40.0
HF140	46.4
HR477	17.4*

* Sum of two interfacial regions

Figure 5.50 displays the deconvolution of the methylene region of the SPE spectrum of the HF10110 blend. While peak ‘d’ and ‘c’ can be attributed to the crystalline and interfacial phases respectively, the assignment of the amorphous phase is ambiguous as the amorphous phase seemed to consist of two regions. While it had previously been assumed that the multiple melting events occurring for these blends observed by DSC was due to formation of different crystalline phases Figure 5.50 suggested that those events were the result of multiple amorphous phases forming within the blends.

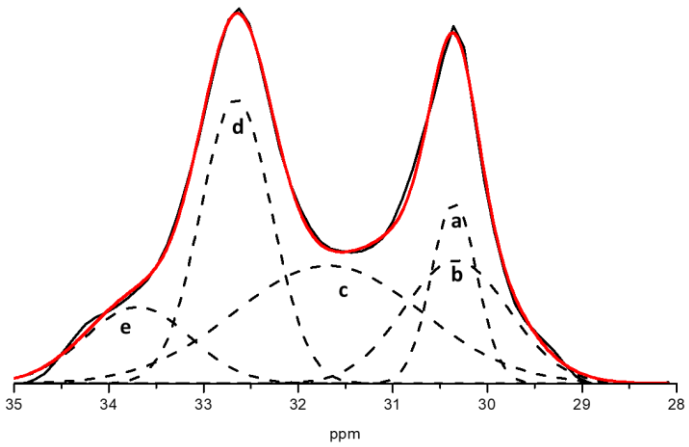

Figure 5. 50 Deconvolution of the methylene region of the ^{13}C SPE spectrum of 90% LDPE SE 10% HF101 blend

Table 5. 22 Mass fractions obtained by deconvolution of 90% LDPE SE 10% HF101 blend SPE spectrum (R^2 = 99.6)

Peak	δ (ppm)	Fraction (%)	Fitting function
a	30.33	18.03	Gaussian
b	30.35	11.49	Gaussian
c	31.68	30.85	Gaussian
d	32.65	28.31	Gaussian
e	33.69	11.28	Gaussian

Figure A.5 in Appendix A displays the deconvolution of the methylene region of the SPE spectrum of the HF12010 blend. Peaks ‘c’ and ‘a’ correspond to the crystalline and amorphous components respectively. Peaks ‘b’ and ‘d’ were tentatively classified as interfacial regions as the contributions were too large to be that of end groups. 72.18% of the signal was therefore contributed by interfacial regions further confirming that the rigidity of the HF120 blends could largely be attributed to the high molar mass of the HF120 blend component and not to crystallinity.

Table 5. 23 Mass fractions obtained by deconvolution of 90% LDPE SE 10% HF120 blend SPE spectrum (R^2 = 99.7)

Peak	δ (ppm)	Fraction (%)	Fitting function
a	30.31	8.83	Gaussian
b	30.50	28.34	Gaussian
c	32.60	18.98	Gaussian
d	32.68	43.84	Gaussian

Figure A.6 in Appendix A displays the deconvolution of the methylene region of the SPE spectrum of the HF14010 blend. Peaks ‘d’ and ‘b’ correspond to the crystalline and amorphous components respectively and peak ‘c’ to the interfacial region. Although the saturated end group was once again visible at peak ‘e’ the peak labelled ‘a’ had too large a contribution to consist solely of the γ signal. It appeared that the resonance due to a second amorphous phase overlapped with that of the end group.

Table 5. 24 Mass fractions obtained by deconvolution of 90% LDPE SE 10% HF140 blend SPE spectrum (R^2 = 99.7)

Peak	δ (ppm)	Fraction (%)	Fitting function
a	30.03	24.43	Gaussian
b	30.29	16.24	Gaussian
c	31.16	24.54	Gaussian Lorentzian Cross
d	32.56	28.71	Gaussian
e	33.69	6.06	Gaussian

Figure A.7 in Appendix A displays the deconvolution of the methylene region of the SPE spectrum of the HR47710 blend. Peaks ‘d’ and ‘a’ correspond to the crystalline and amorphous components respectively and peak ‘c’ to the interfacial region. There was a significant overlap of the interfacial peak ‘c’ and the crystalline peak, suggesting a fairly rigid interfacial region. Peak ‘b’ also appeared to be an interfacial region with more amorphous character. It was possible that the combination of a rigid interfacial and a more mobile interfacial phase was the reason for the enhanced compatibility between the HR477 grade LLDPE and the LDPE.

Table 5. 25 Mass fractions obtained by deconvolution of 90% LDPE SE 10% HR477 blend SPE spectrum (R^2 = 99.9)

Peak	δ (ppm)	Fraction (%)	Fitting function
a	30.25	9.12	Gaussian
b	30.38	39.84	Gaussian
c	32.17	24.93	Gaussian
d	32.54	18.82	Gaussian
e	33.29	7.26	Gaussian

In order to corroborate the deconvolution of the methylene region of the SPE spectra relaxation experiments were also conducted in order to determine the number of components which a relaxation can be attributed to. The form of the spin-spin relaxation spectrum is an exponential decay to which Equation 5.1 can be fitted to obtain the value of T_2 where I is the total intensity of the magnetisation, A_1 is a constant and t is the echo time in µs.

$$I = I_0 + A_1 \exp\left(\frac{t-t_0}{T_2}\right) \quad (5.1)$$

In most cases a three parameter exponential decay yielded the best fit to the T_2 relaxation graphs.

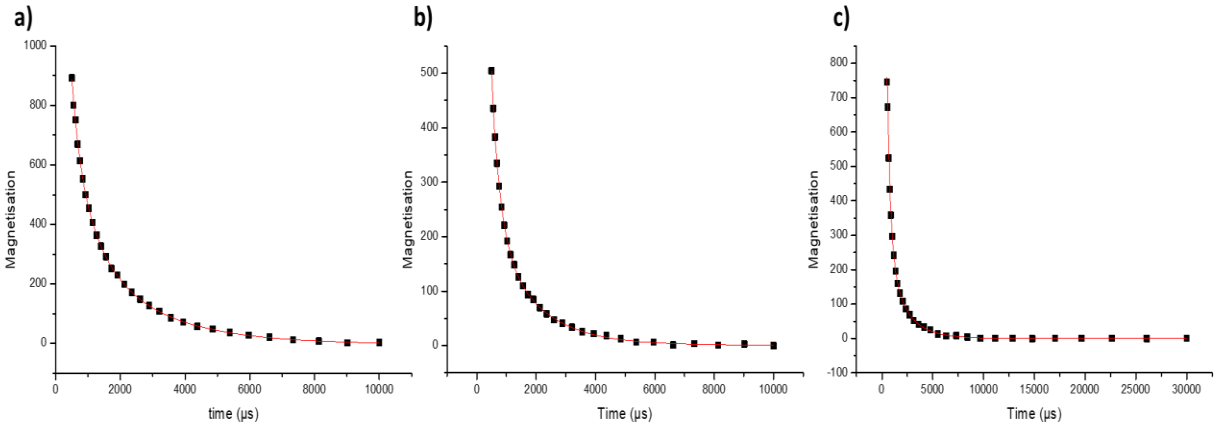

Figure 5. 51 T_2 relaxation curves of a) LDPE SE b) HF10110 and c) HF101

Table 5. 26 Fitting parameters of HF101, HF10110 blend and LDPE SE using three parameter exponential decay (R^2 = 99.8)

Sample	T_2^1	T_2^2	T_2^3
HF101	2282.1756	1177.51486	310.61968
HF10110	298.59442	1453.09826	38.519
LDPE SE	721.37288	236.70969	2267.32099

Since three different values were obtained for the spin-spin relaxation this indicated the presence of three components; a slow relaxing, a moderate relaxing and a fast relaxing component. Long T_2 relaxation times are an indication of averaging of dipolar interactions which generally occur where reorientation and chain diffusion are prevalent,[17] this largely occurs in the amorphous areas. The interfacial region would possess a shorter T_2 relaxation time since more of the dipolar interactions are retained than in the amorphous areas as dipolar interactions are dependent on molecular motions.[17] The necessity of three parameters to provide an accurate fit suggested phase separation within the interfacial and amorphous regions. This was in agreement with the deconvolutions of the SPE spectra which also

suggested multiple regions within the amorphous component of the signal. The relaxation curves for the neat HF101 and its blend is shown in Figure 5.51 with the calculated T_2 values in Table 5.26. For the HF101 the T_2^3 value corresponds to the relaxation of the protons in the interfacial region while the T_2^1 and T_2^2 values were of the order of an amorphous region.[17] For the LDPE SE two of the T_2 values were of the order of an amorphous region while one corresponded to proton relaxation of an interfacial region. The HF10110 blend had one proton relaxation in the amorphous regions and two proton relaxations in the interfacial regions. The T_2^3 value for the blend suggested a significantly more rigid component than was present within the interfacial region implying that the interfacial region was well bound by the crystalline domains.

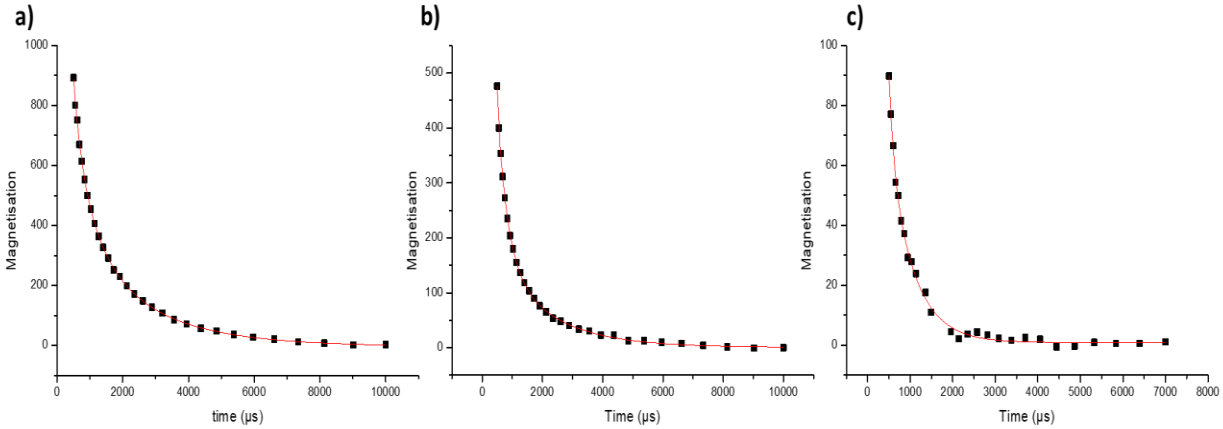

Figure 5. 52 T_2 relaxation curves of a) LDPE SE b) HF12010 and c) HF120

Table 5. 27 Fitting parameters of HF120, HF12010 blend and LDPE SE using three parameter exponential decay (R^2 = 99.6)

Sample	T_2^1	T_2^2	T_2^3
HF120	574.16933	574.625	110.93063
HF12010	344.12713	25.93167	1761.83911
LDPE SE	721.37288	236.70969	2267.32099

The relaxation curves for the neat HF120 and its blend is shown in Figure 5.52 with the calculated T_2 values in Table 5.27. The relaxation curve of the HF120 contained two T_2 values which were equal which indicated that only two components existed within the sample. The values were also not orders of magnitude apart suggesting great similarity between the amorphous and interfacial regions. The proton relaxation in the blend displayed two interfacial regions and a single amorphous region.

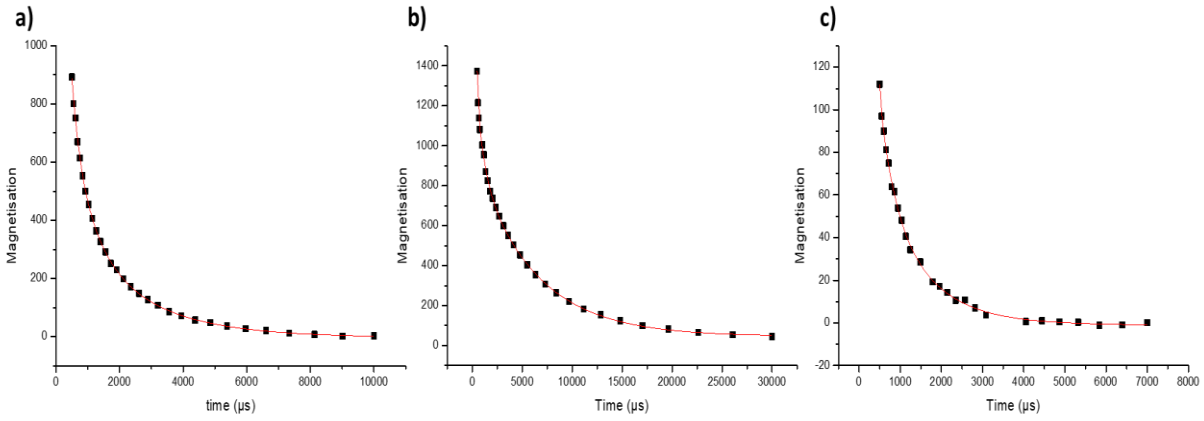

Figure 5. 53 T_2 relaxation curves of a) LDPE SE b) HF14010 and c) HF140

Table 5. 28 Fitting parameters of HF140, HF14010 blend and LDPE SE using three parameter exponential decay (R^2 = 99.8)

Sample	T_2^1	T_2^2	T_2^3
HF140	2.23138	344.22484	1118.14488
HF14010	739.38724	47.46465	5901.44279
LDPE SE	721.37288	236.70969	2267.32099

The relaxation curves for the neat HF140 and its blend is shown in Figure 5.53 with the calculated T_2 values in Table 5.28. The HF140 had two T_2 values corresponding to proton relaxations in interfacial regions and one corresponding to that of protons in the amorphous region. Both the blend and the LDPE SE have two proton relaxations in the amorphous regions. In both cases there was a T_2 value of approximately 700 µs, indicating that one component of the LDPE SE was unaffected by the presence of the HF140. The HF14010 was the only blend containing two amorphous regions. Since the HF140 blends were the least compatible it was likely that this phase separation within the amorphous area was the cause of the incompatibility.

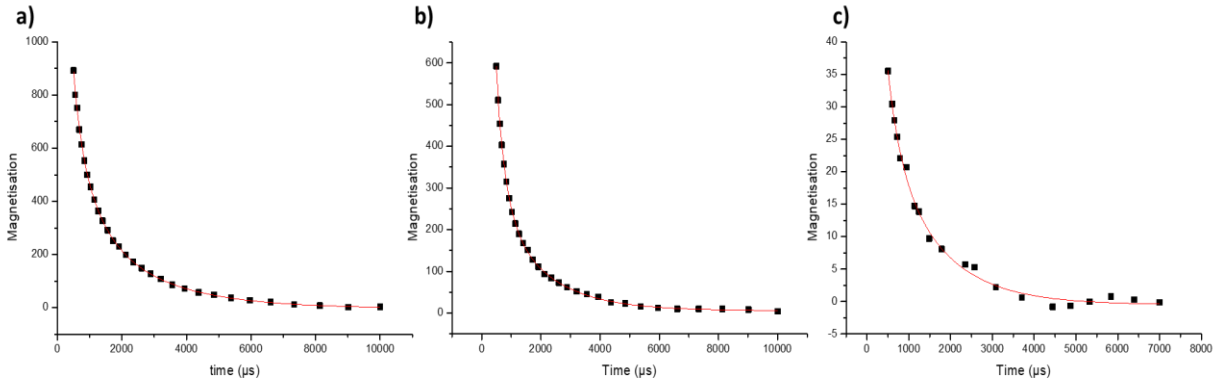

Figure 5. 54 T_2 relaxation curves of a) LDPE SE b) HR47710 and c) HR477

Table 5. 29 Fitting parameters of HR477, HR47710 blend and LDPE SE using three parameter exponential decay (R^2 = 99.2)

Sample	T_2^1	T_2^2	T_2^3
HR477	1225.82455	1225.56525	294.91791
HR47710	31.15549	319.02305	1597.21865
LDPE SE	721.37288	236.70969	2267.32099

The relaxation curves for the neat HR477 and its blend is shown in Figure 5.54 with the calculated T_2 values in Table 5.29.The HR477 once again possessed two T_2's of equal value and therefore only had two components; one interfacial and one amorphous. The blend contained two interfacial regions and one amorphous region.

5.4 Mechanical properties

5.4.1 Tensile properties

Since the crystallinity of the blends does not follow a linear trend it should not be expected that the mechanical properties would display additive behaviour. This was indeed the case, as shown in Figure 5.55. Figure 5.55 shows that the 90/10 blends either possessed a similar or slightly lower tensile modulus to that of the LDPE. The HF10110 blend was the exception in this case with a slightly higher tensile modulus. The HF10150 blend had a lower tensile modulus relative to the other blend ratios while for the HF120, HF140 and HR477 blends the 50/50 blend ratio had a higher modulus relative to the 10% LLDPE blends. Interestingly, the 80% LLDPE blends displayed an appreciably higher tensile modulus than the neat LLDPE, except in the case of the HF12080. The tensile modulus provides information on the amount of stress which the blends can withstand before yielding. Although a polyethylene film is essentially unusable after yielding, the stress at maximum load was included in Figure 5.55 to provide insight into the ultimate properties of the films. The HF10180 and HF14080 blends remained the best performing blends while the HR47780 blend tolerated much less stress than the remaining 80% LLDPE blends. The HR477 blends in general had diminished mechanical strength before the breaking point. The co-crystallised blends, however, all displayed better ultimate properties than the LDPE. The HF101 and HF120 blends seemed to be the most consistent as they showed minimal variation in their relative trends at yield point and before the break point.

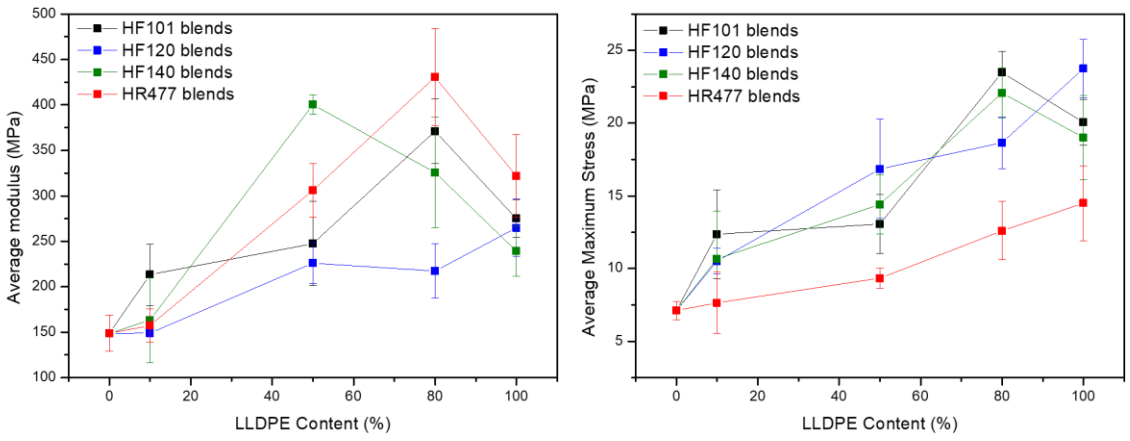

Figure 5. 55 Average tensile moduli and average stress at maximum load for all blends

It is generally believed that crystallinity determines the tensile modulus of the material. In Figure 5.56 a – d the tensile modulus does not appear to correlate with crystallinity, contrary to what was expected. The 80% LLDPE blends which showed the higher tensile modulus than the neat LLDPE also have a lower crystallinity than the neat LLDPE. Clearly crystallinity cannot be the sole contributing factor to the tensile modulus. The correlation with molar mass was therefore also investigated and can be seen in Figure 5.57. The tensile modulus of the HF120 blends in Figure 5.57 b appeared to correlate with molar mass. It was not clear whether the tensile modulus of the remaining blends also followed a molar mass trend. Since the HF120

neat polymer had the highest molar mass it might be that tensile modulus is controlled by molar mass when the molar mass is high. It is likely that the interplay between crystallinity and molar mass means that both of these aspects affect the tensile modulus to varying degrees depending on the blend ratio.

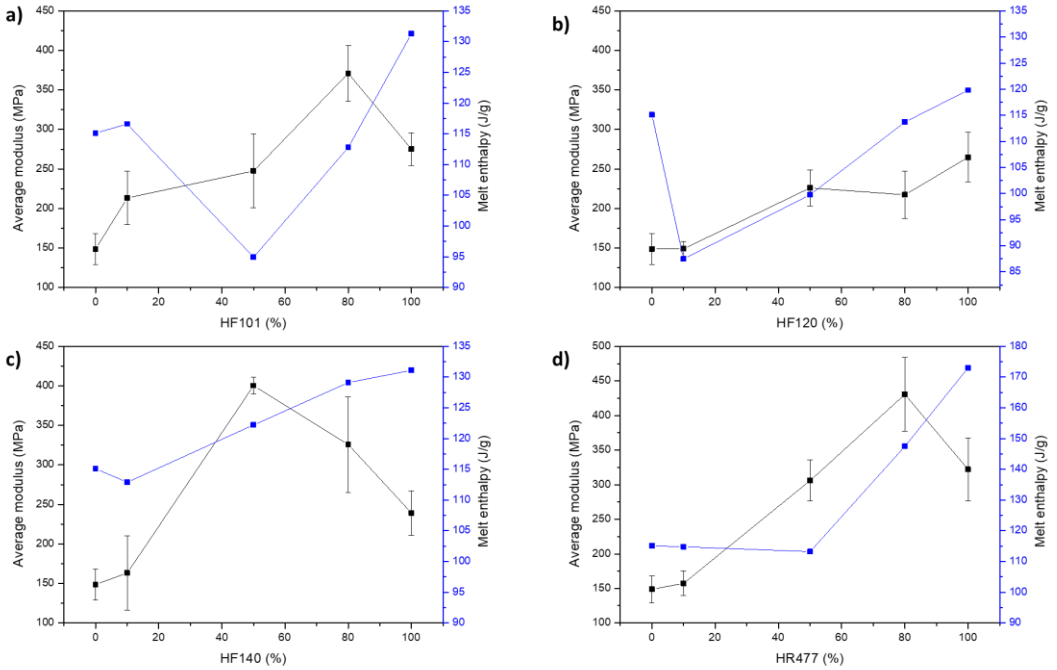

Figure 5. 56 Relationship between average tensile modulus and crystallinity for a) HF101 blends b) HF120 blends c) HF140 blends and d) HR477 blends

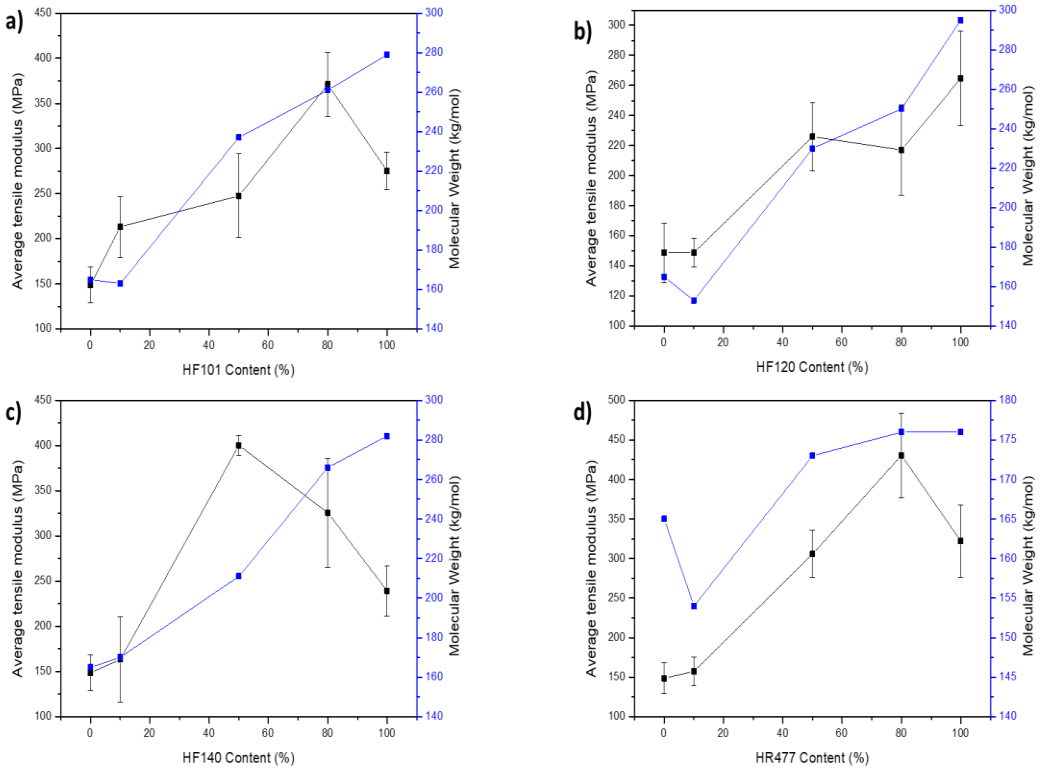

Figure 5. 57 Relationship between average tensile modulus and molar mass for a) HF101 blends b) HF120 blends c) HF140 blends and d) HR477 blends

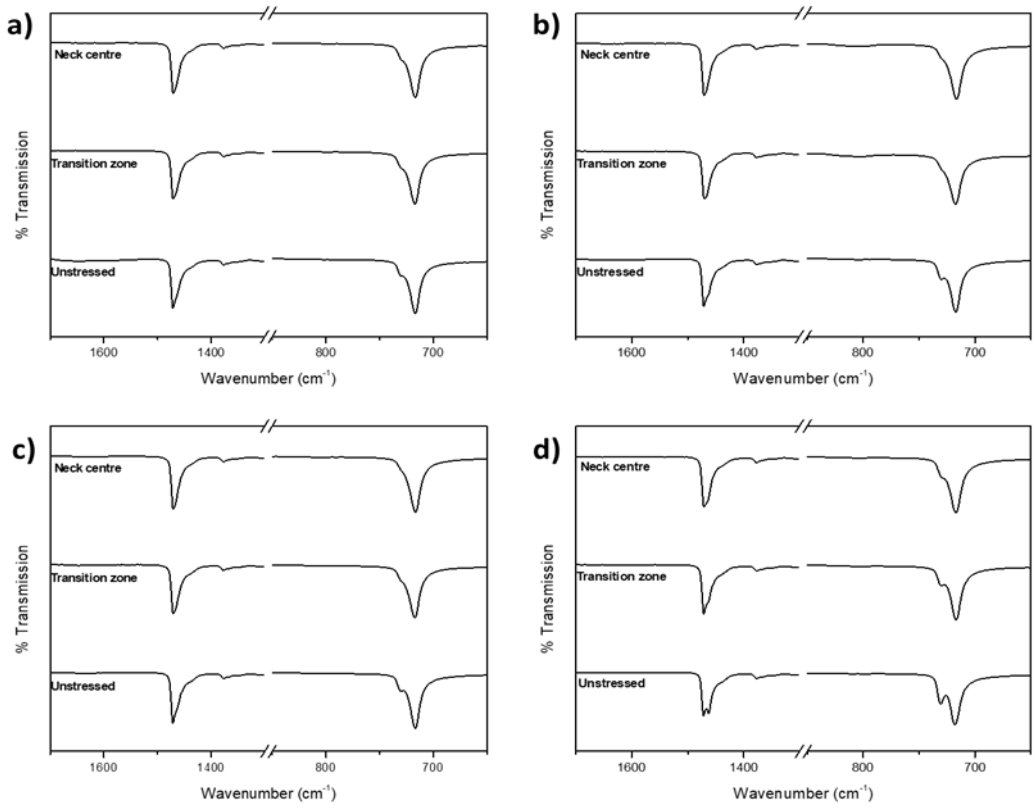

Figure 5. 58 FTIR spectra of tensile samples at different areas for a) HF10110 b) HF12010 c) HF14010 and d) HR47710 blends

When examining the methylene scissoring and rocking regions by FTIR spectroscopy in Figure 5.58 the unstressed sample was once again the most crystalline. The FTIR spectra of the 90/10 blends in different regions after applying a strain resembled that of LDPE shown in Figure 4.33 e which showed minimal splitting of the 730 cm^{-1} peak. The peak splitting for the 90/10 blends was even less than that of neat LDPE, indicating lower crystallinity than the neat LDPE. This confirms that for 90/10 blends crystallisation was hindered and supports the DSC results shown in Section 5.1.2. The decrease in crystalline splitting of the 730 cm^{-1} peak from unstressed through the transition zone to the centre of the necked region once more indicated the chain slippage which occurred before break. The chain slippage seemed to have started from the centre and moved outwards towards the edges of the tensile sample, explaining the decrease in crystalline splitting from the centre outwards. For the 90/10 blends only the most crystalline HR47710 displayed any splitting of the methylene scissoring peak at approximately 1470 cm^{-1}.

In Figure 5.59 the stress fringe patterns could once again be observed for the tensile samples of 90/10 blends. The HF10110 blend in Figure 5.59 a appeared to manage the strain the best of the 90/10 blends as the no clear fringe pattern could be observed and the colours were very dull. The HF14010 displayed slightly more intense colours than the HF10110. In Figure 5.59 c the failure occurred at both stretched edges surrounding the centre of the sample. It was clear that the maximum stress was experienced at the outer edges of this region where the colours were the most intense and not at the centre. The HR47710 and HF12010 showed the most intense colours, with the HF12010 in Figure 5.59 b displaying a clearly defined fringe pattern. These results appeared to follow the same trend as the tensile modulus for 90/10 blends shown in Figure 5.55.

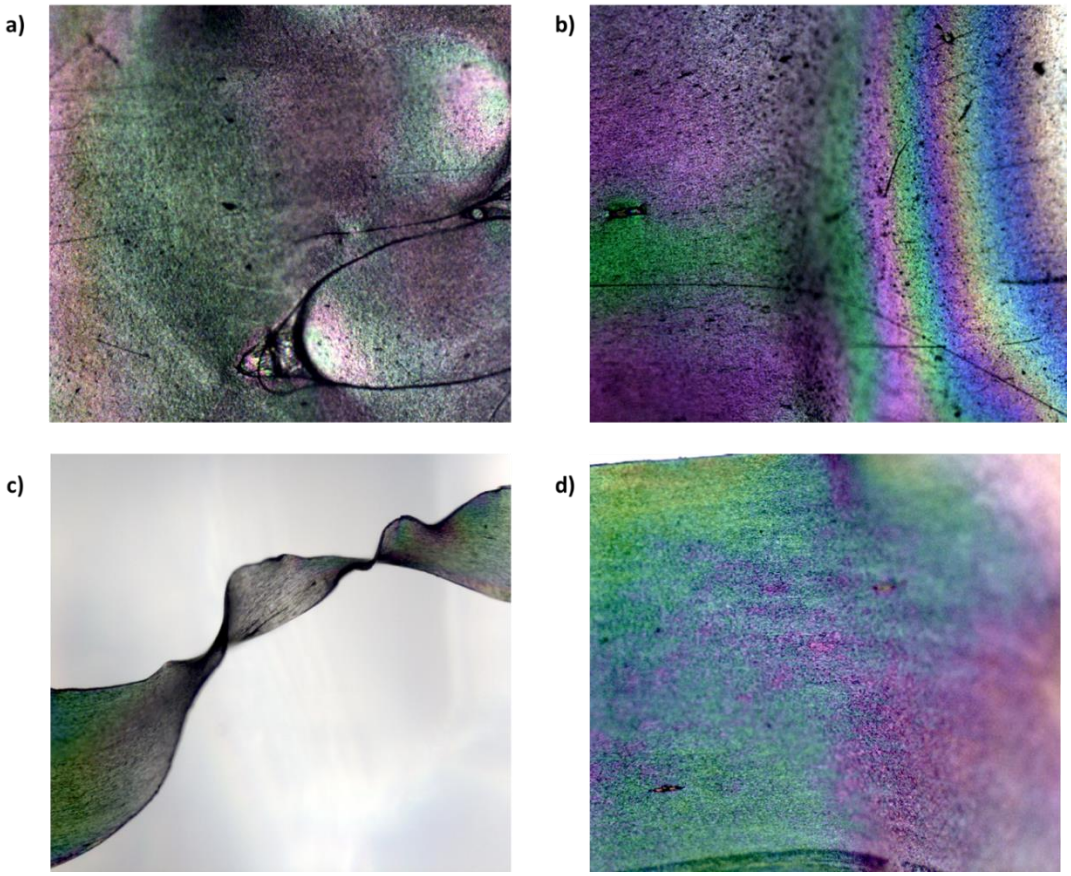

Figure 5. 59 Polarised optical microscopy images of a) HF10110 b) HF12010 c) HF14010 and d) HR47710 in the region above the breaking area. The break occurred to the right in all cases.

Since the binding component was identified as the 30 °C fraction it was of interest to determine how this binding component affected the tensile properties. Blends were made by recombining the LDPE TREF fractions in their corresponding weight percentages without adding the 30 °C fraction to the recombination. This recombined LDPE was blended with the two best performing LLDPEs in terms of mechanical properties, being the HF101 and HF140 grades in an 80/20 blend ratio where the LLDPEs were the majority components. The 80% LLDPE and 20% LDPE blend ratio for the HF101 and HF140 grades exhibited higher tensile moduli than the neat LLDPE in both cases. Figure 5.60 a and b compares the tensile moduli of the neat polymers as well as the 80% LLDPE blends with and without the 30 °C fraction. The tensile modulus of the HF10180 blend without the 30 °C fraction in 5.60 a showed a significant decrease and was similar to the modulus of the LDPE. In 5.60 b the modulus of the HF14080 blend decreased to below that of the LDPE. Despite the presence of all the highly crystalline components in the blends, the absence of the 30 °C had a dramatic effect on the mechanical properties. The 30 °C fraction could thus really be known as a binding fraction since it seems to hold the blends together and act as a compatibiliser between the two different components.

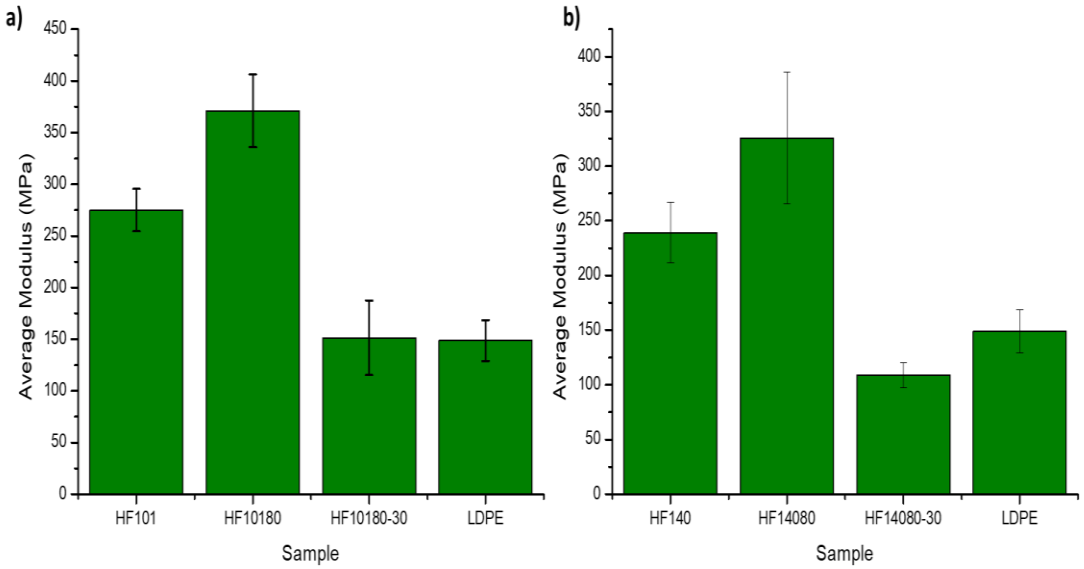

Figure 5. 60 Comparison of tensile moduli of neat polymers with tensile moduli of 80% LLDPE blends with and without 30 °C fraction

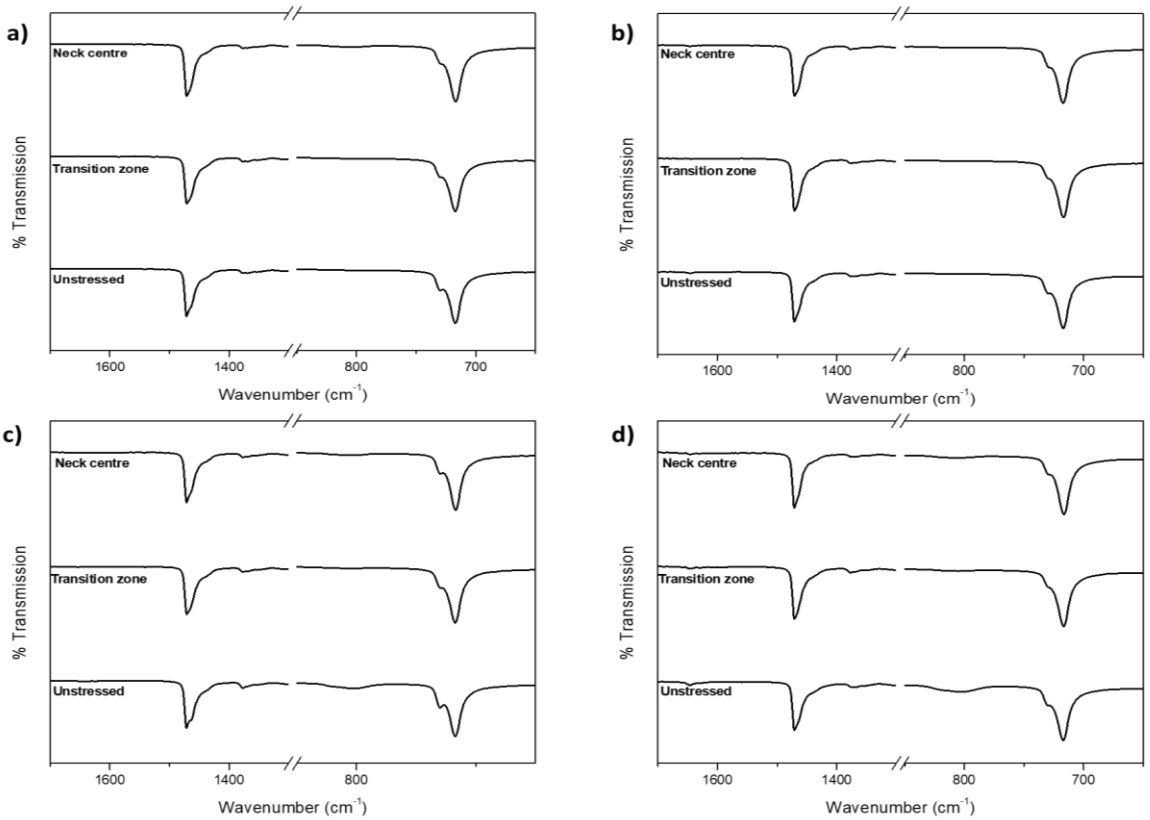

Figure 5. 61 FTIR spectra of tensile samples of a) HF10180 b) HF14080 c) HF10180-30 and d) HF14080-30 blends

In Figure 5.61 the HF10180 (a) and HF14080 (b) are compared to their corresponding blends HF10180-30 (c) and HF14080-30 (d). The splitting of the 720 cm^{-1} peak is not significant in all cases, further confirming that tensile modulus is not solely dependent on crystallinity. The relative intensity of the peaks also appeared to be highly similar, despite the spectra in Figure 5.61 c and d excluding the amorphous fraction. This was most likely due to the low contribution

of the removed amorphous fraction which only constitutes approximately 0.8% of the 20% which was LDPE. Despite the low quantity of LDPE amorphous fraction included, its absence clearly had a remarkable effect on the mechanical properties of the blends.

5.5 References

1. Puig, C. C. On the cocrystallization phenomenon in blends of high density polyethylene and low density polyethylene. *Polym. Bull.* **38,** 715–720 (1997).

2. Müller, A. J., Arnal, M. L., Spinelli, A. L., Cañizales, E., Puig, C. C., Wang, H. & Han, C. C. Morphology and crystallization kinetics of melt miscible polyolefin blends. *Macromol. Chem. Phys.* **204,** 1497–1513 (2003).

3. Wei, X., Bao, R., Cao, Z., Yang, W., Xie, B. & Yang, M. Stereocomplex crystallite network in asymmetric PLLA/PDLA blends: formation, structure, and confining effect on the crystallization rate of homocrystallites. *Macromolecules* **47,** 1439–1448 (2014).

4. Bai, J., Fang, H., Zhang, Y. & Wang, Z. Studies on crystallization kinetics of bimodal long chain branched polylactides. *CrystEngComm* **16,** 2452 (2014).

5. Gao, J., Yu, M. & Li, Z.-T. Nonisothermal crystallization kinetics and melting behavior of bimodal medium density polyethylene/low density polyethylene blends. *Eur. Polym. J.* **40,** 1533–1539 (2004).

6. Kim Piew Chuah, Gan, S. N. & Chee, K. K. Determination of avrami exponent by differential scanning calorimetry for non-isothermal crystallization of polymers. *Polymer (Guildf).* **40,** 253–259 (1999).

7. Paul, D. R. & Bucknall, C. B. *Polymer blends: formulation and performance*. (Wiley, 2000).

8. Ramesh, S. & Arof, A. K. The evaluation of miscibility of poly(vinyl chloride) and poly(ethylene oxide) blends by DSC, refractive index and XRD analyses. *Int. Polym. Process.* **24,** 354–358 (2009).

9. Sinha Ray, S., Pouliot, S., Bousmina, M. & Utracki, L. A. Role of organically modified layered silicate as an active interfacial modifier in immiscible polystyrene/polypropylene blends. *Polymer (Guildf).* **45,** 8403–8413 (2004).

10. Le Grange, M. The use of fluorescence to probe the morphology changes in complex polymers. (Stellenbosch University, 2015).

11. Kameda, T. Molecular structure of crude beeswax studied by solid-state ^{13}C NMR. *J. Insect Sci.* **4,** 29 (2004).

12. Botha, L. & Van Reenen, A. J. The effect of in-process ethylene incorporation on the evolution of particle morphology and molecular characteristics of commercial heterophasic ethylene propylene copolymers (HEPCs). *Eur. Polym. J.* **49,** 2202–2213 (2013).

13. Kuwabara, K., Kaji, H., Tsuji, M. & Horii, F. Crystalline-noncrystalline structure and chain diffusion associated with the 180° flip motion for polyethylene single crystals as revealed by solid-state ^{13}C NMR analyses. *Macromolecules* **33,** 7093–7100 (2000).

14. Russell, K. E., Hunter, B. K. & Heyding, R. D. Monoclinic polyethylene revisited. *Polymer (Guildf).* **38,** 1409–1414 (1997).

15. Kuwabara, K., Kaji, H., Horii, F., Bassett, D. C. & Olley, R. H. Solid-State ^{13}C NMR analyses of the crystalline−noncrystalline structure for metallocene-catalyzed linear low-density polyethylene. *Macromolecules* **30,** 7516–7521 (1997).

16. Assumption, H. J., Vermeulen, J. P., Jarrett, W. L., Mathias, L. J. & Van Reenen, A. J. High resolution solution and solid state NMR characterization of ethylene/1-butene and ethylene/1-hexene copolymers fractionated by preparative temperature rising elution fractionation. *Polymer (Guildf).* **47,** 67–74 (2006).

17. Wang, M., Bernard, G. M., Wasylishen, R. E. & Choi, P. A solid-state ^{13}C NMR investigation of the morphology of single-site and Ziegler-Natta linear low-density polyethylenes with varying branch contents. *Macromolecules* **40,** 6594–6599 (2007).

Chapter 6: Conclusions and Recommendations

6.1 Conclusions

A full characterisation of the neat blend components was presented. Molar mass analysis and crystallinity analysis by DSC revealed the HF101 and HF140 grades to be highly similar while the HF120 possessed the highest molar mass and the lowest crystallinity and in contrast the HR477 grade possessed the highest crystallinity and the lowest molar mass. Solution crystallisation analysis showed that, excluding the main dissolution event, the LLDPEs also contained some material dissolving at lower temperatures, in the same range as the dissolution of the LDPE. Crystal morphology was determined using SEM from which it could be seen that the LLDPEs all exhibit a spherulitic morphology while the LPDE had a two-dimensional axialitic morphology. XRD was used to determine the crystal structure which was orthorhombic in all cases.

The Avrami method was applied to model the crystallisation kinetics under isothermal conditions. According to the calculated Avrami index the crystal morphology ranged from axialitic to spherulitic with nucleation varying from instantaneous to sporadic or a combination of both. The crystallisation half time correlated with the crystallinity values in that the LLDPEs required less time to reach 50% of the full crystallinity while the LDPE required a significantly longer time. The Avrami plots were not parallel indicating that the method was not successful in fully describing these polymer systems. This was most likely due to the Avrami method not considering the process of secondary crystallisation which can affect the results during isothermal crystallisation. Although both the Nadkarni and Ozawa methods yielded adequate results for describing the non-isothermal crystallisation processes the Nadkarni method was deemed the most successful due to the limited temperature range over which the Ozawa method could be applied.

Fractionation of the neat polymers was found to be difficult due to the highly heterogeneous nature of the polymers. SSA fractionation before and after preparative TREF revealed the presence of interactions between the components within the polymer through changes in the methylene sequence length before and after the components were separated.

For the most part the tensile modulus of the neat polymers followed a crystallinity trend, except in the case of the HF120 grade LLDPE where the tensile modulus was dominated by the high molar mass. Using POM the greatest tensile stress was found to be concentrated at the base of the necked region and not within the neck itself.

The crystallisation behaviour of blends of low density polyethylene and various linear low density polyethylenes was studied using different blending methods. For solution blends at least two separate melting events could be observed by DSC for almost all blend ratios at similar peak positions to the neat blend components which was indicative of incompatibility. The 10% LLDPE blend ratio displayed three separate melting events which suggested a certain extent of co-crystallisation. In all cases, except in the case of the HF140 blends, the crystallinity was considerably restricted to values sometimes below that of LDPE even up to 80% LLDPE content. It was then concluded that the individual components interfered with the crystallisation of the other component. The HF140 blends displayed an almost linear increase in crystallinity which indicated that the crystallinity was an additive property implying that no significant interactions took place.

Under isothermal conditions the 80% LLDPE blends crystallised similarly to the neat LLDPEs. At 50% LLDPE and below the crystallisation of the HF101 and HF120 blends was significantly

delayed, while the HF140 and HR477 blends maintained a fairly rapid crystallisation rate until the LLDPE concentration was decreased to 10%. The 50% LLDPE blends also displayed the greatest dependence on crystallisation temperature. Under non-isothermal conditions the crystallisation kinetics of the LLDPE appeared to dominate the behaviour above 50% LLDPE content. The 10% LLDPE blends displayed similar kinetics to that of LDPE. As most commercial processing is done under non-isothermal conditions it appeared that blend ratio will not significantly impact the crystallisation rate above 50% LLDPE content and conditions for neat LLDPE can be used for these systems. Analogously, when using this grade of LDPE similar crystallisation times can be used when adding 10% of a similar LLDPE to those which were used in this study.

The different criteria for co-crystallisation were systematically investigated. It is already known that LDPE and LLDPE have similar chemical structures as both are apolar and (in the case of these Ziegler-Natta LLDPEs) have irregularly distributed branching points. XRD also revealed that the crystal structure was unchanged throughout the solution blending process. By adding cellulose nanowhiskers containing fluorescent labels, either FITC for LLDPEs or RhB for LDPE, and monitoring the movement of the labels by fluorescence microscopy the miscibility in the melt could be assessed. Since no isolated domains of a particular fluorescent marker could be identified it was concluded that the markers, and therefore the polymers, were intimately blended in the melt and were thus melt miscible. The incompatibilities observed by other methods must therefore occur during the crystallisation of the blend components. This idea was supported by the vastly different crystallisation kinetics of the LDPE from all LLDPEs.

It was concluded that the 10% LLDPE blends which showed three melting events by DSC must have possessed some kind of interaction which appeared to be concentration dependent. In order to identify the component of the LDPE which facilitated the interaction, LDPE fractions obtained by prep-TREF were blended with the LLDPEs in 90/10 ratios to test whether any single fraction could reproduce the effect of the three melting events. Only the fraction which eluted at 30 °C, the soluble fraction, was capable of reproducing the three melting events. As the 30 °C fraction only melted at much lower temperatures than the temperature range where the intermediate ‘co-crystallised’ peak occurred, co-crystallisation was no longer an explanation for the intermediate melting peak observed by DSC. Instead it appeared that the presence of the 30 °C fraction caused a phase separation within the LLDPE. As the 30 °C fraction would still be molten at the temperature at which the LLDPE crystallised it was possible that the LDPE 30 °C fraction interfered with the LLDPE amorphous regions, which are also mobile.

Through the use of solid state NMR the solid state morphology of these 90/10 blends could be probed in order to better understand the phase separation which occurred. Due to the majority of the blends consisting of the LDPE 30 °C fraction the proton wideline spectra showed that the blends contain significant mobility. The wideline spectrum of the 10% HF140 blend, which displayed the greatest degree of incompatibility by DSC, displayed a separation of the mobile peak which suggested the presence of two amorphous regions. This was confirmed through the deconvolution of the methylene region of the single pulse spectrum which allowed the identification of both an amorphous and interfacial region in addition to a crystalline peak at higher chemical shift. In most cases an additional region could be attributed to either another amorphous region or interfacial region with the aid of the spin-spin (T_2) relaxation times.

The mechanical properties of these 90/10 blends displayed a similar or slightly lower tensile modulus to that of the LDPE, except the HF10110 blend which had a slightly higher tensile modulus than the LDPE. Tensile modulus displayed a general increase with LLDPE content

with all 80% LLDPE blends, except the HF12080, displaying tensile moduli greater than that of the corresponding LLDPE. No clear trend could be observed between tensile modulus and crystallinity. The HF120 blends displayed a correlation between the tensile modulus and the molar mass. Since the HF120 had the highest molar mass of the LLDPEs it was proposed that a limit exists above which molar mass affects the modulus of the sample while below this limit molar mass was not the dominant factor. Since the LDPE 30 °C fraction was found to be an important factor in the blend morphology a melt blend was made by the recombination of all TREF fractions of LDPE excluding the 30 °C fraction in a 20/80 ratio where the LDPE was the 20 % component. This blend ratio previously displayed the best tensile properties. After the removal of the soluble fraction the tensile modulus was drastically reduced to a similar or lesser value than that of pure LDPE. Thus the 30 °C fraction is key to the mechanical strength of the blends.

6.2 Recommendations

The study requires the inclusion of another grade of LDPE to determine whether the effects observed occur for all LDPE/LLDPE blends.

Blending using LLDPEs with longer and shorter co-monomer lengths could also aid in the interpretation of the observed properties.

Optimisation of solid state NMR relaxation experiments is necessary in order to determine $T_1\rho$ values in addition to the T_2 values presented.

6.3 Future work

In order to fully understand blend miscibility thermodynamic parameters also need to be determined. Physical methods to determine free energy of mixing either have a molar mass dependence which decreases the measured temperature difference to below that which is measurable using regular laboratory methods or require the polymer to be in dilute solutions in which case one cannot probe solid state morphology. Thus a computational study is required to model the blend behaviour. For this study the polymer modification of the reference interaction site model (PRISM) is recommended which has been successfully applied in many cases.

Appendices

Appendix A: Deconvolutions of ^{13}C SPE spectra

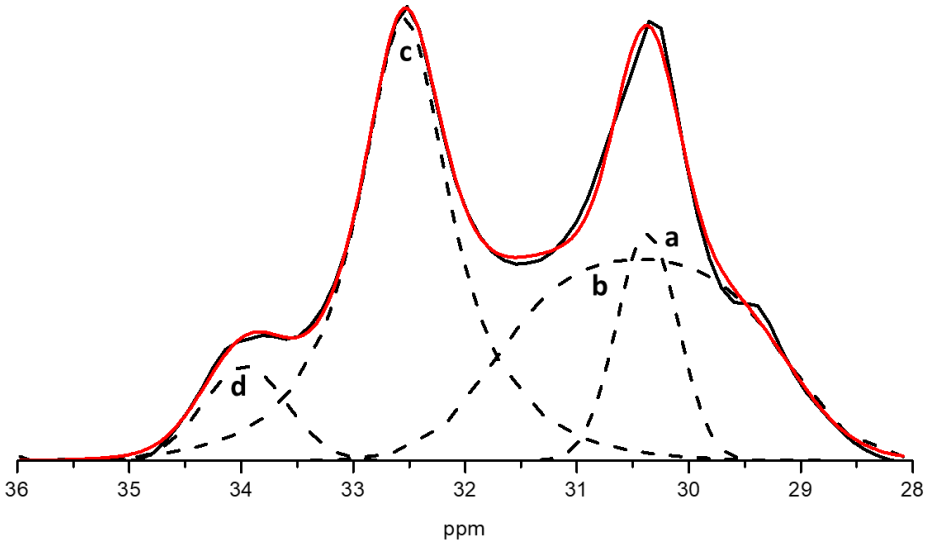

Figure A. 1 Deconvolution of the methylene region of the HF101 ^{13}C SPE spectrum

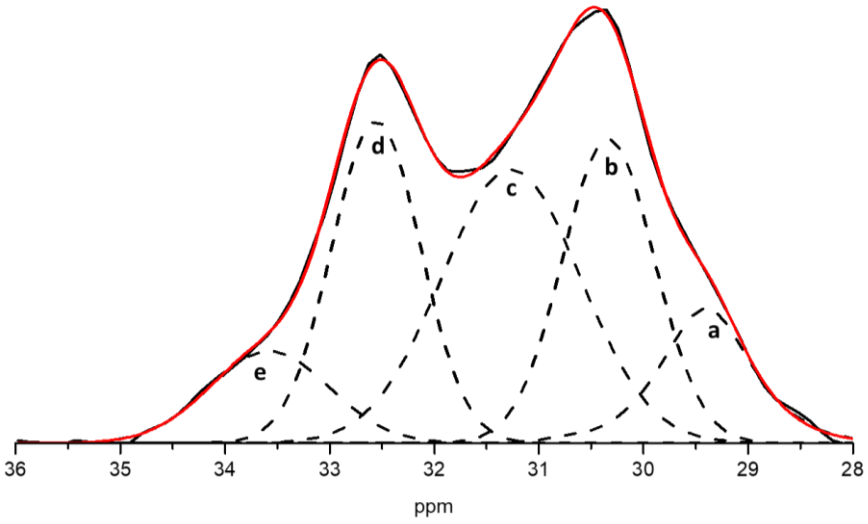

Figure A. 2 Deconvolution of the methylene region of the HF120 ^{13}C SPE spectrum

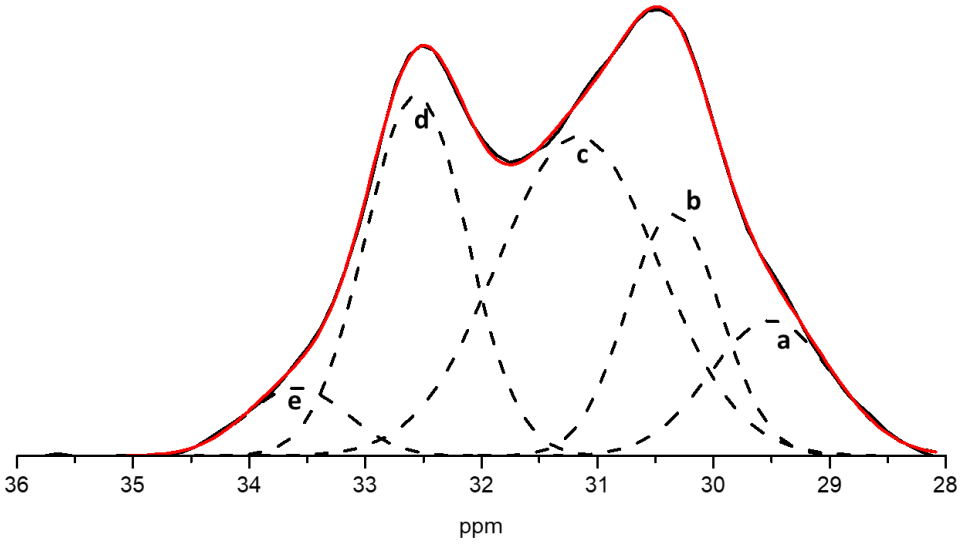

Figure A. 3 Deconvolution of the methylene region of the HF140 ^{13}C SPE spectrum

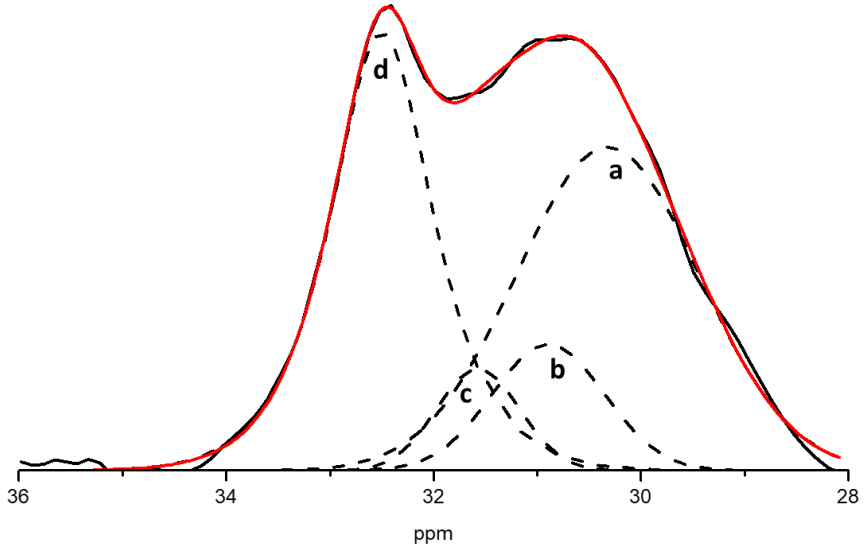

Figure A. 4 Deconvolution of the methylene region of the HR477 ^{13}C SPE spectrum

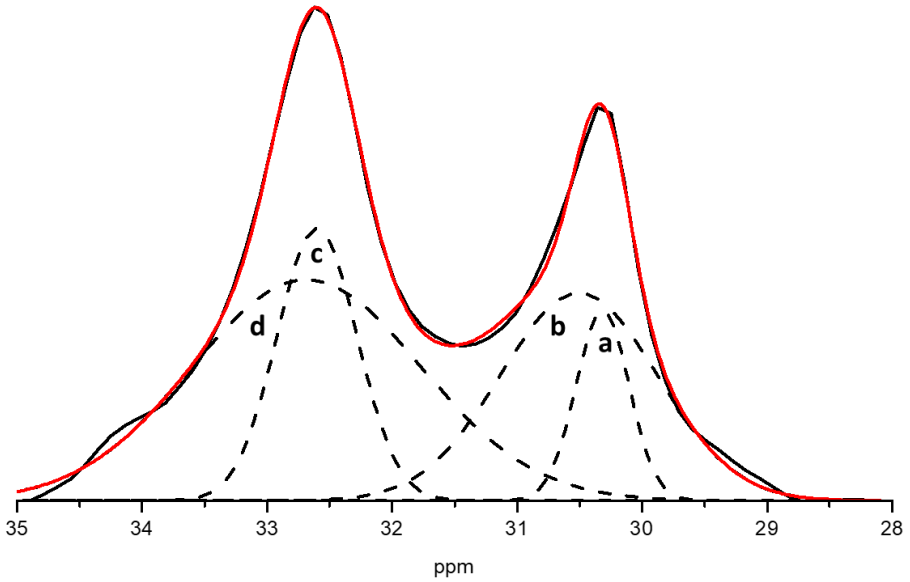

Figure A. 5 Deconvolution of the methylene region of the ^{13}C SPE spectrum of 90% LDPE SE 10% HF120 blend

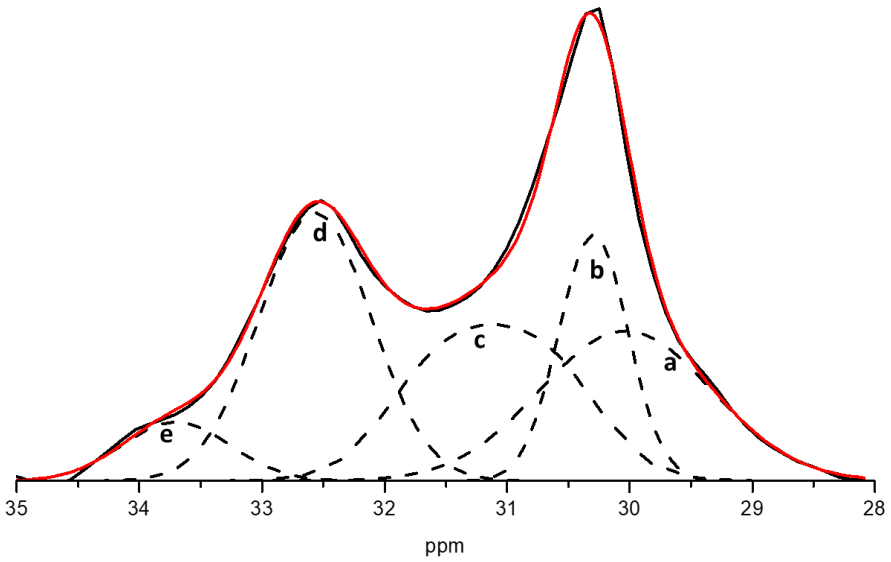

Figure A. 6 Deconvolution of the methylene region of the ^{13}C SPE spectrum of 90% LDPE SE 10% HF140 blend

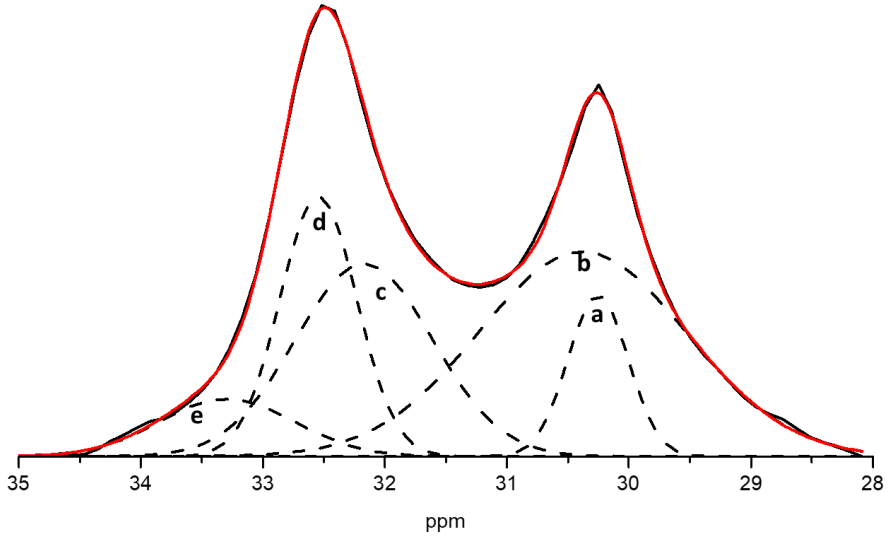

Figure A. 7 Deconvolution of the methylene region of the ^{13}C SPE spectrum of 90% LDPE SE 10% HR477 blend